

**HEPATIC WOUND HEALING FOLLOWING ACUTE AND CHRONIC LIVER  
INJURY: A POTENTIAL ROLE FOR THE HYALURONAN NETWORK**

By  
© 2017

Jennifer McCracken

B.S., Pittsburg State University, 2011

Submitted to the graduate degree program in Toxicology and the Graduate Faculty of  
the University of Kansas in partial fulfillment of the requirements for the degree of  
Doctor of Philosophy.

---

Chair: Michele Pritchard, PhD

---

Wen-Xing Ding, PhD

---

Hartmut Jaeschke, PhD

---

Ken McCarson, PhD

---

Brenda Rongish, PhD

Date Defended: 12 May 2017

The dissertation committee for Jennifer McCracken certifies that  
this is the approved version of the following dissertation:

**HEPATIC WOUND HEALING FOLLOWING ACUTE AND CHRONIC LIVER  
INJURY: A POTENTIAL ROLE FOR THE HYALURONAN NETWORK**

---

Chair: Michele Pritchard, PhD

Date Approved: 12 May 2017

## **Abstract**

Chronic liver disease is the 12<sup>th</sup> leading cause of death in the United States and consists of a continuum of pathologies. Following initial injury, a patient develops steatosis, or excess fat accumulation. While the liver has the remarkable ability to repair itself, if injury persists, the wound healing process becomes deregulated and excess extracellular matrix (ECM) can accumulate resulting in fibrosis. If the etiologic agent is not removed, a patient can progress to cirrhosis and hepatocellular carcinoma. Despite decades of research, there are currently no effective treatments for advanced liver disease and a liver transplantation is the only treatment option for patients. There are two main approaches of developing novel therapeutics to cure liver disease. First, understanding mechanisms of liver injury can lead to potential pharmacologic targets. Second, because the liver has the remarkable capacity to heal itself, understanding the mechanisms that allow this to happen may reveal potential places that can be targeted to enhance this recovery process. This is an appealing approach because wound healing consists of mostly identical steps regardless of the injury-provoking incident and therefore could apply to liver injury of varied etiologies, and maybe even wound repair in extra-hepatic organs. Therefore, I chose to focus my dissertation research on exploring hepatic wound healing after acute and chronic liver injury.

Hyaluronan (HA) is a ubiquitous, anionic glycosaminoglycan in the ECM that can hold 1,000 times its weight in water. HA, HA binding proteins, and HA receptors (the HA network) are implicated in aspects of the wound healing process in the skin, intestine, and lung. The HA network plays roles in injury, inflammation, and fibrogenesis; all primary aspects of wound healing. In fact, high basal HA levels and sustained HA induction in fetal skin are associated with the scarless wound healing that occurs after

injury. Adult dermal tissue, which heals with a scar, has lower basal HA levels and a transient HA induction following injury. HA is elevated in the plasma of patients with liver disease and correlates with disease severity. Despite HA's connection to wound healing and its use as a biomarker for liver disease, little work has been done to investigate if HA is involved in liver wound repair. We hypothesize that the HA network contributes to hepatic wound healing.

Our first focus was on a role for HA itself in hepatic wound healing. HA is synthesized by one of three enzymes (HAS1, 2, or 3) and previous studies show that *Has3*<sup>-/-</sup> mice have decreased dextran sodium sulfate (DSS)-induced colitis and ventilator induced lung injury. We therefore, hypothesized that *Has3*<sup>-/-</sup> mice would be protected from liver injury and fibrosis. Using mice deficient in HAS3, wild-type mice, and carbon tetrachloride (CCl<sub>4</sub>) we induced both acute and chronic liver injury. We found that *Has3*<sup>-/-</sup> mice have increased injury, but also increased wound healing, including inflammation, regeneration, and matrix remodeling compared to wild-type mice after acute CCl<sub>4</sub> exposure. This increased wound healing was associated with an increase in hepatic HA deposition and expression of the HA receptor HA mediated motility receptor (HMMR). After chronic CCl<sub>4</sub>, *Has3*<sup>-/-</sup> mice had increased pro-fibrotic transcripts, but no increase in fibrosis. This disconnect was attributed to increased matrix metabolism and was again associated with increased HMMR expression compared to wild-type mice.

This led us to investigate a role for HMMR in hepatic wound healing. HMMR can be both intracellular and extracellular and plays a role in cell cycle progression and cell migration, important aspects of wound healing. We hypothesized that *Hmmr*<sup>-/-</sup> mice

would have delayed wound healing following acute and chronic liver injury due to impaired hepatocyte proliferation and impaired macrophage-mediated matrix metabolism. Using CCl<sub>4</sub>, we induced both acute and chronic liver injury in *Hmmr*<sup>-/-</sup> and wild-type mice. *Hmmr*<sup>-/-</sup> mice had decreased inflammation, regeneration, and matrix remodeling despite no difference in liver injury compared to wild-type mice after acute liver injury. This was associated with decreased hepatic HA deposition. After chronic liver injury, *Hmmr*<sup>-/-</sup> mice had decreased pro-fibrotic transcripts but no difference in fibrosis. Similar to *Has3*<sup>-/-</sup> mice, this disconnect can be attributed to differences in matrix remodeling, with *Hmmr*<sup>-/-</sup> mice having less matrix metabolism compared to wild-type mice.

My work is the first to demonstrate that HA and HMMR are involved in hepatic wound healing. The culmination of this work led to the development of a working model connecting HA and HMMR with hepatic wound healing. Following liver injury, hepatocytes and resident liver macrophages synthesize pro-inflammatory cytokines and chemokines. These cytokines then stimulate hepatic stellate cells (HSC) to synthesize and deposit HA in the injured areas of the liver, while the chemokines recruit circulating macrophages to the liver. Then, we propose two feed forward loops, the first being where the HA can increase water retention thereby increasing HSC activation by increasing mechanical stress and further increasing HA deposition. Second, we also propose a feed forward loop between HA and inflammation, where the HA contributes to inflammation and increased inflammation further increases HA synthesis by HSC. Additionally, we propose that macrophages that are being recruited to the liver express HMMR and can use the HA:HMMR interaction to localize to the necrotic area and clear

tissue debris. In the case of chronic liver injury, this HA:HMMR interaction can localize scar associated macrophages to the fibrotic septae and increase matrix degradation and facilitate fibrosis resolution. Finally, the increased inflammatory microenvironment of the healing liver, and perhaps intracellular HMMR, promotes hepatocyte proliferation. Together, HA and HMMR contributes to inflammation, regeneration, and matrix remodeling to aid in the hepatic wound healing process.

Taken together, our data demonstrate that the HA network, in particular HA and HMMR, is involved in both acute and chronic liver injury and wound healing. Further work should be completed to evaluate other aspects of the HA network, including other receptors and HA binding proteins. Additionally, exploring what role the HA:HMMR interaction plays in acute and chronic liver injury should be explored further.

## **Acknowledgements**

I would first like to thank my mentor, Dr. Michele Pritchard, who took in someone with very little research experience and taught me everything I know about bench science and the scientific process. Without her guidance and encouragement I would not be where I am today. I know I will take the lessons learned during my time here to all future career endeavors.

Secondly, I would like to thank my dissertation committee. Drs. Wen-Xing Ding, Hartmut Jaeschke, Ken McCarson, and Brenda Rongish have provided invaluable feedback on my project, advice for my future career goals, and guidance through the process of completing my PhD.

I would also like to thank the members of the Department of Pharmacology, Toxicology, and Therapeutics. The faculty and students in this department foster a collaborative environment for which I am immensely grateful. The base of Pharmacology and Toxicology knowledge I received from the classroom lectures will be invaluable to my future. Thank you also to the administrative staff, in particular Elizabeth Jamison, for the help in travel reimbursement, and Cody Tully for making sure I have all requirements completed for graduation. Lastly, thank you to Dr. Mary Lynn Bajt and Huina Cai for their help and work in the histology and cell isolation core.

Thank you to the current and previous members of the Pritchard Lab. In particular, thank you to Lu Jiang, who has been a soundboard for ideas and a great traveling partner to conferences. I would also like to thank Krutika Desphande and Briana Holt for the advancement of my project in the early stages. Whether we were

discussing a new technique or idea, traveling to conferences, or exploring new cities, this experience has been something I will always remember.

Additionally, I want to thank Dr. Prabhakar Chalise in the KUMC Biostatistics department. He has answered numerous emails regarding statistics questions and performed some of the statistical analysis for this project.

I could not have completed the work of this dissertation without the generous donation of the genetically modified mice. Drs. Sean Kessler, Carol de la Motte, and Vince Hascall provided us with *Has1/3*<sup>-/-</sup> mice from which the *Has3*<sup>-/-</sup> mice were derived and Dr. Eva Turley provided us with *Hmnr*<sup>-/-</sup> mice.

The work in this dissertation was supported by National Institutes of Health, National Center for Research Resources [P20 RR021940], National Institute of General Medical Sciences [P20 GM103549, P30GM118247], National Institute of Environmental Health Sciences “Training Program in Environmental Toxicology” [T32 ES007079], the National Institutes of Alcohol Abuse and Alcoholism [K99 AA017918A, R00 AA17918], by an NIH Clinical and Translational Science Award grant [UL1TR000001, formerly UL1RR033179] awarded to the University of Kansas Medical Center, and an internal Lied basic science grant program Communication Corporation of the KUMC Research Institute. In addition, funds from the Center for Reproductive Health after Disease from National Centers for Translational Research in Reproduction and Infertility [P50 HD076188], and National Institute of Diabetes and Digestive and Kidney Diseases [R01 DK098414] were used to complete the work in this study.

I also have to acknowledge several people in my personal life. There have been so many friends who have helped me get through the last five years. I want to

personally thank Jackie Thompson, Kelsey Hampton, Bailey Allard, and Amanda Brinker for the support and encouragement as we all go through this process together, and I want to thank Lindsay Murphy, Anna Capps, Jamie Talbott, and Katie Butler for the friendship over the past 20+ years.

I want to thank my parents, Roger and Drennette, who have been my biggest supporters since day one, regardless of what I chose to do, and are always a great source of encouragement when I need it the most. I would not be the person I am today without their love and support. I also want to thank my future in-laws who have been nothing but encouraging through the past five years.

And last but not least, I want to thank my fiancé Bobby. Despite never actually living in Kansas City, he managed to be my rock, whether it be from Wichita or Houston. His encouragement is what has kept me going and I can't wait to start our life together.

**I would like to dedicate this dissertation to my parents, Roger and Drennette, and my fiancé Bobby for the support and encouragement they have provided over the past five years.**

## Table of Contents

<b>Chapter 1: Introduction .....</b>	<b>1</b>
<b>Hepatic wound healing .....</b>	<b>4</b>
Initial injury .....	7
Inflammation .....	8
Regeneration .....	9
Matrix remodeling .....	12
Chronic Liver Injury and Fibrosis .....	13
<b>Carbon tetrachloride (CCl<sub>4</sub>) as a model of liver disease.....</b>	<b>15</b>
History of CCl <sub>4</sub> .....	15
Modeling Acute Liver Injury.....	15
Modeling Chronic Liver Injury .....	16
Sub-Strain Differences in Mouse Models of Liver Injury .....	17
<b>Hyaluronan.....</b>	<b>18</b>
History.....	18
HA Synthesis .....	19
HA turnover and homeostatic degradation .....	25
HMW-HA signaling.....	26
LMW-HA signaling .....	29
HA and HA mediated motility receptor (HMMR) signaling .....	30
Clinical Uses of HA .....	31
<b>Goals of the studies within this dissertation.....</b>	<b>35</b>
<b>Chapter 2: Materials and Methods.....</b>	<b>39</b>

<b>Materials</b> .....	<b>40</b>
<b>Methods</b> .....	<b>40</b>
Animal use .....	40
Genotyping.....	40
Carbon tetrachloride exposure.....	42
Sample collection and storage.....	43
Hepatocyte isolation and culture.....	43
<i>In vitro</i> , carbon tetrachloride exposure and sample collection .....	45
Lactate dehydrogenase (LDH) assay .....	46
CYP2E1 activity assay.....	47
Injury evaluation.....	47
Hepatic triglyceride determination.....	48
Gene expression.....	49
Immunoblotting .....	50
Cytokine protein array.....	54
Hepatic leukocyte esterase (chloracetate esterase, CAE) localization and quantification.....	54
Ki67 staining .....	56
$\alpha$ SMA immunohistochemistry .....	57
F4/80 immunofluorescence.....	58
Hyaluronan binding protein (HABP) staining for hyaluronan .....	59
Hyaluronan plasma concentration .....	60
Hyaluronan size analysis .....	60

Sirius red staining .....	61
Hydroxyproline assay.....	61
In situ zymography.....	62
Statistical analysis.....	63
<b>Chapter 3: HA produced by HAS3 attenuates liver injury and wound healing after acute CCl<sub>4</sub> exposure .....</b>	<b>64</b>
<b>Abstract.....</b>	<b>65</b>
<b>Introduction.....</b>	<b>66</b>
<b>Results.....</b>	<b>68</b>
Hepatic <i>Has</i> gene transcript accumulation and plasma HA levels in wild-type and <i>Has3</i> <sup>-/-</sup> mice.....	69
Liver injury and steatosis after acute CCl <sub>4</sub> exposure .....	71
Hepatic inflammatory environment after acute CCl <sub>4</sub> exposure in wild-type and <i>Has3</i> <sup>-/-</sup> mice.....	79
Hepatic regeneration following acute CCl <sub>4</sub> exposure in wild-type and <i>Has3</i> <sup>-/-</sup> mice. .....	80
Matrix remodeling following acute CCl <sub>4</sub> exposure in wild-type and <i>Has3</i> <sup>-/-</sup> mice... ..	83
HA receptor expression in wild-type and <i>Has3</i> <sup>-/-</sup> mice following acute CCl <sub>4</sub> exposure. ....	91
<b>Discussion .....</b>	<b>94</b>
<b>Chapter 4: HA mediated motility receptor (HMMR) is required for wound healing after acute liver injury .....</b>	<b>102</b>
<b>Abstract.....</b>	<b>103</b>

<b>Introduction</b> .....	<b>104</b>
<b>Results</b> .....	<b>106</b>
<i>Hmnr</i> expression pattern in C57Bl/6N mice mirrors that of C57Bl/6J mice .....	106
Liver injury in <i>Hmnr</i> <sup>-/-</sup> and wild-type mice following acute CCl <sub>4</sub> exposure.....	108
Hepatic inflammation in <i>Hmnr</i> <sup>-/-</sup> and wild-type mice following acute CCl <sub>4</sub> exposure .....	108
Hepatic regeneration in wild-type and <i>Hmnr</i> <sup>-/-</sup> mice following acute CCl <sub>4</sub> exposure .....	112
Matrix remodeling in wild-type and <i>Hmnr</i> <sup>-/-</sup> mice following acute CCl <sub>4</sub> exposure. .....	115
Hyaluronan accumulation in wild-type and <i>Hmnr</i> <sup>-/-</sup> following acute CCl <sub>4</sub> exposure .....	121
<b>Discussion</b> .....	<b>125</b>
<b>Chapter 5: A critical role for HA and HMMR in liver fibrosis</b> .....	<b>131</b>
<b>Abstract</b> .....	<b>132</b>
<b>Results</b> .....	<b>135</b>
Fibrosis in wild-type and <i>Has3</i> <sup>-/-</sup> mice following chronic CCl <sub>4</sub> exposure .....	135
Matrix remodeling in <i>Has3</i> <sup>-/-</sup> and wild-type mice following chronic CCl <sub>4</sub> exposure .....	137
Macrophage accumulation following chronic CCl <sub>4</sub> exposure in wild-type and <i>Has3</i> <sup>-/-</sup> mice .....	143
HA and HMMR levels in <i>Has3</i> <sup>-/-</sup> and wild-type mice following chronic CCl <sub>4</sub> exposure .....	145

Hepatic fibrosis following chronic CCl <sub>4</sub> exposure in wild-type and <i>Hmmr</i> <sup>-/-</sup> mice .	145
Matrix remodeling following chronic CCl <sub>4</sub> exposure in wild-type and <i>Hmmr</i> <sup>-/-</sup> mice .....	150
Macrophage accumulation following chronic CCl <sub>4</sub> exposure in wild-type and <i>Hmmr</i> <sup>-/-</sup> mice .....	152
<b>Discussion .....</b>	<b>152</b>
 <b>Chapter 6: C57BL/6 sub-strains exhibit different responses to acute carbon tetrachloride exposure: Implications for work involving transgenic mice.....</b>	
<b>Abstract.....</b>	<b>158</b>
<b>Introduction.....</b>	<b>160</b>
<b>Results.....</b>	<b>162</b>
Liver injury and steatosis after CCl <sub>4</sub> exposure .....	162
Baseline CYP2E1 protein and activity .....	163
<i>In vitro</i> hepatocyte sensitivity to CCl <sub>4</sub> .....	166
Antioxidant defense following CCl <sub>4</sub> .....	166
Inflammation following CCl <sub>4</sub> exposure: Hepatic neutrophil accumulation .....	168
Inflammation after CCl <sub>4</sub> exposure: Hepatic macrophage accumulation.....	172
Liver regeneration following CCl <sub>4</sub> exposure.....	176
Matrix remodeling following CCl <sub>4</sub> exposure .....	177
Fibrosis in 6N and 6J mice following chronic CCl <sub>4</sub> exposure.....	179
Genotypes of genetically modified mice used in this dissertation.....	183
<b>Discussion .....</b>	<b>183</b>
 <b>Chapter 7: Discussion, Conclusions, and Future Directions .....</b>	
	<b>192</b>

<b>Role for Hyaluronan (HA) and HA mediated motility receptor (HMMR) in acute and chronic liver injury induced by CCl<sub>4</sub> .....</b>	<b>194</b>
Discussion.....	194
Conclusions .....	206
Future directions .....	207
<b>Differences in C57BL/6 sub-strain response to acute and chronic CCl<sub>4</sub>: implications for genetically modified mice .....</b>	<b>214</b>
Discussion.....	215
Conclusions .....	217
Future Directions.....	217
<b>Chapter 8: References .....</b>	<b>221</b>

## List of Figures and Tables

Figure 1-1: Liver disease progression.....	3
Figure 1-2: Acute wound healing progression.....	5
Figure 1-3: Chronic wound healing progression. ....	6
Figure 1-4: Structure of hyaluronan. ....	20
Figure 1-5: The synthetic capacity of the three mammalian hyaluronan synthases (HAS). ....	22
Figure 1-6: The balance of high molecular weight HA (HMW-HA) and low molecular weight HA (LMW-HA) influences HA signaling. ....	27
Figure 1-7 The HA network.....	28
Table 2-1: Primer table.....	53
Table 2-2: Antibody table. ....	55
Figure 3-1: Hepatic <i>Has</i> enzymes, plasma HA levels, and hepatic HA accumulation in wild-type and <i>Has3</i> <sup>-/-</sup> mice. ....	72
Table 3-1: Total and fractionated plasma HA content in wild-type and <i>Has3</i> <sup>-/-</sup> mice after acute CCl <sub>4</sub> exposure. ....	74
Figure 3-2: Liver injury and steatosis in wild-type and <i>Has3</i> <sup>-/-</sup> mice.....	76
Figure 3-3: CYP2E1 content and activity in wild-type and <i>Has3</i> <sup>-/-</sup> mice.....	78
Figure 3-4: Hepatic and plasma chemokine content in wild-type and <i>Has3</i> <sup>-/-</sup> mice. ....	81
Figure 3-5: Hepatic regeneration following acute CCl <sub>4</sub> exposure. ....	84
Figure 3-6: Ki67 positive hepatocytes after acute CCl <sub>4</sub> exposure.....	86
Figure 3-7: Hepatic stellate cell activation markers in wild-type and <i>Has3</i> <sup>-/-</sup> mice after acute CCl <sub>4</sub> exposure. ....	88

Figure 3-8: Hepatic matrix degradation after acute CCl <sub>4</sub> exposure.....	92
Figure 3-9: Hepatic HA receptor expression following acute CCl <sub>4</sub> exposure. ....	95
Figure 4-1: Hepatic <i>Hmmr</i> expression in C57BL/6N mice. ....	107
Figure 4-2: Hepatic injury in wild-type and <i>Hmmr</i> <sup>-/-</sup> mice following acute CCl <sub>4</sub> exposure. .....	109
Figure 4-3: Basal CYP2E1 expression and activity in wild-type and <i>Hmmr</i> <sup>-/-</sup> mice.....	110
Figure 4-4: Inflammation and pro-inflammatory microenvironment following acute CCl <sub>4</sub> exposure. ....	113
Figure 4-5: Hepatic regeneration following acute CCl <sub>4</sub> exposure in wild-type and <i>Hmmr</i> <sup>-/-</sup> mice. ....	116
Figure 4-6: Ki67 positive hepatocytes following acute CCl <sub>4</sub> exposure in wild-type and <i>Hmmr</i> <sup>-/-</sup> mice. ....	118
Figure 4-7: Hepatic stellate cell activation in wild-type and <i>Hmmr</i> <sup>-/-</sup> mice after acute CCl <sub>4</sub> exposure. ....	120
Figure 4-8: Hepatic matrix remodeling transcripts in wild-type and <i>Hmmr</i> <sup>-/-</sup> mice after CCl <sub>4</sub> exposure. ....	122
Figure 4-9: Matrix remodeling following acute CCl <sub>4</sub> in wild-type and <i>Hmmr</i> <sup>-/-</sup> mice. ...	123
Figure 4-10: Plasma and hepatic HA content following acute CCl <sub>4</sub> exposure in wild-type and <i>Hmmr</i> <sup>-/-</sup> mice. ....	124
Figure 5-1: Hepatic stellate cell activation in wild-type and <i>Has3</i> <sup>-/-</sup> mice following chronic CCl <sub>4</sub> . ....	136
Figure 5-2: Hepatic fibrosis in wild-type and <i>Has3</i> <sup>-/-</sup> mice following chronic CCl <sub>4</sub> exposure. ....	138

Figure 5-3: Markers for matrix metabolism in wild-type and <i>Has3</i> <sup>-/-</sup> mice following chronic CCl <sub>4</sub> exposure. ....	140
Figure 5-4: Active matrix remodeling in wild-type and <i>Has3</i> <sup>-/-</sup> mice following chronic CCl <sub>4</sub> . ....	141
Figure 5-5: Macrophage accumulation in wild-type and <i>Has3</i> <sup>-/-</sup> mice following chronic CCl <sub>4</sub> exposure. ....	144
Figure 5-6: HA accumulation and HMMR levels in wild-type and <i>Has3</i> <sup>-/-</sup> mice following chronic CCl <sub>4</sub> exposure. ....	146
Figure 5-7: Hepatic stellate cell activation in wild-type and <i>Hmmr</i> <sup>-/-</sup> mice following chronic CCl <sub>4</sub> exposure. ....	148
Figure 5-8: Hepatic fibrosis in wild-type and <i>Hmmr</i> <sup>-/-</sup> mice following chronic CCl <sub>4</sub> exposure. ....	149
Figure 5-9: Matrix remodeling in wild-type and <i>Hmmr</i> <sup>-/-</sup> mice following chronic CCl <sub>4</sub> exposure. ....	151
Figure 5-10: Macrophage accumulation in wild-type and <i>Hmmr</i> <sup>-/-</sup> mice following chronic CCl <sub>4</sub> exposure. ....	153
Figure 6-1: Hepatic injury following acute CCl <sub>4</sub> exposure. ....	164
Figure 6-2: CYP2E1 expression, protein content, and activity <i>in vitro</i> and <i>in vivo</i> . ....	167
Figure 6-3: Expression of antioxidants after acute CCl <sub>4</sub> exposure. ....	169
Figure 6-4: Hepatic neutrophil accumulation after acute CCl <sub>4</sub> exposure. ....	171
Figure 6-5: Infiltrating cells and macrophages in liver after acute CCl <sub>4</sub> exposure. ....	174
Figure 6-6: Hepatic regeneration following acute CCl <sub>4</sub> exposure. ....	178
Figure 6-7: Matrix remodeling following acute CCl <sub>4</sub> exposure. ....	180

Figure 6-8: Hepatic fibrosis in C57BL/6J and C57BL/6N mice, after chronic CCl <sub>4</sub> exposure. ....	182
Figure 6-9: <i>Nnt</i> genotypes of genetically modified mice used in this dissertation.....	184
Figure 7-1: Summary of findings for acute and chronic CCl <sub>4</sub> exposure in <i>Has3</i> <sup>-/-</sup> and <i>Hmmr</i> <sup>-/-</sup> mice. ....	197
Figure 7-2: Hyaluronan, inflammation, and hepatic stellate cells influence one another. ....	198
Figure 7-3: Current working model describing a role for HA and HMMR in hepatic wound healing.....	208
Figure 7-4: ALT activity 48 hours after CCl <sub>4</sub> exposure in all four strains of mice used in this dissertation. ....	218

### **List of abbreviations**

6N	=	C57BL/6N mice
6J	=	C57BL/6J mice
ALT	=	alanine amino transferase
APAP	=	acetaminophen
$\alpha$ SMA	=	$\alpha$ smooth muscle actin
BSA	=	bovine serum albumin
BW	=	body weight
C3a	=	complement 3a fragment
C5a	=	complement 5a fragment
CAE	=	chloracetate esterase
CCl <sub>4</sub>	=	carbon tetrachloride
<i>Ccnd1</i>	=	Cyclin D1
CD44	=	Cluster of differentiation 44
CDC	=	Center for Disease Control
CTGF	=	Connective tissue growth factor
CYP	=	Cytochrome P450
Da	=	Dalton
DAMP	=	Danger Associated Molecular Patterns
DAPI	=	4,6-Diamidino-2-phenylindole
ECM	=	Extracellular matrix
EGF	=	Epidermal growth factor
FGF	=	Fibroblast growth factor

GCLC	=	Glutamate-cysteine ligase catalytic subunit
GSH	=	Glutathione
GSSG	=	Glutathione disulfide
H&E	=	Hematoxylin and eosin
HA	=	Hyaluronan
HA-CMC	=	Hyaluronan carboxycellose membrane
HABP	=	Hyaluronan binding protein
HARE	=	Hyaluronan receptor for endocytosis
HAS1	=	Hyaluronan synthase 1
HAS2	=	Hyaluronan synthase 2
HAS3	=	Hyaluronan synthase 3
HCC	=	Hepatocellular carcinoma
HGF	=	Hepatocyte growth factor
HMGB1	=	High mobility group box 1
HMMR	=	Hyaluronan mediated motility receptor
HMW	=	High molecular weight
HRP	=	Horseradish peroxidase
HSC	=	Hepatic stellate cell
HSP47	=	Heat shock protein 47
HYAL	=	Hyaluronidase
IL	=	Interleukin
ILK	=	Integrin linked kinase
ISZ	=	<i>in situ</i> zymography

JNK2	=	c-Jun N-terminal kinase
kDa	=	kilo Dalton
LDH	=	Lactate dehydrogenase
LMW	=	Low molecular weight
LOX	=	Lysyl oxidase
LOXL2	=	Lysyl oxidase like 2
LPS	=	Lipopolysaccharide
LSEC	=	liver sinusoidal endothelial cells
miRNA	=	microRNA
MMP	=	Matrix metalloproteinase
mtDNA	=	mitochondrial DNA
NADP <sup>+</sup> /NADPH	=	Nicotinamide adenine dinucleotide phosphate
NNT	=	Nicotinamide nucleotide transhydrogenase
NPC	=	Non parenchymal cells
NQO1	=	NAD(P)H quinone dehydrogenase 1
OCT	=	Optimal cutting temperature medium
PCNA	=	Proliferating cell nuclear antigen
PCR	=	polymerase chain reaction
PDGF	=	Platelet derived growth factor
PPAR	=	Peroxisome proliferator-activated receptor
qPCR	=	quantitative polymerase chain reaction
ROS	=	Reactive oxygen species
SNP	=	Single nucleotide polymorphisms

TGF $\beta$	=	Transforming growth factor $\beta$
TIMP	=	Tissue inhibitor of matrix metalloproteinase
TLR	=	Toll like receptor
TNF $\alpha$	=	Tumor necrosis factor $\alpha$
TSA	=	Tyramide signal amplification

## Chapter 1: Introduction

*Portions of this chapter are adapted from 1) McCracken, JM et al. "Differential effects of hyaluronan synthase 3 deficiency after acute vs chronic liver injury in mice" Fibrogenesis and Tissue Repair 2016; Licensed under Creative Commons Attribution 4.0 International License and 2) McCracken, JM et al. "C57BL/6 substrains exhibit different responses to acute carbon tetrachloride exposure: Implications for work involving transgenic mice" Gene Expression: The Journal of Basic Liver Research. 17#3, doi: 10.3727/105221617X695050 with permission Cognizant, LLC; [www.cognizantcommunications.com](http://www.cognizantcommunications.com) copyright 2017 in press.*

## **Liver disease**

Liver disease describes a broad range of pathological conditions caused by a number of etiologic agents, including drugs, alcohol or other toxins, viruses, obesity, cholestasis, genetic disorders, and ischemia/reperfusion (Bataller and Brenner, 2005; Abu-Wasel *et al.*, 2013; Leise *et al.*, 2014; Roberts *et al.*, 2014; Thannickal *et al.*, 2014; Woolbright and Jaeschke, 2015). Regardless of the causative agent, patients diagnosed with liver disease follow a similar progression (outlined in Figure 1-1). Patients are initially diagnosed with steatosis, or fatty liver disease, characterized by an excess accumulation of triglycerides in hepatocytes (Charlton, 2004; Postic and Girard, 2008). It is also possible for these patients to develop an acute inflammatory response called steatohepatitis (Yilmaz, 2012; Rosso *et al.*, 2014). A sub-set of patients progress from steatosis to fibrosis, which is characterized by an excess accumulation of extracellular matrix (ECM) in the liver. This ECM can affect the normal structure and function of the liver, however until fibrosis becomes advanced the liver is able to heal itself by degrading this ECM (Bataller and Brenner, 2005; Pellicoro *et al.*, 2014). Some patients progress further to advanced fibrosis and eventually develop cirrhosis, which can lead to hepatocellular carcinoma (HCC) (Pellicoro *et al.*, 2014; Tsochatzis *et al.*, 2014; Zhou *et al.*, 2014). In fact, 80-90% of HCC cases have cirrhosis as an underlying risk factor (Simonetti *et al.*, 1991; Llovet *et al.*, 2003). Once a patient develops advanced cirrhosis or HCC, liver disease is no longer reversible and a liver transplant is the only treatment option available (Rai, 2013). This presents a problem not only because a liver transplant is invasive and costly, but there are a limited number of healthy livers available for

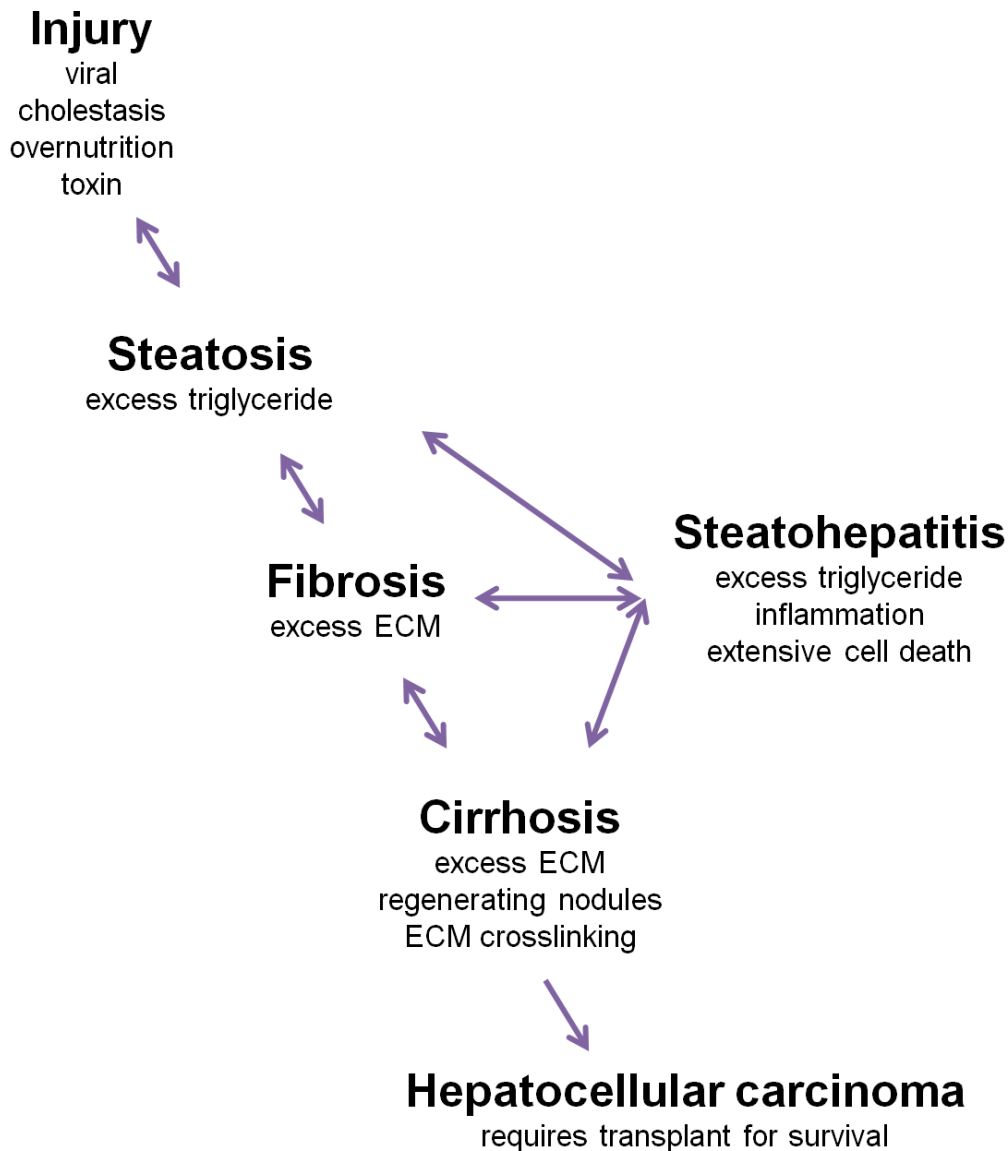


**Figure 1-1: Liver disease progression.**

Following initial injury, a patient is diagnosed with steatosis or excess accumulation of triglyceride. With further injury, some patients progress to fibrosis, characterized by excess extracellular matrix (ECM), and even further to cirrhosis, where the excess ECM forms nodules of regeneration hepatocytes. The ECM also becomes crosslinked in cirrhosis making regression more difficult, which is possible even in early cirrhosis. At any point in this continuum, steatohepatitis can occur. This is a result of extensive cell death and inflammation. Hepatocellular carcinoma can occur in patients who progress past cirrhosis, and cirrhosis underlies 80-90% of HCC cases in the clinics. If advanced cirrhosis or HCC develops, a liver transplant is required for survival.

transplant, partially due to the obesity epidemic (Bilbao *et al.*, 2003; Saidi *et al.*, 2012; Parikh *et al.*, 2015).

According to the Center for Disease Control (CDC), chronic liver disease and cirrhosis was the 12<sup>th</sup> leading cause of death in the United States in 2014. The total number of deaths increased significantly from 2013 to 2014, following an increasing trend over the past 15 years (Kochanek *et al.*, 2016). For some patients, simply removing the etiologic agent, whether that be drugs, alcohol, over nutrition, or reducing the viral load, is enough to allow the liver to heal itself, however, the patients that do progress to advanced liver disease and require a transplant are left without other therapeutic options (Pellicoro *et al.*, 2014; Tsochatzis *et al.*, 2014). There is a need for basic science and translational research to shed light on new mechanisms associated with liver disease pathobiology. It was the goal of my dissertation research to advance our understanding of liver disease by focusing specifically on identifying novel mechanisms of wound repair after acute and chronic liver injury. Identifying ways to halt the progression of liver disease and/or accelerate its reversal would reduce the need for a transplant to cure advanced liver disease.

### **Hepatic wound healing**

Hepatic wound healing is analogous to skin wound healing and includes periods of inflammation, regeneration, and matrix remodeling (Pellicoro *et al.*, 2014; Balaji *et al.*, 2015). Each of these stages in wound healing is discussed in detail below (and outlined in Figure 1-2); with specific focus on hepatic wound healing following toxin-induced liver injury. Liver fibrosis is associated with chronic injury, chronic inflammation, and

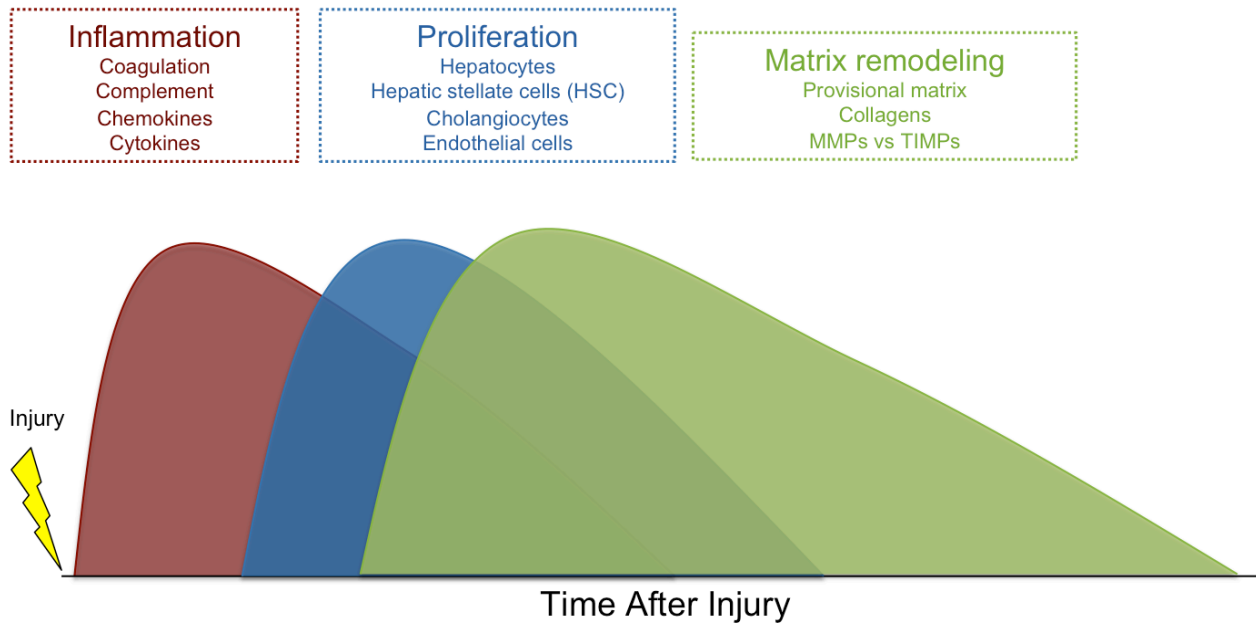


**Figure 1-2: Acute wound healing progression.**

Following acute injury, the liver goes through the wound healing process. Initially coagulation and complement factors are activated and inflammatory chemokines and cytokines are released locally. These factors recruit circulating monocytes and prime the healthy hepatocytes to enter the cell cycle. This is followed by the regeneration and replacement of hepatocytes and the remaining hepatic cells (hepatic stellate cells, cholangiocytes, and endothelial cells). During this regenerative phase, activated hepatic stellate cells are synthesizing a provisional matrix, including laminin and fibronectin, and collagen proteins. These matrices then must be remodeled by matrix metalloproteinases (MMPs) and their inhibitors (TIMPs) in order to restore normal liver structure and function.

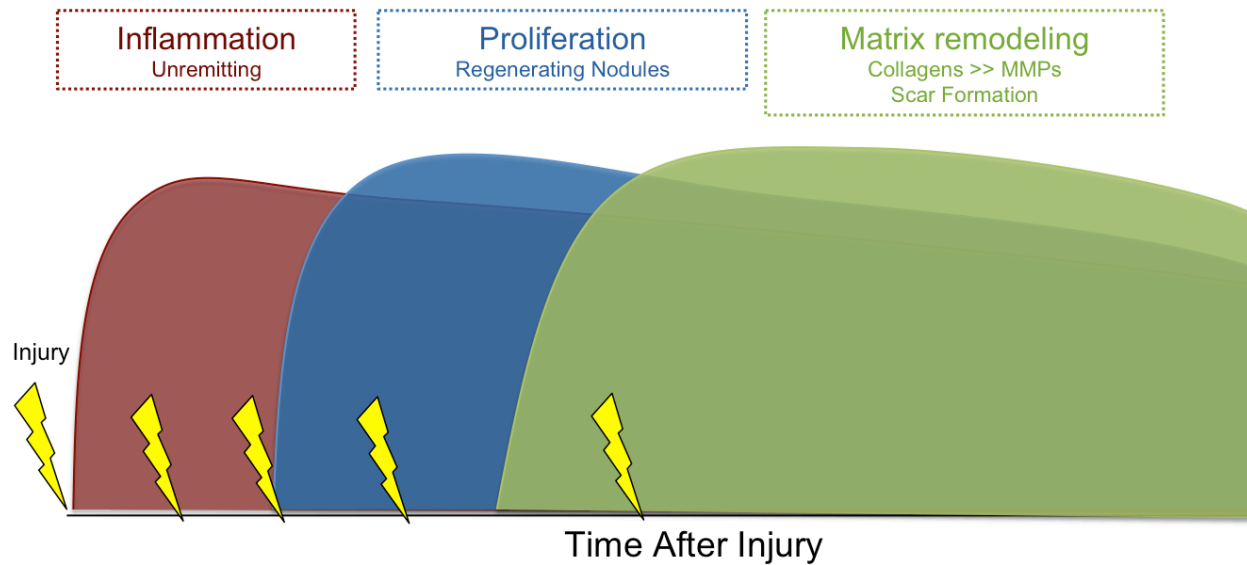


**Figure 1-3: Chronic wound healing progression.**

Following chronic injury, inflammation is induced and remains elevated becoming chronic and unremitting. Similarly, hepatocytes continue regenerating eventually being surrounded by ECM and forming nodules that can later become cancerous. Matrix synthesis by activated hepatic stellate cells outweighs matrix degradation by matrix metalloproteinases (MMPs) and a scar forms that can eventually disrupt normal hepatic structure and function leading to the need for a liver transplant.

incomplete wound repair (outlines in Figure 1-3). The result of the incomplete wound repair is an accumulation of ECM that disrupts the normal structure and function of the liver (Guo and Friedman, 2007; Pellicoro *et al.*, 2014).

## **Initial injury**

Acute liver injury can occur in a number of ways, including viral hepatitis, ischemia/reperfusion, cholestasis, or toxins (Penny, 2013; Leise *et al.*, 2014; Woolbright and Jaeschke, 2015). A portion of liver disease in developed countries, like the United States, is attributed to toxins, specifically acetaminophen (APAP) toxicity due to overdose, and alcohol abuse (Penny, 2013; Jaeschke, 2015). Both APAP toxicity and alcohol abuse cause centrilobular injury, meaning the hepatocytes around the central vein are affected by the toxin (Gujral *et al.*, 2002; Szabo and Mandrekar, 2010; Penny, 2013; Wang *et al.*, 2016a). This is partly due to the increased cytochrome P40 (CYP) enzymes located around the central veins; specifically CYP2E1, one of many enzymes involved in both APAP and ethanol metabolism (Lee *et al.*, 1996; Lu *et al.*, 2008; Abdelmegeed *et al.*, 2010). The reactive/biologically active metabolites produced attack hepatocytes and cause cell death (Gujral *et al.*, 2002; Szabo and Mandrekar, 2010).

Although the focus of the remaining dissertation is on toxin induced liver injury, there are several other ways the liver can be injured. During ischemia/reperfusion, there are periods of hypoxia and subsequently a return of oxygenated blood (Kupiec-Weglinski and Busuttil, 2005; Li *et al.*, 2015). This leads to a shortage of energy sources, production of reactive oxygen species (ROS), and a build-up of toxic metabolites, all of which can cause hepatic cell death (Jaeschke, 2003; Kupiec-

Weglinski and Busuttil, 2005; Li *et al.*, 2015). Cholestasis, whether intrahepatic or extrahepatic, leads to a build-up of toxic bile acids in hepatocytes and results in cell death (Hofmann, 1999; Wagner *et al.*, 2009; Woolbright *et al.*, 2015). In the case of ethanol, the metabolites that cause the liver damage also cause gut leakiness, which leads to increased circulating lipopolysaccharide (LPS) and subsequent LPS-mediated hepatic inflammation (Schaffert, 2009). In all cases, the extent of cellular injury dictates the wound healing process, including inflammation, regeneration, and matrix remodeling.

## **Inflammation**

Necrotic hepatocytes release danger associated molecular patterns (DAMPs) including HMGB1 and mtDNA (Rock and Kono, 2008; McDonald and Kubes, 2016). These DAMPs, along with chemokines like CXCL2, promote neutrophil recruitment and infiltration into the liver, which occurs very early after initial injury (McDonald *et al.*, 2010; Moles *et al.*, 2014; McDonald and Kubes, 2016). These neutrophils migrate to the area of necrosis using a chemoattractant gradient produced by the necrotic tissue (Foxman *et al.*, 1997; Heit *et al.*, 2002). Neutrophils play a role in the removal of cellular debris, but they can also exacerbate hepatic tissue injury (Ramaiah and Jaeschke, 2007; Huang *et al.*, 2015).

DAMPs and LPS activate Kupffer cells, resident liver macrophages, leading to the synthesis of pro-inflammatory cytokines like tumor necrosis factor-alpha (TNF $\alpha$ ) and interleukin 6 (IL6) as well as ROS (Marangoni *et al.*, 2006; Rock and Kono, 2008; Martin-Murphy *et al.*, 2010; Aziz-Seible *et al.*, 2011; Dixon *et al.*, 2013; Woolbright and

Jaeschke, 2015). The dying hepatocytes and activated hepatic stellate cells (HSC) also release pro-inflammatory chemokines (Dambach *et al.*, 2002; Chang *et al.*, 2015b). These cytokines and chemokines, of which CCL2 (also known as monocyte chemoattractant protein 1 (MCP1)) is particularly important, recruit bone marrow derived monocytes to the liver where they differentiate into macrophages and continue to promote the inflammatory microenvironment (Dambach *et al.*, 2002; Baeck *et al.*, 2012). Similar to neutrophils, recruited macrophages can both exacerbate tissue injury and aid in tissue repair (Duffield *et al.*, 2005; Possamai, 2010). For example, the pro-inflammatory microenvironment created by recruited macrophages can lead to increased tissue damage via ROS production (Marangoni *et al.*, 2006). However, recruited macrophages aid in repair during the later stages of wound healing, by removing necrotic debris and making room for the regenerating hepatic cells to expand (Duffield *et al.*, 2005; Mochizuki *et al.*, 2014). The recruited macrophages are also a source of matrix metalloproteinases (MMPs), which are important in matrix degradation as discussed below (Fallowfield *et al.*, 2007a).

## **Regeneration**

The liver performs many vital functions in the body including filtering and detoxifying the blood, absorbing nutrients delivered to the liver from the intestinal tract, producing bile acids to aid in digestion, and by producing complement proteins important for innate immunity, and proteins involved in coagulation (Wagner *et al.*, 2009; Pluta *et al.*, 2010; Dixon *et al.*, 2013). Because these functions are required for organism survival, the liver acquired the remarkable ability to regenerate during

evolution (Michalopoulos and DeFrances, 1997; Cienfuegos *et al.*, 2014; Mao *et al.*, 2014). Historically, this is likely because of the high chances that mammals, including our ancestors, ingested toxins that damaged the liver and required regeneration for organism survival; regeneration-competent survivors then passed their genes on to the next generation who then had a critical survival advantage over those less able to withstand toxin-mediated liver injury (Michalopoulos and DeFrances, 1997; Mao *et al.*, 2014). This same regenerative process still occurs following any liver injury sustained in mammals today (Michalopoulos and DeFrances, 1997; Mao *et al.*, 2014).

Uninjured hepatocytes are primed by DAMPs and pro-inflammatory mediators, including TNF $\alpha$  and complement factors C3a and C5a, to enter the cell cycle, a process that occurs soon after hepatic injury (Grisham, 1962; Webber *et al.*, 1998; Strey *et al.*, 2003; Rock and Kono, 2008; Bohm *et al.*, 2010; Cienfuegos *et al.*, 2014). Growth factors, including hepatocyte growth factor (HGF) and epidermal growth factor (EGF), promote progression through the cell cycle (Huh *et al.*, 2004; Natarajan *et al.*, 2007; Cienfuegos *et al.*, 2014). Once the liver regains lost mass and resumes normal function, regeneration is halted (Michalopoulos and DeFrances, 1997; Mao *et al.*, 2014). While many mechanisms for initiation of regeneration are known, the mechanisms for termination of regeneration are more controversial (Rychtrmoc *et al.*, 2012; Mao *et al.*, 2014). Transforming growth factor  $\beta$  (TGF $\beta$ ), chromatin remodeling proteins, peroxisome proliferator-activated receptor (PPAR) signaling, miRNAs, integrin linked kinase (ILK) and the restoration of normal function may each or all contribute to halting liver regeneration (Apte *et al.*, 2009; Yuan *et al.*, 2011; Rychtrmoc *et al.*, 2012; Jin *et al.*, 2015).

Hepatocytes are not the only cells damaged after toxin-mediated liver injury and a patient requires all cell types, including Kupffer cells, HSC, cholangiocytes and liver sinusoidal endothelial cells (LSECs), to regenerate or be replaced to regain normal liver function (Cienfuegos *et al.*, 2014). After initial hepatic injury, Kupffer cells within the necrotic area can also sustain damage and die, and therefore must be replaced, but there is some controversy on whether the remaining Kupffer cells are able to proliferate or if they must be replaced with bone marrow derived macrophages that differentiate into Kupffer cells (Yamamoto *et al.*, 1996; Scott *et al.*, 2016). HSC store the majority of the body's vitamin A in lipid droplets, and activate (discussed below) or die following liver injury (Friedman, 2008a). The remaining HSC proliferate to restore hepatic function, primarily in response to fibroblast growth factors (FGFs) (Schumacher and Guo, 2016). Similar to the above cell types, cholangiocytes, which line the bile ducts, are damaged during liver injury and also must be replaced (Michalopoulos and DeFrances, 1997). In some instances, it is possible for healthy hepatocytes to transdifferentiate into cholangiocytes, aiding in biliary tree repair (Limaye *et al.*, 2010). LSECs, are normally fenestrated to allow nutrients to pass from the blood to the space of Disse and reach the hepatocytes as well as allow proteins produced in the liver to enter systemic circulation (Herrnberger *et al.*, 2014; Poisson *et al.*, 2017). Following injury, LSECs fuse and lose their fenestration (Poisson *et al.*, 2017). LSEC within the necrotic area will die and must be replaced with proliferating LSEC in the healthy tissue or sinusoidal progenitor cells (DeLeve, 2013; Hu *et al.*, 2014; Poisson *et al.*, 2017). The hepatic regenerative process is tightly controlled with hepatocytes regenerating shortly

after injury, followed by Kupffer cells, HSC, and cholangiocytes, and lastly LSEC (Grisham, 1962; Taub, 2004; Cienfuegos *et al.*, 2014).

### **Matrix remodeling**

Matrix remodeling happens throughout the wound healing process and includes both matrix deposition and matrix metabolism. Following injury, HSC lose their vitamin A depot and activate in response to a number of cytokines and growth factors including, platelet derived growth factor (PDGF) released by inflammatory cells and TGF $\beta$  acting in an autocrine fashion (Friedman, 2000; Friedman, 2008a; Liu *et al.*, 2009; Wells and Schwabe, 2015). The engulfment of dying hepatocytes and changes in the ECM also promote HSC activation (Friedman, 2000; Dechene *et al.*, 2010). Activated HSC express smooth muscle actin ( $\alpha$ SMA) and synthesize ECM proteins like type 1 collagen (Friedman, 2000; Perepelyuk *et al.*, 2013). The liver also contains a population of portal fibroblasts surrounding the biliary tree that can also synthesize ECM components, particularly around the portal tract. However, HSC are likely the main contributor to excess ECM deposition during liver wound healing and fibrosis, even in cholestasis-induced liver fibrosis (Mederacke *et al.*, 2013; Perepelyuk *et al.*, 2013; Wells and Schwabe, 2015).

In order to prevent ECM accumulation, the activated HSC must quit synthesizing ECM components. There is some controversy over how this process is stopped with evidence of HSC returning to a quiescent state, undergoing apoptosis, or becoming senescent all being reported (Issa *et al.*, 2001; Oakley *et al.*, 2005; El Taghdouini *et al.*, 2015; Jin *et al.*, 2016). Matrix degradation occurs throughout the wound healing process

and once HSC stop making ECM, the provisional matrix, including collagen, laminin, and fibronectin, must be removed to restore normal liver architecture and vasculature (Jonker *et al.*, 1992; Alwayn *et al.*, 2008; Duarte *et al.*, 2015; Poole and Arteel, 2016). This is done by the increased production, release, and activation of MMPs (Hemmann *et al.*, 2007; Alwayn *et al.*, 2008; Duarte *et al.*, 2015). MMPs are primarily produced by the macrophages that infiltrated the liver in response to liver injury (Duffield *et al.*, 2005; Fallowfield *et al.*, 2007a). Activated HSC are the major source of tissue inhibitor of MMPs (TIMPs), which inhibit MMP activity and prevent overzealous matrix degradation (Hemmann *et al.*, 2007; Osawa *et al.*, 2013). Once all hepatic cells have regenerated or been repopulated and the matrix has been properly remodeled, the liver has healed completely and hepatic function is successfully restored.

### **Chronic Liver Injury and Fibrosis**

If a patient sustains chronic liver injury through chronic hepatitis, chronic alcohol exposure, or obesity, the above outlined wound healing process continues and becomes deregulated (Pellicoro *et al.*, 2014). Continuing cycles of hepatocyte cell death result in chronic inflammation, a hallmark of chronic liver disease (Czaja, 2014; Seki and Schwabe, 2015). This sustained inflammation results in chronically activated HSC (Friedman, 2000; Imamura *et al.*, 2005; Czaja, 2014). In fact, persistently high levels of TNF $\alpha$  promote HSC survival (Osawa *et al.*, 2013; Yang and Seki, 2015). The increased stiffness of the ECM also promotes HSC activation resulting in unrelenting pro-fibrotic signals, which maintain and exacerbate HSC activation (Dechene *et al.*, 2010). Loss of LSEC fenestration results in capillarization of the sinusoids, which also promotes HSC

activation (DeLeve, 2015; Poisson *et al.*, 2017). These hyper-activated HSC continue to synthesize collagen and other ECM proteins overwhelming macrophage MMP production and MMP-mediated ECM degradation (Gressner and Bachem, 1990; Bataller and Brenner, 2005; Hemmann *et al.*, 2007; Friedman, 2008b; Perepelyuk *et al.*, 2013). This imbalance results in a build-up of ECM, which then disrupts the normal architecture of the liver (Friedman, 2008b; Pellicoro *et al.*, 2014). The excess collagen that accumulates is cross-linked by lysyl oxidase (LOX) enzymes, particularly LOXL2, which promotes collagen stabilization and suppresses the reversal of fibrosis (Ikenaga *et al.*, 2017).

As the progression of liver disease continues, ECM accumulates around nodules of regenerating hepatocytes (Gogel *et al.*, 2000). These nodules disrupt liver function and can lead to decreased blood flow through the liver and portal hypertension, which is a clinical symptom of cirrhosis (Tsochatzis *et al.*, 2014; Garbuzenko, 2015). Cirrhosis is a major risk factor for HCC, with approximately 80-90% of HCC cases occurring in patients with cirrhosis (Gogel *et al.*, 2000; Llovet *et al.*, 2003). For some patients, simply removing the etiologic agent can halt progression of fibrosis to cirrhosis or even reverse fibrosis, unfortunately this is not the case for all patients (Bataller and Brenner, 2005). Parallel to ECM remodeling after acute liver injury, fibrosis can be resolved by increasing MMP activity through macrophage recruitment and by halting collagen synthesis by HSC (Issa *et al.*, 2001; Fallowfield *et al.*, 2007b; Adhyatmika *et al.*, 2015; El Taghdouini *et al.*, 2015). Despite numerous ongoing clinical trials for novel anti-fibrotic drugs based on promising preclinical observations, no treatments have been approved by the FDA (Cohen-Naftaly and Friedman, 2011; Mehal and To, 2016).

Therefore, although fibrosis and early cirrhosis are reversible, once patients progress to advanced cirrhosis or HCC, the only treatment option remains a liver transplant.

## **Carbon tetrachloride (CCl<sub>4</sub>) as a model of liver disease**

### **History of CCl<sub>4</sub>**

Rodent models, including mouse models, have long been used in laboratories to understand the mechanisms driving disease pathogenesis and progression and to test treatment options for those diseases. While dosing mice with APAP and ethanol can be used to study acute toxicity, there are many difficulties in studying the chronic liver injury that patients experience (Schaffert, 2009; McGill *et al.*, 2012). We therefore chose to utilize the hepatotoxicant carbon tetrachloride (CCl<sub>4</sub>), which can be used to induce both acute liver injury and, when administered chronically, liver fibrosis (Weber *et al.*, 2003; Constandinou *et al.*, 2005). In the early 20<sup>th</sup> century, CCl<sub>4</sub> was used as a fire retardant (it was put in glass balls to be thrown at the base of fires), and later it was used as solvent for dry cleaners and machinists (Joron *et al.*, 1957; Faroon *et al.*, 2003). Eventually it was learned that CCl<sub>4</sub> was toxic and could cause liver, lung, and kidney damage and its use as a fire retardant and solvent was largely discontinued (Joron *et al.*, 1957; Faroon *et al.*, 2003).

### **Modeling Acute Liver Injury**

A single intraperitoneal injection of CCl<sub>4</sub> causes significant liver damage in a mouse and can therefore be used as a model of acute liver injury. CCl<sub>4</sub> is bioactivated

by CYP2E1, predominantly in zone 3 hepatocytes, to the trichloromethyl radical (McCay *et al.*, 1984; Wong *et al.*, 1998; Weber *et al.*, 2003). This radical is metabolized further to more reactive metabolites that then attack the lipids in hepatocyte membranes causing lipid peroxidation (McCay *et al.*, 1984; Weber *et al.*, 2003; Knockaert *et al.*, 2012). As the membranes become disrupted and the intrinsic protective response becomes overwhelmed, the cells undergo necrotic cell death (Wang *et al.*, 2013; Xie *et al.*, 2015). Similar to ethanol and APAP, CCl<sub>4</sub> causes centrilobular necrosis, and the liver undergoes the above outlined wound healing process (Taniguchi *et al.*, 2004; Xie *et al.*, 2015). While it is a different mechanism of toxicity, studying the wound healing process following CCl<sub>4</sub> exposure can provide insight into not only toxin induced liver injury, but also other clinically relevant acute liver diseases such as viral hepatitis infections.

### **Modeling Chronic Liver Injury**

While modeling acute liver injury with APAP and ethanol exposure closely mimics the human liver injury seen in the clinic, modeling chronic liver disease has proven more difficult. Exposing mice to CCl<sub>4</sub> at least twice a week for an extended period of time can induce fibrosis, similar to that seen in the clinic (Constandinou *et al.*, 2005). Depending on the exposure time, it is possible to induce fibrosis, early cirrhosis, or advanced cirrhosis (Constandinou *et al.*, 2005; Zhang *et al.*, 2011). This is unique to CCl<sub>4</sub>, as chronic ethanol exposure will not lead to fibrosis in mouse models (Bertola *et al.*, 2013; Crespo Yanguas *et al.*, 2016). Once fibrosis or cirrhosis is established in the mouse, it is then possible to study the resolution of the fibrosis over time after cessation of further

toxin-mediated injury, which can help provide insight into mechanisms responsible for fibrosis regression in patients (Jiao *et al.*, 2012; Ramachandran *et al.*, 2012).

### **Sub-Strain Differences in Mouse Models of Liver Injury**

The mouse is a valuable and universal tool in laboratories all over the world, and different strains of mice exhibit genotypic and phenotypic differences, which can greatly impact experimental outcomes (Reynolds, 2011; Walkin *et al.*, 2013). Recently, mice of the same strain but different sub-strains were evaluated for possible differences in several experimental models of human disease. Sub-strains are defined as branches of an inbred strain that are either known or suspected to be genetically different from the original inbred strain (Mekada *et al.*, 2009). The commonly used C57BL/6 strain has two distinct sub-strains that were established after a breeding pair moved from The Jackson Laboratory (Jackson) to the National Institute of Health (NIH) in the 1950s (Mekada *et al.*, 2009; Zurita *et al.*, 2011). These sub-strains are called C57BL/6J (6J, Jackson) and C57BL/6N (6N, NIH). After separation, the 6J mice developed a spontaneous mutation in the nicotinamide nucleotide transhydrogenase (*Nnt*) gene (Huang *et al.*, 2006; Ronchi *et al.*, 2013). This mutation results in a deletion of exons 7-11 of the *Nnt* gene and leads to a non-functional protein (Huang *et al.*, 2006). The NNT enzyme is partially responsible for antioxidant defense within the mitochondria. It is located on the inner mitochondrial membrane and converts NADP<sup>+</sup> to NADPH using the proton gradient and NADH (Hoek and Rydstrom, 1988; Ronchi *et al.*, 2013). The NADPH produced acts as a cofactor for glutathione reductase to convert oxidized glutathione (GSSG) to reduced glutathione (GSH) (Vogel *et al.*, 1999; Dalton *et al.*, 2004).

Possible differences in hepatotoxicity came to light when two separate groups reported conflicting results in JNK2 deficient mice following acute APAP toxicity (Gunawan *et al.*, 2006; Bourdi *et al.*, 2008). While Gunawan, *et al.* reported *Jnk2*<sup>-/-</sup> mice were partially protected following APAP exposure when compared to wild-type controls, Bourdi, *et al.* reported *Jnk2*<sup>-/-</sup> mice had exacerbated injury following the same dose of APAP (Gunawan *et al.*, 2006; Bourdi *et al.*, 2008). The different outcomes reported in these two studies were explained by the fact that each group used a different C57BL/6 sub-strain control mouse to which the *Jnk2*<sup>-/-</sup> mice were being compared. It was later discovered 6N mice are more susceptible to liver injury compared to 6J mice at the same APAP dose (Bourdi *et al.*, 2011). This was not due to differences in CYP2E1 activity or glutathione depletion, an important antioxidant defense system in APAP toxicity (Duan *et al.*, 2016). Due to the similarities in toxicity between APAP and CCl<sub>4</sub>, it is also important to identify any potential differences in CCl<sub>4</sub>-mediated hepatotoxicity and in the wound healing response between B6 sub-strains. Any potential differences would then become important to consider when using wild-type mice as controls for genetically modified mice. It is imperative to ensure wild-type and transgenic mice are on the same background sub-strain to allow for appropriate data interpretation as was done for this dissertation.

## **Hyaluronan**

### **History**

In 1934, Karl Meyer and John Palmer isolated a high molecular weight substance from the vitreous humor of cow eyes (Meyer and Palmer, 1934). They described the molecule as containing uronic acid, an amino sugar, and possibly a pentose and named it hyaluronic acid, later called hyaluronan (HA), from hyaloid (vitreous) and uronic acid (Meyer and Palmer, 1934; Balazs *et al.*, 1986). In the 1950's, Meyer reported the chemical structure as a repeating disaccharide of glucuronic acid and n-acetylglucosamine (Figure 1.3) (Meyer, 1958). The monosaccharides are linked together through repeating  $\beta$ -1,4 and  $\beta$ -1,3 glycosidic bonds (Figure 1-4) (Necas *et al.*, 2008; Jiang *et al.*, 2011). It is now known that HA is a ubiquitous, highly anionic, glycosaminoglycan found in high levels in the eye, lung, skin, and joints (Fraser *et al.*, 1997; Manasa *et al.*, 2012; Anderegg *et al.*, 2014; Temple-Wong *et al.*, 2016).

## **HA Synthesis**

Endogenous HA is a polydisperse high molecular weight (HMW) molecule and can reach up to  $10^7$  Da (Manasa *et al.*, 2012). Unlike other glycosaminoglycans that are synthesized in the Golgi apparatus and exported to the extracellular space, HA is synthesized and extruded simultaneously at the plasma membrane forming a glycocalyx around cells (Necas *et al.*, 2008). HA is also incorporated into the ECM and performs such functions as space filling, lubrication, and stabilization (Laurent and Fraser, 1992; Anderegg *et al.*, 2014; Temple-Wong *et al.*, 2016). Additionally, HA has no core protein, and because of its unique structure, and anionic properties, HA can hold 1000 times its weight in water (Laurent and Fraser, 1992; Wang *et al.*, 2011; Manasa *et al.*, 2012).

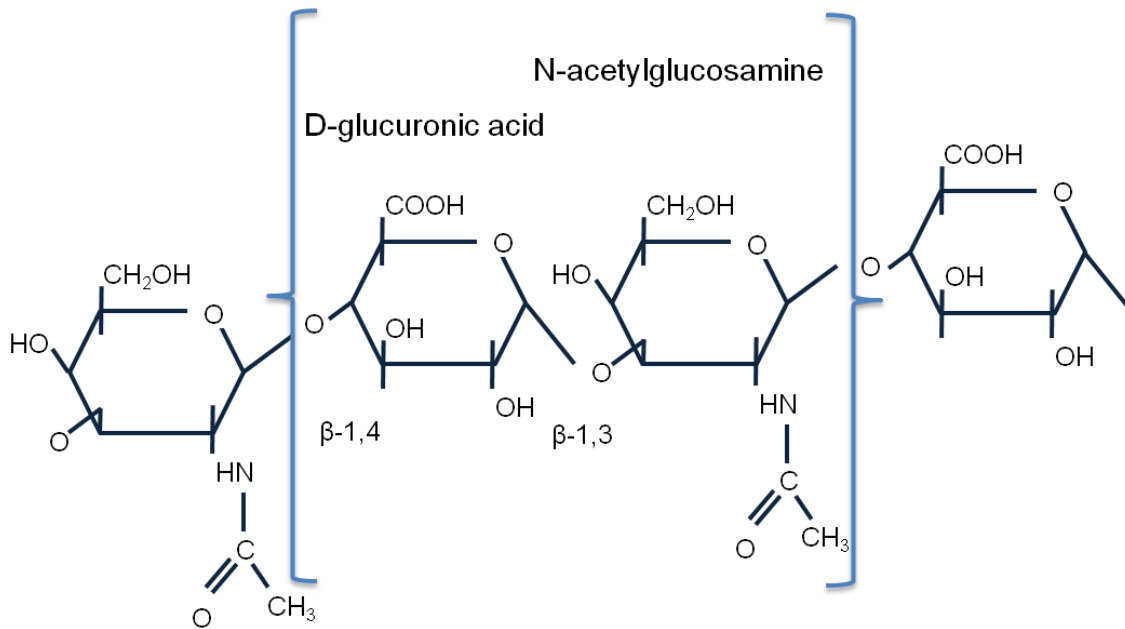


**Figure 1-4: Structure of hyaluronan.**

The structure of hyaluronic acid is a repeating disaccharide consisting of D-glucuronic acid and N-acetylglucosamine. The monosaccharides are linked through repeated  $\beta$ -1,4 and  $\beta$ -1,3 glycosidic bonds.

Three enzymes are responsible for making mammalian HA, hyaluronan synthase (HAS) 1, 2, and 3 (Spicer and McDonald, 1998). Each of the three HAS enzymes is located on different chromosomes suggesting an early gene duplication and divergence (Spicer and McDonald, 1998; Jiang et al., 2011). HAS enzymes differ in the size and amount of HA produced and are described in detail below (and in Figure 1-5) (Spicer and McDonald, 1998; Itano et al., 1999). The HAS enzymes are usually co-expressed, and their expression patterns depend on cell type, developmental stage, and the cellular response to injury (Spicer and McDonald, 1998; Jacobson et al., 2000; Jiang et al., 2011). The expression pattern and activity can also depend on hetero- and homo-dimerization of the HAS enzymes (Bart et al., 2015). The primary postnatal HA-synthesizing cell types are fibroblasts and endothelial cells, and in the liver, activated HSC are the primary source of HA (Spicer and McDonald, 1998; Jiang et al., 2011; Xu et al., 2013; Neuman et al., 2016).

### *HAS1*

HAS1 is the least active HA synthesis enzyme, shown by the smallest pericellular coat/glycocalyx visualized using a particle exclusion assay and Cos-1 cells transfected with mouse *Has1* (Spicer and McDonald, 1998; Itano *et al.*, 1999). Cos-1 cells were used for this study because they are known to have little endogenous HAS activity (Spicer and McDonald, 1998; Itano *et al.*, 1999). Using human *HAS* genes for transfection, HAS1 requires higher sugar substrate concentration, as found in hyperglycemic conditions, to synthesize the same amount of HA as HAS2 and HAS3 in euglycemic conditions (Rilla *et al.*, 2013). Therefore, HAS1 may play a role in diabetes

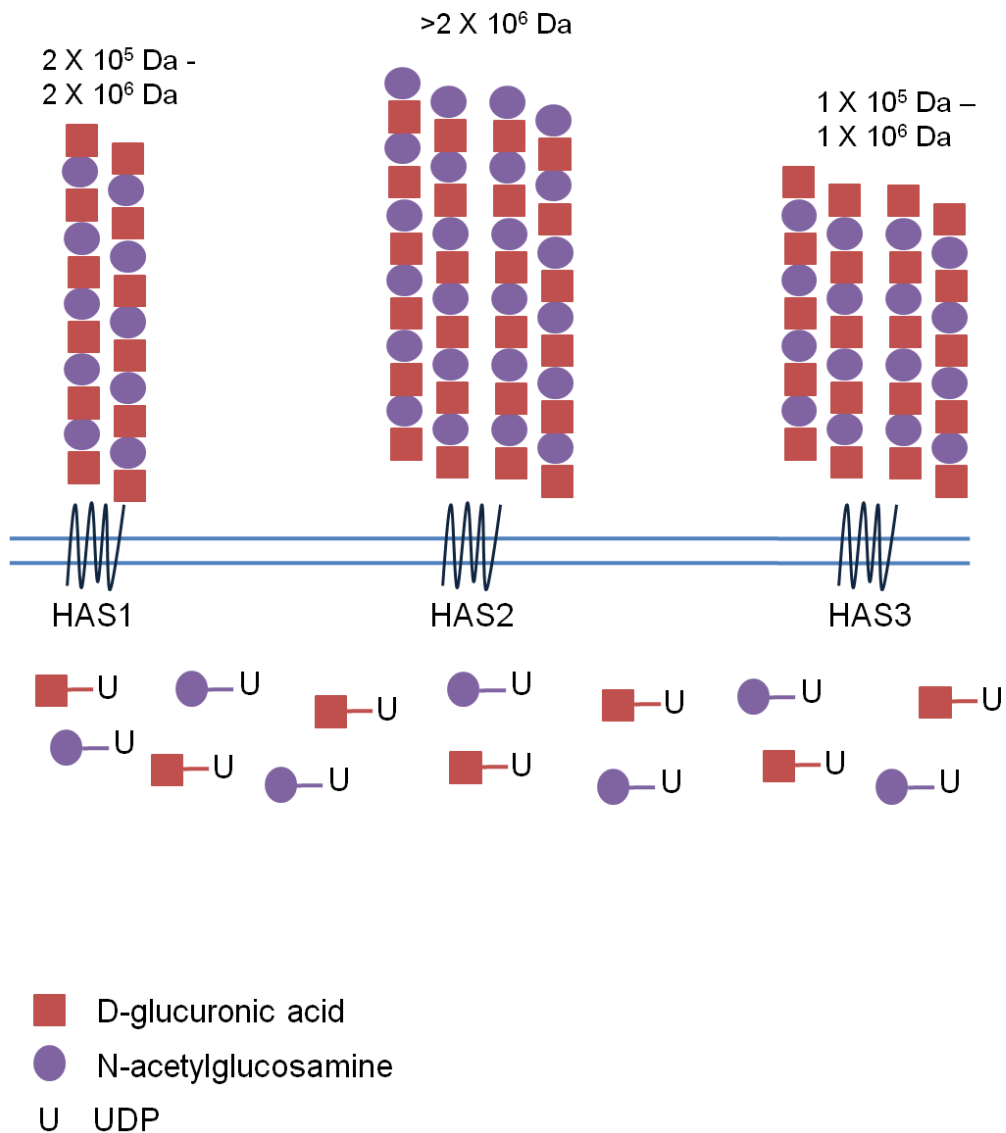


**Figure 1-5: The synthetic capacity of the three mammalian hyaluronan synthases (HAS).**

HAS1 synthesizes HA at an average of  $2 \times 10^5$  Da to  $2 \times 10^6$  and has the lowest synthetic capacity of the three enzymes. HAS2 makes more and larger HA, with an average molecular mass of  $>2 \times 10^6$  Da. HAS3 makes slightly smaller HA at an average of  $1 \times 10^5$  to  $1 \times 10^6$  HA and also has a higher synthetic capacity than HAS1. All HA is synthesized from UDP conjugated D-glucuronic acid and N-acetylglucosamine.

pathologies, where increased glucose levels are correlated with increased HA levels in serum and in the kidney (Mine *et al.*, 2006; Rugheimer *et al.*, 2008). In fact, inflammation and increased glucose, both of which are present in diabetes, can induce *Has1* expression (Bastard *et al.*, 2006; Rilla *et al.*, 2013; Zhuang and Yin, 2013; Siiskonen *et al.*, 2015). When HAS1 is given unlimited substrate, it produces a polydisperse HA population and averages  $2 \times 10^5$  to  $2 \times 10^6$  Da (Spicer and McDonald, 1998; Itano *et al.*, 1999).

## *HAS2*

When Cos-1 cells over expressing mouse *Has2* were provided with unlimited substrate, the cells synthesized HA that had broad polydispersity but averaged  $>2 \times 10^6$  Da, slightly larger than the HA produced by mouse HAS1 (Itano *et al.*, 1999). HAS2 plays a vital role in embryonic development of the heart. In fact, *Has2*<sup>-/-</sup> mice die at E9.5 due to cardiac and vascular abnormalities. Explanted atrioventricular canals from hearts of *Has2*<sup>-/-</sup> mice are rescued back to wild-type phenotype by providing exogenous HA or after transfection with *Has2* cDNA suggesting a critical role for HA synthesized by HAS2 in heart development (Camenisch *et al.*, 2000). Like *HAS1*, *HAS2* expression can be induced. For example, osteopontin induces *HAS2* expression in human mammary epithelial cells and prostaglandins induce *HAS2* expression in human vascular endothelial cells (Meyer-Kirchrath *et al.*, 2004; Cook *et al.*, 2006). In rat keratinocytes, EGF up-regulates *Has2* expression while TGF $\beta$  down-regulates *Has2* expression (Pasonen-Seppanen *et al.*, 2003).

## *HAS3*

HAS3 is unique in terms of the size of HA that it produces. When Cos-1 cells were transfected with mouse *Has3*, the HA produced was slightly smaller than the other two synthases averaging  $1 \times 10^5$  to  $1 \times 10^6$  Da (Itano *et al.*, 1999). Unlike HAS1, human HAS3 synthesizes HA even at low substrate concentrations and its activity is unaffected by additional substrate (Rilla *et al.*, 2013). It is important to note that although HAS3 produces smaller HA compared to HAS1 and HAS2, all endogenously produced HA is considered HMW-HA and pro-homeostatic (Fraser *et al.*, 1997; Cowman *et al.*, 2015). In rat keratinocytes EGF upregulates *Has3* expression and TGF $\beta$  downregulates *Has3* expression (Pasonen-Seppanen *et al.*, 2003). Despite the fact that cells usually express all three enzymes, they can be differentially regulated by various external stimuli and this regulation depends on the cell type being examined (Jacobson *et al.*, 2000).

## *HAS deficient mice*

The creation of animals deficient in HAS enzymes has been a great aid in helping to elucidate roles for HA in health and disease. In *Has1*<sup>-/-</sup> mice, exon five is interrupted with a neomycin cassette that makes it catalytically dead (Kobayashi *et al.*, 2010). HAS3 in *Has3*<sup>-/-</sup> mice is also catalytically dead due to deletion of a portion of exon 4 (Bai *et al.*, 2005). *Has2*<sup>-/-</sup> whole body knockouts are embryonic lethal but viable, conditional knockout mice were created by inserting loxP sites around exon 2, which contains the start codon (Camenisch *et al.*, 2000; Matsumoto *et al.*, 2009). These conditional knockouts allow for exploration into HAS2's role in tissue homeostasis and injury in postnatal life (Matsumoto *et al.*, 2009).

## **HA turnover and homeostatic degradation**

HA is turned over in the body every 2-3 days (Fraser *et al.*, 1997). During normal turnover, HA is degraded by hyaluronidases (Jiang *et al.*, 2011). There are six known vertebrate hyaluronidases that degrade HA into smaller, yet variable sized fragments (Csoka *et al.*, 2001; Jiang *et al.*, 2011). Hyaluronidase (HYAL) 1 and HYAL2 are the most abundant and functionally important in the body (Fraser *et al.*, 1997; Csoka *et al.*, 1999; Csoka *et al.*, 2001). HYAL1 is expressed in high levels in the liver, kidney, heart and spleen, is pH-dependent, and located primarily in lysosomes within the cell (Csoka *et al.*, 1999; McAtee *et al.*, 2015). HYAL2 is ubiquitously expressed (Csoka *et al.*, 1999). It can be membrane bound and act in conjunction with CD44 to bring HMW-HA close to the cell surface for cleavage into low molecular weight (LMW-HA) fragments (Csoka *et al.*, 2001; Rai *et al.*, 2001; Albeiroti *et al.*, 2015). HA that is cleaved initially by HYAL2 can be internalized and further degraded by HYAL1 and glycosidases intracellularly (Csoka *et al.*, 2001; Stern, 2003; de la Motte, 2011). However, in some tissue, HYAL2 is intracellular with no extracellular or membrane localization, suggesting that there are tissue specific localizations for HYAL enzymes (Chow *et al.*, 2006). Platelets are unique in that they have HYAL2 activity but no HYAL1 activity leaving HA degraded by platelets in the extracellular environment and able to act as a potent, pro-inflammatory signaling molecule (discussed below) (Albeiroti *et al.*, 2015). In tissues such as the skin and joints, HA turnover and recycling is done locally, but once HA reaches the blood stream a majority of it (85-90%) is taken up by LSEC, primarily via HA receptor for endocytosis (HARE), and the individual sugar molecules are reused (Fraser *et al.*, 1997; Harris *et*

*al.*, 2007; Gushulak *et al.*, 2012). As more research into HA and HA turnover is being done, new HA degrading enzymes are being discovered including KIAA1199 and TMEM (Yoshida *et al.*, 2013; Yamamoto *et al.*, 2017).

### **HMW-HA signaling**

As stated above, HA is synthesized and released into the extracellular space as a HMW (defined as  $\geq 500\text{kDa}$  unless otherwise stated) polymer and promotes homeostasis (Noble, 2002; Ruppert *et al.*, 2014). For example, U937 cells treated with LPS release pro-inflammatory cytokines like  $\text{TNF}\alpha$ ,  $\text{IL}1\beta$ , and  $\text{IL}6$ , and co-treatment with HMW-HA (800kDa, 2700kDa) reduces the release of each of these cytokines in a concentration-dependent manner (Yasuda, 2007). HMW-HA has similar effects *in vivo*. In a model of T-cell mediated liver disease, HMW-HA (780, 900, 1200kDa) limits liver injury in a size and concentration dependent manner (Nakamura *et al.*, 2004). HMW-HA promotes this homeostatic environment through interactions with HA receptors and HA binding proteins (referred to as the HA network), which are discussed below (and outlined in Figure 1-6 and 1-7) (Manasa *et al.*, 2012; Yang *et al.*, 2012).

Cluster of differentiation 44 (CD44) is a transmembrane adhesion molecule and the most well understood and widely expressed HA receptor (Aruffo *et al.*, 1990; Teder *et al.*, 2002). HMW-HA binds CD44 and links several CD44 receptors together, promoting an anti-inflammatory, homeostatic environment. However, the exact mechanism by which HMW-HA promotes tissue homeostasis is not well established (Bollyky *et al.*, 2009; Yang *et al.*, 2012; Ruppert *et al.*, 2014). CD44 also helps to

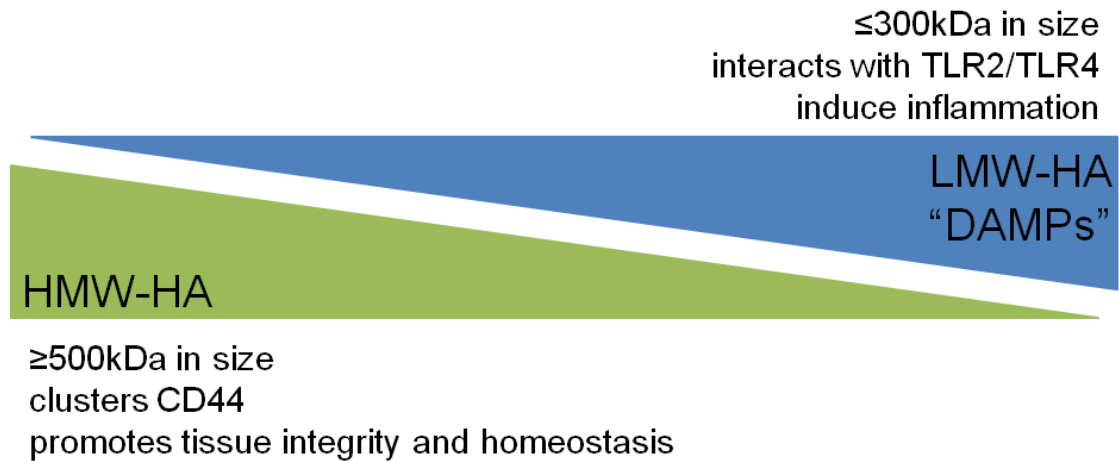


**Figure 1-6: The balance of high molecular weight HA (HMW-HA) and low molecular weight HA (LMW-HA) influences HA signaling.**

HMW-HA, characterized in this dissertation as HA greater than or equal to 500kDa, clusters the receptor CD44 and sends tissue integrity and homeostasis signals intracellularly. LMW-HA, characterized in this dissertation as less than or equal to 300kDa, can interact with TLR2 and TLR4 and induce inflammation.

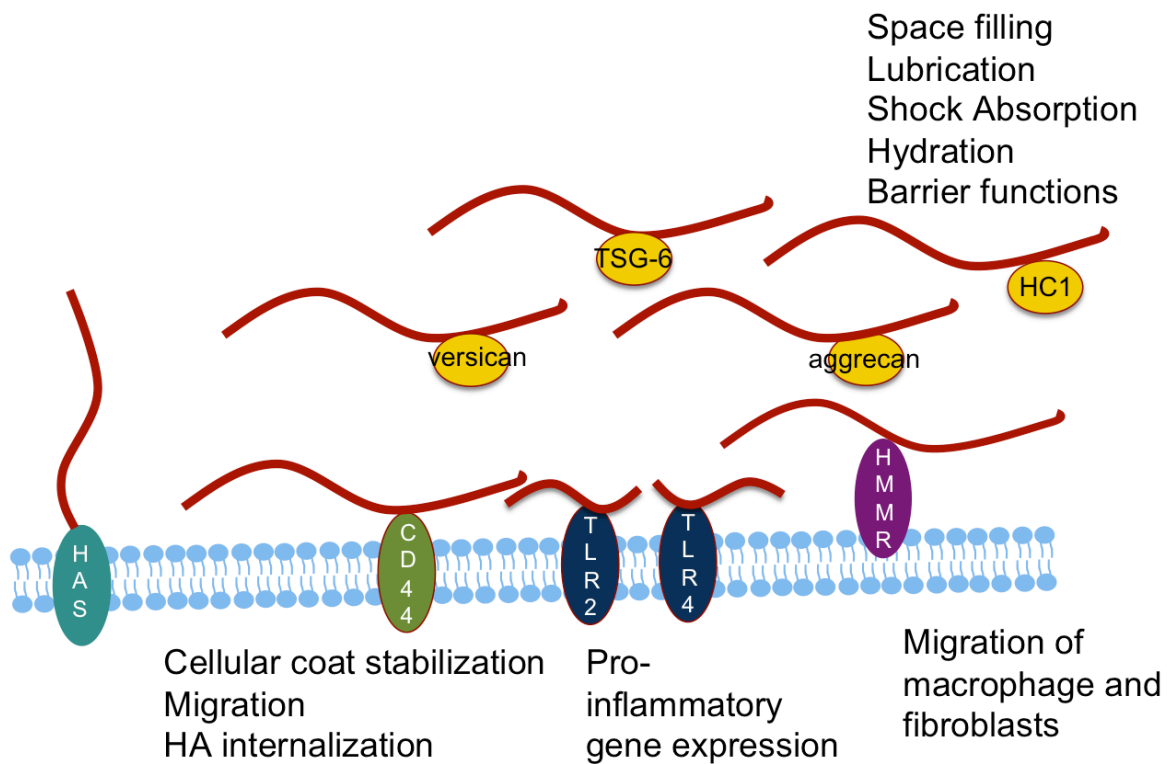


**Figure 1-7 The HA network**

The HA network consists of HA, Hyaluronan synthase (HAS) enzymes, and associated cell surface HA receptors and HA binding proteins. HAS enzymes synthesize HA at the cell surface and simultaneously extrude HA into the extracellular space. There it can bind proteins such as aggrecan and versican to form a stable space filling matrix that can aid in joint lubrication and shock absorption. The stable matrix also aids in hydration and maintaining barrier functions in the skin. HA can also bind cell surface receptors such as CD44 which aids in cell coat stability, migration, and HA internalization. HA bound to toll like receptor (TLR) 2 and TLR4 promotes pro-inflammatory gene expression, and HA bound to HA mediated motility receptor (HMMR) promotes migration of macrophages and fibroblasts.

maintain cell-coat stability (Knudson *et al.*, 1996). HMW-HA can also maintain homeostasis by binding other HA binding proteins like aggrecan and versican to form a stable space filling matrix important in joint lubrication and skin elasticity, respectively (Hasegawa *et al.*, 2007; Seror *et al.*, 2012).

### **LMW-HA signaling**

During tissue injury HMW-HA is degraded to LMW-HA fragments (defined as  $\leq 300$ kDa unless otherwise stated) by HYALs as well as ROS (Moseley *et al.*, 1997; Csoka *et al.*, 2001). Following this degradation, LMW-HA fragments interact with several receptors including CD44 and toll like receptor 2 and 4 (TLR2 and TLR4) (Aruffo *et al.*, 1990; Hardwick *et al.*, 1992; Jiang *et al.*, 2005). These HA receptors are found on many cell types, including macrophages, fibroblasts, and epithelial cells (Teder *et al.*, 2002; Jiang *et al.*, 2005; Ruffell *et al.*, 2011; Tolg *et al.*, 2012). The signaling that occurs during LMW-HA-receptor interaction is specific to the cell type responding to HA and the particular receptor(s) ligated; this is discussed in more detail below (and outlined in Figures 1-6 and 1-7).

The CD44-LMW-HA interaction is implicated in several cellular processes including cell migration and invasion, and glycoalyx stability (Knudson *et al.*, 1996; Marhaba and Zoller, 2004). CD44 also plays a role in the internalization of HA fragments. For example, *Cd44*<sup>-/-</sup> mice exhibit decreased survival and unremitting inflammation following bleomycin induced lung injury due to persistence of pro-inflammatory HA fragments in the injured lung (Knudson *et al.*, 2002; Teder *et al.*, 2002).

TLR2 and TLR4 are part of the innate immune system and are pattern recognition receptors with well-established ligands, Gram-positive and Gram-negative bacterial components, respectively (Mencin *et al.*, 2009). In addition to the bacterial components they recognize, both TLR2 and TLR4 recognize LMW-HA. This is thought to be due to the similar repeating nature of bacterial cell-wall components and the HA molecule (Takeuchi *et al.*, 1999; Jiang *et al.*, 2005; Jiang *et al.*, 2011). During bleomycin induced lung injury, LMW-HA (135kDa) requires TLR2, TLR4, and the adapter protein MYD88 to elicit an innate immune response both *in vitro* and *in vivo* (Jiang *et al.*, 2005). Primary human macrophages stimulated with LMW-HA (200kDa) polarize into M1 pro-inflammatory macrophages primarily through HA interaction with TLR2, TLR4, which again requires the adaptor protein MYD88 (Jiang *et al.*, 2011; Sokolowska *et al.*, 2014).

### **HA and HA mediated motility receptor (HMMR) signaling**

While much is known about the size-dependent interactions of HA with CD44 and TLR2 and 4, much less is known about HA mediated motility receptor (HMMR) or any size-dependent reactions with HA it may have. HMMR (also known as receptor for HA mediated motility or RHAMM) was originally isolated from chick fibroblast cultures (Turley, 1982). It was subsequently cloned by Eva Turley's group and was aptly named for its role in tumor cell migration (Hardwick *et al.*, 1992). Basal HMMR levels are low, but it is rapidly induced following injury (Lovvorn *et al.*, 1998; Bagli *et al.*, 1999; Zaman *et al.*, 2005). Unlike CD44 and the TLRs, HMMR is not a transmembrane protein, however, as the name suggests, HMMR plays a role in migration and motility not only of tumor cells as was first described but also of both macrophages and fibroblasts

(Hardwick *et al.*, 1992; Tolg *et al.*, 2006; Tolg *et al.*, 2012). In fact, a HMMR mimetic that inhibits the interaction between HA and HMMR limits wound closure in a model of excisional skin repair by limiting macrophage and fibroblast migration into the injured tissue (Tolg *et al.*, 2012). Similarly, *Hmmr*<sup>-/-</sup> fibroblasts are unable to migrate in a 3D collagen gel assay when stimulated with HA (Tolg *et al.*, 2006). HMMR is unique in that it is also found intracellularly and aids in cell cycle progression (Assmann *et al.*, 1999; Chen *et al.*, 2014). Specifically, HMMR aids in mitotic spindle integrity during cell division and *Hmmr*<sup>-/-</sup> embryonic fibroblasts exhibit multi-pole spindles and incomplete cytokinesis (Tolg *et al.*, 2010). Together, these receptors allow the simple HA molecule to have a wide range of signaling capabilities.

## **Clinical Uses of HA**

### *HA as a biomarker*

Blood levels of HA are much lower than other tissues and in healthy individuals are between 10 and 100ng/mL (Laurent and Fraser, 1992; Cowman *et al.*, 2015). Patients with advanced liver disease have increased HA blood levels, which have a positive correlation to disease severity (Lee *et al.*, 2010; Lee *et al.*, 2013; Rostami and Parsian, 2013). This is mainly thought to be due to the injured and dysfunctional LSECs, which are the main cell type responsible for systemic HA clearance (Fraser *et al.*, 1997; van den Broek *et al.*, 2013). Similarly, increased HA synthesis is associated with several types of cancer, and HA is currently being investigated as a biomarker for cancer progression (Kuwabara *et al.*, 2003; Auvinen *et al.*, 2013; Peng *et al.*, 2016). For

example, in the case of metastatic breast cancer, plasma HA levels correlate with poor prognosis in patients (Peng *et al.*, 2016).

HA levels from other fluids are also being investigated as potential non-invasive markers of disease. HA levels are increased in lung tissue from human patients with cancer and this is mirrored in sputum samples from the same patients, suggesting sputum HA levels could be used as a biomarker for lung cancer (Rangel *et al.*, 2015). Additionally, urinary HA levels are increased in patients with bladder cancer (Lokeshwar *et al.*, 2000; Shariat *et al.*, 2008). While HA is not the only biomarker used for the diagnosis of any disease, it is becoming increasingly helpful for physicians looking to avoid invasive and costly medical procedures.

#### *HA as treatment for skin aging*

As mentioned above, the skin contains a large portion of the total HA in the body, but the amount of HA in human skin varies depending on age, with young skin containing more HA (Reed *et al.*, 1988; Fraser *et al.*, 1997). There is approximately 200-500 $\mu$ g HA/g skin tissue, with a large percentage of that HA in the dermis (Tammi *et al.*, 1994; Fraser *et al.*, 1997). HA's association with extracellular HA binding proteins, such as aggrecan and versican, as well as CD44, help provide a strong and stable ECM in the skin (Hardingham and Fosang, 1992; LeBaron *et al.*, 1992; Pasonen-Seppanen *et al.*, 2012). Because of its importance in skin homeostasis and hydration, there is great interest in the use of HA as a topical or injectable treatment to renew a youthful appearance in the skin (Anderegg *et al.*, 2014; Paliwal *et al.*, 2014). In fact, in patients with UV damaged skin, injection of a stabilized HA filler increases collagen synthesis

and the study's authors suggest that it is due to the mechanical stretching and activation of the dermal fibroblasts (Wang *et al.*, 2007).

#### *HA as treatment for arthritis*

HA is also a major component of synovial fluid, which contains between 2-4mg HA/mL of fluid (Fraser *et al.*, 1997; Cowman *et al.*, 2015; Temple-Wong *et al.*, 2016). Its ability to hold large amounts of water helps it to aid in the lubrication of the joint and act as a shock absorber (Fraser *et al.*, 1997; Cowman *et al.*, 2015). As we age, the concentration and molecular weight distribution of articular HA changes; the concentration of HA decreases, as does the average molecular weight, resulting in decreased lubrication leading to osteoarthritis and joint pain (Band *et al.*, 2015; Kosinska *et al.*, 2015; Temple-Wong *et al.*, 2016). Currently, intra-articular injection of HA, primarily HMW-HA, is an effective treatment for osteoarthritis by increasing joint lubrication and is associated with decreased IL6 production (Guidolin and Franceschi, 2014; Kusayama *et al.*, 2014; Park *et al.*, 2014). Inflammation, another important component of arthritis, is decreased following HMW-HA injection in a rodent model of collagen induced arthritis primarily due to a decrease in TLR2 and TLR4 and their subsequent downstream signaling pathways (Campo *et al.*, 2011). The increase in joint lubrication and viscosity combined with a decrease in inflammation makes HA, specifically HMW-HA, a viable option for the treatment of joint degeneration and alleviating patients' painful symptoms (Campo *et al.*, 2011; Guidolin and Franceschi, 2014).

### *HA to treat abdominal adhesions*

Post-operative adhesions are a common complication following abdominal surgery and can cause abdominal pain, small bowel obstruction, or infertility in females (Ward and Panitch, 2011). In recent years, a HA-carboxymethyl cellulose (HA-CMC) barrier has been implanted in the abdomen of patients after surgery to aid in abdominal adhesion prevention (Ward and Panitch, 2011; Picaud *et al.*, 2014). This barrier turns to gel 1 day after implantation and is fully absorbed by the body within 1 week (Ward and Panitch, 2011). HA-CMC barriers are used to prevent adhesions after a number of abdominal procedures including both laproscopic and open abdominal surgeries (Stawicki *et al.*, 2014; Ha *et al.*, 2016). Use of the barriers is beneficial by limiting the number and severity of adhesions while having no adverse effects. However a powder version of the same HA-CMC formula shows an increase in adverse outcomes (ten Broek *et al.*, 2014).

### *Targeted drug delivery using HA*

In addition to HA itself being used to treat aging, arthritis, and intra-abdominal adhesions, HA is being tested for use as a vehicle for drug delivery. CD44, a receptor involved in HA endocytosis, is overexpressed in several cancers and contributes to metastasis (Auvinen *et al.*, 2013; Kim and Kumar, 2014; Gao *et al.*, 2015). By taking advantage of this fact, targeted drug delivery is being explored using HA coated anti-cancer drugs (Liu *et al.*, 2015; Wang *et al.*, 2016b). *In vitro*, HA coated nanoparticles containing 5-flourouracil induce apoptosis in colon cancer cells above that of non-HA coated nanoparticles (Liu *et al.*, 2015). Similar results were found in HeLa cells treated

with HA coated nanoparticles containing doxorubicin (Wang *et al.*, 2016b). In an *in vivo* mouse model of breast cancer, mice treated with HA-conjugated liposomes containing gemcitabine had slower drug clearance compared to free gemcitabine and liposome encapsulated gemcitabine, and this correlated with a greater reduction in tumor volume (Han *et al.*, 2016). While these studies are still in the early stages, HA appears to be a promising drug delivery system for cancer treatment.

### **Goals of the studies within this dissertation**

As stated at the beginning of this dissertation, chronic liver disease is an abundant and expensive burden on the United States population (Kochanek *et al.*, 2016). There are few treatments and no cures for advanced liver disease, except for a liver transplant, which comes with a host of problems. These include invasive surgery, the life-long immuno-suppression associated with anti-rejection drugs, cost, and the limited supply of healthy liver donors available (Rai, 2013; Parikh *et al.*, 2015). For these reasons, the objective of my dissertation research was to identify new pathways of liver wound healing with the goal of identifying novel therapeutic targets to improve liver repair after acute and chronic liver injury. To reach this objective, we used mouse models of liver injury to study mechanisms of hepatic wound healing after acute and chronic liver injury induced by CCl<sub>4</sub>.

The HA network, including HA, HA binding proteins, and receptors, plays a role in wound healing in the intestine, lung, and skin (both fetal and adult) (West *et al.*, 1997; de la Motte, 2011; Jiang *et al.*, 2011). The progression of wound healing has been well

defined in the skin, but also occurs in solid organ healing and includes steps of inflammation, regeneration, and matrix remodeling (Gurtner *et al.*, 2008). In fetal skin, the wound healing process that occurs after an injury is referred to as regenerative healing; the result is minimal to no scar formation and this is associated with consistently high levels of HMW-HA, limiting inflammation (Leung *et al.*, 2012). Conversely, in adult skin, wound healing after injury results in scar tissue formation and is associated with a transient increase in HA (West *et al.*, 1997; Bayat *et al.*, 2003). Acute hepatic wound healing can be considered analogous to fetal wound healing where there is no scar formation while chronic wound healing results in a scar, similar to adult skin healing (Pellicoro *et al.*, 2014). However, the role that HA plays in repair after acute and chronic liver injury is unknown.

It has been known for over 30 years that plasma HA levels are elevated in patients with liver disease. However we are the first to explore if the HA network is involved in liver injury or repair (Engstrom-Laurent *et al.*, 1985). As outlined above, liver disease, particularly fibrosis, is described as deregulated cycles of wound healing following chronic injury (Pellicoro *et al.*, 2014). Because HA has been implicated in wound healing responses in other organs and HA is increased in the plasma of patients with liver disease, we hypothesize that the HA network is vital to hepatic wound healing after acute and chronic liver injury.

HA is increased after tissue damage in the lung, skin, and intestine (Bai *et al.*, 2005; Mack *et al.*, 2012; Kessler *et al.*, 2015). If this increase is prevented, as is the case in mice deficient in HAS enzymes, the wound healing process is perturbed. Specifically, *Has3*<sup>-/-</sup> mice are protected from both dextran sodium sulfate (DSS)

induced colitis and ventilator induced lung injury as evident by decreased tissue damage (Bai *et al.*, 2005; Kessler *et al.*, 2015). In DSS-induced colitis, this decreased tissue damage is associated with decreased HA deposition in the colon of these mice (Kessler *et al.*, 2015). In ventilator induced lung injury, the decreased injury is associated with decreased LMW-HA fragments (Bai *et al.*, 2005). We therefore hypothesized that *Has3*<sup>-/-</sup> mice would be protected from CCl<sub>4</sub> induced liver injury and inflammation.

HMMR is unique in that it can be both extracellular and intracellular and plays roles in cell migration and proliferation, respectively (Tolg *et al.*, 2006; Chen *et al.*, 2014). Specifically, preventing the HA:HMMR interaction following dermal wound injury prevents macrophage and fibroblast migration and leads to defective wound repair (Tolg *et al.*, 2006; Tolg *et al.*, 2012). Additionally, *Hmmr* knockdown in HeLa cells results in mitotic spindle defects and aberrant proliferation (Chen *et al.*, 2014). Both cell migration and hepatocyte proliferation are vital parts of the regenerative wound repair process, therefore we hypothesized that *Hmmr*<sup>-/-</sup> mice would have decreased or delayed wound healing following acute CCl<sub>4</sub> exposure.

Unlike the regenerative wound healing observed after acute liver injury, chronic liver injury results in excess ECM accumulation and a fibrotic scar (Pellicoro *et al.*, 2014). Because we hypothesized *Has3*<sup>-/-</sup> mice would have decreased injury after acute CCl<sub>4</sub> exposure, we subsequently hypothesized that *Has3*<sup>-/-</sup> mice would have less fibrosis compared to wild-type mice after chronic CCl<sub>4</sub> exposure. Chronic liver injury and fibrosis are associated with persistent inflammation and deregulated wound healing. We hypothesized that *Hmmr*<sup>-/-</sup> mice would have decreased wound healing after acute CCl<sub>4</sub>

exposure, so we in turn hypothesized that *Hmmr*<sup>-/-</sup> mice would have decreased fibrosis after chronic CCl<sub>4</sub> exposure compared to wild-type mice.

One final goal of this study, which came to light after discovering the genetically deficient mice described above were on different backgrounds, was to identify differences in liver injury, wound healing, and fibrosis between C57BL/6 sub-strains. Specifically, we evaluated acute hepatotoxicity and wound healing following a single injection of CCl<sub>4</sub> in both the 6J and 6N sub-strains of mice. Differences in toxicity occur following APAP induced liver injury, and we hypothesized that these differences will occur following CCl<sub>4</sub> injury as well, with 6N mice having increased injury (Bourdi *et al.*, 2011; Duan *et al.*, 2016). We also hypothesized that this increased injury may contribute to a difference in the wound healing response following acute CCl<sub>4</sub>; i.e. 6N mice will have increased wound healing. We also investigated any potential differences in frank fibrosis between 6J and 6N mice, and hypothesized that 6N mice would have increased fibrosis following chronic CCl<sub>4</sub> exposure compared to 6J mice due to increased liver injury and subsequently more robust repair.

## Chapter 2: Materials and Methods

*Portions of this chapter are adapted from 1) McCracken, JM et al. "Differential effects of hyaluronan synthase 3 deficiency after acute vs chronic liver injury in mice" Fibrogenesis and Tissue Repair 2016; Licensed under Creative Commons Attribution 4.0 International License and 2) McCracken, JM et al. "C57BL/6 substrains exhibit different responses to acute carbon tetrachloride exposure: Implications for work involving transgenic mice" Gene Expression: The Journal of Basic Liver Research. 17#3, doi: 10.3727/105221617X695050 with permission Cognizant, LLC; [www.cognizantcommunications.com](http://www.cognizantcommunications.com) copyright 2017 in press.*

## **Materials**

Olive oil and carbon tetrachloride were purchased from Sigma-Aldrich (St. Louis, MO) and Buprenex (buprenorphine HCL) was manufactured by Reckitt Benckiser Healthcare (UK, Ltd, Hull England) and distributed by Reckitt Benckiser Pharmaceuticals, Inc (Richmond, VA). The anesthetic used was a mixture containing Ketamine (Akom, Inc, Decator, IL), Xylazine (KetaVed, VedCO, Inc., St. Joseph, MO), and Acepromazine (VedCO, Inc) or Isoflurane (Piramal Healthcare).

## **Methods**

### **Animal use**

Animals were treated humanely and in accordance to protocols approved by the University of Kansas Medical Center (KUMC) Institutional Animal Care and Use Committee. Mice were housed in ventilated cages on a 10/14H light/dark cycle with access to standard mouse chow and water *ad libitum*. Wild-type C57BL/6J or C57BL/6N were purchased from Jackson Labs (Bar Harbor, ME) or Charles River (Wilmington, MA), respectively. *Has3*<sup>-/-</sup> animals (Bai *et al.*, 2005) were derived from *Has1/3* double knockout mice, a kind gift from Drs. Vince Hascall, Carol de la Motte, and Sean Kessler from Cleveland Clinic in Cleveland, Ohio and *Hmnr*<sup>-/-</sup> mice (Tolg *et al.*, 2003) were a kind gift from Dr. Eva Turley from London Health Science Centre in Ontario, Canada and were bred at KUMC. Male knockout mice were utilized at 10-12 weeks of age and wild-type mice were age matched.

### **Genotyping**

Mice were ear punched and a small piece (~ 2 mm) of the end of the tail was collected when mice were 14-16 days old, prior to ossification of the distal most tailbones. The tail biopsy was snap frozen in liquid nitrogen and stored at -80°C until DNA was isolated. The tails were digested with ALT buffer and Proteinase K (DNeasy Kit, Qiagen, Valencia, CA) at 57°C overnight (16-18 hours). DNA was isolated using DNeasy Kit and eluted in AE buffer. PCR was completed using parameters specific for each reaction as follows and a MJ Research PTC-200 thermocycler (Bio-Rad). The individual master mixes are listed below and all primers are found in Table 2-1.

*Nnt* genotyping master mix included 1X PCR buffer, 2.5mM MgCl<sub>2</sub>, 0.67mM dNTPs, 1.0µM *Nnt*-Common primer, 0.33µM *Nnt*-Wild-type primer, 0.67µM *Nnt*-Mutant primer, and 1.25 units platinum *Taq* polymerase. The amplification procedure was as follows: initial melt 95°C for 5 minutes, amplification cycle 95°C for 45 seconds, 58°C for 30 seconds, 72°C for 45 seconds for 35 cycles, and a final extension 72°C for 5 minutes (Navarro *et al.*, 2012).

*Has3* genotyping master mix included 1X PCR buffer, 2.0mM MgCl<sub>2</sub>, 0.8mM dNTPs, 1.0µM forward primer, 1.0µM reverse primer, and 2 units of platinum *Taq* polymerase. For *Has3* wild-type the forward primer was *Has3* KO3' and the reverse was *Has3* KO5'. For *Has3* mutant the forward primer was *Has3* KO3' and the reverse was PGK promAS-1. The amplification procedure was as follows: initial melt 94°C for 5 minutes, amplification cycle 94°C for 30 seconds, 67°C for 30 seconds, 72°C for 60 seconds for 37 cycles, and a final extension 72°C for 10 minutes.

*Hmnr* genotyping master mix was the same as above for *Has3*. Each reaction required different amplification procedures and are as follows: For the wild-type

reaction, the initial melting was 94°C for 15 minutes, amplification cycle 94°C for 30 seconds, 50°C for 1 minutes, 72°C for 1 minute repeated 39 times, and a final extension at 72°C for 10 minutes. For *Hmmr* knockout reaction, the initial melting was 94°C for 15 minutes, amplification cycle 94°C for 30 seconds, 60°C for 1 minutes, 72°C for 1 minute repeated 39 times, and a final extension at 72°C for 10 minutes (personal correspondence with Connie Tolg, PhD).

All amplification products were kept at 4°C until they were ran on a 1% agarose gel containing 0.16µg/mL ethidium bromide using a sample loading buffer containing glycerol, bromophenol blue, and xylene cyanol. Gene products for *Nnt* were 579 base pairs for mutant (C57BL/6J background) and 743 base pairs for wild-type (C57BL/6N background). *Has3* gene products were 320 base pairs for mutant and 320 base pairs for wild-type. *Hmmr* gene products were 400 base pairs for mutant and 650 base pairs for wild-type.

### **Carbon tetrachloride exposure**

Animals were given a subcutaneous injection of Buprenex as an analgesic at a concentration of 0.1mg/g body weight (BW). In acute studies, mice were given a single intraperitoneal injection of carbon tetrachloride (CCl<sub>4</sub>, 0.4mg/g BW diluted 1:3 in olive oil) 10 minutes after Buprenex. In the chronic studies, animals were given 2 injections per week for 5 weeks ramping up from 0.1mg/g BW (1 injection) to 0.2mg/g BW (1 injection) to 0.4mg/g BW (8 injections). Control animals received Buprenex and olive oil injection(s). For acute CCl<sub>4</sub> studies, mice were euthanized 12, 24 48, 72, or 96 hours post CCl<sub>4</sub> exposure. For chronic CCl<sub>4</sub> studies, mice were euthanized 72 hours after the

last injection. Animals were euthanized with either a drug cocktail containing ketamine (200mg/kg), xylazine (40mg/kg), and acepromazine (20mg/kg) or isoflurane exposure.

### **Sample collection and storage**

Blood was taken from the inferior vena cava or portal vein in deeply anesthetized mice, collected into a tube containing EDTA and aprotinin, and placed on ice. The diaphragm and aorta were cut to euthanize the animals and a hepatectomy was performed. The liver was weighed and the gall bladder removed. The liver was placed on a glass plate on ice and divided into several pieces: the left lobe of the liver was cut into slices, two slices were snap frozen in liquid nitrogen and saved for Western Blot analysis and another slice was placed in 10% formalin for 16-18 hours and subsequently transferred to 70% ethanol until it was processed. The right lobe was snap frozen to be used for triglyceride analysis and the large portion of the median lobe was embedded in optimal cutting temperature (OCT) medium, incubated on a bed of frozen isopentane until opaque and then wrapped in heavy-duty aluminum foil and stored at -80° C. The small half of the median lobe was placed in RNA later (Ambion, Austin, TX) at room temperature for 5-10 minutes, moved to 4°C for 18-24 hours then transferred to -20°C for further analysis. All remaining liver pieces were snap frozen in liquid nitrogen and stored at -80° for further analysis. Plasma was separated by spinning blood at 10,000g for 3 minutes and 30 seconds at 4° and stored at -80°C for further analysis.

### **Hepatocyte isolation and culture**

Ten to twelve week old C57BL/6N and C57BL/6J mice were anesthetized with a mixture of ketamine (200 mg/kg) and xylazine (10 mg/kg). Once mice were fully anesthetized, the abdomen was shaved using animal clippers. Mice were then affixed to a surgical platform using laboratory tape and the abdomen cleaned using 70% ethanol. The peritoneal cavity was then exposed, and the intestines moved to one side using a sterile cotton swab. Median and left lateral liver lobes were then moved to expose the inferior vena cava and the portal vein. Next, using a pair of sterile curved forceps, a sterile suture was directed under the vena cava and tied loosely around the vein. The vena cava was then cannulated with a 22 gauge i.v. catheter, needle removed, and ligature tightened around the catheter. Perfusion tubing was then attached to the catheter and perfusion started (8.2 mL/min, 100 total mL) using perfusion buffer (1X HBSS  $\text{Ca}^{2+}$ ,  $\text{Mg}^{2+}$ -free, 100 U/mL penicillin, 100  $\mu\text{g}/\text{mL}$  streptomycin, 10 mM HEPES). Immediately after starting the perfusion, the portal vein was cut to allow outflow of perfusate, and then the diaphragm was cut, and superior vena cava clamped using small hemostats. Perfusion continued using 100 mL of a second buffer (1X HBSS with  $\text{Ca}^{2+}/\text{Mg}^{2+}$ , 100 U/mL penicillin, 100  $\mu\text{g}/\text{mL}$  streptomycin, 10 mM HEPES, 0.025 mg/mL Liberase (Roche)). Once complete, perfusion was halted and the liver dissected out of the mouse and placed into a sterile beaker containing 20 – 30 mL ice-cold disruption buffer (1X HBSS  $\text{Ca}^{2+}$ ,  $\text{Mg}^{2+}$ -free, 100 U/mL penicillin, 100  $\mu\text{g}/\text{mL}$  streptomycin, 10 mM HEPES,  $1 \times 10^{-7}$  M insulin). The liver was then cut into large pieces using sterile surgical scissors and then sterile forceps were used to gently agitate the dissected liver pieces in the ice-cold disruption buffer to liberate hepatic cells from the digested hepatic extracellular matrix. The cell suspension was then passed through 3 different sterile

filters (100, 70 and 30  $\mu\text{m}$  mesh sizes) into successive 50 mL centrifuge tubes. The volume of the cell suspension was then brought to 50 mLs using ice-cold disruption buffer and centrifuged at 50 x g for 5 minutes at 4°C. The supernatant was removed by aspiration and cells washed 2 more times in the same buffer. After the third wash, hepatocytes were resuspended in complete Williams E medium (Williams E, 100 U/mL penicillin, 100 U/mL streptomycin, 100 nM insulin, 2 mM GlutaMAX and 5% FBS). Viable cells were counted using a hemacytometer after staining with Trypan blue and plated on collagen-coated plates at  $0.5 \times 10^6$  cells per well in a 24-well plate. Remaining hepatocytes were snap frozen in liquid nitrogen for analysis of *Cyp2e1* expression (details below).

### ***In vitro*, carbon tetrachloride exposure and sample collection**

Two to three hours after plating, medium was aspirated and cells were washed with 1 mL of pre-warmed D-PBS; this was repeated twice. After the second wash, 1 mL of medium (Williams E, 100 U/mL penicillin, 100 U/mL streptomycin, 100nM insulin, 2 mM GlutaMAX, 5% FBS, 1% DMSO) with or without  $\text{CCl}_4$  (0, 1, 5, or 10 mM) was added to each well. One concentration of  $\text{CCl}_4$  was used per plate and each plate was sealed using Parafilm to limit interplate exposure to volatilized  $\text{CCl}_4$ , and placed back into a humidified, 5%  $\text{CO}_2$  incubator. Media addition to each plate was staggered by 15 minutes to allow for the collection of images, culture supernatants and cell lysates 24h after  $\text{CCl}_4$  exposure. A single representative image was taken from each of two replicate wells per treatment using a Zeiss Axio Observer A.1 inverted microscope (Peabody, MA) and Olympus DP71 camera operated by cellSens imaging software (Olympus,

Center Valley, PA). All culture medium (1 mL) was removed, placed into a 1.5 mL microfuge tube, and snap frozen in liquid nitrogen. Hepatocytes remaining in the well were rinsed in 1 mL of room temperature PBS and then lysed in 200  $\mu$ L of ice-cold cell lysis buffer (25 mM HEPES, 5 mM EDTA, 0.1% CHAPS, 1  $\mu$ g/mL pepstatin, 0.5  $\mu$ g/mL leupeptin, 2  $\mu$ g/mL aprotinin, 1X cOmplete, EDTA-free Protease Inhibitor Cocktail). The wells were scraped using a pipette tip to ensure release of hepatocytes from the bottom of each well. Then, the lysate was transferred to a 1.5 mL microfuge tube and allowed to sit at room temperature for 5 minutes prior to snap freezing in liquid nitrogen. Both cell culture media and cell lysates were stored at  $-80^{\circ}\text{C}$  until use. Hepatocytes from one 6N and one 6J mouse were used in each experiment, and the experiment was repeated 3 times on three separate days with two technical replicates completed each day.

### **Lactate dehydrogenase (LDH) assay**

All samples were thawed only once and cell death was determined as described previously (Bajt *et al.*, 2004). In brief, cell lysates were sonicated 2 X 3 seconds and centrifuged for 20 minutes at 20,000 x g at  $4^{\circ}\text{C}$ . A reaction buffer containing 9.64mM  $\text{KH}_2\text{PO}_4$ , 50.42mM  $\text{K}_2\text{HPO}_4$ , 0.91mM pyruvate, and 2.17mM NADH- $\text{Na}_2$  was used for this assay. For LDH release in media, 100 $\mu$ L of media was combined with 700 $\mu$ L of reaction mixture and the kinetics of the reaction were measured at 340nm and the difference in the absorbance determined over time. For LDH contained in cells, 30 $\mu$ L of lysate plus 730 $\mu$ L of reaction mixture were used. The death ratio was determined by the amount of LDH release in the medium divided by the total LDH in the media and cell lysate. The mean of technical replicates (2) from each experimental condition was

calculated and then the mean of experimental replicates (3) was calculated. The data are represented as the fold change over no CCl<sub>4</sub> treatment and experimental replicates are graphed.

### **CYP2E1 activity assay**

Liver microsomes were prepared by homogenizing 100-150mg of frozen liver tissue in 1mL of ice-cold PBS with a loose fitting dounce homogenizer. The homogenate was centrifuged 9,000 x g for 15 min at 4°C. Any fat was removed and the supernatant, plus 10mL of ice-cold PBS, was ultracentrifuged at 105,000 x g for 1 hour at 4°C. The pellet was resuspended in 200µL 0.15M KCL. Total protein was determined using BCA assay (Pierce). The assay reaction mixture consisted of 100µg of protein, 4µL p-nitrophenol, 10µL phosphate buffer (4mL 1M K<sub>2</sub>HPO<sub>4</sub> + 1mL 1M KH<sub>2</sub>PO<sub>4</sub> pH 7.4), water to bring volume to 100µL, and 10µL of 11mM NADPH. The hydroxylation of p-nitrophenol to p-nitrocatechol was used to calculate CYP2E1 activity using the extinction coefficient method. Activity is expressed as nm/min/mg total protein (Wu and Cederbaum, 2008).

### **Injury evaluation**

Plasma alanine aminotransferase (ALT) activity was determined using ALT-SL reagent kit (Sekisui Diagnostics, Exton, PA), by combining 10 µL of sample and 90 µL of working reagent. The mean velocity was determined using Synergy2 multigrade plate reader by taking readings at 340nm every 30 seconds for 5 minutes. The extinction

coefficient method was used to calculate activity based on the extinction coefficient of NADH and the change in absorbance over time.

Formalin-fixed liver tissue was processed using an automated tissue processor (Leica ASP3005, Buffalo Grove, IL) and embedded in paraffin. For histological analysis of necrosis, 5.0 or 6.0  $\mu\text{m}$  sections were stained with hematoxylin and eosin (H&E) using Leica Autostainer XL and coverslipper (Leica CV5030). Necrosis was defined as regions of tissue that were hyper-eosinophilic and lacked hepatocyte nuclei. Total area of necrosis was evaluated by a board certified pathologist by scanning the entire liver section or by using ImageJ to quantify the area of necrosis in three to five non-overlapping images taken at 200x using an Olympus BX51 microscope fitted with an Olympus DP71 camera (Olympus, Waltham, MA). Infiltrating cells were counted in 5 different necrotic areas using an EVOS FL Auto Cell Imaging System (Thermo Fisher, Waltham, MA) or ImageJ and images from an Olympus BX51 microscope fitted with an Olympus DP71 camera. Images were taken at 200X with each image containing at least one central vein. The area of necrosis was determined as defined above, the area of the central vein was subtracted, and the cells infiltrating the necrotic area were counted. Data are represented as the number of cells/ $\mu\text{m}^2$  (EVOS) or cells/pixel (ImageJ). A total of five distinct areas of necrosis were used to determine an average number of infiltrating cells for each mouse.

### **Hepatic triglyceride determination**

The right lobe of the liver was weighed and 50-100mg of tissue was transferred to a new 1.5mL microcentrifuge tube keeping the tissue frozen on dry ice. The liver was

digested with 3M KOH in 65% ethanol for 1 hour at 70°C, and vortexed every 20 minutes. Digested samples were placed at room temperature for 24h. The next day, samples were diluted 1:5 in 2M Tris buffer, pH 7.5. One mL of triglyceride Glycerol Phosphate Oxidase (GPO) Reagent (Pointe Scientific, Canton, MI) was pre-warmed to 37°, 10µL of diluted sample was added, and returned to 37° C for 5 minutes. A standard curve was created using GPO standard and then warmed to 37°C. Two-hundred µL of sample or standard was loaded into a 96-well plate and the absorbance was measured at 500nm. The total hepatic triglyceride (mg/g liver) was calculated using the standard curve and the starting weight of the liver.

### **Gene expression**

Twenty to thirty mg of liver preserved in RNA later (Ambion, Grand Island, NY) was homogenized using RLT (Qiagen RNeasy Mini Kit), 10µL/mL β-mercaptoethanol, and a bead homogenizer at 4m/s for 45 seconds (Fast prep 24, MP Biomedicals, Solon, OH). For RNA isolation from isolated primary mouse hepatocytes, 350µL of RLT + βME per  $3 \times 10^6$  cells was added to pelleted cells. The hepatocytes were further disrupted by passing this lysate through an 18 gauge needle 4 times, followed by 4 times through a 23 gauge needle. The remainder of the procedure was the same for whole liver and isolated primary hepatocytes. Total RNA was isolated using the Qiagen RNeasy Mini Kit and cDNA was synthesized using Retroscript Kit (Life Technologies/Ambion). QPCR was completed to compare genotypes and/or treatment groups using an Applied Bioscience 384-well qPCR machine (model C1000, Bio-rad, Hercules, CA) and SYBR green technology (Bio-rad) or Applied Biosystems 96-well qPCR machine (model Step

One Plus) and TaqMan technology (Applied Biosystems). Data were collected, and results were normalized to *Rn18* (housekeeping gene) and analyzed using Livak method ( $2^{-\Delta\Delta C_t}$  method). Primers used are included in Table 2-1. Sequences were from the Primer Bank (<https://pga.mgh.harvard.edu/primerbank/>) (Wang and Seed, 2003; Spandidos *et al.*, 2008; Spandidos *et al.*, 2010) unless otherwise stated.

## **Immunoblotting**

A 50-100mg slice of snap frozen liver was homogenized in 1X RIPA buffer containing 10mM sodium pyrophosphate, 40  $\mu$ L/mL proteinase inhibitor (Roche, Indianapolis, Indiana), 10  $\mu$ L/mL bacitracin, 10 $\mu$ L/mL leupeptin, 17.5  $\mu$ L/mL aprotinin, 1  $\mu$ L/mL bestatin, and 10  $\mu$ L/mL sodium orthovanadate using the FastPrep24 bead homogenizer at 4 m/sec for 45 seconds. Lysates were kept on ice for 15 minutes and then spun at 21,000 x g at 4°C for 15 minutes. The fat layer floating on top of the lysate/homogenate was removed by aspiration and the total protein concentration of the remaining supernatant was determined using the BCA assay (Pierce/ThermoFisher Scientific). Western blot samples were made to a final concentration of 400  $\mu$ g/200 $\mu$ L in 1X Laemmli buffer, boiled for 5 minutes, aliquoted and stored at -80°C (Pritchard *et al.*, 2007). SDS-PAGE gels were run and separated proteins were transferred to PVDF membranes using a semi-dry transfer apparatus (Bio-Rad, Hercules, CA). Equal protein loading was evaluated by staining membranes with fast green and recorded photographically. Membranes were washed in TBS-T and blocked in either 5% bovine serum albumin (BSA) or 5% non-fat dry milk. Antibodies were applied overnight at 4°, membranes were washed, and then incubated in horseradish peroxidase (HRP)

<b>Gene name</b>	<b>Protein name</b>	<b>Sequence Source</b>	<b>Forward Primer</b>	<b>Reverse Primer</b>
<i>Acta2</i>	asma	Primer Bank ID: 31982518b1	GTCCCAGACATC AGGGAGTAA	TCTATCGGATAC TCAGCGTCA
<i>Ccl2</i>	Ccl2/ Mcp1	(Pascual <i>et al.</i> , 2011)	AGGTCCCTGTCA TGCTTCTG	TCTGGACCCATT CCTTCTTG
<i>Ccnd1</i>	Ccnd1/ CyclinD1	(Pritchard <i>et al.</i> , 2011)	CAGAAGTGCGA AGAGGAGGTC	TCATCTTAGAGG CCACGAACAT
<i>Cd11b</i>	Cd11b	Primer Bank ID: 132626288c3	GGGAGGACAAA AACTGCCTCA	ACAAC TAGGATC TTCGCAGCAT
<i>Cd44</i>	Cd44	Primer Bank ID: 26337169a1	TCGATTTGAATG TAACCTGCCG	CAGTCCGGGAG ATACTGTAGC
<i>Col1a1</i>	Col1a1	(Stefanovic and Stefanovic, 2012)	ATGTT CAGCTTT GTGGACCTC	CAGAAAGCACA GCACTCGC
<i>Col1a2</i>	Col1a2	Primer Bank ID: 6680980a2	GGTGAGCCTGG TCAAACGG	ACTGTGTCCTTT CACGCCTTT
<i>Ctgf</i>	Ctgf	Primer Bank ID: 6753878a1	GGGCCTCTTCT GCGATTTT	ATCCAGGCAAGT GCATTGGTA
<i>Cxcr2</i>	Cxcr2	Primer Bank ID: 6753456a1	ATGCCCTCTATT CTGCCAGAT	GTGCTCCGGTT GTATAAGATGAC
<i>Cxcl1</i>	Cxcl1/ KC/Gro1	Primer Bank ID: 229577225c1	ACTGCACCCAAA CCGAAGTC	TGGGGACACCT TTTAGCATCTT
<i>Cxcl2</i>	Cxcl2/ Mip2	(Tang <i>et al.</i> , 2013)	GCGCCCAGACA GAAGTCATAG	AGCCTTGCCTTT GTT CAGTATC
<i>Cxcl10</i>	Cxcl10/ Ip10	Primer Bank ID: 10946576a1	CCAAGTGCTGC CGTCATTTT	GGCTCGCAGGG ATGATTTCAA
<i>Cyp2e1</i>	Cyp2e1	Primer Bank ID: 57634519b1	CATCACCGTTGC CTTGCTTG	CAGATGGATAC GAGGAGGAGG

<i>Emr1</i>	F4/80	Primer Bank ID: 183583543b1	CTGCACCTGTAA ACGAGGCTT	TTGAAAGTTGGT TTGTCCATTGC
<i>Gclc</i>	Gclc	Primer Bank ID: 33468897A1	GGGGTGACGAG GTGGAGTA	GTTGGGGTTTGT CCTCTCCC
<i>Has1</i>	Has1	Primer Bank ID: 6680169a1	GGCGAGCACTC ACGATCATC	AGGAGTCCATA GCGATCTGAAG
<i>Has2</i>	Has2	(Cheng <i>et al.</i> , 2011)	GGTCCAAGTGC CTTACTGAAAC	TGTACAGCCACT CTCGGAAGTA
<i>Has3</i>	Has3	Primer Bank ID: 6680173a1	GTGGGCACCAG TCTGTTTG	CCACTGAACGC GACCTCTG
<i>Has3</i> KO 3'	Geno- typing	Ryu Miura (Personal communication)	GGAAGCAGGCA TAGGTAGCCTTG	n/a
<i>Has3</i> KO 5'	Geno- typing	Rua Miura (Personal Communication)	TGATCGGCACCT TACCAACCGAG	n/a
<i>Hmmr</i>	Hmmr	Primer Bank ID: 226693395b3	AGCAAAGCTCAA TGCAGCAG	AGTAAGCCGTTT TTCCAGTGAA
<i>Hmmr</i> KO	Geno- typing	Cornelia Tolg (Peronsal Communicaton)	GGC GTC TCC TAT ATG AAG AAC	GAT TTG AGT TGG CTA TTT TCA TC
<i>Hmmr</i> wt	Geno- typing	Cornelia Tolg (Peronsal Communication)	GCC GAG GAT TTG GAA AAA GTG	TCC AAC AAC AAA CTT GTC TGG
<i>Nqo1</i>	Nqo1	Primer Bank ID: 161621259b1	AGGATGGGAGG TACTCGAATC	TGCTAGAGATGA CTCGGAAGG
<i>Mmp2</i>	Mmp2	Primer Bank ID: 47271505b1	GATGTCGCCCC TAAAACAGAC	CAGCCATAGAAA GTGTTTCAGGT
<i>Mmp9</i>	Mmp9	Primer Bank ID: 31560795b2	GGACCCGAAGC GGACATTG	GAAGGGATACC CGTCTCCGT
<i>Mmp13</i>	Mmp13	Primer Bank ID: 291463259b1	TGTTTGCAGAGC ACTACTTGAA	CAGTCACCTCTA AGCCAAAGAAA

<i>Nnt</i> com	Genotyping	(Navarro <i>et al.</i> , 2012)	GTAGGGCCAAC TGTTTCTGCATG A	n/a
<i>Nnt</i> Mut	Genotyping	(Navarro <i>et al.</i> , 2012)	GTGGAATTCCG CTGAGAGAACTC TT	n/a
<i>Nnt</i> wt	Genotyping	(Navarro <i>et al.</i> , 2012)	GGGCATAGGAA GCAAATACCAAG TTG	n/a
<i>Pcna</i>	Pcna	Primer Bank ID: 7242171a1	TTTGAGGCACG CCTGATCC	GGAGACGTGAG ACGAGTCCAT
PGKPro m-AS1	Genotyping	Rua Miura (Personal Communication)	GAGGCCACTTG TGTAGCGCCAA G	n/a
<i>Rn18s</i>	18S	(Tang <i>et al.</i> , 2013)	ACGGAAGGGCA CCACCAGGA	CACCACCACCC ACGGAATCG
<i>Serpinh</i> <i>1</i>	Hsp47	Primer Bank ID: 6753304a1	GCCGAGGTGAA GAAACCCC	CATCGCCTGATA TAGGCTGAAG
<i>Tgfb</i>	Tgf $\beta$	Primer Bank ID: 6755774b1	AGCTGGTGAAA CGGAAGCG	GCGAGCCTTAG TTTGGACAGG
<i>Timp1</i>	Timp1	Primer Bank ID: 6755795a1	GCAACTCGGAC CTGGTCATAA	CGGCCCGTGAT GAGAACT
<i>Tlr2</i>	Tlr2	Primer Bank ID: 158749637b2	TCTAAAGTCGAT CCGCGACAT	CTACGGGCAGT GGTGAAAACCT
<i>Tnfa</i>	Tnfa	(Pritchard <i>et al.</i> , 2010)	CCCTCACACTCA GATCATCTTCT	GCTACGACGTG GGCTACAG

Table 2-1: Primer table.

conjugated secondary antibodies for 1-2 hours at room temperature. Proteins of interest were visualized using enhanced chemiluminescent substrate (GE Healthcare, Piscataway, NJ) and luminescence was captured on radiographic film. ImageJ was used to quantify intensity of bands present for each protein of interest and loading normalization was done using GAPDH or HSC70. Antibodies used can be found in Table 2-2.

### **Cytokine protein array**

Plasma cytokine protein content was measured using a Proteome Profiler: Mouse Cytokine Array Panel A (R&D Systems, Minneapolis, MN) to evaluate inflammatory mediators present in pooled plasma samples from the mice exposed to CCl<sub>4</sub> and euthanized 48 hours later or in animals exposed to olive oil (control). In brief, pooled plasma samples (n = 6–8 individual mice per group) were applied to the provided membrane impregnated with capture antibodies. Streptavidin-HRP-conjugated secondary antibodies were then applied, and chemiluminescent technology was used to detect proteins captured by the array. All arrays were done on the same day with the same exposure time. ImageJ was used to semi-quantify pixel density of resultant cytokine-positive areas recorded using radiographic film.

### **Hepatic leukocyte esterase (chloracetate esterase, CAE) localization and quantification**

Chloracetate esterase (CAE) was detected in liver sections from all mice using a naphthol-AS-D CAE kit, according to the manufacturer's instructions (Sigma-Aldrich).

<b>Antibody</b>	<b>Clone</b>	<b>Secondary</b>	<b>Company</b>
$\alpha$ sma	1A4	anti-rabbit	AbCam Cambridge, MA
Cyclin D1	92g2	anti-rabbit	Cell Signaling Danvers, MA
Cyp2e1	n/a	anti-rabbit	AbCam Cambridge, MA
F4/80	MCA497	Cl:A3-1	Bio-rad Hercules, CA
Gapdh	14C10	anti-rabbit	Cell Signaling
Hmmr (CD168)	EPR4054	anti-rabbit	AbCam
Hsc70	6i2	anti-rat	Santa Cruz Dallas, TX
Ki67	ab66155	anti-rabbit (fluorescent)	AbCam
Mmp13	n/a	anti-rabbit	AbCam
Pcna	PC10	anti-mouse	EMD-Millipore Billerica, MA
biotinylated goat anti-rat	n/a	n/a	Vector
donkey anti-rabbit IgG-Alexa Fluor 488 conjugate	n/a	n/a	Life Technologies Waltham, WA
goat anti-mouse IgG-HRP	n/a	n/a	Santa Cruz
goat anti-rabbit IgG-HRP	n/a	n/a	AbCam
Goat anti-rat IgG2b-HRP	n/a	n/a	BioRad

Table 2-2: Antibody table.

Briefly, formalin-fixed, paraffin-embedded liver tissues were cut into 5.0  $\mu\text{M}$  thick sections, heated to 60°C for 20 minutes, deparaffinized in 3 changes of Safeclear (5 minutes each) and then rehydrated in a series of graded ethanols. After staining, sections were dehydrated and mounted for analysis. Quantification of CAE+ cells was performed by an individual blinded to sub-strain and time point. Due to the small number of CAE+ cells observed, all CAE+ cells in one entire liver section per mouse were counted.

### **Ki67 staining**

Liver embedded in OCT medium was cut to 5.0  $\mu\text{M}$  sections and placed on SuperFrost + slides (Fisher, Waltham, MA) and stored at -80°C for less than one week before use. Slides were removed from -80°C and allowed to warm at room temperature for 2 minutes and then fixed in 10% formalin for 10 minutes. The formalin was removed and slides were then incubated in 0.1% Triton X-100 in PBS for 15 minutes, washed in PBS 3 x 2 minutes, then blocked in 10% donkey serum in PBS for 1 hour at room temperature. Ki67 primary (see Table 2-2) antibody was applied to slides at a concentration of 1:500 in 1% donkey serum overnight at 4°C. The following day, slides were washed 3 x 2 minutes, incubated with a Alexa Fluor 488 conjugated donkey anti-rabbit secondary antibody at a dilution of 1:500 for one hour, and washed again in PBS 3 x 2 minutes. Nuclei were counter stained with 4',6-diamidino-2-phenylidole (DAPI, Vector Labs) and clear nail polish was used to seal a glass coverslip over the sections. Three to five non-overlapping images were taken of each section using an Olympus BX51 microscope with an Olympus BH2RFLT3 burner and Olympus DP71 camera at

200X using DP Controller software (Olympus, Waltham, MA). Ki67-positive cells were manually counted using images taken through the GFP filter and ImageJ.

### **$\alpha$ SMA immunohistochemistry**

Formalin-fixed, paraffin-embedded liver tissues were cut into 5.0  $\mu$ m sections, deparaffinized using Citrisolv (Fisher Scientific) and rehydrated in a series of graded ethanol. Antigens were exposed using 10% Reveal Decloaker (BioCare Medical, Concord, CA), and microwaving slides for 2 minutes at 50% power followed by 7 minutes at 10% power. Slides were allowed to cool for 1 hour then washed in TBS 2 x 15 minutes and endogenous peroxidase activity was blocked using 3% H<sub>2</sub>O<sub>2</sub> for 15 minutes. Following a wash in TBS, endogenous avidin and biotin (Vector Laboratories, Burlingame, CA) were blocked. Mouse-on-mouse (MOM) (Vector Laboratories) IgG blocking diluent was applied to sections for 1 hour. Next, slides were washed in TBS and MOM blocking diluent was applied for 5 minutes.  $\alpha$ SMA antibody (see Table 2) was diluted 1:100 and applied to sections for 30 minutes. Slides were washed in TBS and then biotin-conjugated anti-mouse IgG reagent (MOM kit) was applied to slides for 10 minutes. Following a TBS wash, the signal was amplified using avidin biotin-HRP complex (Vectastain ABC, Vector Laboratories). 3,3'-diaminobenzidine was used to detect positive staining, and hematoxylin was used as a counterstain. Slides were immersed in a bluing reagent, dehydrated in a series of graded ethanol and Citrisolv, and sealed using glass coverslips and Cytoseal mounting medium (Thermo Fisher Scientific). Five non-overlapping 200X images were taken of each section using an Olympus BX51 microscope and Olympus DP71 camera operated by DP Controller

software (Olympus, Waltham, MA). ImageJ was used to quantify the area of positive staining above a threshold that remained constant for all images.

### **F4/80 immunofluorescence**

Formalin-fixed, paraffin-embedded sections were cut to 5.0  $\mu$ M sections. Paraffin was removed by SafeClear (Protocol/Thermo Fisher Scientific) and tissues were rehydrated by putting slides through a series of graded ethanols (100% 2 x 3 minutes, 95% 1 x 3 minutes, 85% 1 x 3 minutes, 70% 1 x 3 minutes, 50% 1 x 3 minutes, and RO water). Slides were immersed in 1 X Reveal Decloaker and microwaved for 2 minutes at 50% power followed by 7 minutes at 10% power then allowed to cool for 1 hour at room temperature. Slides were then washed in TBS-T, endogenous peroxidase was blocked using 3% H<sub>2</sub>O<sub>2</sub> for 15 minutes, followed by another wash in TBS. Endogenous avidin and biotin were blocked using avidin/biotin blocking kit (Vector Labs). Slides were rinsed in TBS after both avidin and biotin blocking steps and 10% goat serum, 0.4% TritonX 100 in TBS was used to block sections. F4/80 primary antibody (see Table 2-2) was diluted in blocking solution at a concentration of 1:100 and applied to sections overnight at 4°C. The following day, primary antibody was removed and slides were washed in TBS-T and incubated in biotinylated anti-rat secondary antibody diluted in block (10% goat serum, 0.4% TritonX 100 in TBS) 1:100 for 2 hours at room temperature. Following a wash in TBS-T slides were incubated in avidin/biotin complex (Vector Labs) to amplify signal, washed again in TBS-T, and a second amplification step was completed using tyramide signal amplification (TSA) kit (Perkin Elmer, Waltham, MA) diluted 1:400. Nuclei were stained with DAPI following a wash in TBS-T. Slides were cover slipped

and then sealed with clear nail polish. Three to five non-overlapping 200X images were taken of each section using an Olympus BX51 microscope with an Olympus BH2RFLT3 burner and Olympus DP71 camera operated by DP Controller software (Olympus, Waltham, MA). ImageJ was used to quantify the area of positive staining above a threshold that remained constant for all images.

### **Hyaluronan binding protein (HABP) staining for hyaluronan**

Formalin-fixed, paraffin-embedded liver tissue was cut into 5.0  $\mu\text{m}$  sections and rehydrated in Safe Clear (2 x 3 minutes) and a series of graded ethanols and PBS (100% 1 x 1 minute, 100% 1 x 2 minutes, 95% 1 x 1 minute, 95% 1 x 2 minutes, running water 1 minute, PBS 1 x 10 minutes). Endogenous avidin and biotin was blocked (avidin/biotin Blocking kit, Vector). Sections were incubated with normal goat serum at a concentration of 150  $\mu\text{L}/10\text{mL}$  PBS for 20 minutes followed by a 1 hour incubation with 1mg/mL hyaluronidase (Sigma) in 0.9% normal saline for negative controls or 0.9% normal saline. After a rinse in PBS, biotinylated-HABP (Calbiochem) at 1:100 in normal goat serum at a concentration of 150  $\mu\text{L}/10\text{mL}$  was applied to sections for 1 hour at room temperature. After washing with PBS, the signal was amplified using the Avidin/Biotin complex applied for 30 minutes. A second amplification step using TSA diluted 1:400 was followed by nuclear staining using DAPI, cover slipping, and sealing the sections with clear nail polish. Three to five non-overlapping 200X images were taken of each section using an Olympus BX51 microscope with an Olympus BH2RFLT3 burner and Olympus DP71 camera operated by DP Controller software (Olympus, Waltham, MA). Each image was taken using the same exposure and ImageJ was used

to quantify the area and intensity of positive staining above a threshold that remained constant for all images.

### **Hyaluronan plasma concentration**

Because HA is a carbohydrate a traditional ELISA using antibody technology cannot be used. Therefore an “ELISA-like” assay was used to quantify HA, which utilized HA binding proteins (HABP) for both capture and detection reagents (R&D systems). The wells of a 96-well plate were coated with capture HABP and mouse plasma was diluted 1:40-1:100 with manufacturer-supplied calibrator diluent and applied to the wells. The plate was placed on an orbital microplate shaker (0.12” orbit) at 500 rpm for 2 hours at room temperature, washed with supplied wash buffer, after which recombinant aggrecan-HRP conjugate was applied to the wells and the plate was again placed on the orbital microplate shaker at 500 rpm for 2 hours at room temperature. After a second wash, substrate was applied to the wells for 30 minutes and the reaction was stopped with the supplied stop solution. The plate was read at 450nm and 540nm to correct for wavelength. myassays.com was used to complete a four parametric analysis based on a standard curve prepared to determine total HA in each well.

### **Hyaluronan size analysis**

HMW-HA and LMW-HA were separated as described previously (Decleves *et al.*, 2012) with modifications. Fifty  $\mu$ L of pooled plasma was digested 1:1 with 1mg/mL Proteinase K (Invitrogen, Grand Island, NY) with 0.01% SDS for 4 hours at 60°. Saline was added to bring volume to 1mL and Centriscart® 1 Centrifugal Ultrafiltration units

(Sigma) with a molecular weight cut off of 100kDa or 300kDa were used to separate HMW-HA from LMW-HA. Quantikine HA ELISA-like assay was used as described above to quantify amount of HA in each fraction per manufacturer's instructions. Similar to above, myassays.com was used to complete a four parametric analysis based on a standard curve prepared to determine total HA in each fraction.

### **Sirius red staining**

Formalin-fixed, paraffin-embedded liver tissue sections cut to 5.0  $\mu\text{M}$  were heated at 60°C for 20 minutes. SafeClear II (Protocol, Pittsburgh, PA) was used to deparaffinize sections and a series of graded ethanols (100% 2 x 1 minute, 70% 1 x 1 minute, 30% 1 x 1 minute, RO water 2 x 1 minute) were used to rehydrate the tissue. Slides were then immersed in 0.1% Sirius red solution (Direct Red 80, Sigma) for 40 minutes to 1 hour at room temperature. Acidified water (0.5% acetic acid in water) was used to wash slides 3 times for 5 minutes each, then slides were dehydrated in a 100% ethanol 3 x 1 minute and 2 x 5 minutes SafeClear II solutions, mounted with Permount and allowed to dry. Three to five non-overlapping 200X images were taken of each section using an Olympus BX51 microscope and Olympus DP71 camera operated by DP Controller software. ImageJ was used to quantify area of positive staining above a threshold that was kept constant for all images.

### **Hydroxyproline assay**

Ten mg of snap frozen tissue was hydrolyzed using 100 $\mu\text{L}$  12.1N HCl and 100 $\mu\text{L}$  water at 120°C for 3 hours, vortexing every 30 minutes. Samples were centrifuged at

10,000 x g for 10 minutes to remove particulate matter. A standard curve was made using 1mg/mL hydroxyproline and 10 $\mu$ L of standard and sample were added to a 96-well plate. One hundred  $\mu$ L Chloramine T solution (45mM chloramine t, 10% 1-propanol in acetate-citrate buffer: 1.46M sodium acetate trihydrate, 239.43mM citric acid, 1.21% acetic acid, 850.06mM sodium hydroxide pH 6.5) was added to each well and plate was incubated at room temperature for 25 minutes. One hundred  $\mu$ L of Ehrlich's solution (1.22M 4-(dimethylamino)benzaldehyde, 27% perchloric acid, 82% 1-propanol) was added to each well and the plate was incubated at 60°C for 35 minutes in a dry heat oven. Following incubation, absorbance of each well at 550nm was determined and hydroxyproline concentration was calculated from the standard curve. Collagen concentration was calculated by dividing hydroxyproline concentration by 12.5% (Reddy and Enwemeka, 1996).

### **In situ zymography**

Matrix metabolism was determined as described previously with modifications (Lindsey *et al.*, 2001). Frozen tissue sections cut 7.0  $\mu$ m thick were taken directly from -80°C and developing buffer (Tris, pH 7.4- final concentration 100mM, NaCl- 100mM, CaCl<sub>2</sub>- 5mM, Brij-35- 0.05%, PMSF- 0.25mM, and Oregon green, dye quenched (DQ) gelatin (Molecular probes)- 0.1mg/mL) was applied. Inhibitor for MMP13 (444283, Calbiochem, Billerica, MA) was added to one section in a subset of slides. The slides were incubated in a humid chamber at 37°C for 16-18 hours, washed in MQ-water, and DAPI mounting medium was used as a nuclear stain. Clear nail polish was used to seal tissue sections. Three to five non-overlapping 200X images were taken of each section

using an Olympus BX51 microscope with an Olympus BH2RFLT3 burner and Olympus DP71 camera operated by DP Controller software. ImageJ was used to quantify the area of positive staining above a threshold that remained constant for all images.

### **Statistical analysis**

All data are represented as mean  $\pm$  standard error of mean. Significance was calculated by two-way analysis of variance (SAS Institute, Inc, Cary, NC or GraphPad Prism, La Jolla, CA). Post hoc analysis was done using Tukey's, Dunnett's, or multiple t-tests depending on comparisons being performed. The comparisons having p-value of less than 0.05 were considered statistically significant. For the cases having only two groups, Student's t-test was used to determine significance. A Pearson's correlation was done to determine the relationship between two independent variables.

## **Chapter 3: HA produced by HAS3 attenuates liver injury and wound healing after acute CCl<sub>4</sub> exposure**

*Portions of this chapter are adapted from McCracken, JM et al. "Differential effects of hyaluronan synthase 3 deficiency after acute vs chronic liver injury in mice"*

*Fibrogenesis and Tissue Repair 2016; Licensed under Creative Commons Attribution*

*4.0 International License*

## **Abstract**

Hyaluronan (HA) is a ubiquitous extracellular matrix (ECM) glycosaminoglycan synthesized by three different enzymes, hyaluronan synthase (HAS) 1, 2, and 3. HA synthesis mediated by HAS3 promotes inflammation and is pathogenic in animal models of human lung and intestinal disease. Although plasma HA is a commonly used biomarker for liver disease, if and how HA contributes to disease pathogenesis remains unclear. Wound healing follows acute liver injury, and includes periods of inflammation, regeneration, and matrix remodeling. Here, we tested the hypothesis that HA synthesized by HAS3 enhances inflammation and wound healing. To test this hypothesis, we exposed wild-type or *Has3*<sup>-/-</sup> mice to carbon tetrachloride (CCl<sub>4</sub>) once to induce acute liver injury. Acute CCl<sub>4</sub> induced expression of hepatic *Has* enzymes, increased plasma HA, and increased hepatic HA accumulation in both genotypes. *Has3*<sup>-/-</sup> mice had reduced plasma HA compared to wild-type but increased hepatic HA. *Has3*<sup>-/-</sup> mice also had a perturbation of LMW-HA/HMW-HA ratio compared to wild-type mice following liver injury. This was associated with an increase in injury and wound healing, including inflammation, regeneration, and matrix remodeling (specifically matrix degradation). Acute CCl<sub>4</sub> exposure also induced the expression of the HA receptors CD44, TLR2, TLR4, and HMMR. *Has3*<sup>-/-</sup> mice had increased HMMR both at the mRNA and protein level compared to wild-type mice following acute CCl<sub>4</sub> exposure. These data suggest that HA, and HA receptors, should be investigated further to determine their specific roles in liver injury and repair.

## **Introduction**

Hyaluronan (HA) is a ubiquitous, non-sulfated glycosaminoglycan that is part of the extracellular matrix (ECM) (Jiang *et al.*, 2011; Manasa *et al.*, 2012). HA is synthesized by many cell types including fibroblasts and vascular endothelial cells (Stern *et al.*, 2006; Jiang *et al.*, 2007). HA is synthesized by three HA synthases (HAS1, 2, or 3) (Itano *et al.*, 1999; Jiang *et al.*, 2011). These enzymes differ in their expression levels depending on cell type and tissue (Spicer and McDonald, 1998; Itano *et al.*, 1999). The three HAS enzymes also differ in their biosynthetic capacity and the size of HA produced (Itano *et al.*, 1999; Rilla *et al.*, 2013). For example, HAS1 and HAS2 make high molecular weight (HMW-HA) and HAS3 slightly smaller HA, although all endogenously produced HA is considered HMW-HA (described in more detail in Chapter 1) (Spicer and McDonald, 1998; Itano *et al.*, 1999). HAS1 is least enzymatically active in euglycemic conditions while HAS3 is enzymatically active even in low glucose conditions (Itano *et al.*, 1999; Rilla *et al.*, 2013).

When tissues are injured, HA is synthesized and degraded and participates in the wound healing response (Fraser *et al.*, 1997; Jiang *et al.*, 2011). The size of HA dictates its signaling properties with low molecular weight HA (LMW-HA,  $\leq 300$ kDa) promoting inflammation and HMW-HA ( $\geq 500$ kDa) promoting homeostasis (Stern *et al.*, 2006; Jiang *et al.*, 2007). HMW-HA is a major component of healthy joints, the vitreous humor of the eye, and skin, and when synthesized in these injured tissues, dampens inflammation (Meyer and Palmer, 1934; Guidolin and Franceschi, 2014; Paliwal *et al.*, 2014). HA is degraded by hyaluronidases and reactive oxygen species under normal circumstances and when tissues are injured, into a polydisperse population containing

LMW-HA fragments ( $\leq 300$  kDa), which exacerbate inflammation (McKee *et al.*, 1996; Moseley *et al.*, 1997; Csoka *et al.*, 2001). Consistently, persistence of LMW-HA in chronically wounded tissue contributes to disease pathogenesis in animal models of idiopathic pulmonary fibrosis (Jiang *et al.*, 2005).

The use of genetically deficient mice has led to great advances in understanding the role of HA in various diseases. *Has2*<sup>-/-</sup> mice are embryonic lethal due to abnormal cardiac development but conditional knockouts as well as whole body *Has1*<sup>-/-</sup> and *Has3*<sup>-/-</sup> mice have been utilized in a number of studies (Camenisch *et al.*, 2000; Bai *et al.*, 2005; Matsumoto *et al.*, 2009). *Has3*<sup>-/-</sup> mice are protected from ventilator induced liver injury as well as dextran sodium sulfate (DSS) induced colitis (Bai *et al.*, 2005; Kessler *et al.*, 2015). It is suggested that this is due to the relatively smaller HA produced by HAS3 being more easily degraded into LMW-HA fragments (Bai *et al.*, 2005).

Elevated plasma HA is associated with liver disease (Engstrom-Laurent *et al.*, 1985; Laurent and Fraser, 1992). In fact, the more advanced the liver disease the higher plasma HA concentrations (Lee *et al.*, 2010; Lee *et al.*, 2013). This is likely due to a combination of increased HA synthesis by hepatic stellate cells (HSC) and other cells, as well as a reduced capacity for HA uptake by dysfunctional liver sinusoidal endothelial cells (LSEC) found in diseased liver (Gressner and Bachem, 1990; Harris *et al.*, 2007; van den Broek *et al.*, 2013). Despite this being known for over 30 years, little additional work has explored if a causative role exists for HA in liver disease. HA does play a role in skin wound healing, which is analogous to hepatic wound healing in that it follows the same steps: injury, inflammation, regeneration, and matrix remodeling

(Pellicoro *et al.*, 2014; Balaji *et al.*, 2015). More specifically, acute hepatic wound healing which does not result in scar formation is analogous to fetal wound healing where elevated HA levels are associated with the scarless wound healing that occurs in fetal tissue (Longaker *et al.*, 1991; Leung *et al.*, 2012). This led us to explore a role for HA in liver wound healing.

Because HAS3 is the most enzymatically active HAS enzyme, we chose to focus on *Has3*<sup>-/-</sup> mice. Additionally, previous literature supports a detrimental role for HA produced by HAS3 in models of lung and intestinal injury. Specifically, in ventilator induced lung injury, *Has3*<sup>-/-</sup> mice are protected from injury and inflammation compared to wild-type mice, and in a DSS-induced mouse model for colitis, *Has3*<sup>-/-</sup> mice are again protected from injury compared to wild-type mice (Bai *et al.*, 2005; Kessler *et al.*, 2015). In this study we tested the hypothesis that HAS3, or HA produced by HAS3, contributes to liver injury and inflammation, similar to what has been shown in the lung and intestine. To test this hypothesis, we utilized the well-characterized carbon tetrachloride (CCl<sub>4</sub>)-induced liver injury model in wild-type mice and mice deficient in HAS3 (Constandinou *et al.*, 2005). We evaluated parameters of injury, as well as the parameters for the subsequent wound healing response, including inflammation, regeneration, and matrix remodeling. Due to a lack of HA synthesized by HAS3, we predicted *Has3*<sup>-/-</sup> mice would exhibit reduced injury, inflammation, and wound healing compared to wild-type mice after acute CCl<sub>4</sub> exposure, similar to the previously published studies (Bai *et al.*, 2005; Kessler *et al.*, 2015).

## **Results**

## **Hepatic *Has* gene transcript accumulation and plasma HA levels in wild-type and *Has3*<sup>-/-</sup> mice**

Real time PCR was used to determine the relative amounts of *Has1*, 2, and 3 in livers from wild-type and *Has3*<sup>-/-</sup> mice, at baseline. The accumulation of *Has1* transcripts was not different between genotypes (Figure 3-1A). *Has3* transcripts were most abundant in livers from wild-type mice and were ~5-fold more than *Has1* transcripts. *Has2* transcripts were least abundant in both genotypes, between 1 – 5 % of total *Has1* levels. However, *Has2* was 40% greater in livers from *Has3*<sup>-/-</sup> mice relative to wild-type mice suggesting this enzyme may compensate, at least in part, for HAS3 deficiency at baseline.

Real time PCR was again used to evaluate hepatic *Has* gene transcript levels after acute CCl<sub>4</sub> exposure. In wild-type mice, *Has1* levels were increased 20-fold above baseline 24 hours after CCl<sub>4</sub> exposure and declined thereafter (Figure 3-1B). In *Has3*<sup>-/-</sup> mice, hepatic *Has1* transcripts also increased 24 hours after CCl<sub>4</sub> exposure, but this level was not different from that found in wild-type mice (Figure 3-1B). *Has1* transcript levels were higher in *Has3*<sup>-/-</sup> mice compared to wild-type mice 72 hours after CCl<sub>4</sub> exposure. *Has2* transcripts peaked in wild-type mice 48 hours after CCl<sub>4</sub> exposure, but only 1.8-fold above baseline, which was not significantly different from basal levels (Figure 3-1C). *Has2* transcripts in *Has3*<sup>-/-</sup> mice also peaked 48 hours after CCl<sub>4</sub> exposure, and this difference was significant at 4-fold over baseline, and again 72 hours after CCl<sub>4</sub> *Has3*<sup>-/-</sup> mice had increased *Has2* transcript levels compared to wild-type mice (Figure 3-1C). Finally, *Has3* transcripts were induced approximately 20-fold over

baseline 24 and 48 hours after CCl<sub>4</sub> exposure in wild-type mice and returned to baseline 72 hours after CCl<sub>4</sub> (Figure 3-1D). Taken together, acute CCl<sub>4</sub> exposure induced all 3 *Has* transcripts in liver; *Has1* and *Has3* were robustly induced. It is possible that the greater induction of *Has1* and *Has2* transcripts in *Has3*<sup>-/-</sup> mice was an attempt to compensate for the lack of the HAS3 enzyme.

Using an ELISA-like assay, we measured plasma HA levels in wild-type and *Has3*<sup>-/-</sup> mice. *Has3*<sup>-/-</sup> mice had reduced plasma HA levels when compared to wild-type mice at baseline, 24 and 48 hours after CCl<sub>4</sub> exposure (Figure 3-1E). HA levels were similar between genotypes at 72 hours but greater in *Has3*<sup>-/-</sup> mice 96 hours after CCl<sub>4</sub> exposure (Figure 3-1E). These data suggested that other HAS enzymes did not completely compensate for reduced HA biosynthetic capacity in *Has3*<sup>-/-</sup> mice. Next, using specific molecular weight cut-off columns to fractionate plasma HA into three groups (<100 kDa, 100 – 300 kDa, and >300 kDa), we found that wild-type mice had more HA in the 100-300 kDa molecular weight range, compared to *Has3*<sup>-/-</sup> mice, while the absolute amounts of HA in the other fractions did not exhibit such large differences between genotypes (Figure 3-1F). However, relative to wild-type mice, *Has3*<sup>-/-</sup> mice exhibited an increased percentage of the <100 kDa HA fraction, decreased percentage of the 100 – 300 kDa fraction and increased percentage of the >300 kDa HA fraction at almost every time point after CCl<sub>4</sub> exposure (Table 3-1). These data suggested that, in addition to a reduction in total HA level, HA molecular mass distribution was also perturbed in *Has3*<sup>-/-</sup> mice, favoring lower molecular weight populations, relative to wild-type mice.

We also evaluated HA content in the liver following acute CCl<sub>4</sub> exposure using HA binding protein (HABP). Using this method, we detected HA in the centrilobular regions of livers from wild-type and *Has3*<sup>-/-</sup> mice after CCl<sub>4</sub> exposure (Figure 3-1G). This is the same area where necrotic cell death occurs. There was no HA present at baseline or 24 hours following CCl<sub>4</sub> (not shown), however HA was detected in *Has3*<sup>-/-</sup> mice 48 hours after CCl<sub>4</sub> exposure; very little HA was observed in livers from wild-type mice at this time point (Figure 3-1G and H). Surprisingly, despite *Has3*<sup>-/-</sup> mice lacking one enzyme responsible for HA synthesis, there was more HA present in the *Has3*<sup>-/-</sup> mice compared to wild-type mice 48 and 72 hours after CCl<sub>4</sub> exposure. Together, these data demonstrate that *Has3* has the highest expression in wild-type mouse liver at baseline and acute liver injury increases expression of all *Has* enzymes in both wild-type and *Has3*<sup>-/-</sup> mice. Increased *Has* expression in wild-type mice results in increased HA in the plasma and in the centrilobular region of the liver, however as the liver heals, the plasma HA and hepatic HA return to baseline. These data also demonstrate that *Has3*<sup>-/-</sup> mice compensate for the lack of HAS3 and have increased hepatic HA accumulation compared to wild-type mice. However, content and the size distribution of plasma HA is perturbed and could lead to differences in hepatic injury and healing following acute CCl<sub>4</sub> exposure.

### **Liver injury and steatosis after acute CCl<sub>4</sub> exposure**

CCl<sub>4</sub> induced liver injury in both strains of mice, but this injury was greater in livers from *Has3*<sup>-/-</sup> mice. Specifically, peak plasma ALT activity occurred in both wild-type and *Has3*<sup>-/-</sup> mice 48 hours after CCl<sub>4</sub> exposure but ALT activity was 41% greater in

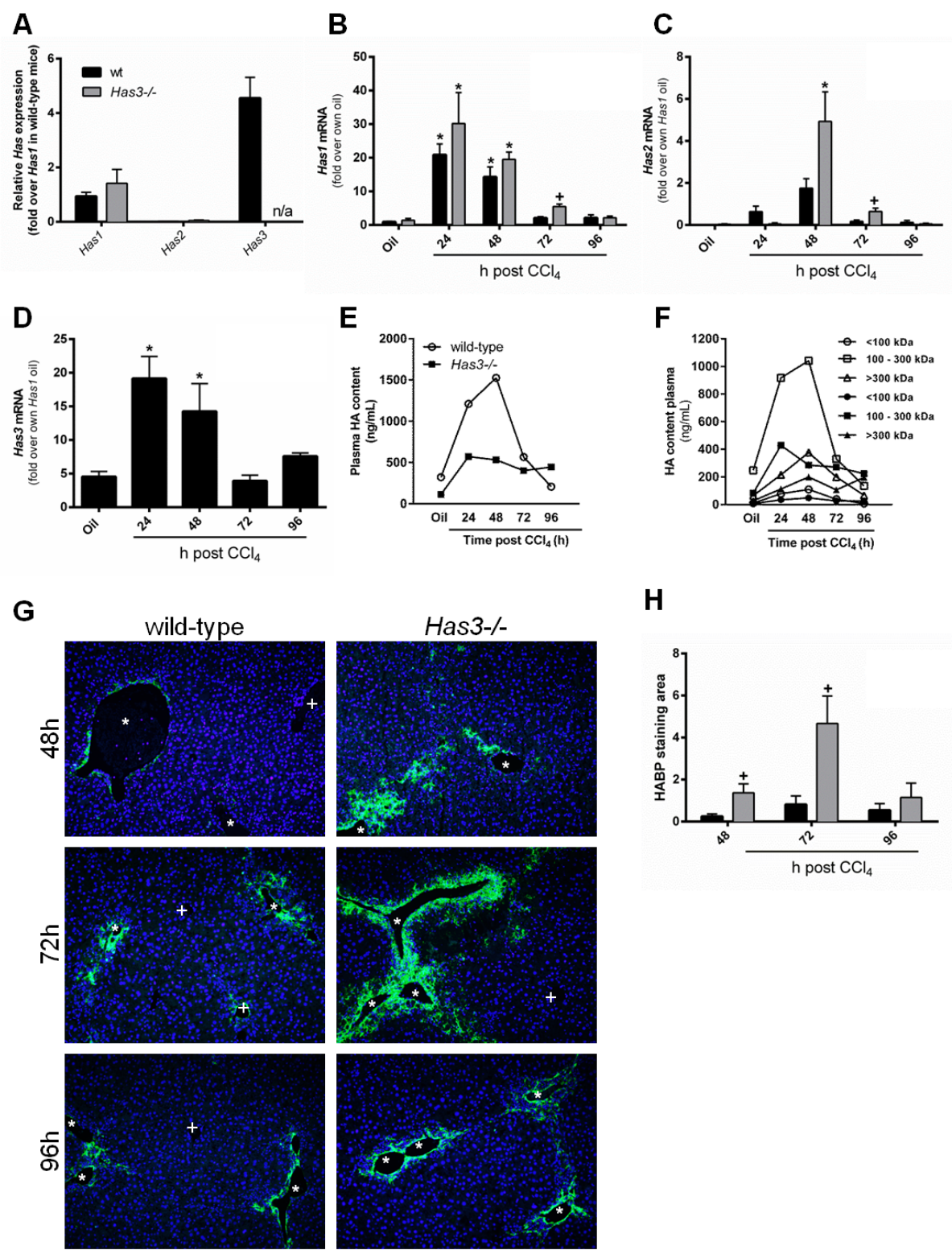


**Figure 3-1: Hepatic *Has* enzymes, plasma HA levels, and hepatic HA accumulation in wild-type and *Has3*<sup>-/-</sup> mice.**

A. Real time PCR was used to measure basal levels of hepatic *Has* enzyme transcript accumulation in wild-type and *Has3*<sup>-/-</sup> mice. B – D. Mice were exposed to CCl<sub>4</sub> and euthanized 24, 48, 72 or 96 hours later. Control animals received an olive oil (Oil) injection. Real time PCR was used to measure hepatic *Has1* (B), *Has2* (C) and *Has3* (D) in livers from wild-type and *Has3*<sup>-/-</sup> mice. Here and throughout this chapter, data were calculated using the  $2^{-\Delta\Delta Ct}$  method after normalization to 18S. Data in A-D are expressed as fold change over wild-type hepatic *Has1* content. An ELISA-like assay (see Material and Methods for details on this antibody-independent assay) was used to determine HA concentration in pooled plasma from wild-type and *Has3*<sup>-/-</sup> mice either before (E) or after (F) HA fractionation using molecular weight cut-off columns. In E and F, open symbols indicate wild-type mice while closed symbols indicated *Has3*<sup>-/-</sup> mice. Circles indicate HA pools less than 100 kDa, squares indicate HA pools between 100 – 300 kDa and triangles indicate HA pools greater than 300 kDa. Statistical analysis was not performed on these pooled samples. See Table 3-1 for additional details. G. Representative images and H. quantification of HABP staining used to localize hepatic HA accumulation in wild-type and *Has3*<sup>-/-</sup> mice 48, 72, and 96 hours after CCl<sub>4</sub> exposure. \* denotes central veins and + signs denotes the portal triad in images. All data is presented as mean + SEM and throughout this chapter black bars represent wild-type mice and grey bars represent *Has3*<sup>-/-</sup> mice. \* represents p<0.05 when comparing CCl<sub>4</sub> exposure to baseline within a genotype, + represents p<0.05 when comparing wild-type and *Has3*<sup>-/-</sup> mice within a time point n/a = not applicable. N = 6 – 8 mice per experimental group.

<b>Group</b>	<b>&lt;100kDa (ng/mL)</b>	<b>% of total</b>	<b>100- 300kDa (ng/mL)</b>	<b>% of total</b>	<b>&gt;300kDa (ng/mL)</b>	<b>% of total</b>	<b>Total (ng/mL)</b>
<i>Wild-type mice</i>							
Oil	10	3	247	22	64	20	322
24h	78	6	917	76	215	18	1210
48h	109	7	1041	68	376	25	1526
72h	38	7	330	58	199	35	567
96h	7	3	135	65	66	32	208
<i>Has3<sup>-/-</sup> mice</i>							
Oil	6	5	82	72	27	23	115
24h	34	3	428	75	112	20	574
48h	48	9	285	54	199	37	532
72h	26	7	271	67	106	26	403
96h	26	6	223	50	196	44	445

Table 3-1: Total and fractionated plasma HA content in wild-type and *Has3<sup>-/-</sup>* mice after acute CCl<sub>4</sub> exposure.

*Has3*<sup>-/-</sup> mice relative to control mice 48 hours after CCl<sub>4</sub> exposure (Figure 3-2A). By 72 hours post CCl<sub>4</sub> exposure, ALT activity had decreased in both wild-type and *Has3*<sup>-/-</sup> mice, but *Has3*<sup>-/-</sup> mice still had higher ALT levels compared to wild-type mice. Consistent with increased plasma ALT values; hepatic architecture was more severely disrupted in *Has3*<sup>-/-</sup> mice 48 hours after CCl<sub>4</sub> exposure (Figure 3-2D). Specifically, histopathological assessment revealed more necrosis in livers from *Has3*<sup>-/-</sup> mice compared to wild-type mice at peak injury, 48 hours post CCl<sub>4</sub> exposure (Figure 3-2B and D).

Hepatic triglyceride accumulation increased 24 hours after CCl<sub>4</sub> in both genotypes, and was 31% greater in HAS3-deficient mice compared to controls (Figure 3-2B). Liver histology paralleled this biochemical measure of the liver's response to CCl<sub>4</sub> in wild-type and *Has3*<sup>-/-</sup> mice (Figure 3-2D). Increased macrovesicular steatosis was more abundant in livers from *Has3*<sup>-/-</sup> mice compared to wild-type mice 24 hours after CCl<sub>4</sub> (Figure 3-2D). Together, these data demonstrate *Has3*<sup>-/-</sup> mice have increased injury and steatosis compared to wild-type mice following acute CCl<sub>4</sub> exposure.

CCl<sub>4</sub> must be bioactivated by cytochrome P450 2E1 (CYP2E1) to reactive metabolites to induce hepatotoxicity (Wong *et al.*, 1998; Weber *et al.*, 2003). To ensure that the increased liver injury in *Has3*<sup>-/-</sup> mice was not due to differences in CCl<sub>4</sub> bioactivation, we measured CYP2E1 protein levels (Figure 3-3A and B). There was no difference in baseline CYP2E1 protein between genotypes. We also measured CYP2E1 activity by measuring the hydroxylation of p-nitrophenol to p-nitrocatechol. Again, similar to CYP2E1 total protein, there was no difference in CYP2E1 activity (Figure 3-3C)

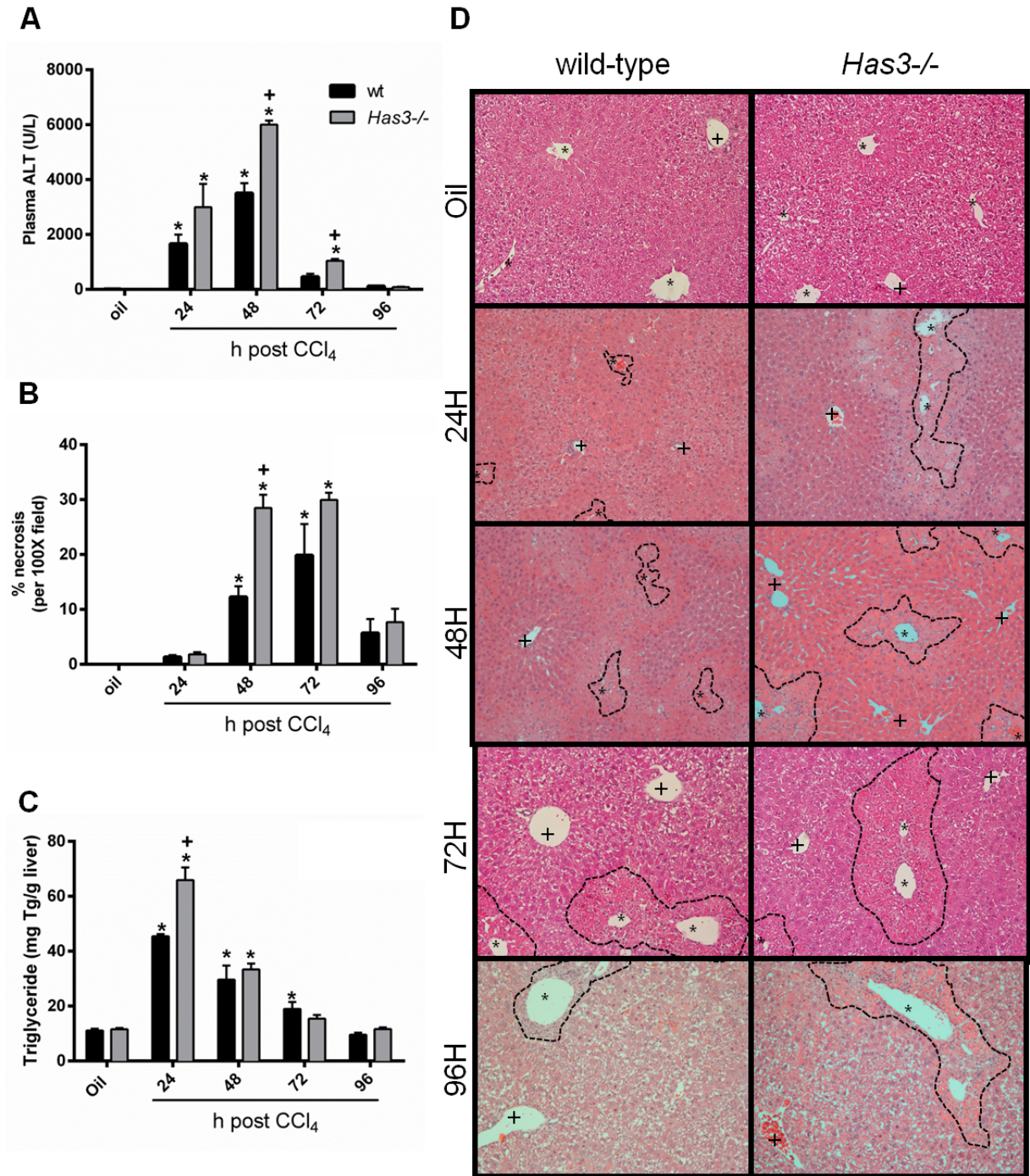
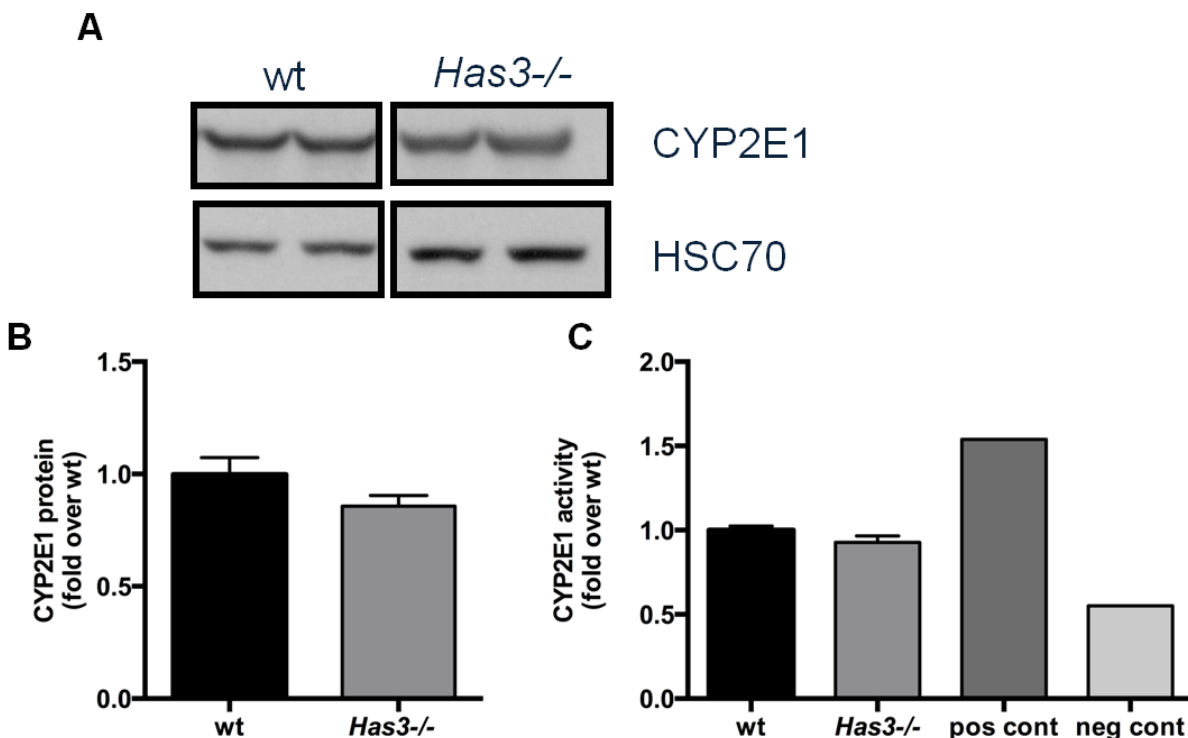


Figure 3-2: Liver injury and steatosis in wild-type and *Has3*<sup>-/-</sup> mice.

Mice were exposed to CCl<sub>4</sub> and euthanized 24, 48, 72 or 96 hours later. Control animals received an olive oil (oil) injection. A. Plasma ALT activity was determined using an enzymatic assay. B. Histopathologic assessment of the percent necrosis. C. Total hepatic triglycerides were measured using a biochemical assay. D. Representative H&E histology in wild-type and *Has3*<sup>-/-</sup> mice (200X). \* denotes central veins and + signs denotes the portal triads in H&E images. The necrotic areas are outlined with black dashed lines. \* represents p<0.05 when comparing CCl<sub>4</sub> exposure to baseline within a genotype, + represents p<0.05 when comparing wild-type and *Has3*<sup>-/-</sup> mice within a time point. N = 4 – 7 mice per experimental group.



**Figure 3-3: CYP2E1 content and activity in wild-type and *Has3*<sup>-/-</sup> mice.**

A. Representative CYP2E1 immunoblot using samples from olive oil-treated wild-type and *Has3*<sup>-/-</sup> mice. GAPDH was used as a loading control. B. Semi-quantification of hepatic CYP2E1 content after normalization to GAPDH. Data are expressed as fold change over wild-type mice. C. Hepatic CYP2E1 activity assay using microsomes isolated from wild-type and *Has3*<sup>-/-</sup> mice at baseline (before CCl<sub>4</sub> exposure). The data are expressed as fold-change over wild-type. N = 6 mice per experimental group. Pos cont: microsomes prepared from a single mouse fed an ethanol-containing diet for 5 weeks (ethanol increases CYP2E1). Neg cont: microsomes prepared from a single mouse exposed to CCl<sub>4</sub> and euthanized 24h later (CCl<sub>4</sub> consumptively depletes CYP2E1).

suggesting that a difference in CCl<sub>4</sub> bioactivation was not contributing to the increase in liver injury observed in *Has3*<sup>-/-</sup> mice. Surprisingly, and in contrast to the pathogenic role HAS3 plays in injury in other animal models of human disease, our data suggest that HA produced by HAS3 plays a protective role in the liver after acute CCl<sub>4</sub> exposure.

### **Hepatic inflammatory environment after acute CCl<sub>4</sub> exposure in wild-type and *Has3*<sup>-/-</sup> mice**

Inflammation follows injury and can both exacerbate injury and contribute to tissue repair (Duffield *et al.*, 2005; You *et al.*, 2013; Mohanraj *et al.*, 2014). Thus, we next investigated the impact of HAS3-deficiency on hepatic inflammation. While pro-inflammatory markers increased in livers from both strains of mice after CCl<sub>4</sub> exposure, these markers tended to be greater in *Has3*<sup>-/-</sup> mice compared to wild-type mice. Specifically, *Ccl2* transcripts, a chemokine vital to macrophage migration (Lu *et al.*, 1998; Baeck *et al.*, 2012), are increased in *Has3*<sup>-/-</sup> mice compared to wild-type mice 48 hours after CCl<sub>4</sub> exposure (Figure 3-4A). Similarly, hepatic transcript levels of *Cxcl10*, another chemokine important for the migration of inflammatory cells including macrophages (Tomita *et al.*, 2016), showed the same trend as *Ccl2*. *Cxcl10* is induced in both wild-type and *Has3*<sup>-/-</sup> mice following CCl<sub>4</sub> exposure and was greater in *Has3*<sup>-/-</sup> mice compared to wild-type mice 48 hours post CCl<sub>4</sub> exposure (Figure 3-4B). Hepatic transcript levels of *Cxcl1*, a chemokine that is more important in neutrophil migration following injury (Dominguez *et al.*, 2009; Chang *et al.*, 2015a), increased in both wild-type and *Has3*<sup>-/-</sup> mice, but the increase was not different between genotypes at any time point (Figure 4C). Consistent with the gene expression analysis, using a cytokine

protein array to evaluate plasma inflammatory mediator levels 48 hours after CCl<sub>4</sub>, we found plasma CCL2, CXCL10, and CXCL1 chemokine proteins were also increased in *Has3*<sup>-/-</sup> mice compared to wild-type mice at the time of peak injury (Figure 3-4D – F). Evaluation of the mouse macrophage marker *Emr1* revealed a peak of hepatic transcripts 72 hours post CCl<sub>4</sub> exposure (Figure 3-4G). *Has3*<sup>-/-</sup> mice had increased *Emr1* levels compared to wild-type mice 48 hours post CCl<sub>4</sub> exposure. High *Cd11b* expression is associated with pro-inflammatory, infiltrating macrophages after acute liver injury (Mohanraj *et al.*, 2014), however there was no difference in the accumulation of *Cd11b* transcripts at any time point between wild-type and *Has3*<sup>-/-</sup> mice (Figure 3-4H). *Ccr2*, the receptor for CCL2, increased in both genotypes following acute CCl<sub>4</sub> exposure, but was not different between wild-type and *Has3*<sup>-/-</sup> mice at any time point (Figure 3-4I). This suggests that although the inflammatory microenvironment is increased, there may not be an increase in hepatic macrophage content.

#### **Hepatic regeneration following acute CCl<sub>4</sub> exposure in wild-type and *Has3*<sup>-/-</sup> mice.**

The wound healing process continues following injury and inflammation and includes regeneration. Acute CCl<sub>4</sub> exposure causes massive centrilobular necrosis leading to loss of liver mass and function so liver regeneration is required to restore the functional capacity of the liver (Michalopoulos and DeFrances, 1997). We evaluated the hepatic expression of proteins vital to the cell cycle. *Ccnd1* (Cyclin D1) is important throughout the cell cycle and *Ccnd1* transcripts were increased in both genotypes following acute CCl<sub>4</sub> exposure (Figure 3-1A), peaking at 48 hours post CCl<sub>4</sub> exposure. *Ccnd1* transcript levels were increased in *Has3*<sup>-/-</sup> mice compared to wild-type mice 48

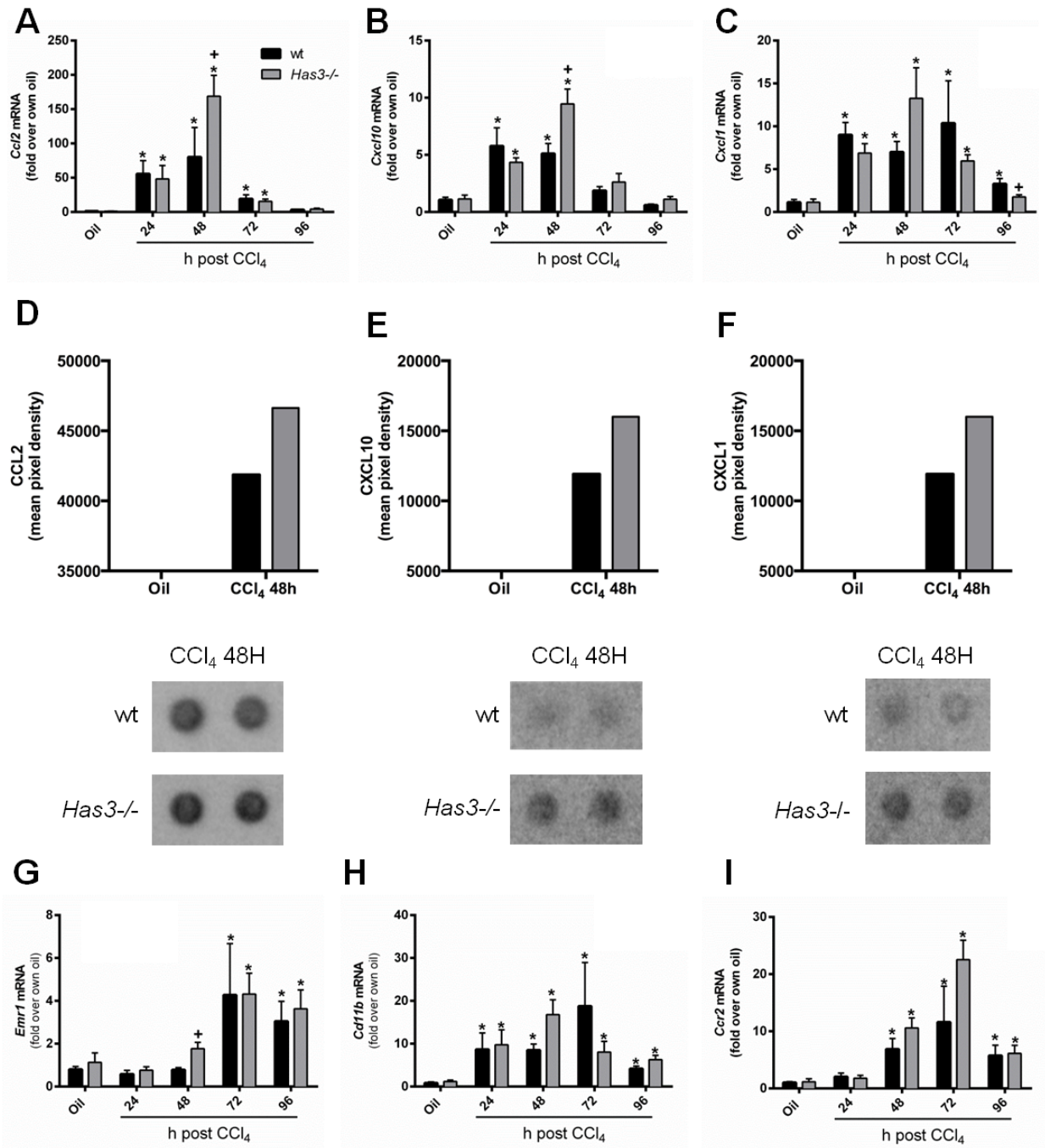


Figure 3-4: Hepatic and plasma chemokine content in wild-type and *Has3*<sup>-/-</sup> mice.

Mice were exposed to CCl<sub>4</sub> and euthanized 24, 48, 72, and 96 hours later. Control animals received an olive oil (oil) injection. Real time PCR was used to measure relative levels of A. *Ccl2*, B. *Cxcl10*, and C. *Cxcl1* transcripts in both genotypes. Data are expressed as fold change over each genotypes' own oil. Plasma isolated from blood collected 48 hours after CCl<sub>4</sub> exposure and pooled to determine the relative amounts of CCL2 (D), CXCL1 (E), CXCL10 (F) peptides using a protein array. For this assay, plasma samples were pooled per experimental group (n = 6 – 8 mice). The bar graphs in D – F were created after semi-quantification of chemokine spot density from the array shown directly below each graph. Real time PCR was used to measure hepatic transcript levels of G. *Emr1*, H. *Cd11b*, and I. *Ccr2* in wild-type and *Has3*<sup>-/-</sup> mice after acute CCl<sub>4</sub> exposure. Data are expressed as fold change over each genotypes' own oil. \* represents p<0.05 when comparing CCl<sub>4</sub> exposure to baseline within a genotype, + represents p<0.05 when comparing wild-type and *Has3*<sup>-/-</sup> mice within a time point N = 4 – 7 mice per experimental group.

and 72 hours after CCl<sub>4</sub> exposure. Cyclin D1 protein levels increased in both genotypes, and similar to *Ccnd1* expression pattern, the levels were higher in *Has3*<sup>-/-</sup> mice, compared to baseline, 48 and 72 hours after CCl<sub>4</sub> exposure (Figure 3-5B and C). Hepatic accumulation of proliferating cell nuclear antigen (*Pcna*) transcript, another component of cell cycle regulation, showed a delay in regeneration in *Has3*<sup>-/-</sup> mice with the levels of *Pcna* being lower in *Has3*<sup>-/-</sup> mice compared to wild-type mice 24 and 48 hours after CCl<sub>4</sub> exposure (Figure 3-5D). This trend is opposite that seen in *Ccnd1* mRNA expression. However, PCNA protein follows a similar trend as Cyclin D1 protein. PCNA was higher in *Has3*<sup>-/-</sup> mice compared to wild-type mice at both 48 and 72 hours after CCl<sub>4</sub> exposure (Figure 3-5E and F). *Has3*<sup>-/-</sup> mice also had increased Ki67 positive cells at 48, 72, and 96 hours post CCl<sub>4</sub> exposure compared to wild-type mice (Figure 3-6A and B). Together, these data suggest that following increased injury and increased pro-inflammatory microenvironment, hepatic regeneration is increased in *Has3*<sup>-/-</sup> mice compared to wild-type mice.

### **Matrix remodeling following acute CCl<sub>4</sub> exposure in wild-type and *Has3*<sup>-/-</sup> mice.**

Matrix remodeling consists of two stages: matrix synthesis and matrix degradation. Acute CCl<sub>4</sub> exposure induces activation of HSC, cells integral to hepatic wound healing. HSC are the main cell type in the liver that produce ECM components, including HA, after acute liver injury (Friedman, 2008a; Perepelyuk *et al.*, 2013). Many factors contribute to HSC activation including proinflammatory cytokines, oxidative stress, and phagocytosis of tissue debris (Nieto *et al.*, 2002; Imamura *et al.*, 2005; Zhan *et al.*, 2006; Friedman, 2008a; He *et al.*, 2015). Because liver injury and inflammation

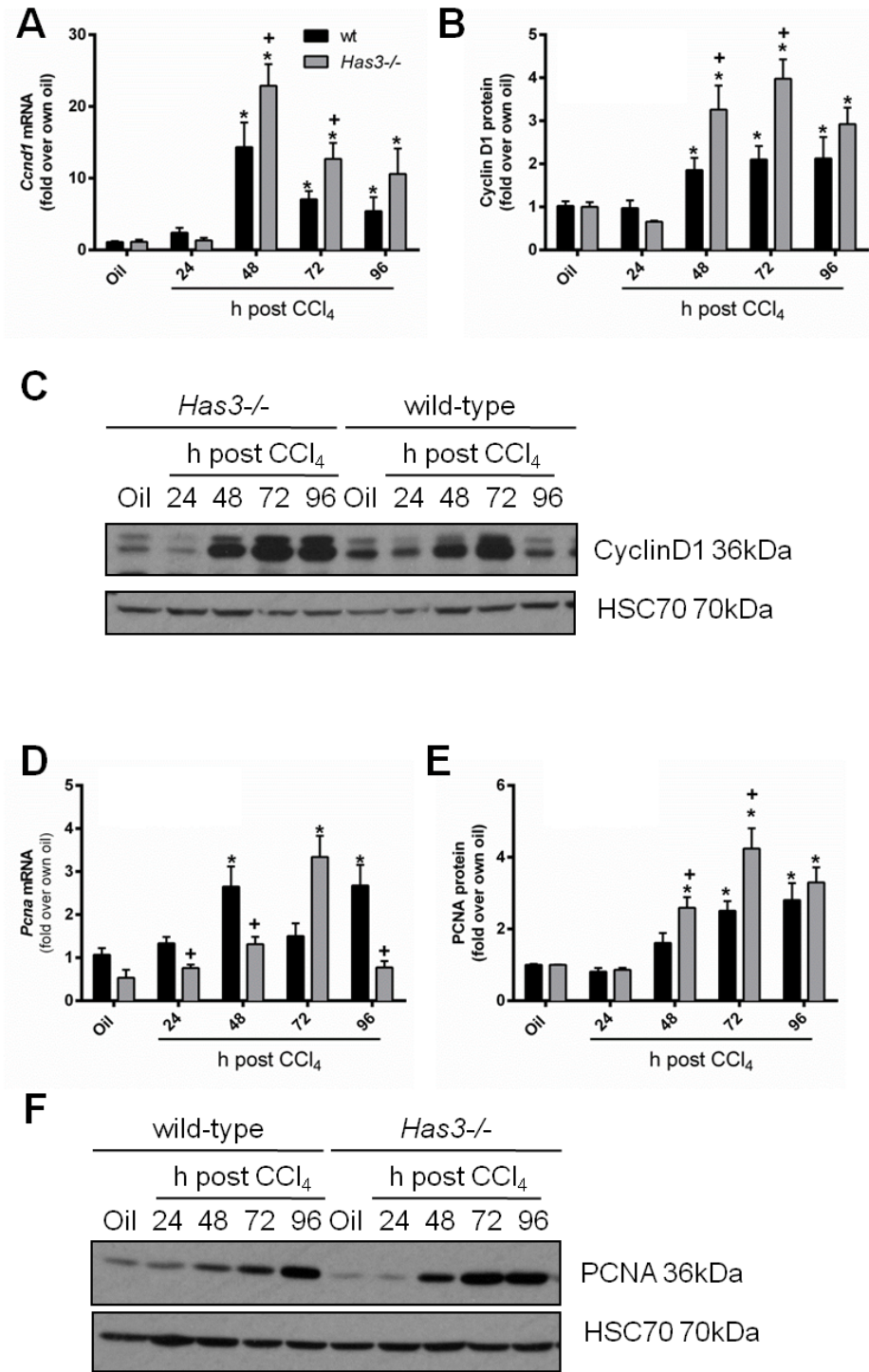


**Figure 3-5: Hepatic regeneration following acute CCl<sub>4</sub> exposure.**

Mice were exposed to CCl<sub>4</sub> and euthanized 24, 48, 72, and 96 hours later. Control animals received an olive oil (oil) injection. A. Hepatic *Ccnd1* transcript levels were measured using real-time PCR. B. Quantification and C. representative Cyclin D1 western blot. HSC70 was used as a loading control. D. Real-time PCR was used to evaluate hepatic *Pcna* transcript levels. E. Quantification and F. representative PCNA Western blot. HSC70 was used as a loading control. All data are expressed as fold change over each genotype's own baseline. \* represents p<0.05 when comparing CCl<sub>4</sub> exposure to baseline within a genotype, + represents p<0.05 when comparing wild-type and *Has3*<sup>-/-</sup> mice within a time point. N = 4 – 7 mice per experimental group.

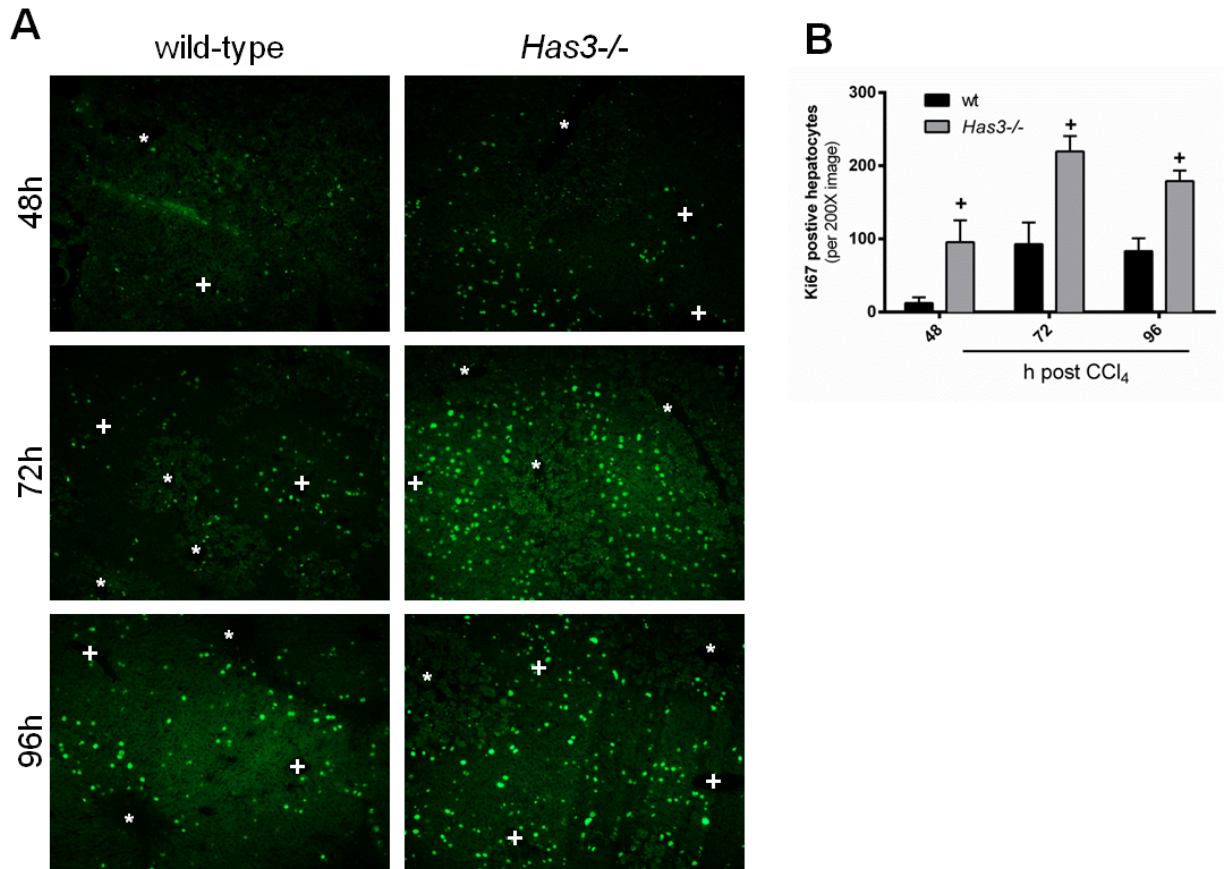


**Figure 3-6: Ki67 positive hepatocytes after acute CCl<sub>4</sub> exposure.**

Mice were exposed to CCl<sub>4</sub> and euthanized 48, 72, or 96 hours later. A. Representative images of Ki67-positive, regenerating hepatocytes. \* denotes central veins and + signs denotes the portal triads in images. B. Quantification of the number of Ki67-positive hepatocytes per 200X image, 3-5 images counted per sample. + represents  $p < 0.05$  comparing wild-type and *Has3*<sup>-/-</sup> mice within a time point. N = 4 – 7 mice per experimental group.

were increased in *Has3*<sup>-/-</sup> mice after acute CCl<sub>4</sub> exposure and we observed increased hepatic HA content in *Has3*<sup>-/-</sup> mice compared to wild-type mice, we predicted that HSC activation would also be increased. After acute CCl<sub>4</sub> exposure, markers associated with HSC activation were increased in both mouse strains. Several of these markers were greater in livers from *Has3*<sup>-/-</sup> mice. Specifically, using real-time PCR, we found that hepatic pro-fibrotic growth factor transcript accumulation, transforming growth factor (*Tgf*) *b1*, and connective tissue growth factor (*Ctgf*), were increased in both wild-type and *Has3*<sup>-/-</sup> mice following acute CCl<sub>4</sub>. Both transcripts were increased in livers from *Has3*<sup>-/-</sup> mice compared to wild-type mice at 48 hours after CCl<sub>4</sub> exposure (Figure 3-7A and B). Consistent with a role for these mediators in HSC activation, hepatic *Acta2* ( $\alpha$  smooth muscle actin,  $\alpha$ SMA) transcript, a marker for HSC activation, is also increased in *Has3*<sup>-/-</sup> mice relative to wild-type mice 48 and 72 hours post-CCl<sub>4</sub> exposure (Figure 3-7C). Despite increased transcript accumulation, the protein level of  $\alpha$ SMA was not different between genotypes at any time point after CCl<sub>4</sub> exposure (Figure 3-7D and E). Activated HSC make type I collagen (*Col1a1*, *Col1a2*), mRNAs for which increased in both wild-type and *Has3*<sup>-/-</sup> mice following CCl<sub>4</sub> exposure (Figure 3-7F and G). *Col1a1* transcript accumulation was greater 48 and 72 hours after CCl<sub>4</sub> exposure in *Has3*<sup>-/-</sup> mice relative to wild-type mice at the same time point. Similarly, *Col1a2* transcript levels were higher in *Has3*<sup>-/-</sup> mice compared to wild-type mice 72 hours after CCl<sub>4</sub> exposure. *Serpinh1* transcripts (the gene for heat shock protein (HSP) 47-a collagen-specific chaperone) increased following acute CCl<sub>4</sub> exposure in both wild-type and *Has3*<sup>-/-</sup> mice and was increased in *Has3*<sup>-/-</sup> mice relative to wild-type mice at 48 and 72 hours after acute CCl<sub>4</sub> exposure (Figure 3-7H). However, and similar to  $\alpha$ SMA, HSP47 protein

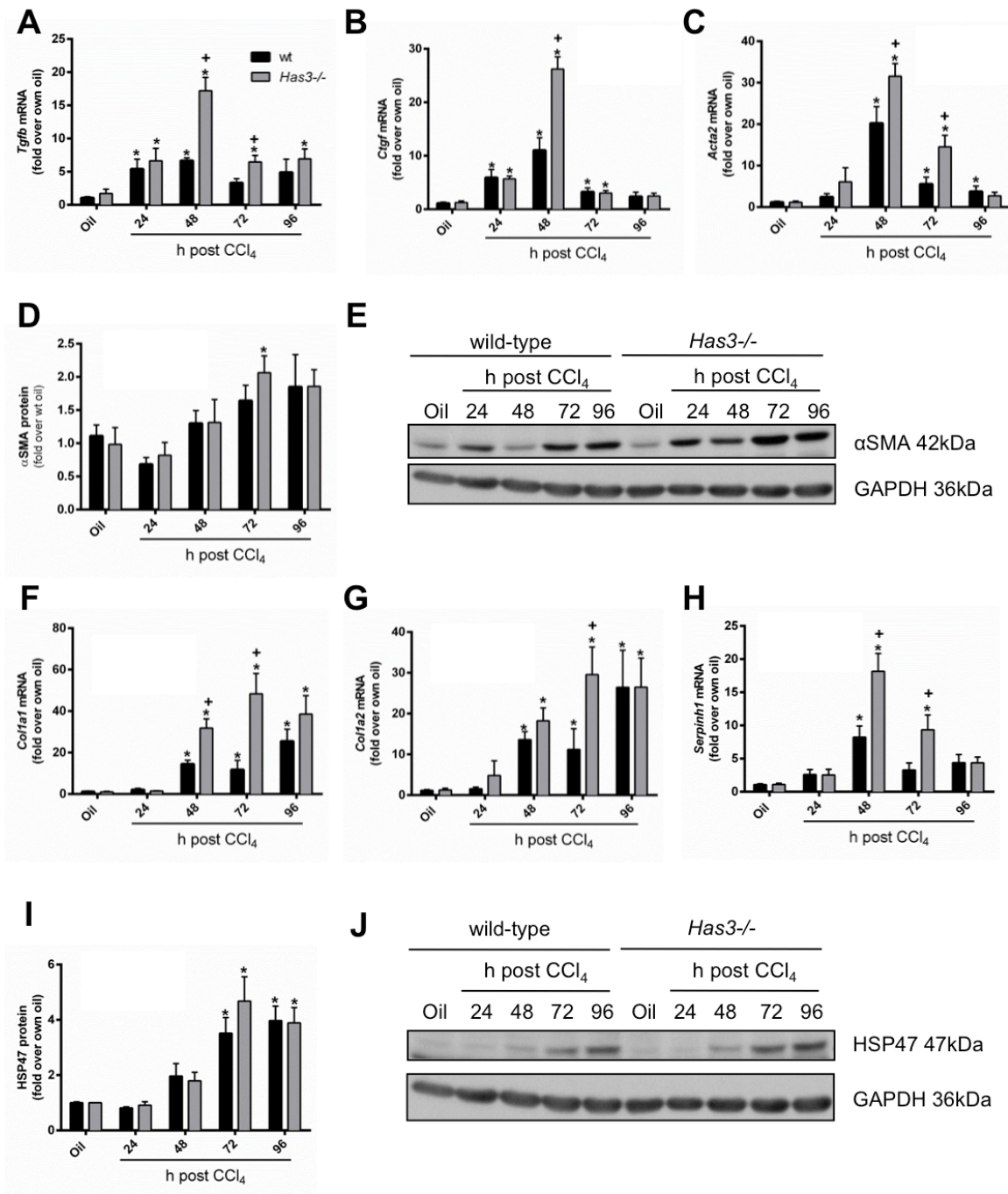


**Figure 3-7: Hepatic stellate cell activation markers in wild-type and *Has3*<sup>-/-</sup> mice after acute CCl<sub>4</sub> exposure.**

Mice were exposed to CCl<sub>4</sub> and euthanized 24, 48, 72, or 96 hours later. Control animals received an olive oil (oil) injection. Hepatic A. *Tgfb1*, B. *Ctgf*, C. *Acta2*, were measured using real time PCR and are expressed as fold change over each strain's oil control. D. Quantification and E. representative  $\alpha$ SMA western blot. GAPDH was used as a loading control. Hepatic F. *Col1a1*, G. *Col1a2* and H. *Serpinh1* were measured using real-time PCR. The data are expressed as fold change over each strain's oil control. I. Quantification and J. representative HSP47 western blot. GAPDH was used as a loading control. \* represents  $p < 0.05$  when comparing CCl<sub>4</sub> exposure to baseline within a genotype, + represents  $p < 0.05$  when comparing wild-type and *Has3*<sup>-/-</sup> mice within a time point. N = 4 – 7 mice per experimental group.

levels were not different between the genotypes (Figure 3-7I andJ). Collectively, these data demonstrate that increased injury and inflammation in *Has3*<sup>-/-</sup> mice is associated with more robust expression of genes involved in the hepatic wound healing response after acute CCl<sub>4</sub> but not an increase in the proteins associated with HSC activation.

Matrix remodeling includes not only matrix synthesis by activated HSC but also matrix degradation, which is primarily accomplished by recruited macrophages (Duffield *et al.*, 2005; Fallowfield *et al.*, 2007b). There are several matrix metalloproteinases (MMPs) synthesized following hepatic injury. *Mmp2* and *Mmp9* are two gelatinases (Hemmann *et al.*, 2007; Duarte *et al.*, 2015) that increase following CCl<sub>4</sub> exposure in both genotypes. *Mmp2* transcripts did not increase until 96 hours after CCl<sub>4</sub> exposure and were not different between wild-type and *Has3*<sup>-/-</sup> mice at any time point (Figure 3-8A). *Mmp9* increased earlier relative to *Mmp2* in both genotypes, increasing above baseline levels at 24 and 48 hours post CCl<sub>4</sub> exposure but again was not different between genotypes (Figure 3-8B). *Mmp13* is the main mouse collagenase and is equivalent to *Mmp1* in humans (Hemmann *et al.*, 2007). Hepatic transcripts of *Mmp13* were induced 24 and 48 hours after CCl<sub>4</sub> exposure in both genotypes (Figure 3-8C). These transcripts were higher in *Has3*<sup>-/-</sup> mice compared to wild-type mice 48 and 72 hours post-CCl<sub>4</sub> exposure. Tissue inhibitors of MMPs (TIMPs) inhibit MMPs (Hemmann *et al.*, 2007). *Timp1* was increased in both genotypes following CCl<sub>4</sub> exposure and was not different between genotypes at any time point (Figure 3-8D).

Real time PCR does not provide data on MMP enzymatic activity. To determine this, alternative techniques must be used. *In situ* zymography (ISZ) is a technique that allows visualization of active areas of matrix degradation (Lindsey *et al.*, 2001; Yan and

Blomme, 2003). To perform ISZ, a dye quenched gelatin or collagen suspended in an enzymatically permissive buffer is layered on top of freshly cut, OCT-embedded liver sections and placed at 37°C overnight. Any place in the liver section where gelatinase or collagenase activity is present will result in green fluorescence, which can be recorded and quantified using standard morphometry techniques (Lindsey *et al.*, 2001; Yan and Blomme, 2003). We used ISZ to evaluate matrix degradation activity in livers from *Has3*<sup>-/-</sup> and wild-type mice and it revealed that *Has3*<sup>-/-</sup> mice had increased gelatinase activity (matrix degradation) relative to wild-type mice 72 hours post CCl<sub>4</sub> exposure (Figure 3-8E-G). Because MMP13 can activate MMP2 and MMP9 (Leeman *et al.*, 2002), these data suggest that the observed increase in matrix degradation observed in *Has3*<sup>-/-</sup> mice is likely due to the increased *Mmp13* seen at the transcript level.

#### **HA receptor expression in wild-type and *Has3*<sup>-/-</sup> mice following acute CCl<sub>4</sub> exposure.**

HA interacts with several different receptors expressed on various cell types. Using real time PCR, we evaluated the expression of many of these receptors in wild-type and *Has3*<sup>-/-</sup> mice following acute CCl<sub>4</sub> exposure. *Cd44* is the most well characterized HA receptor and plays a role in cell migration and adhesion (Marhaba and Zoller, 2004; McDonald and Kubes, 2015). *Cd44* expression increased in both genotypes following acute CCl<sub>4</sub> exposure and at 48 hours post CCl<sub>4</sub> it was increased in *Has3*<sup>-/-</sup> mice compared to wild-type mice (Figure 3-9A). Toll like receptors (TLR) also interact with HA and are required for HA-stimulated inflammatory signals

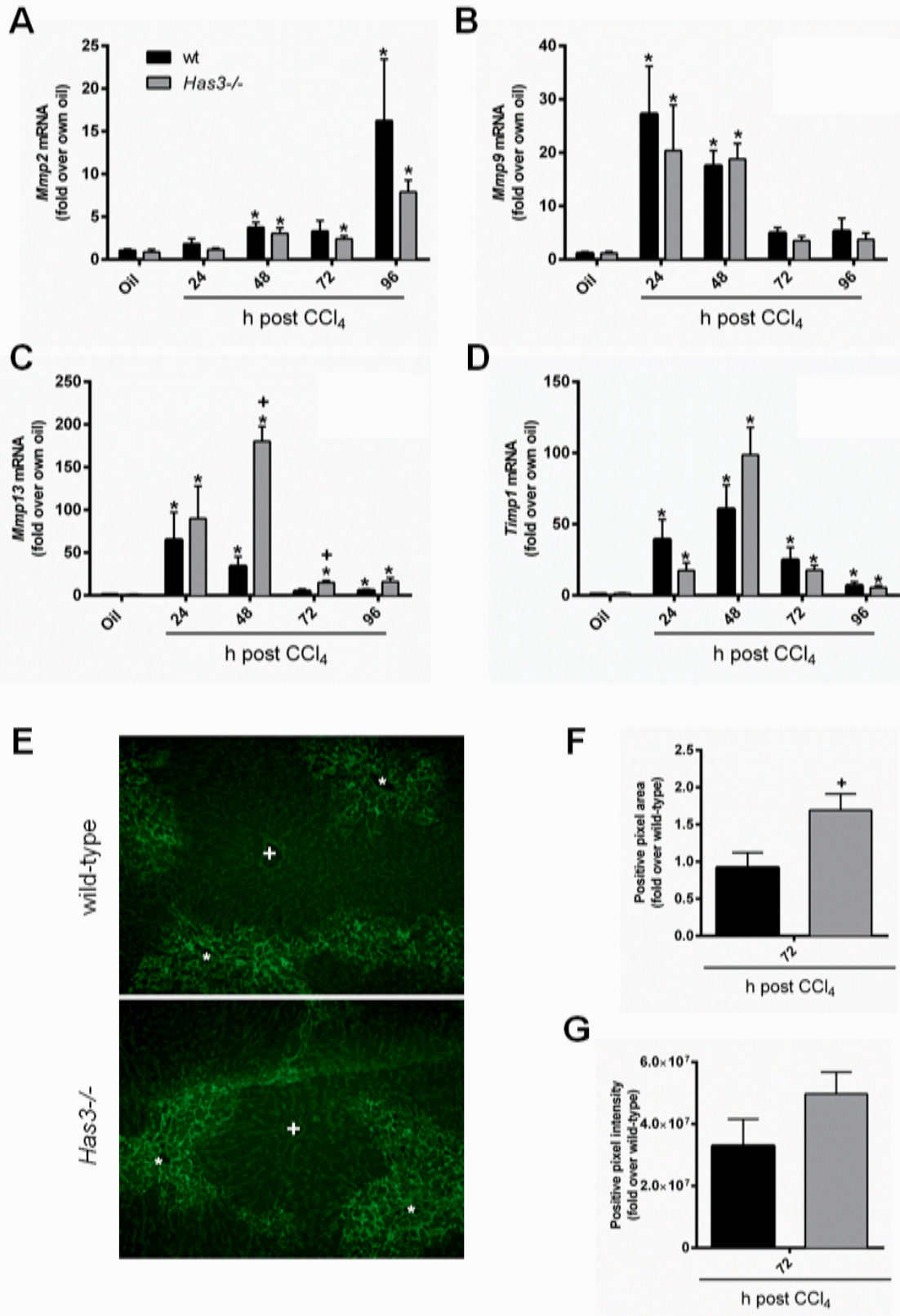


Figure 3-8: Hepatic matrix degradation after acute CCl<sub>4</sub> exposure.

Mice were exposed to CCl<sub>4</sub> and euthanized 24, 48, 72, or 96 hours later. Control mice received an olive oil (oil) injection. Hepatic transcript accumulation of A. *Mmp2*, B. *Mmp9*, C. *Mmp13*, D. *Timp1* were measured using real-time PCR. Data are expressed as fold change over each strain's own oil control. E. Representative *in situ* zymography showing active matrix metabolism. \* denotes central veins and + signs denotes the portal triads in images. F. Area and G. intensity of positive *in situ* zymography as a measure of total matrix metabolism. \* represents p<0.05 when comparing CCl<sub>4</sub> exposure to baseline within a genotype, + represents p<0.05 when comparing wild-type and *Has3*<sup>-/-</sup> mice within a time point N. = 4 – 7 mice per experimental group.

(Jiang *et al.*, 2005; Jiang *et al.*, 2011; Sokolowska *et al.*, 2014). *Tlr2* increases in both genotypes following acute CCl<sub>4</sub> exposure and the transcript levels were higher in *Has3*<sup>-/-</sup> mice compared to wild-type mice 48 hours post CCl<sub>4</sub> exposure (Figure 3-9B). Similarly, *Tlr4* expression increased in both wild-type and *Has3*<sup>-/-</sup> mice following CCl<sub>4</sub> exposure, however the increase was not different between genotypes at any time point (Figure 3-9C). The receptor with the highest induction after acute CCl<sub>4</sub> and the biggest differential expression between genotypes was HA mediated motility receptor (*Hmmr*). HMMR plays roles in macrophage and fibroblast migration (Zaman *et al.*, 2005; Tolg *et al.*, 2012) and in spindle pole stability (Maxwell *et al.*, 2003; Tolg *et al.*, 2010). Transcript levels for *Hmmr* were not increased above baseline until 48 hours in either genotype, however they were then robustly increased (Figure 3-9D). At 48 and 72 hours post CCl<sub>4</sub>, expression of *Hmmr* was almost 200-fold higher in *Has3*<sup>-/-</sup> mice compared to wild-type mice (Figure 3-9D). HMMR protein showed a similar trend, albeit not as dramatic. HMMR protein was increased in *Has3*<sup>-/-</sup> mice compared to wild-type mice 48 hours post CCl<sub>4</sub> and there was a trend toward a difference 72 hours post CCl<sub>4</sub> (Figure 3-9E and F). Taken together, the many differences observed between wild-type and *Has3*<sup>-/-</sup> mice in injury, inflammation, regeneration, and matrix remodeling suggest that HA and possibly interactions between HA with one or more of its receptors play critical roles in liver injury and wound healing following acute CCl<sub>4</sub> exposure.

## **Discussion**

Despite a well-appreciated role for plasma HA as a hepatic function biomarker, few studies have explored a possible role for HA in the pathogenesis of liver disease

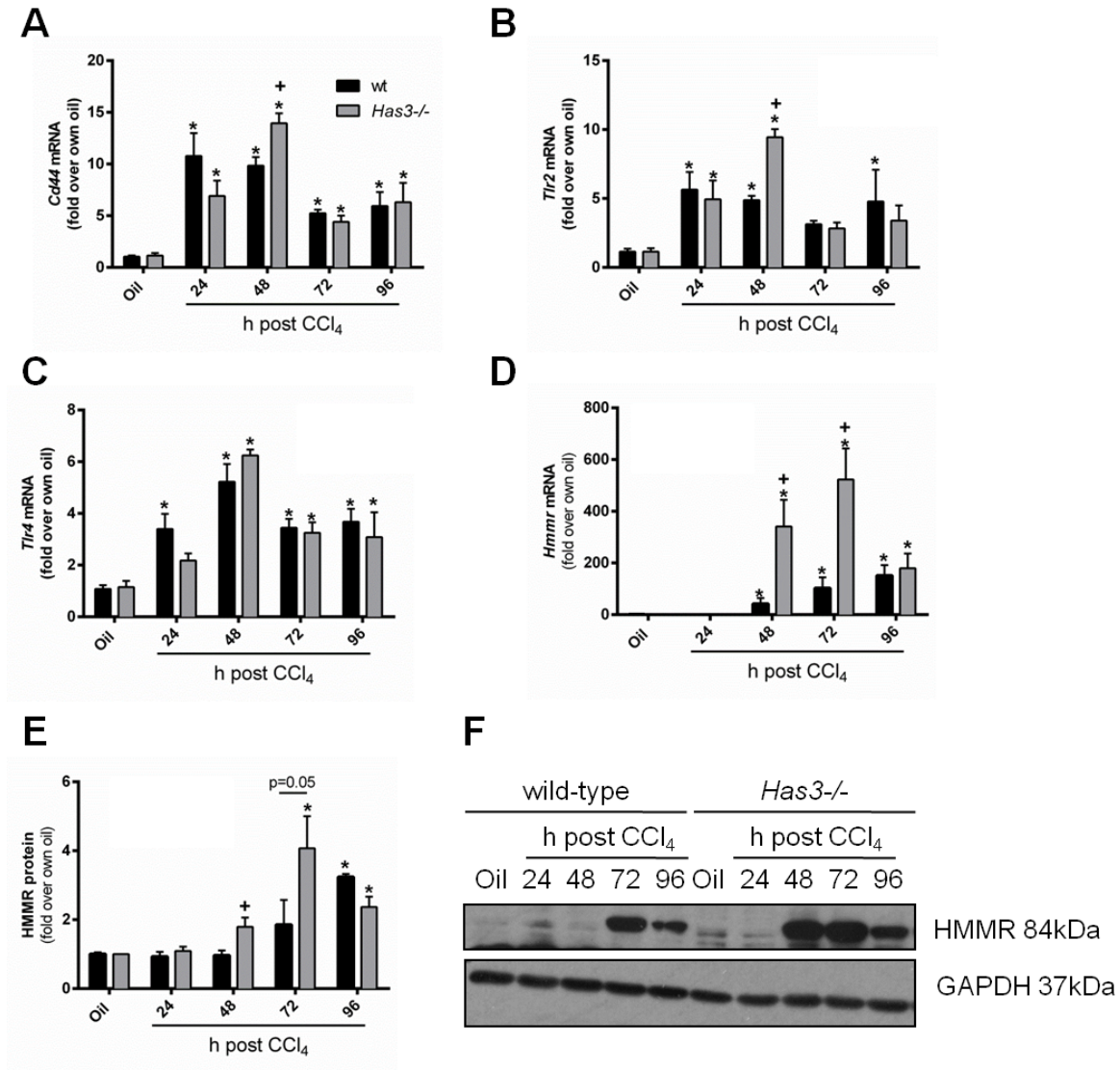


**Figure 3-9: Hepatic HA receptor expression following acute CCl<sub>4</sub> exposure.**

Mice were exposed to CCl<sub>4</sub> and euthanized 24, 48, 72, or 96 hours later. Control mice received an olive oil (oil) injection. Real time PCR was used to measure hepatic accumulation of A. *Cd44*, B. *Tlr2*, C. *Tlr4*, and D. *Hmnr* transcript levels. Data are expressed as fold change over each strain's own oil control. E. Quantification and F. representative Western blot for hepatic HMMR. GAPDH was used as a loading control. \* represents  $p < 0.05$  when comparing CCl<sub>4</sub> exposure to baseline within a genotype, + represents  $p < 0.05$  when comparing wild-type and *Has3*<sup>-/-</sup> mice within a time point. N = 4 – 7 mice per experimental group.

(Engstrom-Laurent *et al.*, 1985; Lee *et al.*, 2013; Neuman *et al.*, 2016). We provide the first evidence to suggest that HAS3, and presumably HA produced by HAS3, plays opposing roles in liver injury and wound healing after hepatotoxin mediated acute liver injury. Specifically, we show that HAS3, or HA produced by HAS3, protects the liver after acute liver injury by dampening hepatic inflammation. However, this alters subsequent wound healing by also dampening regeneration and matrix remodeling. Our data suggest that this protective effect may be due to the total amount and relative proportions of critical molecular weight HA pools and/or may be related to the amount of HA deposited in the liver following acute liver injury.

It is known that HSC can synthesize HA and do so in response to partial hepatectomy, a surgical model of liver regeneration (Vrochides *et al.*, 1996). In addition, treating mice with HMW-HA (780, 900 or 1200 kDa), but not LMW-HA (250 and 470 kDa), can prevent T-cell mediated liver injury (concanavalin A and galactosamine/lipopolysaccharide models) and this occurs through a reduction in pro-inflammatory cytokines, including tumor necrosis factor  $\alpha$  (TNF $\alpha$ ), interferon gamma, macrophage inflammatory protein 2 (MIP2) and interleukin 4 (Nakamura *et al.*, 2004). Administration of human umbilical vein HA (HMW-HA) also exerts some protection against CCl<sub>4</sub>-induced liver injury, lipid peroxidation, and fibrosis in rats when used in combination with chondroitin sulfate, but not when either molecule was used alone (Campo *et al.*, 2004). Collectively, these studies, as well as our study, suggest that HA can exhibit a protective effect in animal models of acute liver disease.

While no one has yet explored the effect of HAS enzyme deficiency in animal models of liver injury, investigators have evaluated the impact HAS3-deficiency has in

other animal models of human disease; these studies largely support a pathogenic role for HAS3. For example, in the lung, Bai *et al.*, demonstrated that high-tidal volume ventilator-induced pulmonary MIP2 production and neutrophil infiltration is robust in wild-type mice, but suppressed in mice deficient in HAS3 (Bai *et al.*, 2005). The increase in inflammation in wild-type mice is associated with increased pulmonary accumulation of HA favoring lower molecular weight species (178 – 370 kDa); this was not observed in *Has3*<sup>-/-</sup> mice. Likewise, Kessler *et al.*, demonstrated that HAS3-null mice are protected from DSS-induced colitis when compared to wild-type mice (Kessler *et al.*, 2015). In the absence of HAS3, HA deposition and leukocyte infiltration are profoundly attenuated and associated with reduced weight loss and reduced pro-inflammatory cytokine production after DSS exposure (Kessler *et al.*, 2015). In both of these studies, and in contrast to our study, HAS3 drives tissue inflammation.

The specific mechanisms behind the pathogenic function of HAS3 in the lung and in the gut remain controversial. One hypothesis is that because HAS3 can make smaller HA polymers compared to HAS1 and HAS2 (Spicer and McDonald, 1998; Itano *et al.*, 1999), perhaps HAS3-synthesized HA is small enough to be pro-inflammatory on its own. Conversely, perhaps LMW-HA synthesized by HAS3 is not directly pro-inflammatory but because it is smaller initially, it is more rapidly degraded into HA species which are pro-inflammatory. Another possible explanation is that HAS enzymes are differentially expressed in various tissues, cell types or in response to different stimuli (Jacobson *et al.*, 2000). Therefore, loss of one enzyme could profoundly influence the nature of the inflammatory response to injury in a tissue or cell type-specific fashion (Spicer and McDonald, 1998). Therefore HAS3's differential effect,

pathologic vs protective depending on animal model, should be explored further by evaluating in which cell types HAS3 is expressed as well as by elucidating the local production and turnover of HA after tissue injury. Indeed, in the DSS-induced colitis model, HAS3 expression is predominantly localized to the endothelial cells found in gut microvessels where it produces a leukocyte-adhesive HA and contributes to inflammation (Kessler *et al.*, 2015). Further exploration of cell-type specific hepatic HAS enzyme expression, hepatic HA accumulation and hepatic HA molecular weight distribution during liver disease pathogenesis is required to understand the differences between our study and the other studies discussed above.

In this study, we observed increases in hepatic mRNA and plasma protein levels for several pro-inflammatory chemokines in *Has3*<sup>-/-</sup> mice compared to wild-type mice after acute CCl<sub>4</sub> exposure (Mohanraj *et al.*, 2014). These chemokines can attract a number of cells involved in innate and adaptive immune responses to tissue injury including monocytes/macrophages (CCL2, CXCL10), neutrophils (CXCL1), natural killer cells (CXCL10), dendritic cells (CCL2, CXCL12) and T-cells (CCL2, CXCL10). We believe that chemokine production is at a critical nexus between the promotion of liver injury and, paradoxically, wound healing. Indeed, while CYP2E1-mediated bioactivation is required for CCl<sub>4</sub>'s hepatotoxic effects (Wong *et al.*, 1998), macrophages and macrophage recruitment also contribute to liver injury in this model. For example, if macrophages are depleted using gadolinium chloride, liver injury after CCl<sub>4</sub> exposure is reduced (Edwards *et al.*, 1993). Similarly, mice deficient in CCL2 or the CCL2 receptor, CCR2, exhibit reduced plasma ALT activities, intrahepatic inflammatory cytokine expression and macrophage recruitment after CCl<sub>4</sub> exposure (Zamara *et al.*, 2007;

Mitchell *et al.*, 2009a). Therefore, increased chemokine production in *Has3*<sup>-/-</sup> mice could be contributing to increased inflammatory macrophage recruitment, which could contribute to increased injury after CCl<sub>4</sub> exposure. Future work should evaluate markers of macrophage mediated TNF $\alpha$  and ROS as well as protein levels of macrophage markers by IHC or FACS analysis to determine if this is occurring in *Has3*<sup>-/-</sup> mice.

In addition to contributing to liver injury, inflammation promotes hepatic regeneration. We observed increased inflammatory microenvironment in *Has3*<sup>-/-</sup> mice compared to wild-type mice and it is possible that this may also play a role in the increased regeneration in the *Has3*<sup>-/-</sup> mice. TNF $\alpha$  treatment *in vitro* increases rat hepatocyte proliferation, suggesting a role for pro-inflammatory mediators in “priming” hepatocytes for regeneration (Webber *et al.*, 1998). In addition, treating mice with a CCR2 antagonist following a partial hepatectomy results in decreased mitotic figures associated with a decrease in hepatic macrophage content (Nishiyama *et al.*, 2015). Likewise, depletion of Kupffer cells using clodronate-encapsulated liposomes, results in a decrease of ethanol-induced DNA synthesis (Owumi *et al.*, 2014). While we observed increased chemokine expression, further work should be completed (as described above) to determine if there is in fact increased macrophage infiltration or if there is increased TNF $\alpha$  production, but overall our data suggest that increased inflammation may also provide a mechanism to improve liver regeneration.

Additionally, hepatic macrophages and macrophage recruitment are also critical determinants of ECM regulation. Macrophages are the primary source of MMPs required for matrix degradation/metabolism, which can also influence regeneration and is required to restore hepatic structure and function (You *et al.*, 2013; Duarte *et al.*,

2015). In this study, we found increased matrix metabolism in livers from *Has3*<sup>-/-</sup> mice compared to wild-type mice. Treatment of mice following a partial hepatectomy with a broad spectrum MMP inhibitor limited regeneration (Alwayn *et al.*, 2008). This suggests that, similar to the increased inflammation, the increased matrix metabolism may also be aiding in the increased regeneration seen in *Has3*<sup>-/-</sup> mice. It is likely that increased matrix metabolism is caused by the increase in *Mmp13* transcript accumulation in the *Has3*<sup>-/-</sup> mice. *Mmp13* transcript accumulation is increased following low dose D-galactosamine exposure in rats and is associated with survival (Yata *et al.*, 1999). However in high dose D-galactosamine exposure, *Mmp13* transcript expression is dysregulated and associated with non-survival (Yata *et al.*, 1999). HA oligosaccharides are known inducers of MMP13 (Fieber *et al.*, 2004). It is tempting to speculate that increased HA levels found in *Has3*<sup>-/-</sup> mice after exposure to CCl<sub>4</sub> may have contributed to the increase in *Mmp13* levels we found in this study. Together these data suggest that the increased matrix metabolism in the *Has3*<sup>-/-</sup> mice is promoting the wound healing process, and this may be caused by the imbalance in LMW-HA and HMW-HA fragments or increased hepatic HA found in *Has3*<sup>-/-</sup> mice following acute CCl<sub>4</sub>.

Finally, we evaluated HA receptor expression in wild-type and *Has3*<sup>-/-</sup> mice after acute liver injury. We observed increased expression of all receptors evaluated, CD44, TLR2, and TLR4, but the largest differential expression was in HMMR. This was mirrored, although to a lesser degree relative to mRNA, in the hepatic HMMR protein content. This receptor is unique in that it can be both intracellular and extracellular and it can play a role in cell migration, for macrophage and fibroblasts, as well as cell proliferation (Tolg *et al.*, 2006; Tolg *et al.*, 2012; Chen *et al.*, 2014). The increased

expression of *Hmmr*, may therefore be contributing to several aspects of the wound parameters that were found to be different in *Has3*<sup>-/-</sup> mice compared to wild-type mice after acute CCl<sub>4</sub>. This possible contribution of HMMR to liver wound healing will be explored further in the following chapter.

Despite increased plasma HA levels being linked to liver disease severity for years, we are the first to show a link between HA and acute hepatic wound healing. We conclude that HA produced by HAS3 protects against hepatotoxin-induced liver injury. However in *Has3*<sup>-/-</sup> mice, we uncovered an unexpected increase in hepatic HA, which is associated with increased hepatic wound healing, including inflammation, regeneration, and matrix remodeling. We also observe an induction in hepatic *Has* enzymes, hepatic HA content, and the transcription of several HA receptors following acute liver injury, further supporting a role for HA and the HA network in hepatic wound healing.

**Chapter 4: HA mediated motility receptor (HMMR) is required  
for wound healing after acute liver injury**

## **Abstract**

Hepatic wound healing occurs following acute liver injury and includes stages of inflammation, regeneration, and matrix remodeling. Hyaluronan (HA) is a ubiquitous glycosaminoglycan that is increased following dermal injury and plays a role in the skin wound healing process. HA is also increased in the plasma of patients with liver disease, however a role for HA in the hepatic wound healing process has not been investigated. We showed in Chapter 3 that mice deficient in HAS3 have increased injury and increased wound healing associated with increased HA and HA mediated motility receptor (HMMR) expression after acute carbon tetrachloride (CCl<sub>4</sub>) exposure. HMMR plays a role in the migration of fibroblasts and macrophages to wounded tissue and in mitotic spindle stability and proliferation. We therefore hypothesized that HMMR aids in wound healing following acute liver injury. Using *Hmmr*<sup>-/-</sup> and wild-type mice, we induced liver injury and evaluated parameters of wound healing. We found that *Hmmr*<sup>-/-</sup> mice have reduced pro-inflammatory cytokine and chemokine expression compared to wild-type mice that is independent of injury. This was associated with reduced matrix degradation. Further evaluation indicated that removal of dead tissue was delayed in mice lacking HMMR. *Hmmr*<sup>-/-</sup> mice also have delayed hepatic regeneration compared to wild-type mice. Finally, *Hmmr*<sup>-/-</sup> mice have delayed hepatic HA deposition. Together, our data suggest a role for HMMR and HA in both macrophage localization and hepatic regeneration after toxin induced acute liver injury. We propose macrophages are utilizing HA via an interaction with HMMR to localize to the necrotic area and aid in hepatic wound healing.

## **Introduction**

Toxins like acetaminophen or alcohol, when consumed in large quantities, are a primary cause of acute liver injury in developed countries like the United States (Penny, 2013; Jaeschke, 2015). Once toxin-mediated injury occurs, the liver works to heal itself. This process is analogous to skin wound healing and includes periods of inflammation, regeneration, and matrix remodeling (Balaji *et al.*, 2015). Hepatic wound healing after acute injury is analogous to fetal wound healing and results in minimal scar formation. If injury is sustained, this process becomes deregulated and results in liver fibrosis, analogous to adult dermal wound healing (Guo and Friedman, 2007; Friedman, 2008b). If injury and inflammation continue to persist, fibrosis can progress to cirrhosis and even hepatocellular carcinoma at which point a liver transplant becomes necessary for survival (Rai, 2013; Tsochatzis *et al.*, 2014). Studying the mechanisms of acute liver wound healing can provide novel insight into the progression of chronic liver disease and lead to possible therapeutic options to avoid the need for a transplant.

Hyaluronan is a non-sulfated, ubiquitous, glycosaminoglycan implicated in a number of disease pathologies (Jiang *et al.*, 2011). For example, the molecular weight and concentration of HA in articular joints decreases as we age and is associated with the progression of osteoarthritis (Campo *et al.*, 2011; Band *et al.*, 2015). In fact, intra-articular HMW-HA injections are currently used as a treatment for osteoarthritis, demonstrating the importance of HMW-HA in preventing inflammation (Guidolin and Franceschi, 2014). In lung injury, HA fragments accumulate and can induce an inflammatory response via interaction with toll like receptor (TLR) 2 and 4 (Jiang *et al.*, 2005). HA is increased in the plasma of patients with liver disease, and this increase is

correlated with the disease severity (Engstrom-Laurent *et al.*, 1985; Lee *et al.*, 2010; Lee *et al.*, 2013).

HA is synthesized by three different hyaluronan synthase (HAS) enzymes, HAS1, HAS2, and HAS3 (Jiang *et al.*, 2011). These enzymes differ in their tissue-specific expression and synthetic capacity, but each creates high molecular weight HA (HMW-HA) (Spicer and McDonald, 1998; Itano *et al.*, 1999). We have shown previously (Chapter 3), that mice bearing an enzymatically inactive HAS3 have increased injury compared to wild-type controls following acute liver injury induced by carbon tetrachloride (CCl<sub>4</sub>). These mice also have increased wound healing, evident by increased liver regeneration and matrix remodeling after acute injury. Interestingly, these mice have increased hepatic HA accumulation and also display an increase in the expression of the HA receptor, HA mediated motility receptor (HMMR) at both the mRNA and protein level compared to wild-type controls.

HMMR is a unique HA receptor in that it does not contain a transmembrane domain, and it can be either intracellular or extracellular (Savani *et al.*, 2000; Jiang *et al.*, 2010). Extracellular HMMR interacts with HA in the extracellular matrix (ECM) and promotes the migration of fibroblasts and macrophages to wounded tissue to facilitate dermal wound healing (Tolg *et al.*, 2006; Tolg *et al.*, 2012). Intracellular HMMR plays a role in cell proliferation; specifically it is a component of the mitotic spindle complex and promotes progression through the cell cycle (Maxwell *et al.*, 2003; Chen *et al.*, 2014). Cells lacking functional HMMR arrest at the G2/M transition of the cell cycle, resulting in either delayed mitosis or mitotic arrest (Chen *et al.*, 2014). Because of the unique properties of HMMR in migration and cell proliferation, as well as HMMR expression

being associated with increased wound healing observed in *Has3*<sup>-/-</sup> mice, we sought to examine hepatic wound healing in *Hmmr*<sup>-/-</sup> mice following acute CCl<sub>4</sub> exposure. We hypothesized that *Hmmr*<sup>-/-</sup> mice would exhibit a delay in inflammation, regeneration, and matrix metabolism after acute liver injury, the reciprocal of what we observed in *Has3*<sup>-/-</sup> mice after acute liver injury.

## **Results**

### ***Hmmr* expression pattern in C57Bl/6N mice mirrors that of C57Bl/6J mice**

As described previously, *Has3*<sup>-/-</sup> mice have increased wound healing, which is associated with increased HMMR levels (see Chapter 3). In addition, because HMMR has been implicated in cell migration and regeneration, we hypothesized that *Hmmr*<sup>-/-</sup> mice would have delayed wound healing (Tolg *et al.*, 2006; Tolg *et al.*, 2010; Tolg *et al.*, 2012; Chen *et al.*, 2014) after acute liver injury. The *Hmmr*<sup>-/-</sup> mice are on a C57Bl/6N background, which is in contrast to the *Has3*<sup>-/-</sup> mice, which are on a C57Bl/6J background (See Figure 6-9). Therefore, we first evaluated *Hmmr* expression and protein levels in C57Bl/6N wild-type mice. Similar to the C57Bl/6J mice used in the *Has3*<sup>-/-</sup> studies, *Hmmr* expression was induced only at 48, 72, and 96 hours post CCl<sub>4</sub> exposure, peaking at 48 hours (Figure 4-1A). A similar pattern was seen when HMMR protein levels were measured (Figure 4-1B). Thus indices of liver injury, inflammation, and repair were measured only at 48, 72, and 96 hours post CCl<sub>4</sub> *Hmmr*<sup>-/-</sup> mice and C57Bl/6N mice.

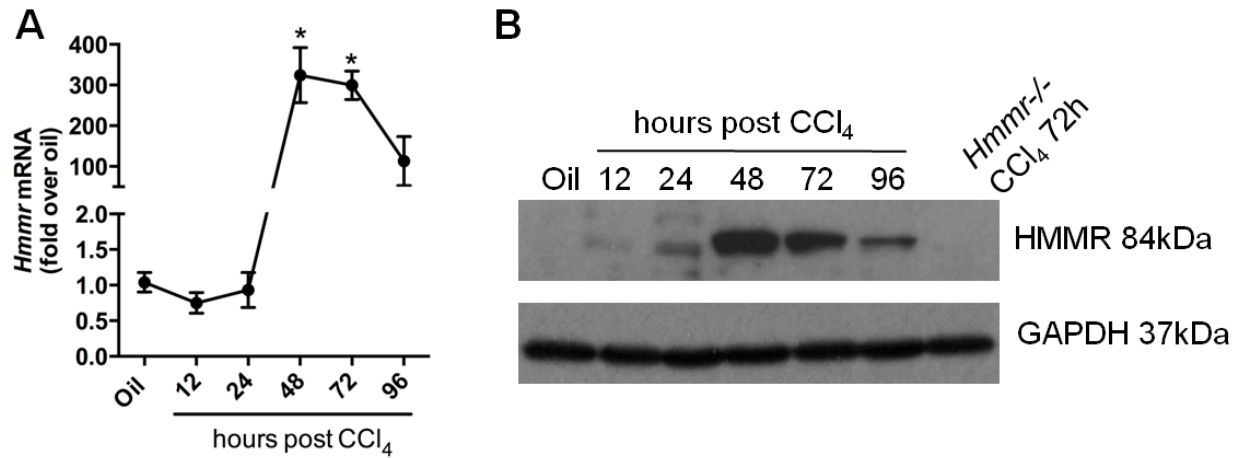


**Figure 4-1: Hepatic *Hmnr* expression in C57BL/6N mice.**

Mice were exposed to CCl<sub>4</sub> and euthanized 12, 24, 48, 72, or 96 hours later. Control mice received an olive oil (oil) injection. A. Wild-type hepatic *Hmnr* expression was evaluated using real time PCR. Data were normalized to 18s and expressed as fold change over oil. B. Western blot samples were pooled and separated on a SDS-PAGE gel, transferred to a PVDF membrane, and probed for HMMR. GAPDH served as a loading control. All data are represented as mean + SEM throughout this chapter. \* represents p<0.05 compared to oil. N = 5 – 6 mice per group.

### **Liver injury in *Hmmr*<sup>-/-</sup> and wild-type mice following acute CCl<sub>4</sub> exposure**

Plasma ALT activity and the area of necrosis in H&E stained liver sections were used to assess liver injury following CCl<sub>4</sub> exposure in *Hmmr*<sup>-/-</sup> mice and wild-type controls. Plasma ALT activity was elevated in both genotypes 48 hours after CCl<sub>4</sub> exposure, and there was no difference between genotypes (Figure 4-2A). While there was no difference in peak necrosis at 48 hours between wild-type and *Hmmr*<sup>-/-</sup> mice, by 72 hours after CCl<sub>4</sub> exposure, there was more necrosis remaining in *Hmmr*<sup>-/-</sup> mice compared to wild-type mice. This suggests a delay in necrotic cell removal (Figure 4-2B and C). Similar to the *Has3*<sup>-/-</sup> mice (Chapter 3), there was no difference in basal CYP2E1 protein or activity levels between *Hmmr*<sup>-/-</sup> mice and wild-type mice (Figure 4-3A-C). Taken together, these data suggest that wound repair is delayed in *Hmmr*<sup>-/-</sup> mice and this effect is independent of liver injury.

### **Hepatic inflammation in *Hmmr*<sup>-/-</sup> and wild-type mice following acute CCl<sub>4</sub> exposure**

Because HMMR plays a role in cell migration, we evaluated the number of cells infiltrating into the necrotic area. *Hmmr*<sup>-/-</sup> mice had lower infiltrating cells at 48 hours, but trended toward an increase at 72 hours compared to wild-type. This could account for the delay in necrotic healing but the ability for *Hmmr*<sup>-/-</sup> mice to recover to wild-type levels by 96 hours (Figure 4-4A). In fact, the number of infiltrating cells is negatively correlated to the area of necrosis (Figure 4-4B). While this does not distinguish between types of cell infiltrating necrotic areas or if they are removing tissue debris, it does suggest that HMMR is important for early cell infiltration after acute liver injury.

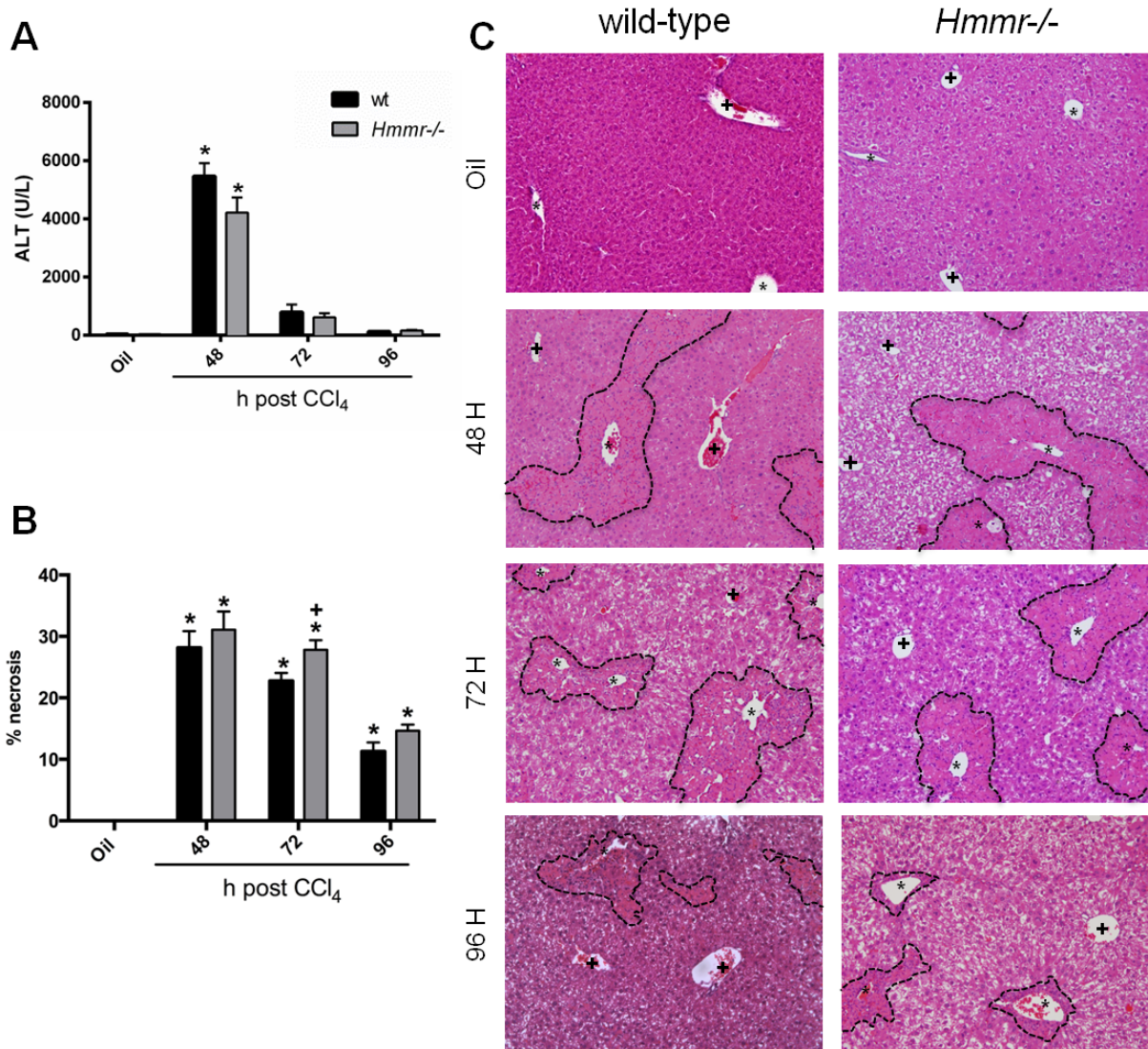


**Figure 4-2: Hepatic injury in wild-type and *Hmnr*<sup>-/-</sup> mice following acute CCl<sub>4</sub> exposure.**

Mice were exposed to CCl<sub>4</sub> and euthanized 48, 72, or 96 hours later. Control mice received an olive oil (oil) injection. A. Plasma ALT activity and B. the area of necrosis was measured to evaluate hepatic injury. Necrosis was defined as hyper eosinophilic tissue area with the absence of hepatic nuclei. C. Representative H&E stained liver sections with the necrotic area outlined with a black dashed line. \* denotes central vein and + denotes portal veins in the images. Throughout this chapter, black bars represent wild-type mice and grey bars represent *Hmnr*<sup>-/-</sup> mice. In the graphs, \* represents  $p < 0.05$  when compared to each genotype's own oil control, + represents  $p < 0.05$  when comparing genotypes within a time point. N = 6 – 13 mice per group.

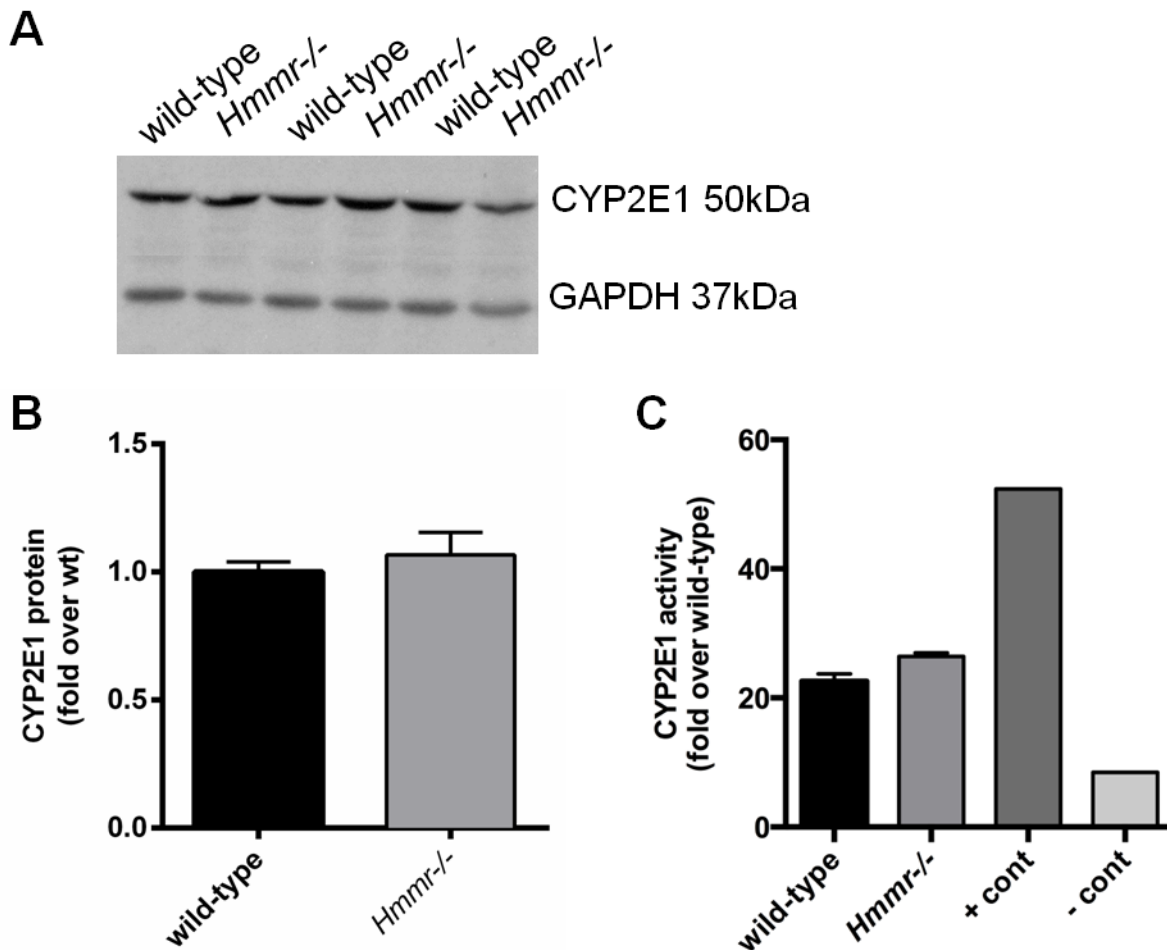


**Figure 4-3: Basal CYP2E1 expression and activity in wild-type and *Hmnr*<sup>-/-</sup> mice.**

Control mice received olive oil (oil) injections and were euthanized 72 hours later. A. Representative blot for CYP2E1 protein. GAPDH was used as a loading control. B. Quantification of CYP2E1 protein levels were completed using ImageJ. C. CYP2E1 activity was measured in microsomes isolated from the livers of control mice. + cont samples were from mice exposed to ethanol, a known inducer of CYP2E1 and – cont samples were from mice exposed to CCl<sub>4</sub>, known to deplete CYP2E1 levels. \* represents  $p < 0.05$ . N = 6 – 9, N = 2 for positive and negative controls.

HMMR is important for macrophage migration in skin wound healing (Tolg *et al.*, 2012). Macrophages are important in both initial injury and hepatic wound healing, but there was no difference in hepatic injury (Figure 4-2) and HMMR is only expressed when hepatic repair is ongoing (Figure 4-1). We therefore hypothesized that HMMR is more important in hepatic wound healing rather than initial injury (Duffield *et al.*, 2005; Zigmond *et al.*, 2014). *Ccl2* (encodes CCL2, also known as monocyte chemoattractant protein 1, MCP1) and aids in the recruitment of macrophages to the damaged liver (Zamara *et al.*, 2007). *Ccl2* transcripts were induced in both wild-type and *Hmmr*<sup>-/-</sup> mice 48 hours post CCl<sub>4</sub>, and the transcript levels were lower in the *Hmmr*<sup>-/-</sup> mice compared to wild-type mice at this time point (Figure 4-4C). *Ccr2*, the receptor for MCP1 and a marker of recruited macrophages (Mitchell *et al.*, 2009a), was elevated above baseline in both wild-type and *Hmmr*<sup>-/-</sup> mice 48 hours post CCl<sub>4</sub> exposure and remained elevated in *Hmmr*<sup>-/-</sup> mice through 96 hours post CCl<sub>4</sub> exposure (Figure 4-4D). *Emr1* transcripts, which encode for F4/80, a mouse macrophage marker, increased in wild-type mice by 48 hours post CCl<sub>4</sub> exposure and were significantly lower at that same time point in *Hmmr*<sup>-/-</sup> mice (Figure 4-4E). In fact, *Emr1* transcript levels were not elevated above baseline until 72 hours post CCl<sub>4</sub> exposure in *Hmmr*<sup>-/-</sup> mice. *Tnfa*, the gene for the pro-inflammatory cytokine TNF $\alpha$ , is produced mainly by macrophages (Mohanraj *et al.*, 2014). Hepatic *Tnfa* transcript levels increased in both wild-type and *Hmmr*<sup>-/-</sup> mice 48 hours after CCl<sub>4</sub> exposure, however this increase was greater in wild-type mice (Figure 4-4F). Together, these data suggest that due to a decrease in pro-inflammatory chemokine gene expression, macrophage recruitment may be delayed. However as evidenced by sustained levels of *Ccr2* transcripts in *Hmmr*<sup>-/-</sup> mice,

recruited macrophages may persist in the liver compared to macrophages from wild-type mice. These gene expression analyses do not mean that macrophages are recruited to the necrotic area where they are required to clear the dead and dying hepatocytes (Kinoshita *et al.*, 2010; Ikarashi *et al.*, 2013). In fact, when evaluating F4/80 staining, there is a trend towards a decrease in total area of F4/80+ cells in liver from *Hmmr*<sup>-/-</sup> mice compared to wild-type mice (Figure 4-4G and H). In addition, F4/80+ cells in wild-type mice are infiltrating the necrotic area, while the F4/80+ cells in *Hmmr*<sup>-/-</sup> mice are not yet infiltrating into the necrotic area (Figure 4-4H). Combined with the sustained necrosis level in *Hmmr*<sup>-/-</sup> mice, this suggests that macrophage localization to necrotic tissue was delayed in *Hmmr*<sup>-/-</sup> mice.

### **Hepatic regeneration in wild-type and *Hmmr*<sup>-/-</sup> mice following acute CCl<sub>4</sub> exposure**

Hepatic regeneration is a vital step in hepatic wound healing after acute CCl<sub>4</sub> exposure (Cienfuegos *et al.*, 2014). HMMR is unique in that it is not only important in cell motility, but it also plays a role in cell cycle progression, and is particularly important during the G2/M phase transition (Tolg *et al.*, 2010; Hatano *et al.*, 2012). Inflammatory cytokines including TNF $\alpha$ , aid in the priming of hepatocytes for regeneration (Webber *et al.*, 1998; Owumi *et al.*, 2014). Due to the reduced *Tnfa* transcripts and the role of HMMR in proliferation, we predicted that *Hmmr*<sup>-/-</sup> mice would have decreased or delayed hepatic regeneration following acute CCl<sub>4</sub> exposure. To test this hypothesis, we evaluated several indices of cell proliferation associated with liver regeneration. Hepatic *Pcna* transcripts were induced in both wild-type and *Hmmr*<sup>-/-</sup> mice following CCl<sub>4</sub>

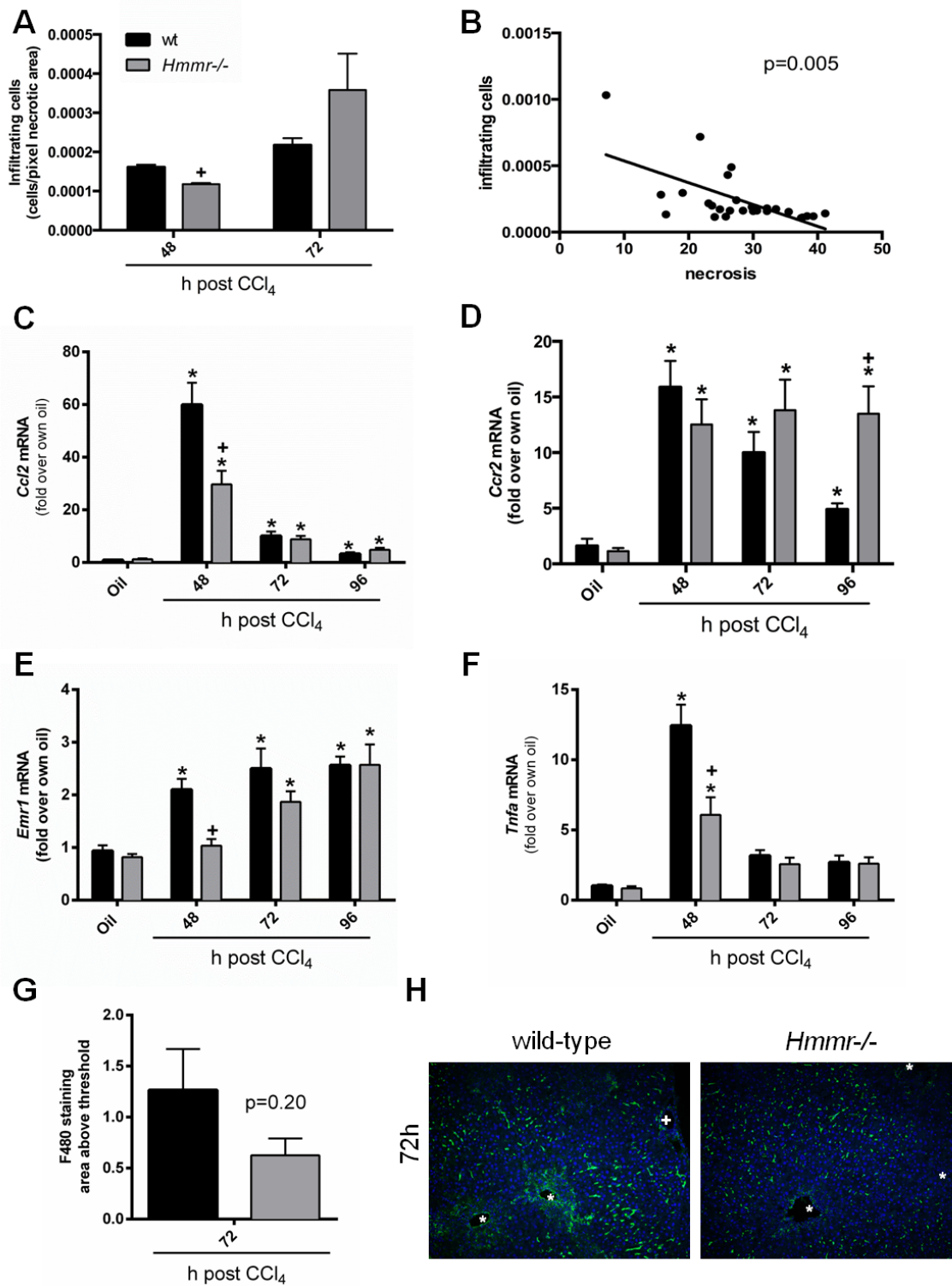


**Figure 4-4: Inflammation and pro-inflammatory microenvironment following acute CCl<sub>4</sub> exposure.**

Mice were exposed to CCl<sub>4</sub> and euthanized 48, 72, or 96 hours later. Control mice received an olive oil (oil) injection. A. Cells that had infiltrated the necrotic area were counted and represented as number of cells/pixel of necrotic area. B. The infiltrating cells were correlated with % necrotic tissue for mice euthanized 48 and 72 hours after CCl<sub>4</sub> exposure. Real time PCR was used to evaluate hepatic accumulation of C. *Ccl2*, D. *Ccr2*, E. *Emr1*, and F. *Tnfa* transcripts. Data are expressed as fold change over own oil. G. Quantification of total area of positive staining and H. representative histology of F4/80 staining 72 hours after CCl<sub>4</sub> exposure. \* denotes central veins and + denotes portal veins in the images. In the graphs, \* represents p<0.05 compared to each genotype's own oil, + represents p<0.05 comparing the two genotypes at one timepoint. N = 6 – 13 mice per group.

exposure, however, 48 hours after exposure wild-type mice had increased *Pcna* transcript compared to *Hmmr*<sup>-/-</sup> mice (Figure 4-5A). PCNA protein increased in both genotypes in response to CCl<sub>4</sub>, but there were no differences at any time point between wild-type and *Hmmr*<sup>-/-</sup> mice (Figure 4-5B and C). *Ccnd1*, the gene that encodes Cyclin D1, was induced in both wild-type and *Hmmr*<sup>-/-</sup> mice by 48 hours after CCl<sub>4</sub> exposure; there were no differences in transcript levels between the genotypes at any time point (Figure 4-5D). A similar trend was observed in Cyclin D1 protein (Figure 4-5E and F). Ki67, a marker for cell proliferation, was used to observe actively proliferating hepatocytes in liver sections. Despite limited differences in Cyclin D1 and PCNA protein, wild-type mice had almost twice as many Ki67 positive cells 48 hours after CCl<sub>4</sub> exposure compared to *Hmmr*<sup>-/-</sup> mice (Figure 4-6A and 4-6B). Together, these data suggest that despite similar gene expression profiles, *Hmmr*<sup>-/-</sup> mice have a delay in hepatocyte proliferation following acute liver injury.

### **Matrix remodeling in wild-type and *Hmmr*<sup>-/-</sup> mice following acute CCl<sub>4</sub> exposure.**

Matrix remodeling is another vital component of the hepatic wound healing process and includes both matrix synthesis and matrix degradation. In addition to HMMR's role in macrophage migration, it also plays a role in fibroblast migration in dermal wound healing (Tolg *et al.*, 2006). In the injured liver, hepatic stellate cells (HSC) are activated and transdifferentiate into myofibroblasts, cells phenotypically and functionally similar to the fibroblasts that participate in skin wound healing (Wells and Schwabe, 2015). A common marker for myofibroblasts is  $\alpha$ SMA, a protein that is encoded by the *Acta2* gene (Wells and Schwabe, 2015). Hepatic *Acta2* transcripts

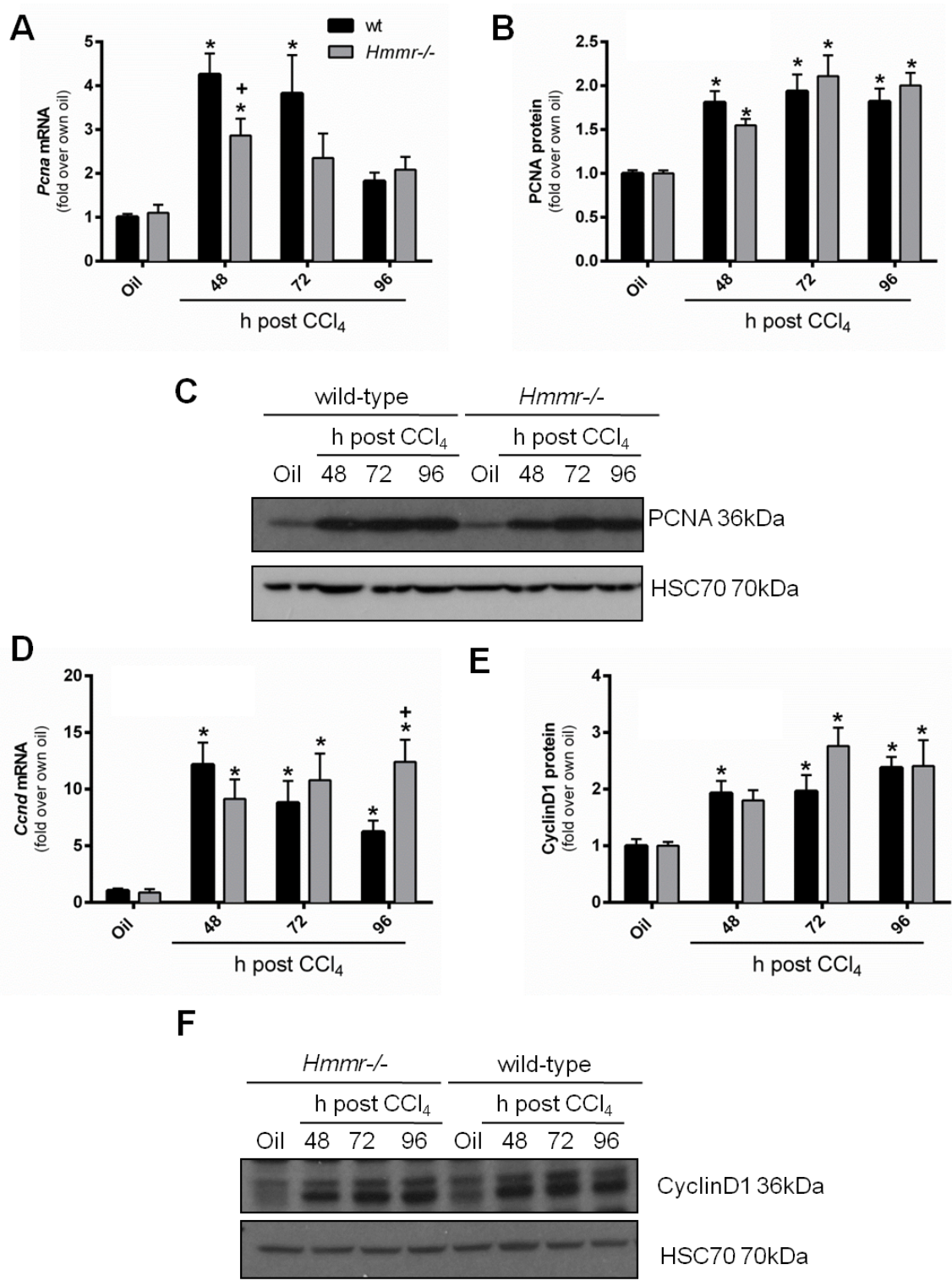


**Figure 4-5: Hepatic regeneration following acute CCl<sub>4</sub> exposure in wild-type and *Hmnr*<sup>-/-</sup> mice.**

Mice were exposed to CCl<sub>4</sub> and euthanized 48, 72, or 96 hours later. Control mice received an olive oil (oil) injection. A. Hepatic *Pcna* transcript accumulation was measured using real time PCR. B. Quantification and C. representative blot for PCNA protein. E. Hepatic *Ccnd1* transcripts were measured using real time PCR. F. Quantification and G. representative Cyclin D1 Western blot. Data are expressed as fold change over each genotype's own oil. \* represents p<0.05 compared to each genotype's own oil. + represents p<0.05 when comparing the two genotypes at one time point. N = 6 – 13 mice per group.

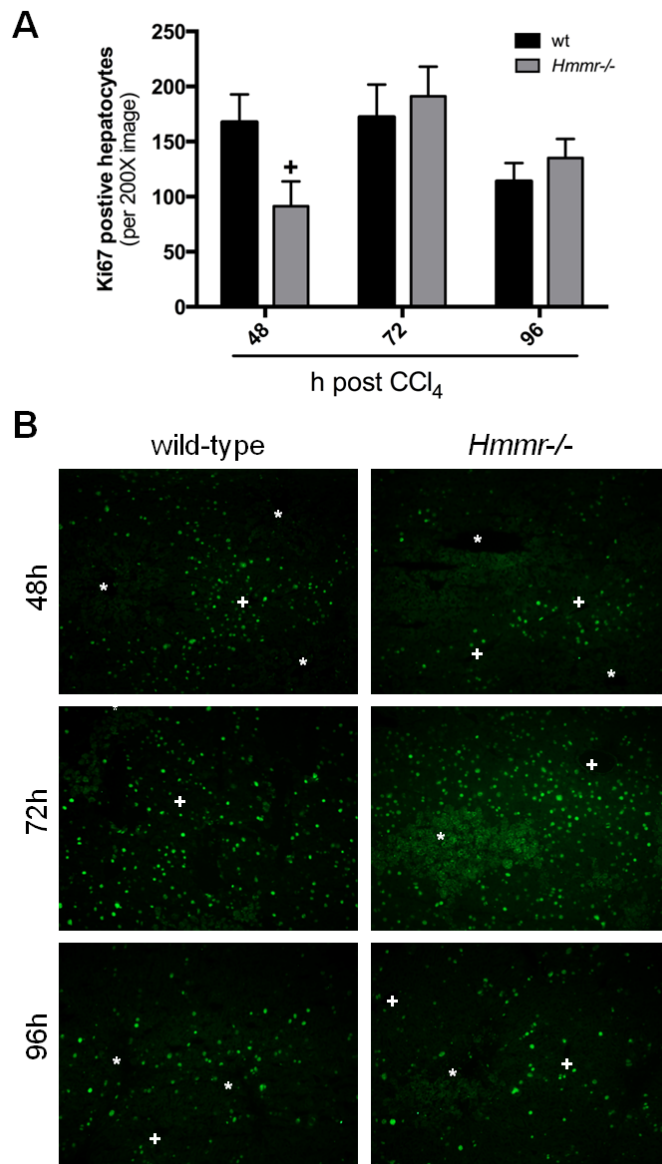


**Figure 4-6: Ki67 positive hepatocytes following acute CCl<sub>4</sub> exposure in wild-type and *Hmnr*<sup>-/-</sup> mice.**

Mice were exposed to CCl<sub>4</sub> and euthanized 48, 72, or 96 hours later. A. Quantification and B. representative histology of Ki67 positive hepatocytes. Data are expressed as number of positive hepatocytes per 200X image. \* denotes central veins and + denotes portal veins in the images. In the graphs, + represents p<0.05 when comparing the two genotypes at one time point. N = 6 – 13 mice per group.

increased in both genotypes above baseline following CCl<sub>4</sub> exposure but there was no difference between genotypes at any time point (Figure 4-7A). The amount of  $\alpha$ SMA protein was actually lower in *Hmmr*<sup>-/-</sup> mice compared to wild-type mice 48 hours after CCl<sub>4</sub> exposure (Figure 4-7B and C). This suggests that HMMR may not be required for HSC activation following acute liver injury, however it does not prove conclusively that HMMR is not important for HSC localization to injured areas of the liver.

As mentioned above, matrix remodeling consists of not only matrix synthesis by activated HSC, but also of matrix degradation. This degradation occurs due to a coordinated effort by several matrix metalloproteinases (MMPs), synthesized primarily by macrophages (Fallowfield *et al.*, 2007b; Duarte *et al.*, 2015). Due to the apparent decrease in hepatic inflammation, we hypothesized that *Hmmr*<sup>-/-</sup> mice would have decreased matrix degradation. MMP13 is the main mouse collagenase, and hepatic *Mmp13* transcripts were elevated in both wild-type and *Hmmr*<sup>-/-</sup> mice 48 hours after CCl<sub>4</sub> exposure. However, this induction was not different between genotypes (Figure 4-8A). MMP13 degrades collagen molecules to gelatin that are then degraded by gelatinases (Chung *et al.*, 2004). Expression of *Mmp2*, a mouse gelatinase, increased in both genotypes, however not until 72 hours after CCl<sub>4</sub> exposure (Figure 4-8B). The transcript levels were not different between genotypes at any time point. *Mmp9* transcripts, which encode for another mouse gelatinase, increased in both wild-type and *Hmmr*<sup>-/-</sup> mice 48 hours after CCl<sub>4</sub> exposure (Figure 4-8C). In contrast to our hypothesis, *Mmp9* transcript levels were increased in *Hmmr*<sup>-/-</sup> mice compared to wild-type mice 72 and 96 hours post CCl<sub>4</sub> exposure. Tissue inhibitors of MMPs (TIMPs) act to balance the

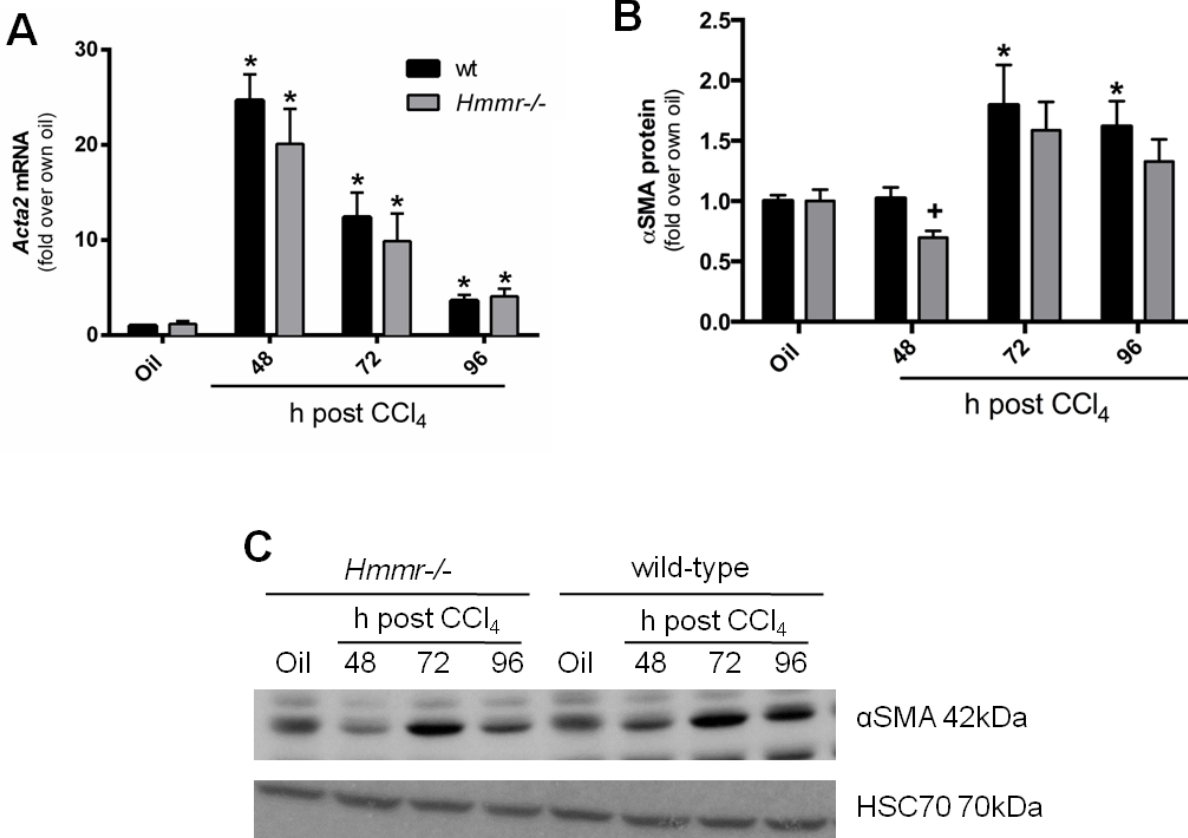


**Figure 4-7: Hepatic stellate cell activation in wild-type and *Hmnr*<sup>-/-</sup> mice after acute CCl<sub>4</sub> exposure.**

Mice were exposed to CCl<sub>4</sub> and euthanized 48, 72, or 96 hours later. Control mice received olive oil (oil) injection. A. Real time PCR was used to measure hepatic *Acta2* transcripts. B. Quantification and C. representative blot for αSMA protein levels. HSC70 was used as a loading control. Data are expressed as fold change over each genotype's own oil control. \* represents p<0.05 compared to each genotype's own oil. + represents p<0.05 when comparing the two genotypes at one time point. N = 6 – 13 mice per group.

MMP activity following acute liver injury. *Timp1* transcripts also increased in both genotypes but the increase was greater in wild-type mice 48 hours after CCl<sub>4</sub> exposure (Figure 4-8D). Using *in situ* zymography (described in Chapter 2 and Chapter 3), active matrix remodeling was decreased in *Hmmr*<sup>-/-</sup> mice compared to wild-type mice 72 hours post CCl<sub>4</sub> exposure (Figure 4-9A, B, and C). These data demonstrated that despite no difference, or an increase in the expression level of any MMP evaluated, and in spite of the decreased *Timp1* expression, *Hmmr*<sup>-/-</sup> mice have decreased matrix metabolism. This suggests that *Hmmr*<sup>-/-</sup> mice are able to induce gene expression to promote wound healing, but may be unable to localize cells to the necrotic area to facilitate matrix metabolism.

#### **Hyaluronan accumulation in wild-type and *Hmmr*<sup>-/-</sup> following acute CCl<sub>4</sub> exposure**

HMMR is a receptor for HA, and blocking this interaction can effect dermal wound healing (Tolg *et al.*, 2012). It was therefore important to evaluate plasma HA and intrahepatic HA levels in *Hmmr*<sup>-/-</sup> and wild-type mice. Plasma HA levels increased following CCl<sub>4</sub> exposure in the wild-type mice, but not the *Hmmr*<sup>-/-</sup> mice (Figure 4-10A). While very little HA is present in healthy liver, hepatic HA increased in livers from both genotypes following injury. However, HA accumulation at 48 hours post CCl<sub>4</sub> exposure was less in *Hmmr*<sup>-/-</sup> mice compared to wild-type mice (Figure 4-10B and C). By 72 hours after CCl<sub>4</sub> exposure, hepatic HA levels in *Hmmr*<sup>-/-</sup> mice had increased to the level of wild-type mice. This suggests that there was a delay in HA synthesis following injury in *Hmmr*<sup>-/-</sup> mice and that this may contribute to delayed wound healing in *Hmmr*<sup>-/-</sup> mice.

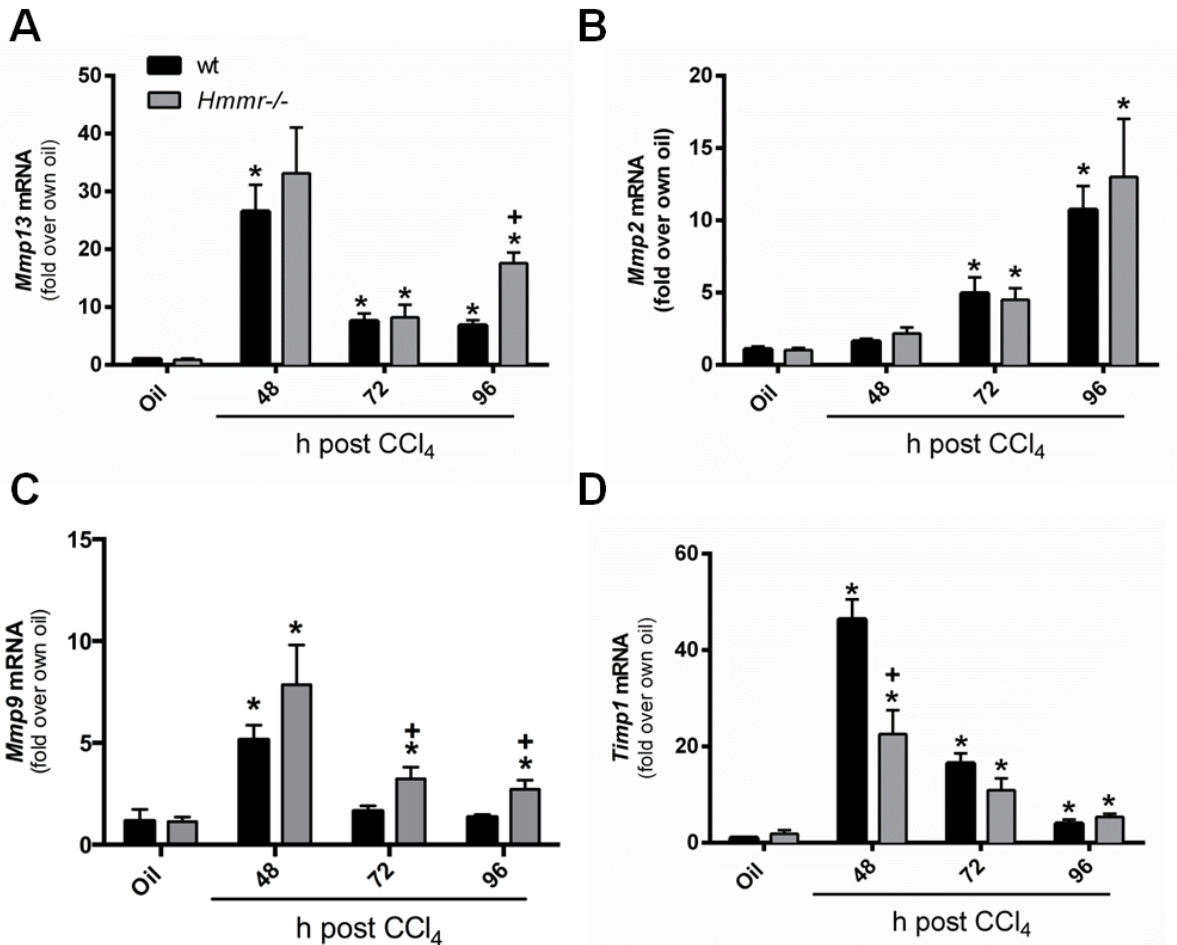


**Figure 4-8: Hepatic matrix remodeling transcripts in wild-type and *Hmnr*<sup>-/-</sup> mice after CCl<sub>4</sub> exposure.**

Mice were exposed to CCl<sub>4</sub> and euthanized 48, 72, or 96 hours later. Control mice received olive oil (oil) injection. Hepatic A. *Mmp13*, B. *Mmp2*, C. *Mmp9*, and D. *Timp1* mRNAs were measured using real time PCR. Data are expressed as fold change over own oil. \* represents p<0.05 compared to each genotype's own oil. + represents p<0.05 when comparing the two genotypes at one time point. N = 6 – 13 mice per group.

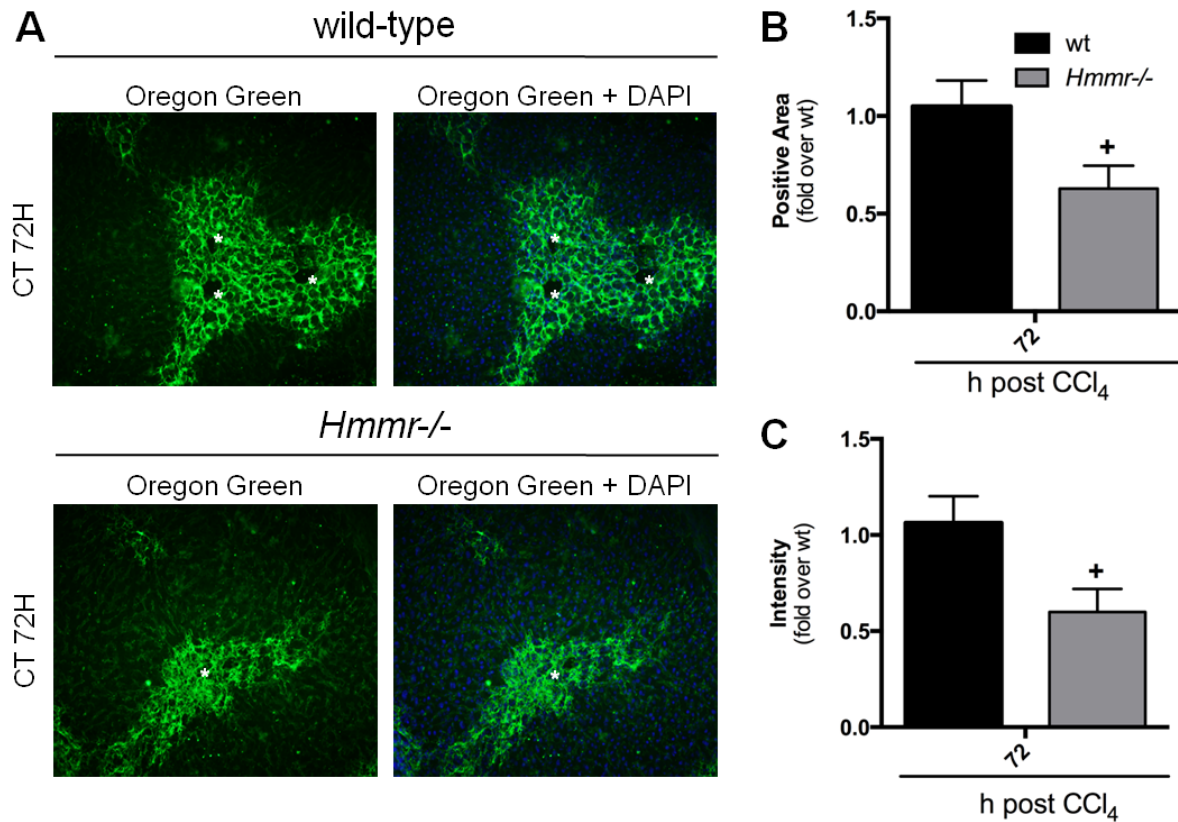


**Figure 4-9: Matrix remodeling following acute CCl<sub>4</sub> in wild-type and *Hmmr*<sup>-/-</sup> mice.**

Mice were exposed to CCl<sub>4</sub> and euthanized 72 hours later. A. Representative *in situ* zymography histology and quantification of B. area of positive signal and C. intensity were used to evaluate active matrix metabolism following acute CCl<sub>4</sub> exposure. \* denotes central vein, + denotes portal veins in the images. In the graphs, + represents  $p < 0.05$  when comparing the two genotypes at one time point. N = 7 – 8 mice per group.

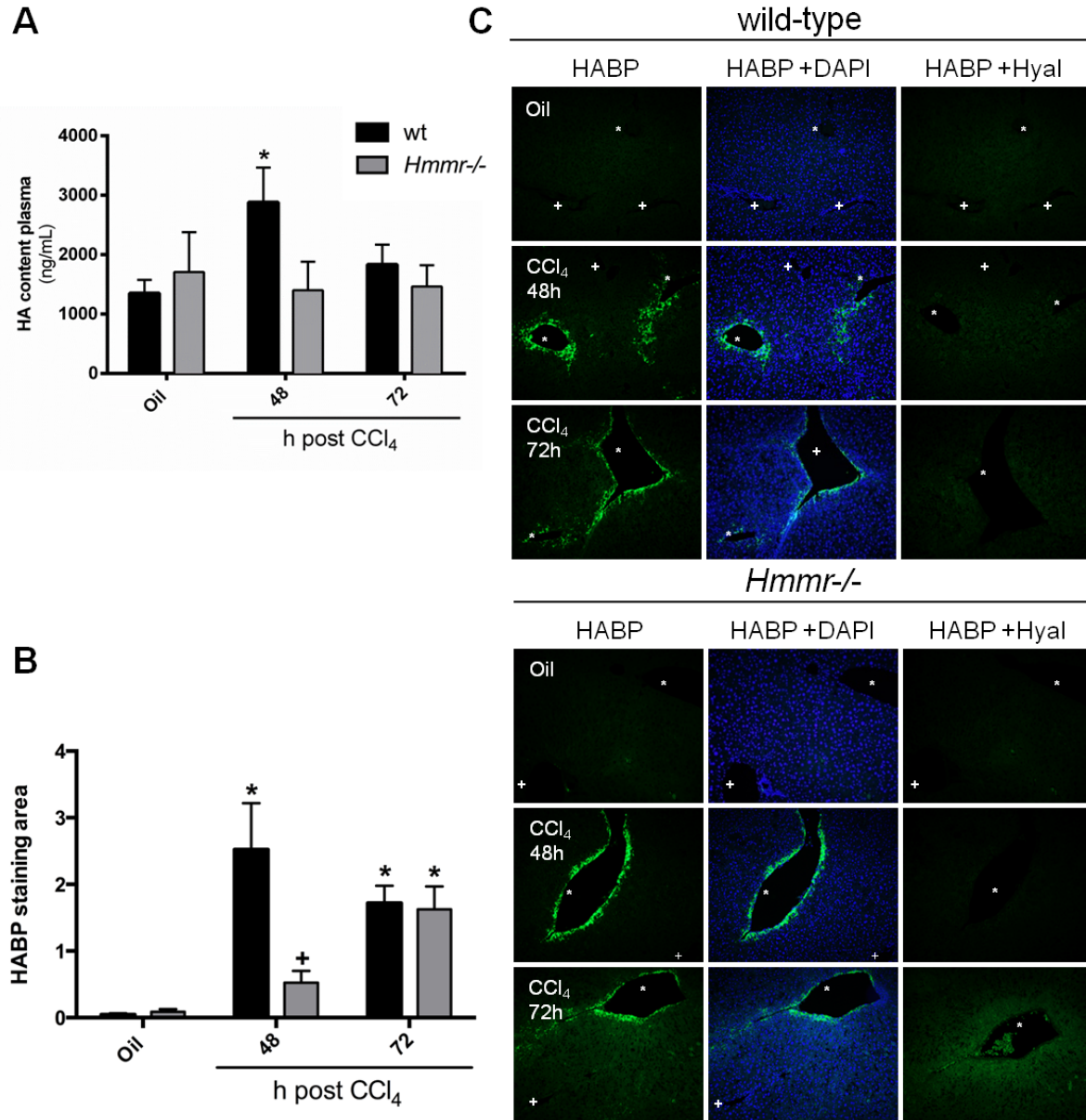


**Figure 4-10: Plasma and hepatic HA content following acute CCl<sub>4</sub> exposure in wild-type and *Hmnr*<sup>-/-</sup> mice.**

Mice were exposed to CCl<sub>4</sub> and euthanized 48 or 72 hours later. Control mice received an olive oil (oil) injection. A. An ELISA-like assay was used to measure plasma HA content. B. Quantification and C. representative histology of HABP staining used to localize hepatic HA content. \* denotes central vein, + denotes portal veins in the images. In the graphs, \* represents p<0.05 compared to each genotype's own oil. N = 6 – 9 mice per group.

## **Discussion**

HMMR is a unique HA receptor in that it has both intracellular and extracellular localization and has different effects on cell behavior depending on its location (Jiang *et al.*, 2010; Telmer *et al.*, 2011). Extracellular HMMR is tethered to the cellular membrane via a GPI anchor and acts with CD44 in aiding in cell migration and motility (Tolg *et al.*, 2006; Nikitovic *et al.*, 2013). Intracellular HMMR interacts with the mitotic spindle and binds to microtubules aiding in cell proliferation (Jiang *et al.*, 2010; Telmer *et al.*, 2011). Healthy adult tissue has very low levels of HMMR, however, following injury HMMR expression is drastically upregulated (Tolg *et al.*, 2006). In addition, tissues with extensive proliferation, like testis and bone marrow, express high levels of HMMR (Jiang *et al.*, 2010). HMMR is implicated in a number of biological process and diseases including dermal wound healing and lung inflammation (Zaman *et al.*, 2005; Tolg *et al.*, 2006). We provide the first evidence of a role for HMMR in hepatic wound healing following hepatotoxin induced liver injury, with possible implications for both inflammation and regeneration associated with wound repair.

In dermal wound healing, HMMR plays a role in both macrophage and fibroblast migration. HMMR and CD44 are required for ERK1/2 phosphorylation and subsequent migration of fibroblasts *in vitro* (Tolg *et al.*, 2006). Using a HMMR mimetic that prevents HMMR from interacting with HA, Tolg, *et al.*, show a decrease in both inflammation and fibrogenesis following full-thickness skin wounds (Tolg *et al.*, 2012). Specifically, the mimetic decreased macrophage and fibroblast numbers in the wound bed and this was associated with a decrease in wound collagen content (Tolg *et al.*, 2012). Our study closely mimics the inflammatory data from this published study in that we show a

decrease in the inflammatory microenvironment (i.e. decreased *Ccl2* and *Tnfa* expression) in the liver following acute hepatotoxin exposure. Decreased matrix metabolism suggests a decreased ability for the wound healing macrophages to localize to the necrotic area and aid in clean up. This is further supported by the delay in necrotic tissue removal. *Hmmr*<sup>-/-</sup> mice are able to recover to wild-type levels in terms of necrosis removal and inflammation, which may be due to compensation by another HA receptor CD44, which plays roles in cell migration as well.

HMMR plays a role in macrophage migration in other models of human diseases. A HMMR blocking antibody prevented macrophage migration both *in vitro* and *in vivo* in the lung following bleomycin exposure (Zaman *et al.*, 2005). Similarly, blocking HMMR prevented macrophage migration in response to the known macrophage chemotaxis stimulator, surfactant protein A (SPA), in a Boyden chamber assay (Foley *et al.*, 2012). Additionally, *Hmmr*<sup>-/-</sup> bone marrow derived macrophages have decreased migration in response to SPA, HA, or TGF $\beta$  (Foley *et al.*, 2012). We have shown in this study, that mice lacking HMMR have a lower inflammatory microenvironment compared to wild-type mice after acute CCl<sub>4</sub>. These mice also have decreased necrotic tissue removal and decreased matrix degradation. All of these things together strongly suggest a role for HMMR in macrophage migration in the liver following toxin induced acute liver injury.

HA is induced during injury and implicated in wound healing in other tissues, however no one has evaluated a role for HA in hepatic wound healing (Jiang *et al.*, 2007; Cowman *et al.*, 2015). What is interesting to note in our study is the delay in hepatic HA accumulation in *Hmmr*<sup>-/-</sup> mice compared to wild-type mice. This could be an indirect response to the decreased inflammation, specifically the delayed *Tnfa*

expression observed in the *Hmnr*<sup>-/-</sup> mice. In human umbilical cord vein endothelial cells (HUVEC), TNF $\alpha$  induces *HAS2* expression and subsequently HA synthesis (Vigetti *et al.*, 2010). This increased HA, in turn, increases the adhesion of U937 cells, a human monocyte cell line, to HUVEC, *in vitro* (Vigetti *et al.*, 2010). Conversely, reduced accumulation of hepatic HA in *Hmnr*<sup>-/-</sup> mice may be why inflammation was reduced relative to inflammation in wild-type mice. For example, LMW-HA induces expression of TNF $\alpha$  in peritoneal macrophages, *in vitro* (Jiang *et al.*, 2005). Additionally, persistent LMW-HA in mouse lungs following bleomycin-induced injury is associated with increased inflammation (Teder *et al.*, 2002). Because we see both a decrease in inflammation and a decrease in hepatic HA in *Hmnr*<sup>-/-</sup> mice compared to wild-type mice, it is impossible to distinguish if the HA is stimulating the inflammation or aiding in macrophage migration into the wound. It might also be possible that there exists a feed-forward loop involving inflammation and HA synthesis, where inflammation influences HA synthesis and subsequent HA and/or HA degradation influences inflammation. It is known that a transient increase in inflammation is required for wound repair, but we propose that the transient increase in HA synthesis and its subsequent degradation, coupled to HMMR-mediated recruitment of macrophages to injured tissue are critical and previously unrecognized components of the hepatic wound healing process.

HMMR plays a role in fibroblast migration during dermal wound healing (Tolg *et al.*, 2006; Tolg *et al.*, 2012). In fact, *Hmnr*<sup>-/-</sup> mice have a delay in fibroblast localization and defective wound repair (Tolg *et al.*, 2012). Despite this, no one has evaluated a role for HMMR in HSC migration in injured liver. Following liver injury, HSC become activated and differentiate into myofibroblasts that then begin synthesizing ECM

components, including HA (Vrochides *et al.*, 1996; Chang *et al.*, 2015b). While we evaluated HSC activation, we do not know if HMMR deficiency impaired the migration of HSC to the injured areas of the liver, or if that could be the cause of the delayed hepatic HA accumulation. Regardless, we did not observe a difference in HSC activation between genotypes, as evident by *Acta2* transcript levels and  $\alpha$ SMA protein quantification. Interestingly, while HA supplementation results in increased macrophage migration and faster dermal wound healing, this is not associated with an increase in  $\alpha$ SMA staining or collagen content (Tolg *et al.*, 2014). This increased wound healing induced by HA required HMMR and CD44 (Tolg *et al.*, 2014) and suggests that HMMR may be important for fibroblast localization, but not fibroblast activation. This stresses the importance of assessing HSC localization in *Hmmr*<sup>-/-</sup> mice following acute CCl<sub>4</sub> exposure.

The processes described above are all in relation to extracellular HMMR and the receptor's interaction with HA. However, as noted, HMMR can be intracellular as well. Intracellular HMMR is not as well studied with the majority of work having been done *in vitro*, and it is currently unknown whether its actions are HA dependent or independent (Savani *et al.*, 2000; Tolg *et al.*, 2010; Esguerra *et al.*, 2015). Our data suggest that HMMR is playing a role in hepatocyte proliferation, either directly within hepatocytes or indirectly by influencing inflammation. HMMR binds microtubules and is important in the G2/M phase transition of the cell cycle (Tolg *et al.*, 2010; Chen *et al.*, 2014). In fact, HMMR deficiency results in multi-pole mitotic spindles in mouse embryonic fibroblasts (Tolg *et al.*, 2010). The silencing of HMMR in HeLa cells results in an increase in multinucleated cells and cells with spindle pole defects (Chen *et al.*, 2014). HMMR

silenced HeLa cells were, however, able to initiate proliferation, but became stalled mid-mitosis, suggesting a problem with the final proliferative stages, not the initiation of proliferation (Chen *et al.*, 2014). If hepatocytes are able to initiate cell proliferation, but become “stuck” mid-mitosis, this may be why we see no difference in PCNA or Cyclin D1 protein levels, but a decrease in Ki67 positive hepatocytes.

The delay in regeneration observed in HMMR deficient mice could be secondary to the delay in inflammation observed. It is well known that inflammation plays a critical role in hepatocyte proliferation following hepatic wound healing (Webber *et al.*, 1998; Nishiyama *et al.*, 2015). Specifically, complement protein proteolytic fragments C3a and C5a as well as TNF $\alpha$  prime rat hepatocytes for proliferation *in vitro* (Webber *et al.*, 1998; Strey *et al.*, 2003), and Kupffer cell depletion limits DNA synthesis following ethanol induced liver injury *in vivo* (Owumi *et al.*, 2014). In our study, we observed a decrease in the expression of pro-inflammatory molecules, *Tnfa* and *Ccl2*, which could contribute to the delay in regeneration we observe. HMMR deficiency could therefore be the indirect cause of the delayed regeneration due to decreased inflammation. HMMR is present on macrophages, which further supports this idea (Zaman *et al.*, 2005). In fact, when we evaluated *Hmmr* expression in hepatocytes and non-parenchymal cells (NPC), the NPC fraction had approximately 20 times the amount of *Hmmr* expression compared to the hepatocyte fraction at both 48 and 72 hours after CCl<sub>4</sub> exposure (data not shown). Despite this, no one has specifically evaluated HMMR in hepatocytes, or proliferation of hepatocytes with or without HMMR. Therefore, further exploration into cell type specific expression patterns should be completed to determine if HMMR is contributing to hepatocyte regeneration directly or indirectly via inflammation.

Our initial interest in HMMR came from the increased HMMR expression observed in *Has3*<sup>-/-</sup> mice, which occurred concomitant with hepatic wound healing after acute liver injury (see Chapter 3). Specifically, *Has3*<sup>-/-</sup> mice have increased injury and inflammation but, in turn, they also display increased regeneration and matrix metabolism. This was associated with increased HMMR expression compared to wild-type mice. Conversely, in HMMR mice, we observe no difference in liver injury, but a delay in inflammation, regeneration, and matrix remodeling. This inverse relationship between *Has3*<sup>-/-</sup> and *Hmmr*<sup>-/-</sup> mice strongly suggests a positive role for HMMR in hepatic wound healing and will be further discussed in Chapter 7.

In conclusion, we are the first to show that HMMR is involved in liver repair. This is supported by our data which demonstrated that mice lacking HMMR exhibit decreased hepatic inflammation despite no differences in liver injury, delayed clearance of necrotic tissue, decreased hepatic HA deposition, delayed hepatocyte proliferation, and decreased matrix remodeling. This suggests roles for HMMR in multiple cell types, including macrophages, HSC, and perhaps even hepatocytes, and lays the foundation for future work exploring cell-type specific roles for HMMR in liver repair.

## Chapter 5: A critical role for HA and HMMR in liver fibrosis

*Portions of this chapter are adapted from 1) McCracken, JM et al. "Differential effects of hyaluronan synthase 3 deficiency after acute vs chronic liver injury in mice"*

*Fibrogenesis and Tissue Repair 2016; Licensed under Creative Commons Attribution*

*4.0 International License*

## **Abstract**

Following acute liver injury, the liver undergoes periods of inflammation, regeneration, and matrix remodeling and completely restores normal structure and function. Following chronic injury, persistent inflammation results in activation of hepatic stellate cells that synthesize extracellular matrix resulting in fibrosis. If the injurious agent is removed, matrix degradation can remodel and remove the scar. We have previously shown that HA and the HA receptor HMMR play a role in hepatic wound healing following acute liver injury. Specifically, mice deficient in HAS3 have increased injury but they also have increased matrix metabolism. This led us to hypothesize that *Has3*<sup>-/-</sup> mice will have a similar increase in matrix metabolism following chronic carbon tetrachloride (CCl<sub>4</sub>) exposure resulting in less fibrosis compared to wild-type mice. We have also shown that mice deficient in HMMR have similar injury after acute CCl<sub>4</sub> exposure but decreased matrix metabolism compared to wild-type mice. We therefore hypothesize that *Hmmr*<sup>-/-</sup> mice will have increased fibrosis after chronic CCl<sub>4</sub> due to decreased matrix metabolism. To induce fibrosis, we exposed each genotype to CCl<sub>4</sub> twice a week for five weeks and evaluated both matrix synthesis and matrix degradation parameters. *Has3*<sup>-/-</sup> mice had increased fibrotic transcript levels, but similar fibrosis compared to wild-type mice. This disconnect was attributed to increased matrix metabolism in *Has3*<sup>-/-</sup> mice, likely due to increased MMP13 activity. *Hmmr*<sup>-/-</sup> mice had lower levels of pro-fibrotic transcripts, but no difference in frank fibrosis compared to wild-type mice. Like *Has3*<sup>-/-</sup> mice, this disconnect was attributed to decreased matrix metabolism in *Hmmr*<sup>-/-</sup> mice. Together these data suggest that HA and HMMR play a role in chronic liver injury.

## **Introduction**

Chronic liver injury can be caused by a number of etiologic agents including viral hepatitis, obesity, and chronic alcohol abuse (Sebastiani *et al.*, 2014; Stal, 2015; Crespo Yanguas *et al.*, 2016). Liver disease can progress from simple steatosis to early and advanced fibrosis if exposure to the etiologic agent persists (Bataller and Brenner, 2005; Crespo Yanguas *et al.*, 2016). Following acute liver injury, there are periods of inflammation, regeneration, and matrix remodeling that result in a complete recovery, or regenerative repair (Bohm *et al.*, 2010; Balaji *et al.*, 2015; Pritchard and McCracken, 2015). In chronic liver injury, inflammation is sustained and fibrosis can occur (Friedman, 2008b; Pellicoro *et al.*, 2014). Fibrosis is characterized by an excess accumulation of extracellular matrix (ECM), primarily type-I collagen fibers (Bataller and Brenner, 2005; Friedman, 2008b). The excess ECM disrupts normal tissue structure and function (Bataller and Brenner, 2005; Crespo Yanguas *et al.*, 2016). Fibrosis can resolve, to a point, but if it progresses to advanced stages such as cirrhosis, a liver transplant becomes the only treatment option (Bataller and Brenner, 2005; Tsochatzis *et al.*, 2014; Crespo Yanguas *et al.*, 2016). Due to the shortage of livers available, as well as the cost and invasiveness of organ transplant, there is need for novel therapeutics to halt and reverse the progression of fibrosis (Saidi *et al.*, 2012; Rai, 2013).

Hyaluronan (HA) is a non-sulfated glycosaminoglycan that is synthesized by one of three hyaluronan synthases (HAS1, 2, or 3) (Jiang *et al.*, 2007; Jiang *et al.*, 2011). These enzymes differ in their synthetic capacity and expression profiles depending on tissue and developmental stage (Spicer and McDonald, 1998; Itano *et al.*, 1999).

Following tissue injury, HA is both synthesized and degraded and has different signaling capabilities depending on the size of HA and HA receptors present (Turley *et al.*, 2002; Decleves *et al.*, 2012; Tolg *et al.*, 2014). There are several cell surface receptors that can interact with HA and our focus is on HA mediated motility receptor (HMMR) due to its unique properties related to wound repair (Savani *et al.*, 2001; Turley *et al.*, 2002). For example, HMMR can be both intracellular and extracellular and plays roles in cell migration and cell proliferation, respectively (Savani *et al.*, 2000; Jiang *et al.*, 2010; Telmer *et al.*, 2011). In the context of chronic injury and fibrotic wound repair, it is likely that extracellular HMMR plays a more prominent role. For example, in mice, following an excisional skin wound, HMMR promotes macrophage and fibroblast migration and wound closure, two processes that are vitally important in liver fibrosis progression (Tolg *et al.*, 2006; Tolg *et al.*, 2012). We raise the question-does HA or HMMR play a role in chronic liver injury and fibrosis.

We have previously shown (Chapters 3 and 4), that HA and HMMR play a role in the hepatic response to acute carbon tetrachloride (CCl<sub>4</sub>) exposure. Specifically, mice deficient in HAS3, one of the enzymes that makes HA, have increased liver injury and inflammation compared to wild-type mice after acute CCl<sub>4</sub> exposure. They also had, however, increased matrix metabolism. These differences were associated with an increase in hepatic HA content in *Has3*<sup>-/-</sup> mice compared to wild-type mice and upregulation of several HA receptors, including HMMR. This led us to examine *Hmmr*<sup>-/-</sup> mice after acute liver injury. We showed in Chapter 4, that these mice had decreased matrix metabolism, despite no difference in liver injury compared to wild-type mice after acute CCl<sub>4</sub> exposure. Based on the data collected following acute CCl<sub>4</sub> (Chapters 3 and

4), we hypothesize that *Has3*<sup>-/-</sup> mice will have increased matrix remodeling compared to wild-type after chronic CCl<sub>4</sub> exposure which would result in decreased fibrosis. Further we hypothesize that *Hmmr*<sup>-/-</sup> mice will have a delayed wound healing including matrix remodeling resulting in increased fibrosis compared to wild-type mice. To test these hypotheses, we used chronic CCl<sub>4</sub> exposure to induce fibrosis in wild-type, *Has3*<sup>-/-</sup>, and *Hmmr*<sup>-/-</sup> mice.

## **Results**

### **Fibrosis in wild-type and *Has3*<sup>-/-</sup> mice following chronic CCl<sub>4</sub> exposure**

To evaluate a possible role for HA in hepatic fibrosis and resolution, wild-type and *Has3*<sup>-/-</sup> mice were exposed CCl<sub>4</sub> twice a week for five weeks. *Has3*<sup>-/-</sup> mice have increased injury and inflammation following acute liver injury induced by a single exposure to CCl<sub>4</sub>. They also display faster wound healing, including increased matrix metabolism. We therefore hypothesized that *Has3*<sup>-/-</sup> mice will have decreased fibrosis following chronic CCl<sub>4</sub> exposure. Following chronic CCl<sub>4</sub>, hepatic *Acta2* increased in both wild-type and *Has3*<sup>-/-</sup> mice and this induction was higher in *Has3*<sup>-/-</sup> mice compared to wild-type mice (Figure 5-1A). Despite this increase in *Acta2* transcripts, there was no difference in  $\alpha$ SMA protein after chronic CCl<sub>4</sub> between wild-type or *Has3*<sup>-/-</sup> mice (Figure 5-1B and C). Hepatic transcripts for *Col1a1*, *Col1a2*, and *Serpinh1* (the gene encoding for HSP47-a collagen specific chaperone) were all increased in both genotypes following chronic CCl<sub>4</sub> exposure (Figure 5-1D-F). The induction in each of these transcripts was higher in *Has3*<sup>-/-</sup> mice compared to wild-type mice suggesting an

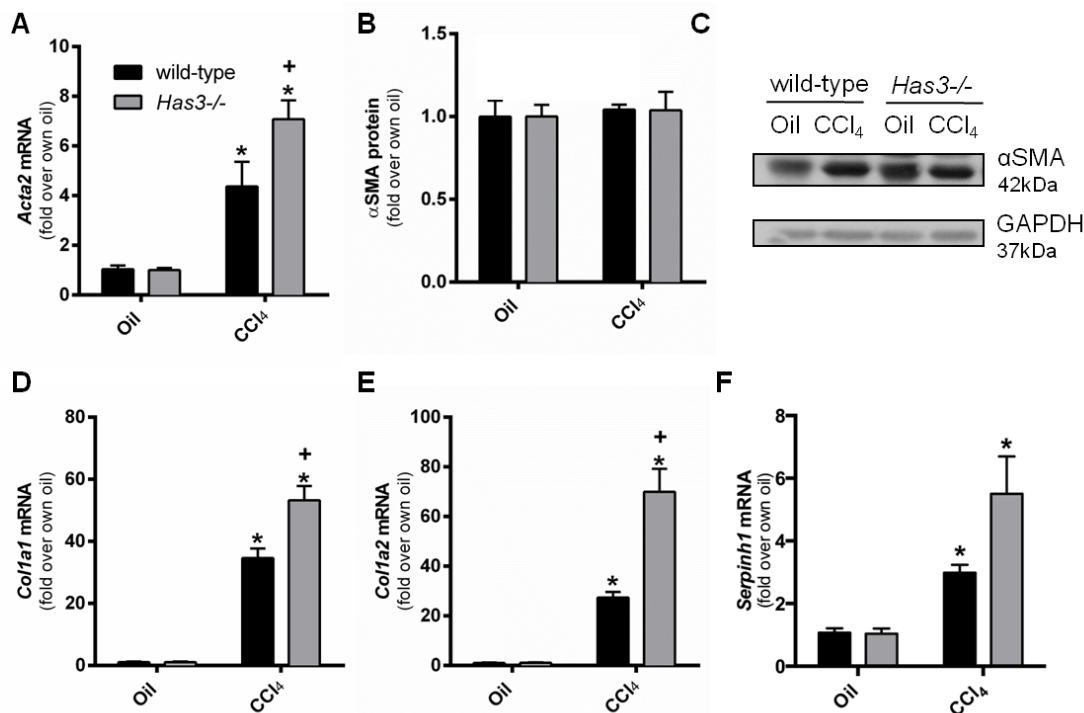


**Figure 5-1: Hepatic stellate cell activation in wild-type and *Has3*<sup>-/-</sup> mice following chronic CCl<sub>4</sub>.**

Mice were exposed to CCl<sub>4</sub> twice a week for five weeks and euthanized 72 hours after the last injection. Control mice received olive oil (oil) injections twice a week for five weeks. Hepatic transcript accumulation of A. *Acta2* was evaluated using real time PCR. B. Quantification and C. representative blot for  $\alpha$ SMA protein. GAPDH was used as a loading control. Real time PCR was used to measure transcript accumulation of D. *Col1a1*, E. *Col1a2*, and F. *Serpinh1* in wild-type and *Has3*<sup>-/-</sup> livers following chronic CCl<sub>4</sub> exposure. Black bars represent wild-type mice and grey bars represent *Has3*<sup>-/-</sup> mice for figures 1-6. Data are presented as fold change over each genotypes own oil. \* represents p<0.05 comparing each genotypes CCl<sub>4</sub> value to its own oil, + represents p<0.05 comparing CCl<sub>4</sub> between genotypes. N = 5 – 6

increase in the pro-fibrotic environment.

Surprisingly, despite the increased pro-fibrotic signature observed in *Has3*<sup>-/-</sup> mice compared to wild-type mice, there is not increased fibrosis in *Has3*<sup>-/-</sup> mice. Picrosirius red staining was used to evaluate ECM accumulation, and while there was an increase in hepatic ECM in both wild-type and *Has3*<sup>-/-</sup> mice following chronic CCl<sub>4</sub>, there was not a difference between genotypes (Figure 5-2A and B). Similarly, there is no difference in total collagen content (extrapolated from measured hydroxyproline content) between wild-type and *Has3*<sup>-/-</sup> mice following chronic CCl<sub>4</sub> (Figure 5-2C). These data suggest that there are increased hepatic pro-fibrotic signatures in chronically injured livers from *Has3*<sup>-/-</sup> mice, but this did not lead to an increase in fibrosis in *Has3*<sup>-/-</sup> mice compared to wild-type mice.

### **Matrix remodeling in *Has3*<sup>-/-</sup> and wild-type mice following chronic CCl<sub>4</sub> exposure**

Fibrosis is counterbalanced by matrix metalloproteinases (MMPs) produced primarily by recruited macrophages. Because there was an obvious disconnect between pro-fibrotic gene signatures in the liver and the extent to which this influenced fibrosis, we hypothesized that there was an increase in matrix metabolism in *Has3*<sup>-/-</sup> mice compared to wild-type mice. This is similar to what we observed in *Has3*<sup>-/-</sup> mice compared to wild-type mice after acute CCl<sub>4</sub> exposure. Hepatic accumulation of mRNAs encoding for *Mmp2*, a mouse gelatinase, increased in both genotypes after chronic CCl<sub>4</sub> exposure and this induction was not different between *Has3*<sup>-/-</sup> and wild-type mice (Figure 5-3A). A similar trend was seen for *Mmp9*, another mouse gelatinase (Figure 5-3B). Hepatic transcript accumulation of *Mmp13*, the main mouse collagenase, was

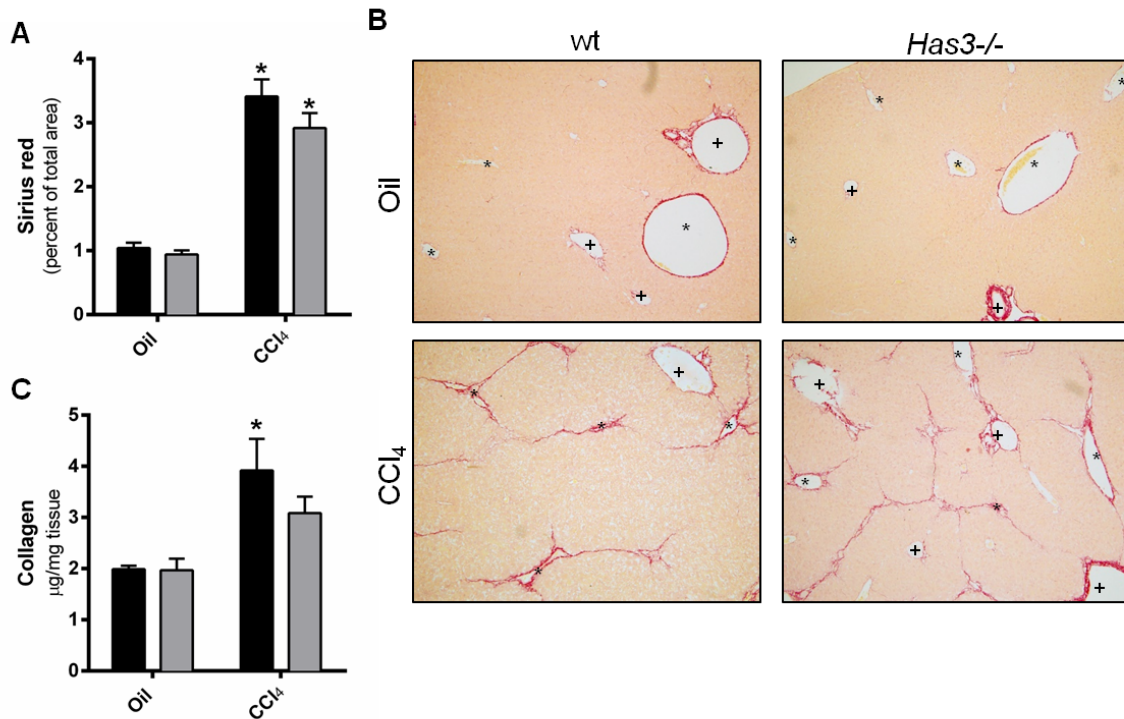


**Figure 5-2: Hepatic fibrosis in wild-type and *Has3*<sup>-/-</sup> mice following chronic CCl<sub>4</sub> exposure.**

Mice were exposed to CCl<sub>4</sub> twice a week for five weeks and euthanized 72 hours after the last injection. Control mice received olive oil (oil) injections twice a week for five weeks. A. Quantification and B. representative histology of picosirius red staining used to measure ECM accumulation by morphometry in wild-type and *Has3*<sup>-/-</sup> livers following chronic CCl<sub>4</sub> exposure. \* denotes central veins and + denotes the portal triads in images. C. Hydroxyproline was measured and extrapolated to collagen content in both wild-type and *Has3*<sup>-/-</sup> mice. \* represents  $p < 0.05$  comparing each genotypes CCl<sub>4</sub> value to its own oil, N = 6 – 7

induced by repeated CCl<sub>4</sub> exposure, and similar to what we observed in acute CCl<sub>4</sub> exposure, this induction was higher in *Has3*<sup>-/-</sup> mice compared to wild-type mice (Figure 5-3C). MMP enzymes are released into the extracellular space in a pro-form and must be cleaved to their active form (Duarte *et al.*, 2015). We, therefore, measured the ratio of active to pro form of MMP13 in liver following chronic CCl<sub>4</sub> exposure and found this ratio was increased in *Has3*<sup>-/-</sup> mice compared to wild-type mice, suggesting increased MMP13 activity (Figure 5-3D and E). Tissue inhibitors of MMPs (TIMPs) inhibit MMP activity and provide a counterbalance to matrix metabolism (Duarte *et al.*, 2015). *Timp1* transcripts were increased in both genotypes following chronic CCl<sub>4</sub> exposure and this induction was not different between genotypes (Figure 5-3F).

While transcript and protein data suggest that matrix remodeling is increased in *Has3*<sup>-/-</sup> mice compared to wild-type mice following chronic CCl<sub>4</sub> exposure, this is not a direct measurement of matrix degradation. In order to evaluate the actual matrix metabolism, *in situ* zymography was used (described in detail in Chapters 2 and 3). Chronic CCl<sub>4</sub> exposure increased both the area and intensity of signal measured in wild-type and *Has3*<sup>-/-</sup> mice (Figure 5-4A-C). This matrix metabolism (area and intensity) was increased in *Has3*<sup>-/-</sup> mice compared to wild-type mice. Due to the difference in *Mmp13* mRNAs, as well as the increased ratio of active-MMP13 to pro-MMP13, we utilized a MMP13 specific inhibitor to inhibit MMP13 activity. When the inhibitor was used, matrix degradation in *Has3*<sup>-/-</sup> mice was inhibited while the matrix degradation in wild-type mice was unaffected. These data together demonstrate that matrix metabolism was

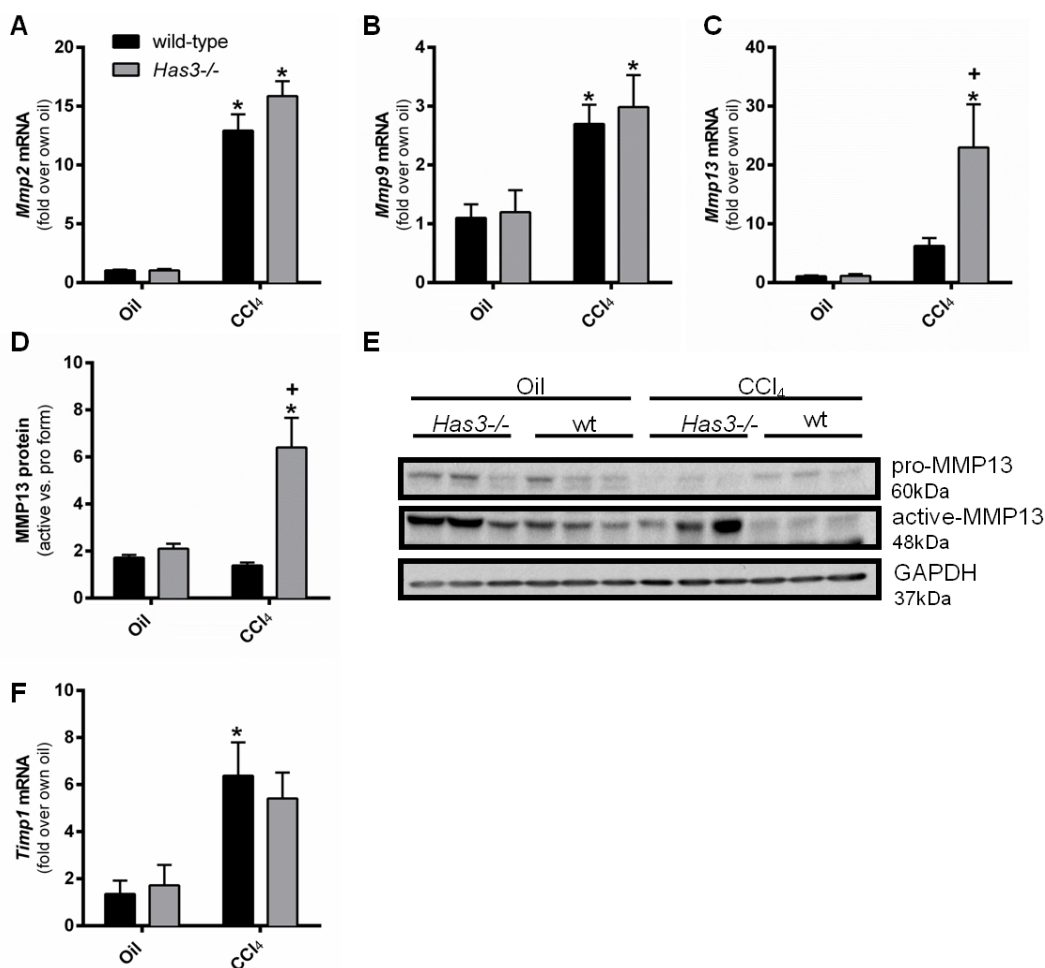


**Figure 5-3: Markers for matrix metabolism in wild-type and *Has3*<sup>-/-</sup> mice following chronic CCl<sub>4</sub> exposure.**

Mice were exposed to CCl<sub>4</sub> twice a week for five weeks and euthanized 72 hours after the last injection. Control mice received olive oil (oil) injections twice a week for five weeks. Real time PCR was used to evaluate hepatic transcript accumulation of A. *Mmp2*, B. *Mmp9*, and C. *Mmp13* in wild-type and *Has3*<sup>-/-</sup> mice after chronic exposure to CCl<sub>4</sub>. Data are presented as fold over each genotypes own oil. D. Quantification and E. representative blot for the active and pro form of MMP13. GAPDH was used as a loading control. Data are presented as a ratio of active to pro form. F. Hepatic transcript levels of *Timp1* were measured using real time PCR. Data are presented as fold change over each genotypes own oil. \* represents p<0.05 comparing each genotypes CCl<sub>4</sub> value to its own oil, + represents p<0.05 comparing CCl<sub>4</sub> between genotypes. N = 6 – 7

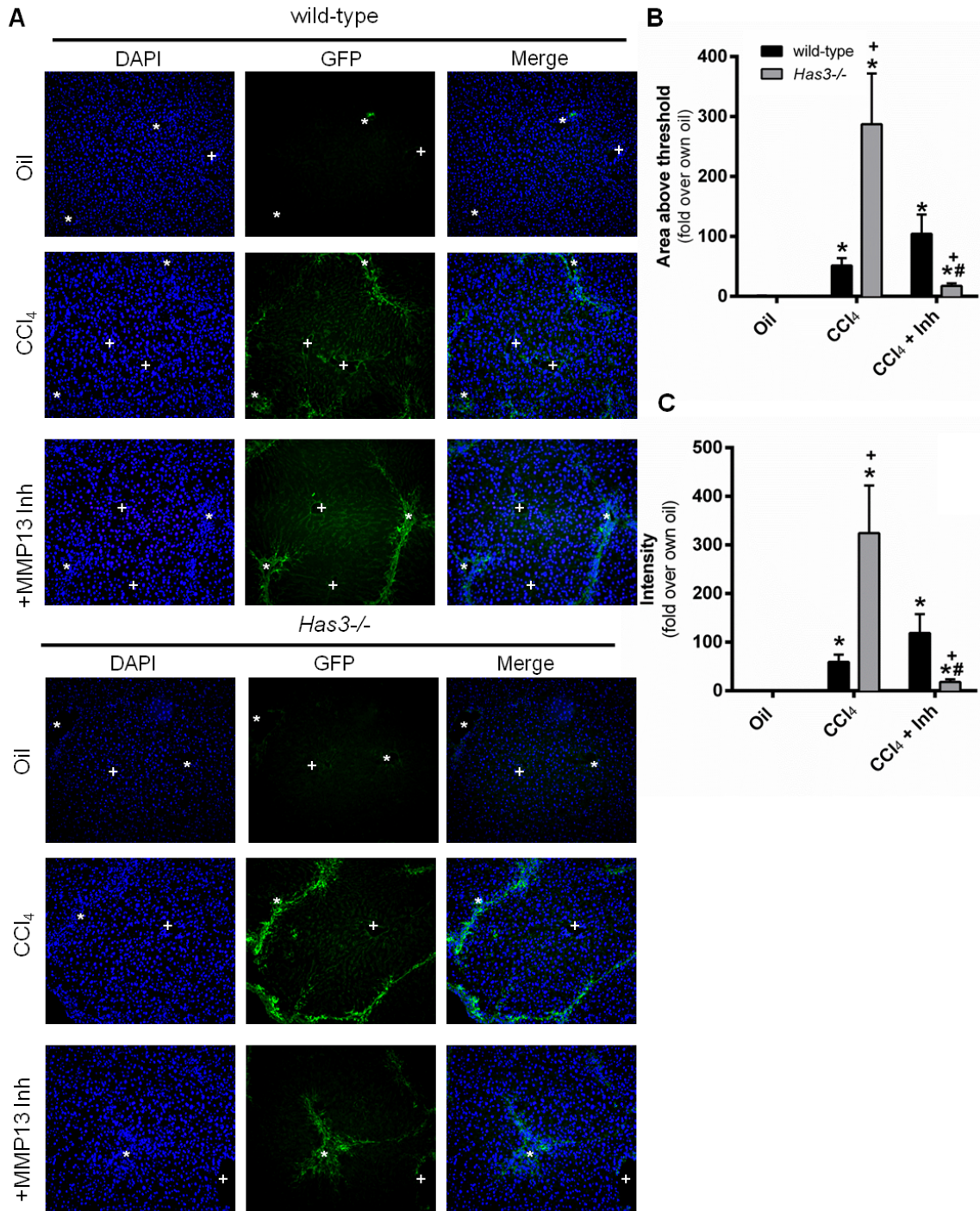


**Figure 5-4: Active matrix remodeling in wild-type and *Has3*<sup>-/-</sup> mice following chronic CCl<sub>4</sub>.**

Mice were exposed to CCl<sub>4</sub> twice a week for five weeks and euthanized 72 hours after the last injection. Control mice received olive oil (oil) injections twice a week for five weeks. A. Representative *in situ* zymography (ISZ) histology used to evaluate active matrix metabolism in fresh frozen liver sections of wild-type and *Has3*<sup>-/-</sup> mice. The top panel is ISZ for wild-type mice and the bottom panel is ISZ for *Has3*<sup>-/-</sup> mice. The left-most column is DAPI staining for nuclei, the middle column is Oregon green signal, and the right most column is the merged images. An MMP13-specific inhibitor was used to determine MMP13's contribution to matrix metabolism. B. Quantification of the total area above a set threshold and C. intensity of the signal. \* denotes central veins and + denotes the portal triads in images. Data are presented as fold change over own oil. \* represents p<0.05 comparing each genotypes CCl<sub>4</sub> value to its own oil, + represents p<0.05 comparing CCl<sub>4</sub> between genotypes, # represents p<0.05 between CCl<sub>4</sub> and CCl<sub>4</sub> + Inh within each genotype. N = 6 – 7

increased in *Has3*<sup>-/-</sup> mice compared to wild-type mice likely due to increased MMP13 activity.

### **Macrophage accumulation following chronic CCl<sub>4</sub> exposure in wild-type and *Has3*<sup>-/-</sup> mice**

The primary source of matrix degrading enzymes is recruited macrophages (Duarte *et al.*, 2015). We therefore evaluated macrophage accumulation following chronic CCl<sub>4</sub> exposure in both wild-type and *Has3*<sup>-/-</sup> mice. As a surrogate marker for macrophage content, we evaluated the hepatic transcript accumulation of two macrophage markers, *Emr1* and *Cd11b*. *Emr1* (the gene that encodes for F4/80) transcripts trend toward an increase in both genotypes, however neither genotype was significantly higher than its own baseline (Figure 5-5A). Hepatic *Cd11b* accumulation was increased in *Has3*<sup>-/-</sup> mice but not in wild-type mice in response to chronic CCl<sub>4</sub> (Figure 5-5B). Immunofluorescent staining for F4/80 showed no difference between wild-type and *Has3*<sup>-/-</sup> mice in total amount of F4/80 positive cells in the liver following chronic CCl<sub>4</sub> (Figure 5-5C and D). This demonstrates that there was no increase in macrophage recruitment to the liver, but it does not prove there is no difference in localization of those macrophages to fibrotic septae. In fact, the increased matrix metabolism suggests either there was increased macrophage localization to the fibrotic scar or that each macrophage reaching the fibrotic scar had greater matrix degrading activity in *Has3*<sup>-/-</sup> mice than wild-type mice. Future work should be done to more closely evaluate macrophage localization.

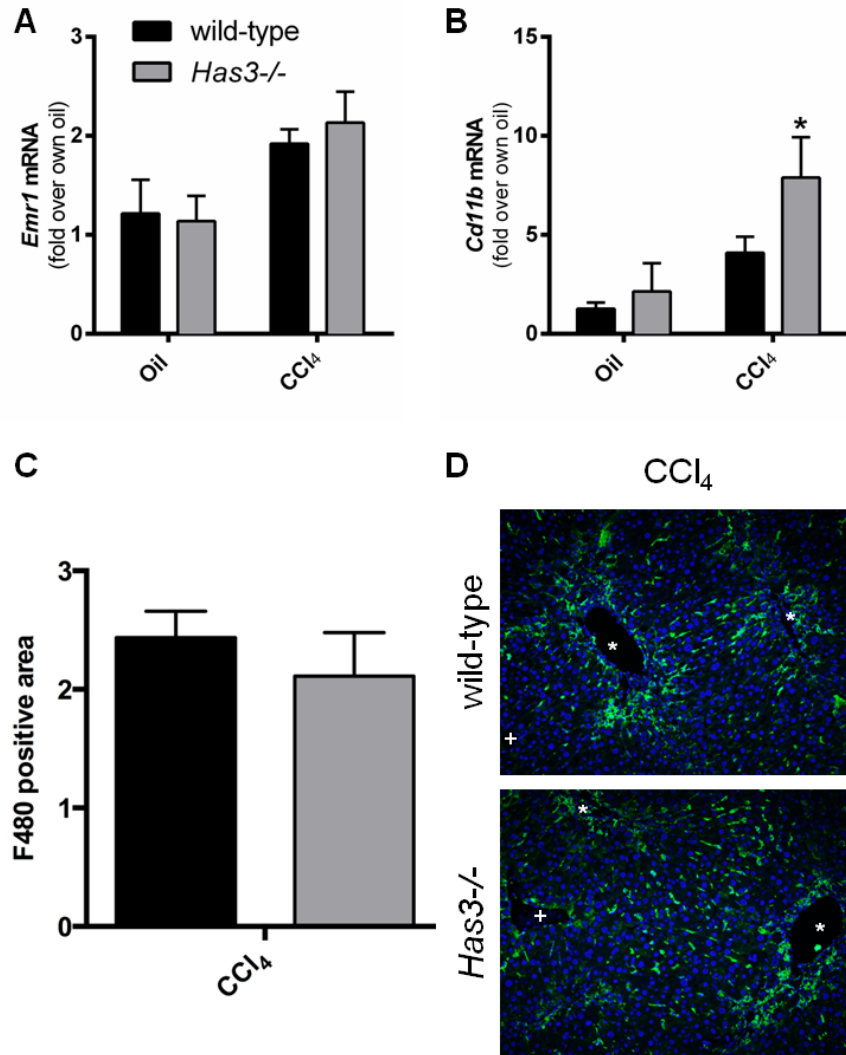


**Figure 5-5: Macrophage accumulation in wild-type and *Has3*<sup>-/-</sup> mice following chronic CCl<sub>4</sub> exposure.**

Mice were exposed to CCl<sub>4</sub> twice a week for five weeks and euthanized 72 hours after the last injection. Control mice received olive oil (oil) injections twice a week for five weeks. Real time PCR was used to evaluate hepatic transcript accumulation of A. *Emr1* and B. *Cd11b*. Data are presented as fold change over each genotypes own oil. C. Quantification and D. representative histology for F4/80 positive macrophages in wild-type and *Has3*<sup>-/-</sup> livers after chronic CCl<sub>4</sub> exposure. The green signal is F4/80 and DAPI was used to visualize nuclei. \* denotes central veins and + denotes the portal triads in images. \* represents p<0.05 comparing each genotypes CCl<sub>4</sub> value to its own oil. N = 6 – 7

## **HA and HMMR levels in *Has3*<sup>-/-</sup> and wild-type mice following chronic CCl<sub>4</sub> exposure**

Following acute CCl<sub>4</sub> exposure, hepatic HA content was greater in *Has3*<sup>-/-</sup> mice, despite lacking one enzyme that makes HA. Following chronic CCl<sub>4</sub>, there was limited HA accumulation near the fibrotic scar in both wild-type and *Has3*<sup>-/-</sup> mice (Figure 5-6A and B). This accumulation was not different between the two genotypes.

We took a particular interest in the HA receptor HMMR due to its role in cell migration, including migration of macrophages and fibroblasts. HMMR induction was increased in *Has3*<sup>-/-</sup> mice compared to wild-type mice following acute CCl<sub>4</sub> exposure. Similarly, hepatic *Hmmr* transcripts were induced following chronic CCl<sub>4</sub> in both genotypes and this induction was greater in *Has3*<sup>-/-</sup> compared to wild-type mice (Figure 5-6C). HMMR protein levels were increased above baseline in *Has3*<sup>-/-</sup> mice but not wild-type mice following chronic CCl<sub>4</sub> (Figure 5-6D and E). Taken together, although we observed increased pro-fibrotic transcripts, there was not increased fibrosis, likely because of the increased matrix metabolism in *Has3*<sup>-/-</sup> mice compared to wild-type mice.

## **Hepatic fibrosis following chronic CCl<sub>4</sub> exposure in wild-type and *Hmmr*<sup>-/-</sup> mice**

Due to the importance of macrophage migration in fibrosis resolution, HMMR's role in macrophage migration following excisional skin wounds, and the induction of HMMR after chronic CCl<sub>4</sub> we wanted to explore a possible role for HMMR in hepatic fibrosis. To do this we exposed wild-type and *Hmmr*<sup>-/-</sup> to CCl<sub>4</sub> twice a week for five weeks to establish fibrosis. Following acute liver injury induced by CCl<sub>4</sub> exposure,

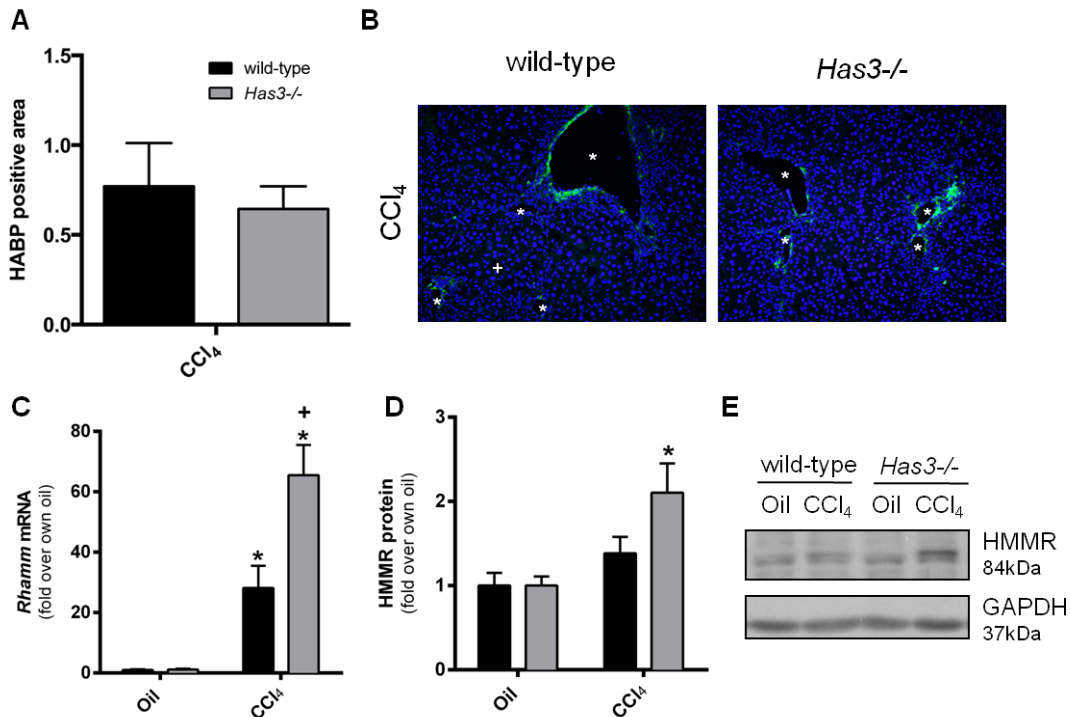


**Figure 5-6: HA accumulation and HMMR levels in wild-type and *Has3*<sup>-/-</sup> mice following chronic CCl<sub>4</sub> exposure.**

Mice were exposed to CCl<sub>4</sub> twice a week for five weeks and euthanized 72 hours after the last injection. Control mice received olive oil (oil) injections twice a week for five weeks. A. Quantification and B. representative histology for hepatic HA accumulation measured using HA binding protein (HABP). The green signal is HABP and DAPI was used to visualize nuclei. \* denotes central veins and + denotes the portal triads in images. C. Real time PCR was used to measure hepatic accumulation of *Hmmr* in wild-type and *Has3*<sup>-/-</sup> livers after chronic CCl<sub>4</sub> exposure. D. Quantification and E. representative blot for HMMR protein. GAPDH was used as a loading control. Data are presented as fold change over each genotypes own oil. \* represents p<0.05 comparing each genotypes CCl<sub>4</sub> value to its own oil, + represents p<0.05 comparing CCl<sub>4</sub> between genotypes. N = 6 – 7

*Hmmr*<sup>-/-</sup> mice have a delay in wound healing, including matrix metabolism. This led us to hypothesize that *Hmmr*<sup>-/-</sup> mice would have increased fibrosis compared to wild-type mice after chronic CCl<sub>4</sub>.

Hepatic *Acta2* mRNAs were increased in wild-type mice following chronic CCl<sub>4</sub> but not in *Hmmr*<sup>-/-</sup> mice (Figure 5-7A). Similar to what was found in *Has3*<sup>-/-</sup> mice, protein levels of  $\alpha$ SMA were not different in either wild-type or *Hmmr*<sup>-/-</sup> mice after chronic CCl<sub>4</sub> (Figure 5-7B and C). Transcript levels of *Col1a1* and *Col1a2*, the genes that encode for type 1-collagen proteins, were induced in both genotypes after chronic CCl<sub>4</sub> and this induction was greater in wild-type mice compared to *Hmmr*<sup>-/-</sup> mice (Figure 5-7D and E). This trend was similar for *Serpinh1*, the gene encoding HSP47-a collagen specific chaperone; this transcript was induced in both genotypes but the induction was stunted in *Hmmr*<sup>-/-</sup> mice compared to wild-type mice (Figure 5-7F). These transcript data suggest that HSC activation is impaired in *Hmmr*<sup>-/-</sup> mice compared to wild-type mice after chronic CCl<sub>4</sub> exposure.

To evaluate frank fibrosis, picrosirius red was again used to measure total ECM accumulation. Despite the decreased fibrotic markers observed in *Hmmr*<sup>-/-</sup> mice, there was no difference in ECM accumulation between genotypes (Figure 5-8A and B). This is further supported by no difference in collagen levels, extrapolated from measured hydroxyproline content, between wild-type and *Hmmr*<sup>-/-</sup> mice following chronic CCl<sub>4</sub> exposure (Figure 5-8C). Together, these data demonstrate that despite a decrease in pro-fibrotic transcripts, the frank fibrosis was not different between wild-type and *Hmmr*<sup>-/-</sup> mice following chronic liver injury.

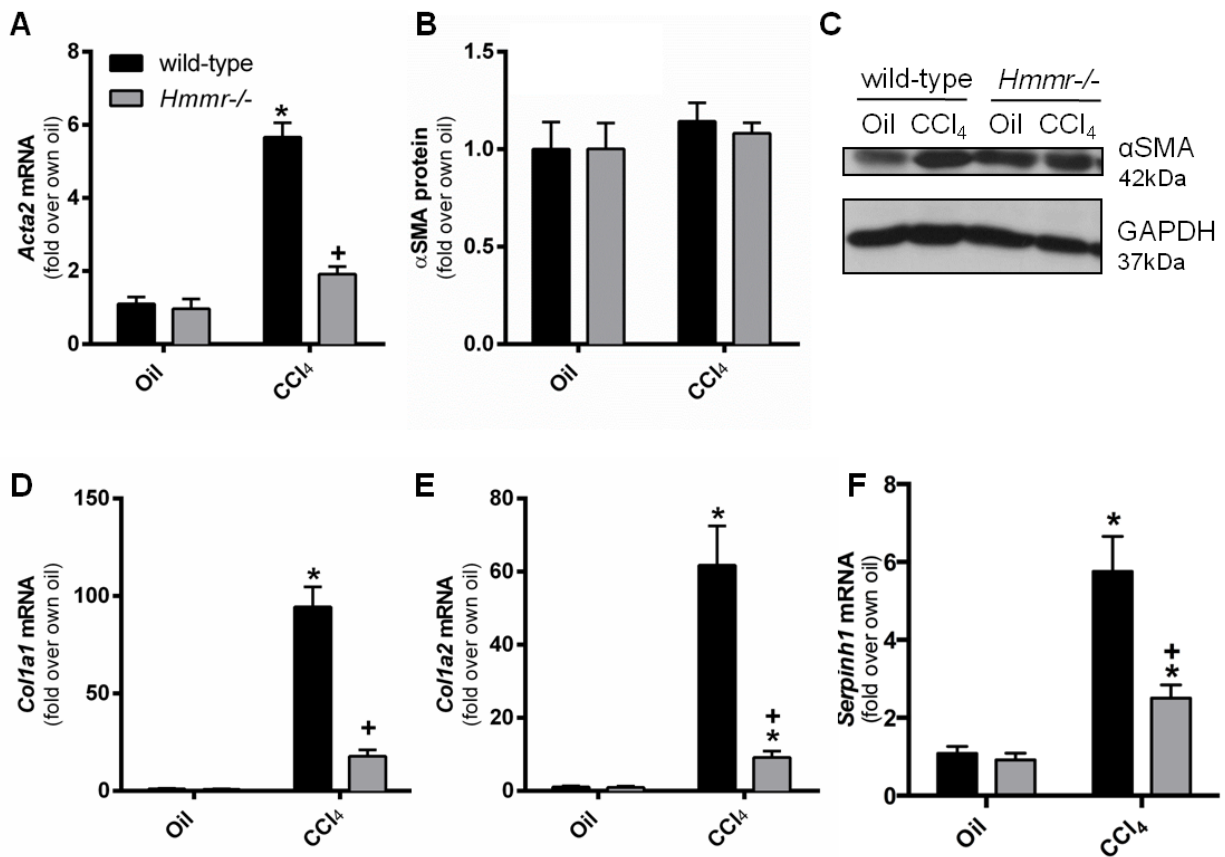


**Figure 5-7: Hepatic stellate cell activation in wild-type and *Hmmer*<sup>-/-</sup> mice following chronic CCl<sub>4</sub> exposure.**

Mice were exposed to CCl<sub>4</sub> twice a week for five weeks and euthanized 72 hours after the last injection. Control mice received olive oil (oil) injections twice a week for five weeks. A. Real time PCR was used to evaluate *Acta2* transcript levels in livers of wild-type and *Hmmer*<sup>-/-</sup> mice following chronic CCl<sub>4</sub> exposure. B. Quantification and C. representative blot for  $\alpha$ SMA protein. GAPDH was used as a loading control. Hepatic accumulation of D. *Col1a1*, E. *Col1a2*, and F. *Serpinh1* transcripts were measured using real time PCR. Data are presented as fold change over each genotypes' own oil. Black bars represent wild-type mice and grey bars represented *Hmmer*<sup>-/-</sup> mice for figures 7-10. \* represents  $p < 0.05$  comparing each genotypes CCl<sub>4</sub> value to its own oil, + represents  $p < 0.05$  comparing CCl<sub>4</sub> between genotypes. N = 5 – 7

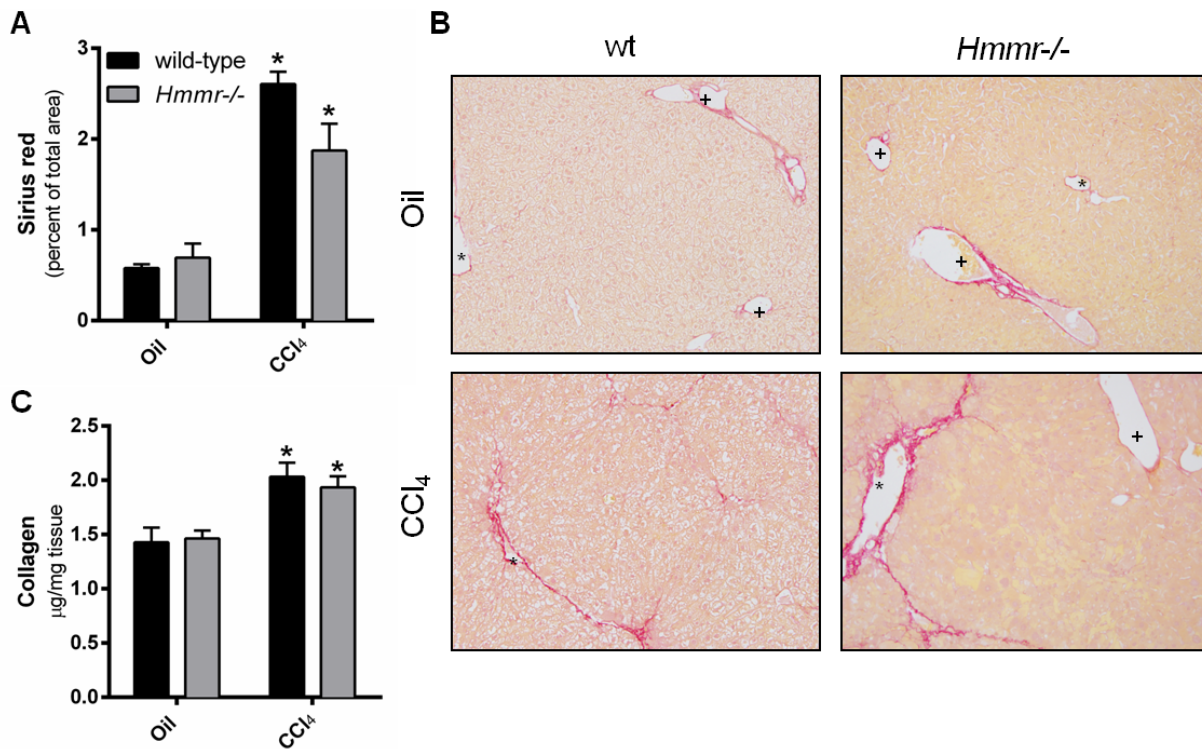


**Figure 5-8: Hepatic fibrosis in wild-type and *Hmmer*<sup>-/-</sup> mice following chronic CCl<sub>4</sub> exposure.**

Mice were exposed to CCl<sub>4</sub> twice a week for five weeks and euthanized 72 hours after the last injection. Control mice received olive oil (oil) injections twice a week for five weeks. A. Quantification and B. representative histology of picosirius red staining, which was used to evaluate ECM accumulation, in wild-type and *Hmmer*<sup>-/-</sup> livers following chronic CCl<sub>4</sub> exposure. \* denotes central veins and + denotes the portal triad in images. C. Collagen content was measured via extrapolation from hepatic hydroxyproline content. \* represents p<0.05 comparing each genotypes CCl<sub>4</sub> value to its own oil. N = 6 – 7

### **Matrix remodeling following chronic CCl<sub>4</sub> exposure in wild-type and *Hmmr*<sup>-/-</sup> mice**

After acute CCl<sub>4</sub>, matrix metabolism was lower in *Hmmr*<sup>-/-</sup> mice compared to wild-type mice. We, therefore, hypothesized that decreased matrix metabolism could account for the disconnect between lower collagen transcripts and no difference in fibrosis between wild-type and *Hmmr*<sup>-/-</sup> mice after chronic CCl<sub>4</sub>. There was no difference in the induction of *Mmp2* transcripts between wild-type and *Hmmr*<sup>-/-</sup> mice after chronic hepatotoxin exposure (Figure 5-9A). *Mmp9* transcripts, however, were induced in wild-type mice following chronic CCl<sub>4</sub> but not in *Hmmr*<sup>-/-</sup> (Figure 5-9B). MMP13 appeared to be the main player in the increased matrix remodeling observed in *Has3*<sup>-/-</sup> mice, but *Mmp13* induction was not different between wild-type and *Hmmr*<sup>-/-</sup> mice following chronic CCl<sub>4</sub> exposure (Figure 5-9C). *Timp1*, the primary inhibitor of MMPs, was also not different after chronic CCl<sub>4</sub> exposure between wild-type and *Hmmr*<sup>-/-</sup> mice (Figure 5-9D).

Again, transcript levels cannot evaluate matrix metabolism directly, so *in situ* zymography was used (Figure 5-9E). After chronic CCl<sub>4</sub>, there was a trend toward a decrease ( $p=0.07$ ) in the total area matrix degrading activity in *Hmmr*<sup>-/-</sup> mice compared to wild-type mice (Figure 5-9F) and the intensity of the signal detected was lower in *Hmmr*<sup>-/-</sup> compared to wild-type mice (Figure 5-9G). These data suggest that matrix metabolism is lower following chronic CCl<sub>4</sub> exposure in *Hmmr*<sup>-/-</sup> mice compared to wild-type mice. This helps to explain the lower pro-fibrotic transcripts but lack of a difference in frank fibrosis between genotypes.

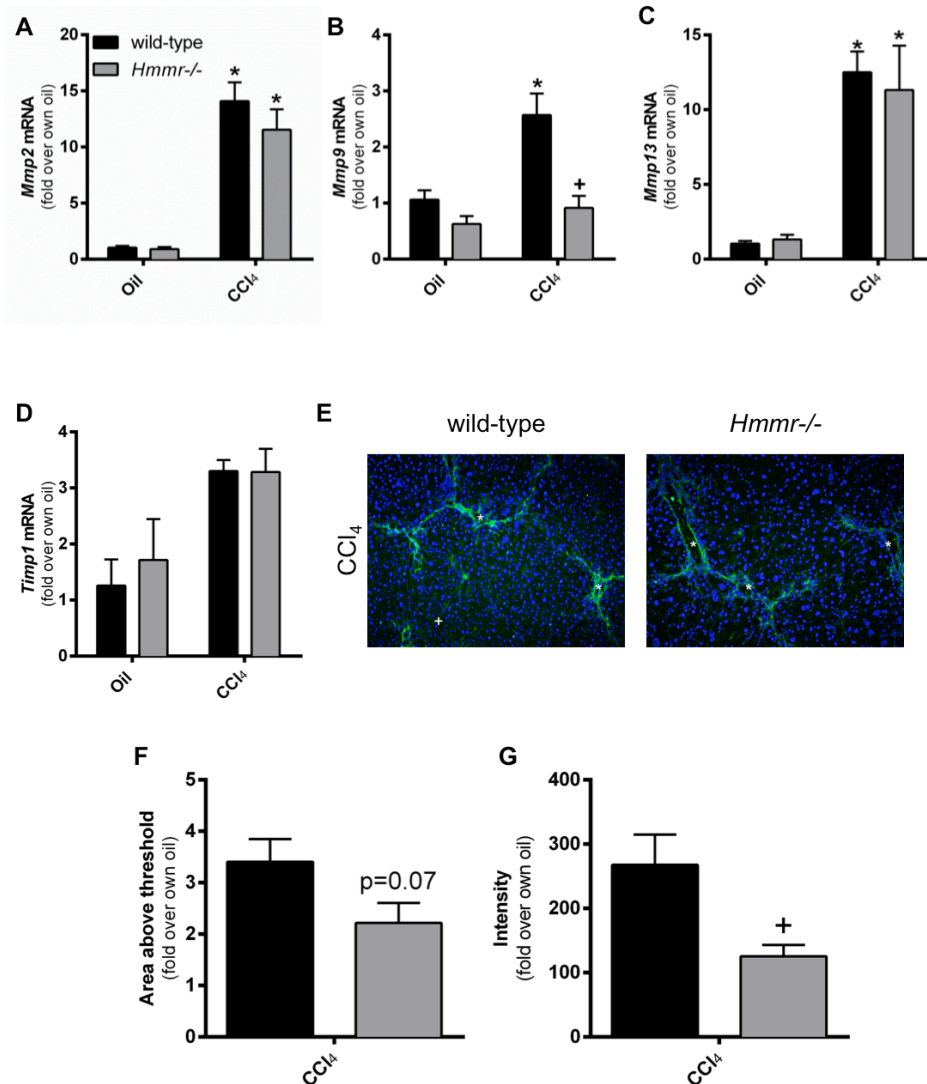


**Figure 5-9: Matrix remodeling in wild-type and *Hmmer*<sup>-/-</sup> mice following chronic CCl<sub>4</sub> exposure.**

Mice were exposed to CCl<sub>4</sub> twice a week for five weeks and euthanized 72 hours after the last injection. Control mice received olive oil (oil) injections twice a week for five weeks. Real time PCR was used to evaluate hepatic transcript accumulation of A. *Mmp2*, B. *Mmp9*, C. *Mmp13*, and D. *Timp1*. Data are presented as fold change over each genotypes' own oil. E. Representative histology for *in situ* zymography to evaluate matrix remodeling. The green signal indicates active matrix metabolism and DAPI was used to visualize nuclei. \* denotes central veins and + denotes the portal triad in images. F. Area and G. intensity of positive signal in arbitrary units. \* represents p<0.05 comparing each genotypes CCl<sub>4</sub> value to its own oil, + represents p<0.05 comparing CCl<sub>4</sub> between genotypes. N = 5 – 7

## **Macrophage accumulation following chronic CCl<sub>4</sub> exposure in wild-type and *Hmmr*<sup>-/-</sup> mice**

Macrophages that have localized to the fibrotic scar are the primary source of MMPs contributing to fibrosis regression. HMMR is important in macrophage migration in skin wound healing, so we hypothesized that *Hmmr*<sup>-/-</sup> mice would have decreased macrophage accumulation in the liver, which would then account for the decreased matrix metabolism we observe in *Hmmr*<sup>-/-</sup> mice compared to wild-type mice. We evaluated transcripts for the macrophage markers *Emr1*, *Cd11b*, and *Ccr2*. *Emr1* transcripts increased in both genotypes following chronic CCl<sub>4</sub> exposure and this accumulation was not different between wild-type and *Hmmr*<sup>-/-</sup> mice (Figure 5-10A). Unlike *Emr1*, *Cd11b* and *Ccr2* transcripts were increased above baseline in wild-type mice following chronic CCl<sub>4</sub> but not in *Hmmr*<sup>-/-</sup> mice (Figure 5-10B and C). These transcript data, together with decreased matrix remodeling, suggests that there was a decrease in macrophage accumulation in *Hmmr*<sup>-/-</sup> mice relative to macrophage accumulation in wild-type mice, although more work should be done to localize macrophages *in situ*.

## **Discussion**

Chronic inflammation is a hallmark of organ fibrogenesis and HA is implicated in the pathogenesis of chronic inflammatory diseases including asthma and irritable bowel disease (IBD). Specifically, HA is increased in the bronchial alveolar lavage fluid (BALF) from asthma patients compared to healthy controls and is associated with increased inflammation (Bousquet *et al.*, 1991; Teder *et al.*, 2002; Liang *et al.*, 2011). Increased

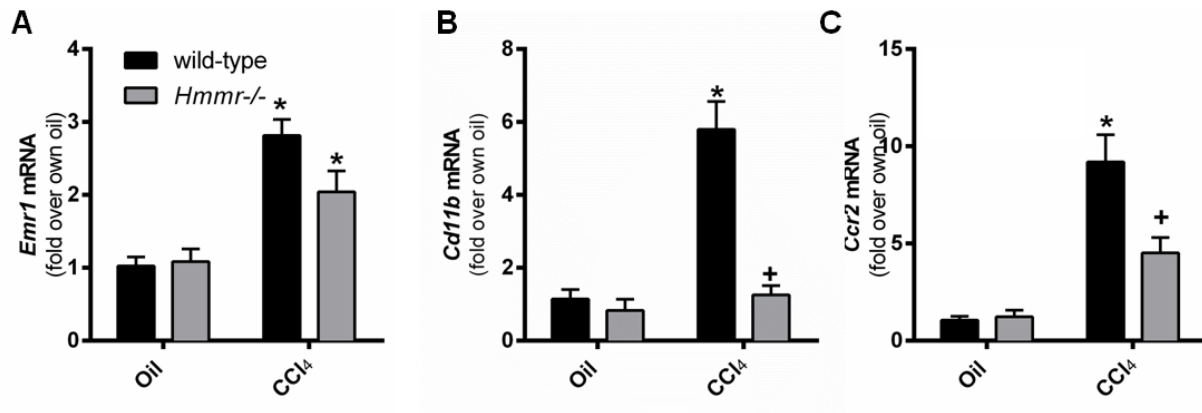


**Figure 5-10: Macrophage accumulation in wild-type and *Hmnr*<sup>-/-</sup> mice following chronic CCl<sub>4</sub> exposure.**

Mice were exposed to CCl<sub>4</sub> twice a week for five weeks and euthanized 72 hours after the last injection. Control mice received olive oil (oil) injections twice a week for five weeks. Real time PCR was used to evaluate total hepatic accumulation of A. *Emr1*, B. *Cd11b*, and C. *Ccr2* in wild-type and *Hmnr*<sup>-/-</sup> liver following chronic CCl<sub>4</sub> exposure. \* represents p<0.05 comparing each genotypes CCl<sub>4</sub> value to its own oil, + represents p<0.05 comparing CCl<sub>4</sub> between genotypes. N = 5 – 7

HA is also found in the BALF from patients with idiopathic lung fibrosis and correlates with white blood cell counts (Bjermer *et al.*, 1989). Patients with IBD have increased HA deposition in their colon, and this HA is thought to form cable-like structures that bind and trap leukocytes and promote chronic inflammation, which can lead to fibrosis (de la Motte *et al.*, 2003; Kessler *et al.*, 2008; de la Motte, 2011). HA is increased in the plasma of patients with chronic liver disease (Engstrom-Laurent *et al.*, 1985; Gudowska *et al.*, 2016). In fact, this increase is correlated to disease severity (Lee *et al.*, 2010; Gudowska *et al.*, 2016). Like other solid organs, chronic hepatic injury results in chronic inflammation and fibrosis (Pellicoro *et al.*, 2014). Despite the connection between HA and fibrosis and the use of HA as a biomarker for liver disease, little work has been done to investigate if a pathogenic role for HA in advanced liver disease exists. In order to investigate a role for HA in the progression of liver fibrosis, we utilized *Has3*<sup>-/-</sup> and wild-type mice and exposed them to chronic CCl<sub>4</sub> injections. Following acute liver injury, *Has3*<sup>-/-</sup> mice display increased matrix metabolism compared to wild-type mice. Therefore, we hypothesized that *Has3*<sup>-/-</sup> mice would also have increased matrix metabolism compared to wild-type mice following chronic CCl<sub>4</sub> exposure, resulting in decreased fibrosis in *Has3*<sup>-/-</sup> mice. While we did observe increased matrix metabolism in *Has3*<sup>-/-</sup> mice compared to wild-type mice, we also found increased pro-fibrotic transcripts. This disconnect between matrix synthesis and matrix metabolism resulted in similar fibrosis between wild-type and *Has3*<sup>-/-</sup> mice after chronic CCl<sub>4</sub> exposure.

While chronic inflammation promotes fibrosis, a decrease in recruited macrophages can also be detrimental when it comes to regression of the hepatic scar. In fact, Duffield, *et al.*, used CD11b-DTR transgenic mice to deplete macrophages at

various stages of fibrosis and found that depleting macrophages during CCl<sub>4</sub> induced fibrosis progression attenuated fibrosis, but deleting them after fibrosis was established attenuated the removal of the fibrotic scar (Duffield *et al.*, 2005). The macrophages responsible for matrix degradation, scar-associated macrophages (SAMs), are the main source of MMPs including MMP13 and this MMP13 activity is vital to removing the fibrotic scar formed after chronic CCl<sub>4</sub> exposure (Fallowfield *et al.*, 2007b). We found that *Has3*<sup>-/-</sup> mice have an increase in active MMP13 and a subsequent increase in matrix remodeling. This helps to explain the disconnect between the pro-fibrotic transcript levels and frank fibrosis in *Has3*<sup>-/-</sup> mice. It also suggests that *Has3*<sup>-/-</sup> mice are better able to recruit macrophages to the fibrotic scar compared to wild-type mice after chronic CCl<sub>4</sub> exposure, although more work should be done to localize SAMs to the fibrotic septae. Additionally, *Has3*<sup>-/-</sup> mice have increased HMMR, a receptor known to promote macrophage migration, suggesting the HA:HMMR interaction may be important for macrophage migration and subsequent matrix degradation.

HA itself is a known inducer of MMP13 (Fieber *et al.*, 2004), and because *Has3*<sup>-/-</sup> mice have increased hepatic HA deposition following acute CCl<sub>4</sub> exposure, it is possible that they also have increased HA deposition following chronic CCl<sub>4</sub> exposure, which leads to increased matrix metabolism. Although, we do see increased hepatic HA accumulation following chronic CCl<sub>4</sub> exposure in both wild-type and *Has3*<sup>-/-</sup> mice, we do not observe any differences between the two genotypes. Additionally, this increase is not the same extent as we observed following acute CCl<sub>4</sub> exposure. This does not, however, conclusively rule out any differences in hepatic HA deposition between genotypes, since we only measured a single time point in a process that occurs over

several days. Thus it is possible we missed the peak of hepatic HA accumulation, and a more thorough characterization of the resolution of fibrosis in *Has3*<sup>-/-</sup> mice should be done.

Similar to results found in acute CCl<sub>4</sub> studies (Chapter 3), *Has3*<sup>-/-</sup> mice had an increase in *Hmnr* transcript accumulation compared to wild-type mice following chronic CCl<sub>4</sub> exposure. HMMR protein levels in *Has3*<sup>-/-</sup> mice were elevated above baseline after chronic CCl<sub>4</sub> exposure; this was not the case in wild-type mice. HMMR plays a role in macrophage and fibroblast migration and wound healing in models of excisional skin wounds, resulting in a collagen scar similar to that observed in hepatic fibrosis (Tolg *et al.*, 2006; Tolg *et al.*, 2012). Therefore, we hypothesized that HMMR is playing a role in hepatic fibrogenesis and/or fibrosis regression. In order to investigate HMMR's role in hepatic fibrosis more closely, *Hmnr*<sup>-/-</sup> mice were exposed to chronic CCl<sub>4</sub> and fibrosis, and subsequent matrix metabolism parameters were measured. After acute liver injury, *Hmnr*<sup>-/-</sup> mice had decreased matrix metabolism, and we hypothesized a similar phenomenon would occur after chronic CCl<sub>4</sub> exposure, resulting in increased fibrosis in *Hmnr*<sup>-/-</sup> mice compared to wild-type mice.

We first evaluated several pro-fibrotic transcripts to evaluate matrix synthesis. We found that hepatic pro-fibrotic markers were lower in *Hmnr*<sup>-/-</sup> mice compared to wild-type mice following chronic CCl<sub>4</sub> exposure. This, however, did not translate to decreased fibrosis. In fact, the *Hmnr*<sup>-/-</sup> mice had the same amount of fibrosis as their wild-type controls after chronic hepatotoxin exposure. Although we did not observe increased fibrosis in *Hmnr*<sup>-/-</sup> mice compared to wild-type mice, the disconnect between lower pro-fibrotic transcripts and no difference in fibrosis still supports our hypothesis.

HMMR contributes to the macrophage migration in both the skin and the lung (Zaman *et al.*, 2005; Tolg *et al.*, 2012). Specifically, a HMMR mimetic delays macrophage migration into an excisional skin wound (Tolg *et al.*, 2012). Similarly, a HMMR blocking antibody prevents the accumulation of macrophages following bleomycin induced lung injury (Zaman *et al.*, 2005). In the current study, we observed a decrease in hepatic *Cd11b* and *Ccr2* transcripts, two macrophage-associated markers, in *Hmmr*<sup>-/-</sup> mice compared to wild-type mice after chronic CCl<sub>4</sub> exposure. We also showed a decrease in the matrix metabolism measured by *in situ* zymography in the *Hmmr*<sup>-/-</sup> mice compared to wild-type mice. Our data demonstrate that the absence of HMMR is associated with a decrease in macrophage localization to the fibrotic scar. By contrast, in *Has3*<sup>-/-</sup> mice, increased HMMR levels may be contributing to the increased macrophage localization and subsequent increase in matrix metabolism compared to wild-type mice following chronic CCl<sub>4</sub> exposure. This suggests that HMMR likely plays a role in the localization of macrophages to the hepatic scar for its subsequent degradation following chronic CCl<sub>4</sub> exposure. Therefore, we propose that HMMR, likely on macrophages, plays a role in the regression of the fibrotic scar after chronic liver injury and not in the development of fibrosis. Future work will directly explore the impact of HMMR on fibrosis resolution.

## **Chapter 6: C57BL/6 sub-strains exhibit different responses to acute carbon tetrachloride exposure: Implications for work involving transgenic mice**

*Portions of this chapter are adapted from McCracken, JM et al. "C57BL/6 substrains exhibit different responses to acute carbon tetrachloride exposure: Implications for work involving transgenic mice" Gene Expression: The Journal of Basic Liver Research. 17#3, doi: 10.3727/105221617X695050 with permission Cognizant, LLC; www.cognizantcommunications.com copyright 2017 in press*

## **Abstract**

Biological differences exist between strains of laboratory mice, and it is becoming increasingly evident that there are differences between sub-strains. In the C57BL/6 mouse, the primary sub-strains are 6J and 6N. Previous studies have demonstrated that 6J and 6N mice differ in response to many experimental models of human disease. The aim of our study was to determine if differences exist between 6J and 6N mice in terms of their response to acute and chronic carbon tetrachloride (CCl<sub>4</sub>) exposure. Mice were given CCl<sub>4</sub> once and were euthanized 12 to 96 hours later or given CCl<sub>4</sub> twice a week for five weeks and euthanized 72 hours after the last injection. Control mice received olive oil injection(s). Relative to 6J mice, we found that 6N mice had increased liver injury but more rapid repair. This was due to the increased speed with which necrotic hepatocytes were removed in 6N mice and was directly related to increased recruitment of macrophages to the liver. In parallel, enhanced liver regeneration was observed in 6N mice relative to 6J mice. Hepatic stellate cell activation occurred earlier in 6N mice, but there was no difference in matrix metabolism between sub-strains. Following chronic CCl<sub>4</sub> exposure, 6N mice had increased pro-fibrotic markers and increased fibrosis. Taken together, these data demonstrate specific and significant differences in how the C57BL/6 sub-strains respond to acute and chronic CCl<sub>4</sub>, which has important implications for all mouse studies utilizing this model, including those in the previous chapters involving *Has3*<sup>-/-</sup> and *Hmnr*<sup>-/-</sup> mice.

## **Introduction**

Differences in biological responses between strains of mice have been known for several years and recently biological differences have been discovered between sub-strains of mice. The C57BL/6 mouse strain has several sub-strains, the two most common being C57BL/6N (6N) and C57BL/6J (6J). Recently, there have been reports on these two sub-strains having differential responses in several models including in alcohol preferences and diet-induced obesity (Ramachandra *et al.*, 2007; Nicholson *et al.*, 2010). These two sub-strains are characterized by having a wild-type nicotinamide nucleotide transhydrogenase (*Nnt*), 6N, or mutated *Nnt*, 6J. *Nnt* is important for the production of NADPH in the inner mitochondrial membrane and is used in mitochondrial antioxidant defense.

Sub-strain differences are also important to consider when using genetically modified mice. For example, two separate laboratories reported conflicting results on the role JNK2 plays in acetaminophen (APAP)-induced liver injury. Nakagawa, H. *et al.* reported that *Jnk2*<sup>-/-</sup> mice are partially protected from APAP-induced liver injury while Bourdi *et al.* reported that *Jnk2*<sup>-/-</sup> mice have exacerbated liver injury relative to wild-type mice. It was determined that each lab used a different B6 sub-strain as a control, and that these two sub-strains (6N and 6J) differentially responded to APAP exposure (Bourdi *et al.*, 2008; Nakagawa *et al.*, 2008; Bourdi *et al.*, 2011). Recently, Duan, L *et al.* reported that the 6N mice have increased liver injury, likely due to increase APAP adduct formation and increased mitochondrial dysfunction (Duan *et al.*, 2016). Not only does this point out the importance of utilizing the correct sub-strain as a control for any genetically modified mouse study, but it raises the question of a potential differential

response between these sub-strains in other commonly used mouse models of liver injury.

Given the findings in APAP-induced liver injury, we hypothesized that a differential response would occur between 6N and 6J mice after acute and chronic CCl<sub>4</sub> exposure; another commonly used model of liver injury and disease. CCl<sub>4</sub> causes centrilobular necrosis shortly after exposure (Weber *et al.*, 2003). This liver injury and its subsequent repair is analogous to the well-established model of wound healing that occurs in the skin; the stages include inflammation, regeneration, and matrix remodeling (Pellicoro *et al.*, 2014; Balaji *et al.*, 2015). In the liver, inflammatory chemokines and cytokines are synthesized primarily by Kupffer cells, liver resident macrophages, which, in turn, recruit circulating neutrophils and monocytes to the liver that continue to synthesize inflammatory mediators (Aziz-Seible *et al.*, 2011; Dixon *et al.*, 2013). These infiltrating cells can exacerbate injury as well as remove dead and dying hepatocytes and, therefore, also actively participate in wound healing (Ramaiah and Jaeschke, 2007; Kiso *et al.*, 2012; Mochizuki *et al.*, 2014; Moles *et al.*, 2014; Zigmond *et al.*, 2014). Following injury, the liver regenerates to restore normal mass and function (Cienfuegos *et al.*, 2014; Mao *et al.*, 2014). Similar to skin wound healing, matrix remodeling occurs at the later stages of liver repair. This involves matrix synthesis, primarily by activated hepatic stellate cells (HSC), as well as matrix metabolism, primarily by macrophages (Guo and Friedman, 2007; Friedman, 2008a). Here we explored whether or not differences exist in hepatic injury and wound healing, including the inflammation, regeneration, and matrix remodeling stages, following acute CCl<sub>4</sub> exposure between 6J and 6N mice.

Following chronic liver injury, there are repeated cycles of injury and wound healing (Bataller and Brenner, 2005; Friedman, 2008b). The wound healing process becomes deregulated and excess extracellular matrix accumulates resulting in a fibrotic scar (Bataller and Brenner, 2005; Friedman, 2008b). Because 6N mice have increased injury following acute APAP overdose and we believe that a similar increase in 6N injury will be observed after acute CCl<sub>4</sub> exposure, we hypothesized that 6N mice will have increased fibrosis after chronic liver injury. We induced chronic liver injury and fibrosis by exposing mice to CCl<sub>4</sub> twice a week for five weeks (Constandinou *et al.*, 2005). Any differences observed in injury, the wound healing response, or fibrosis between these two sub-strains is particularly important for this dissertation because the genetically modified mice utilized are on either the 6J (*Has3*<sup>-/-</sup>) or 6N (*Hmmr*<sup>-/-</sup>) background.

## **Results**

### **Liver injury and steatosis after CCl<sub>4</sub> exposure**

To determine if 6N and 6J mice have a differential response to acute CCl<sub>4</sub> exposure, liver injury was evaluated by measuring plasma ALT activity. This enzyme is released into circulation by dead and dying hepatocytes. Both strains had increased plasma ALT activity following CCl<sub>4</sub> exposure, but 6N mice had greater plasma ALT activity compared to 6J mice 48 hours after CCl<sub>4</sub> exposure (Figure 6-1A). By 72 hours after CCl<sub>4</sub> exposure, ALT activity in 6N mice was not different than baseline, while ALT activity remained elevated in 6J mice (Figure 6-1A). By 96 hours after CCl<sub>4</sub> exposure, plasma ALT returned to baseline in 6J mice (Figure 6-1A). Because CCl<sub>4</sub> causes

centrilobular necrosis, we also evaluated liver injury by histopathology. Necrosis increased in both sub-strains following CCl<sub>4</sub>, however the area of necrosis increased in 6N mice 12 hours following CCl<sub>4</sub> exposure while the area of necrosis did not increase above baseline in the 6J mice until 48 hours after CCl<sub>4</sub> exposure (Figure 6-1B and D). At 96 hours post-CCl<sub>4</sub> exposure, 6N mice had less necrosis compared to 6J mice (Figure 6-1B and 1D). Together, these data demonstrate that 6N mice had increased injury, but also a faster recovery from that injury, after acute CCl<sub>4</sub> exposure.

Hepatic triglyceride accumulation, measured biochemically and evident in H&E-stained liver sections, also increased in both strains following CCl<sub>4</sub> exposure (Figure 6-1C and D). Contrary to plasma ALT levels and area of necrosis, 6J mice had more hepatic triglyceride than 6N mice 24h post CCl<sub>4</sub> exposure. While the triglyceride levels in 6N mice returned to baseline by 48h post CCl<sub>4</sub> exposure, levels in 6J mice did not return to baseline until 72h post CCl<sub>4</sub> exposure (Figure 6-1C and D).

### **Baseline CYP2E1 protein and activity**

In order for CCl<sub>4</sub> to induce liver injury it must undergo bioactivation by CYP2E1 (Weber *et al.*, 2003). Therefore, to eliminate the possibility that differential CYP2E1 activity accounted for variation in the liver injury between sub-strains, we measured baseline hepatic CYP2E1. There was no difference in hepatic CYP2E1 mRNA or protein levels between 6N and 6J mice (Figure 6-2A - C) or in *Cyp2e1* mRNA from isolated primary hepatocytes (Figure 6-2D). Similarly, there was no difference in the CYP2E1 activity between the two sub-strains as assessed by the hydroxylation of p-nitrophenol to p-nitrocatechol using microsomes isolated from whole liver (Figure 6-2E).

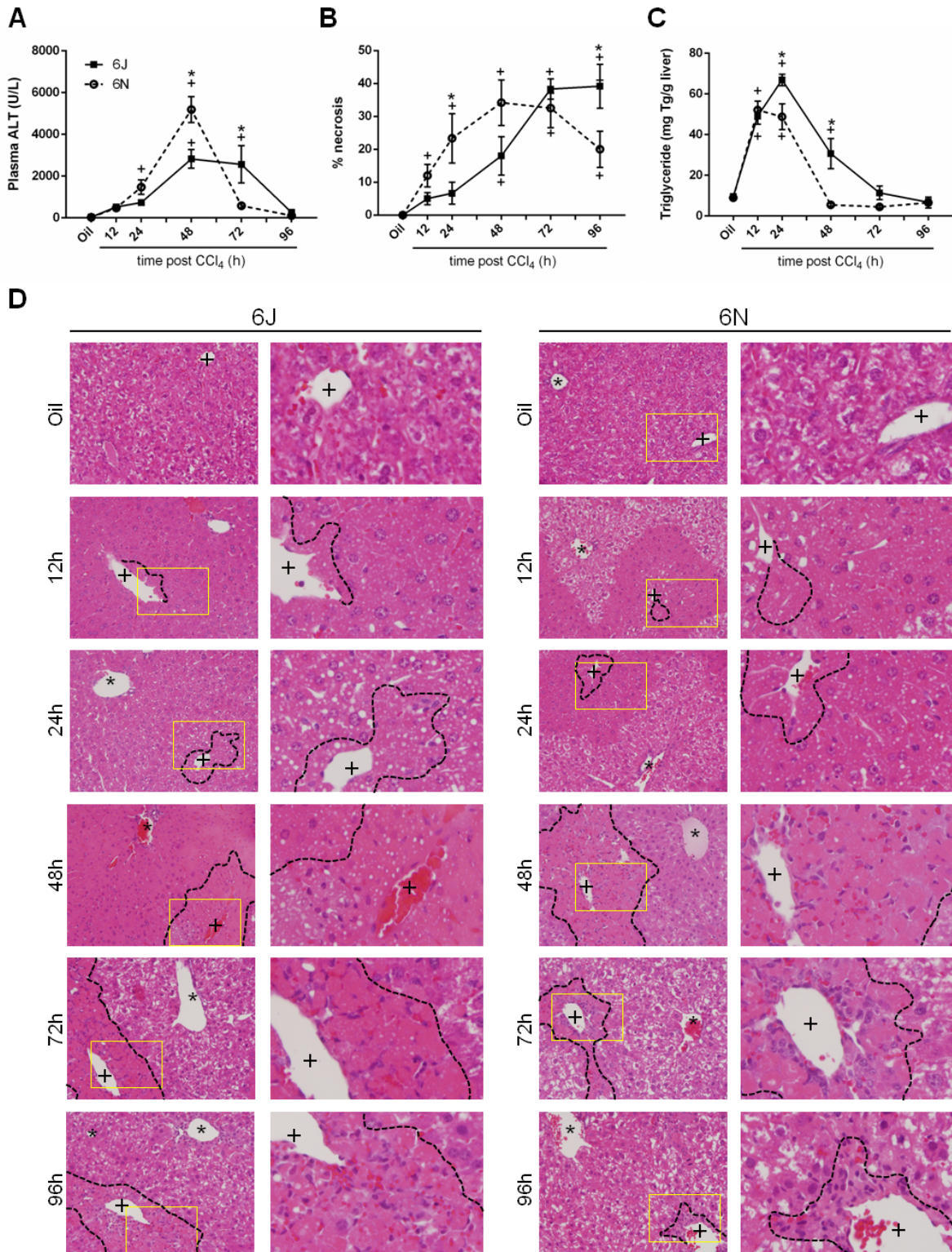


**Figure 6-1: Hepatic injury following acute CCl<sub>4</sub> exposure.**

Mice were exposed to CCl<sub>4</sub> and euthanized 12, 24, 48, 72, or 96 hours later. A. Plasma ALT was determined by enzymatic assay. B. Quantification of necrosis evaluated by a board-certified pathologist blinded to experimental group. C. Total hepatic triglyceride content was determined by a biochemical assay. D. Representative histology of hematoxylin and eosin (H&E) stained liver sections showing necrosis around the central veins (+) of the liver, asterisks (\*) indicate portal veins. A black dashed line outlines necrotic areas, defined as hyper-eosinophilic and lacking hepatocyte nuclei. The yellow-boxed area is enlarged in the right panel next to each image to better depict steatosis at each time point. Throughout the chapter, the black squares/bars/solid lines represent data from 6J mice and white circles/bars/dashed lines represent data from 6N mice. Data are presented as mean ± standard error of mean. n=5-6, \*, p ≤ 0.05 when comparing sub-strains at a single time point; +, p ≤ 0.05 when comparing the indicated CCl<sub>4</sub> time point to the oil (control) of the same sub-strain

These findings suggest that the observed differences in liver injury were not due to sub-strain specific differences in CCl<sub>4</sub> bioactivation.

### ***In vitro* hepatocyte sensitivity to CCl<sub>4</sub>**

To determine if the increased liver injury observed in 6N mice was due to an increase in hepatotoxin sensitivity, primary hepatocytes from 6N and 6J mice were exposed to CCl<sub>4</sub> for 24 hours at three different CCl<sub>4</sub> concentrations. The higher concentrations (5 and 10mM) induced hepatocyte cell death detectable by lactate dehydrogenase (LDH) release 24h after CCl<sub>4</sub> exposure (Figure 6-2F); morphological changes were obvious at all CCl<sub>4</sub> concentrations (Figure 6-2G). However, there was no difference in the cell death between the two sub-strains (Figure 6-2F). This suggests that increased hepatocyte sensitivity to CCl<sub>4</sub> is not responsible for the increased injury observed in the 6N mice compared to the 6J mice.

### **Antioxidant defense following CCl<sub>4</sub>**

6J mice have a mutation in the *Nnt* gene, which can attenuate antioxidant defense (Arkblad *et al.*, 2005; Sheeran *et al.*, 2010; Ronchi *et al.*, 2013). However, reduced NNT activity does not make 6J mice more sensitive to CCl<sub>4</sub>-mediated liver injury as one might expect. In fact, the reverse was true: 6N mice are more sensitive to CCl<sub>4</sub>-induced liver injury than 6J mice. Therefore, we evaluated two additional parameters associated with antioxidant defense to determine if they were increased in 6J mice to compensate for lack of functional NNT and perhaps responsible for the observed protection from CCl<sub>4</sub>-induced liver injury. *Gclc*, glutamate-cysteine ligase

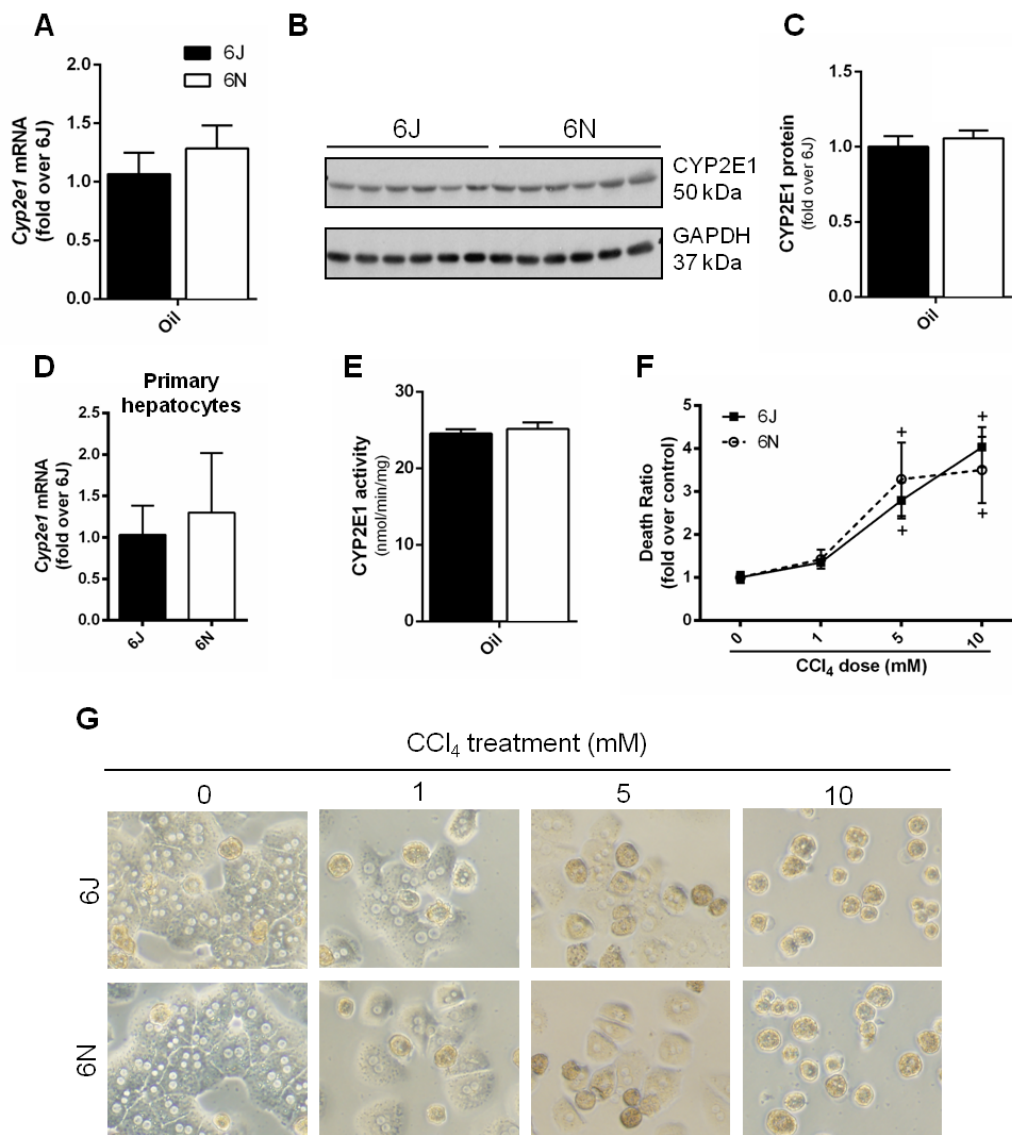


**Figure 6-2: CYP2E1 expression, protein content, and activity *in vitro* and *in vivo*.**

A – C. Control mice given an olive oil injection and euthanized 72 hours later were evaluated for A. *Cyp2e1* mRNA and B, C. CYP2E1 protein from whole liver. D. *Cyp2e1* expression was determined in isolated hepatocytes. E. CYP2E1 activity in microsomes isolated from whole liver was determined by the hydroxylation of *p*-nitrophenol to *p*-nitrocatechol. F, G. Primary hepatocytes were isolated from 6N and 6J mice and exposed to 0, 1, 5, 10mM CCl<sub>4</sub> for 24 hours. F. Death ratio was calculated from the amount of LDH released in the media versus the total amount of LDH in the cells and media. G. Cell morphology was evaluated in micrographs taken at the end of the 24h incubation.

catalytic domain, is the rate-limiting step in glutathione synthesis, and important for antioxidant defense after CCl<sub>4</sub> induced liver injury (Ip and Ko, 1996; Wong *et al.*, 2014). *Gclc* mRNA increases rapidly in liver in both sub-strains of mice early following CCl<sub>4</sub> exposure and is not different between sub-strains at any time point (Figure 6-3A). *Nqo1*, NAD(P)H dehydrogenase, is another vital part of the liver's antioxidant defense against many hepatotoxins (Hwang *et al.*, 2015). While hepatic *Nqo1* mRNA is increased in 6N mice compared to the 6J mice 12, 48 and 72 hours after CCl<sub>4</sub> (Figure 6-3B), hepatic NQO1 protein levels in 6N mice do not parallel these changes. In fact, NQO1 protein decreases over time in both strains (Figure 6-3C and D). Although a trend to a decrease in NQO1 protein is observed in 6N mice 72 and 96 hours after CCl<sub>4</sub> exposure, NQO1 protein is not different between sub-strains when plasma ALT levels are different between sub-strains (compare Figure 6-1A and Figure 6-3C, D). Together, these data suggest that antioxidant defense is equivalent between 6J and 6N mice following CCl<sub>4</sub> exposure and does not account for observed differences in CCl<sub>4</sub>-induced liver injury between sub-strains.

### **Inflammation following CCl<sub>4</sub> exposure: Hepatic neutrophil accumulation**

Because hepatocyte sensitivity to CCl<sub>4</sub> and anti-oxidant defenses were not different between sub-strains, we hypothesized that another mechanism must be responsible for increased liver injury observed in 6N mice. Neutrophils are recruited rapidly after CCl<sub>4</sub>-mediated injury and can exacerbate hepatocyte cell death (Ramaiah and Jaeschke, 2007; Moles *et al.*, 2014), therefore we measured several neutrophil-related markers in 6J and 6N mice. First, we evaluated *Cxcl2* (MIP2) and *Cxcr2*, a major

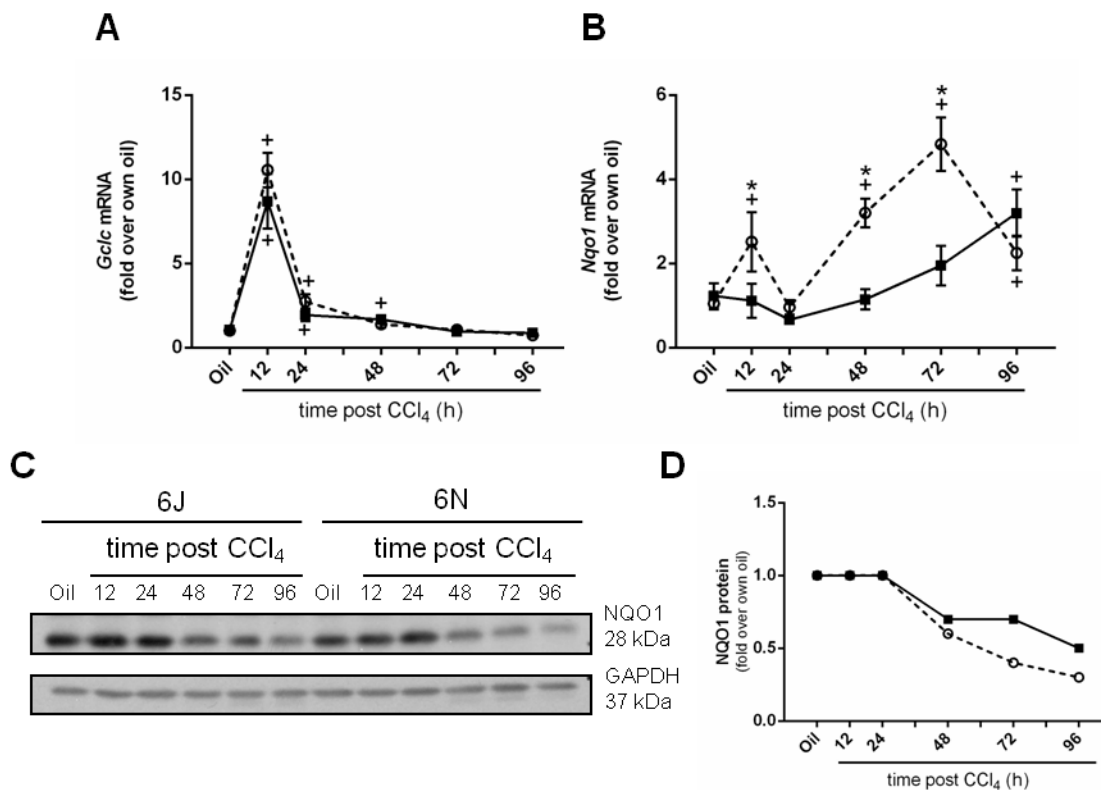


**Figure 6-3: Expression of antioxidants after acute CCl<sub>4</sub> exposure.**

Mice were exposed to CCl<sub>4</sub> and euthanized 12, 24, 48, 72, or 96 hours later and the hepatic transcript accumulation of A. *Gclc* and B. *Nqo1* was determined. Individual mouse liver samples were pooled to evaluate NQO1 protein concentration throughout the time course. C. Immunoblot and D. densitometry of the immunoblot shown in C. n=5-6 per group, \*, p ≤ 0.05 when comparing sub-strains at a single time point; +, p ≤ 0.05 when comparing the indicated CCl<sub>4</sub> time point to the oil (control) of the same sub-strain.

neutrophil chemotactic protein and its receptor, respectively, at the mRNA level. *Cxcl2* transcripts increased in 6J and 6N mice 12 hours after CCl<sub>4</sub> and are not different between sub-strains (Figure 6-4A). However, 24 and 48 hours after CCl<sub>4</sub> exposure, 6N mice have increased *Cxcl2* expression (Figure 6-4A). *Cxcr2* is increased 12 hours after CCl<sub>4</sub> and remains elevated in both strains until 48 hours post CCl<sub>4</sub> exposure (Figure 6-4B). Thereafter, *Cxcr2* transcripts decrease in 6N mice but remain elevated in 6J (Figure 6-4B).

To further evaluate neutrophils, we localized chloracetate esterase (CAE), a leukocyte esterase, in livers from 6J and 6N mice. CAE was not found in control livers from either sub-strain (Figure 6-4C and D). However, CAE-positive cells were apparent in livers from both sub-strains 12 and 24 hours after CCl<sub>4</sub> exposure (Figure 5-4C and D). Although there was a trend to an increase in CAE-positive cells in livers from 6N mice when compared to 6J mice 24 hours after CCl<sub>4</sub>, this difference was not significant ( $p=0.0682$ , Figure 6-4C and D). No CAE-positive cells were found in livers from mice 48, 72 or 96 hours after CCl<sub>4</sub> exposure (data not shown). Taken together, these data suggest that neutrophil-mediated hepatocyte injury may partially contribute to increased liver injury observed in 6N mice. It is interesting to note that CAE staining data do not parallel hepatic *Cxcr2* transcript levels (Figure 6-4B). This suggests that the sustained rise in *Cxcr2* mRNA observed, in particular, in 6J mice, is due to *Cxcr2* expression in other hepatic cells, such as hepatocytes, as observed following APAP overdose and ischemia-reperfusion-induced liver injury (Hogaboam *et al.*, 1999; Dixon *et al.*, 2013).

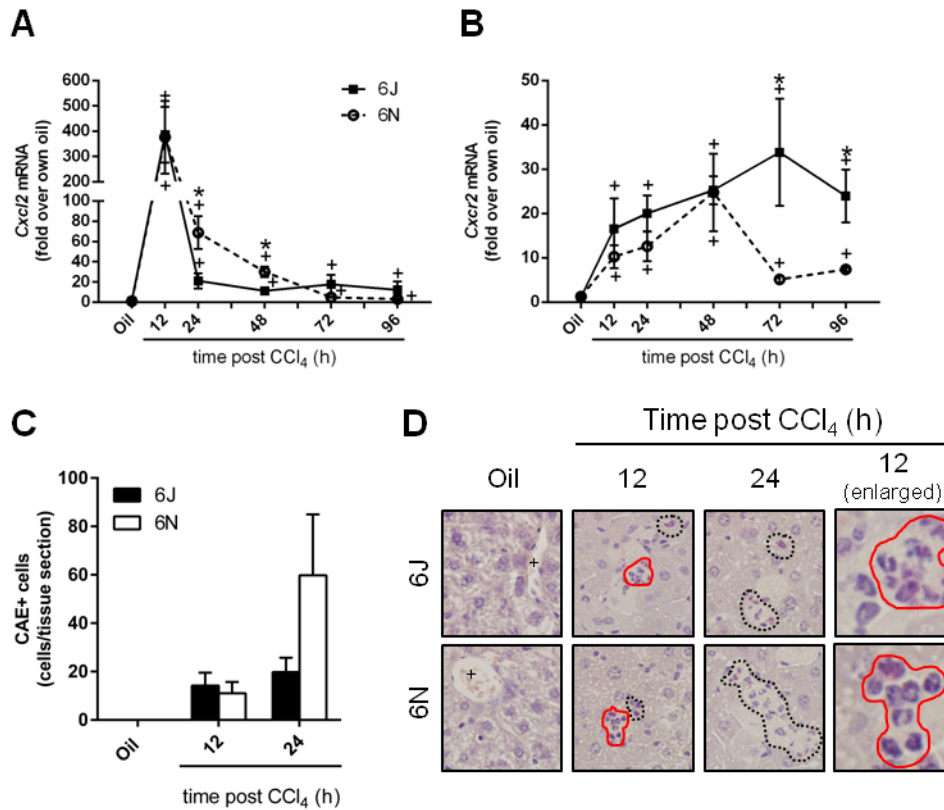


**Figure 6-4: Hepatic neutrophil accumulation after acute CCl<sub>4</sub> exposure.**

Mice were exposed to CCl<sub>4</sub> and euthanized 12, 24, 48, 72, or 96 hours later. A. *Cxcl2* and B. *Cxcr2* transcripts were quantified in whole liver cDNA samples using real time PCR. C. Quantification of CAE staining used to assess the number of neutrophils in the liver at baseline (oil) and 12 and 24h after CCl<sub>4</sub>. D. Representative images of CAE+ cells with neutrophil morphology (pink staining within the dotted black lines, area within solid red line is enlarged to the right). The + indicates central veins in the images. n=5-6 per group, \*, p ≤ 0.05 when comparing sub-strains at a single time point; +, p ≤ 0.05 when comparing the indicated CCl<sub>4</sub> time point to the oil (control) of the same sub-strain.

### **Inflammation after CCl<sub>4</sub> exposure: Hepatic macrophage accumulation**

Macrophages are also recruited to the liver after injury and can play roles in sustaining injury as well as promoting repair (You *et al.*, 2013; Zigmond *et al.*, 2014). Because we observed a more rapid removal of necrotic tissue in livers from 6N mice, we hypothesized that cell recruitment was increased in this sub-strain and contributed to more rapid repair, compared to 6J mice. To determine whether or not this relationship existed, we first counted the number of non-parenchymal cells (NPC) within the pericentral (necrotic) areas in livers from 6J and 6N mice. There were very few NPC in the necrotic area 12 and 24 hours after CCl<sub>4</sub> (not quantified). However by 48 hours, NPC increased in necrotic areas from both sub-strains (Figure 6-1D, 6-5A), and at 72 and 96 hours post CCl<sub>4</sub> exposure, 6N mice had more necrosis-infiltrating cells compared to 6J mice (Figure 6-1D and 6-5A). While infiltration of cells into necrotic areas 72 and 96 hours after CCl<sub>4</sub> does not support a role for inflammation-mediated exacerbation of liver injury in 6N mice, it does support a role for these cells in removal of necrotic hepatocytes. In fact, the number of infiltrating cells was negatively correlated with the area of necrosis (Figure 6-5B).

Next, we wanted to verify that macrophages were associated with this repair response. After CCl<sub>4</sub>-exposure, resident hepatic macrophages and other liver cells produce chemokines, which attract peripheral monocytes into the liver leading to an increase in hepatic macrophage number (Dixon *et al.*, 2013). *Ccl2* is the gene that encodes monocyte chemoattractant protein 1 (MCP1), a chemokine that aids in the recruitment of inflammatory cells, including macrophages (Baeck *et al.*, 2012). Hepatic *Ccl2* transcripts increased above baseline 12 hours after CCl<sub>4</sub> exposure in both 6N and

6J mice (Figure 6-5C). However, 6N mice had increased *Ccl2* transcripts 24 and 48 hours post CCl<sub>4</sub> relative to 6J mice at the same time point (Figure 5-5C). Conversely, 96 hours post CCl<sub>4</sub>, *Ccl2* transcripts were higher in 6J mice relative to 6N mice (Figure 6-5C). To assess hepatic macrophage content, we examined expression of *Emr1*, the F4/80 gene, a common mouse macrophage marker. *Emr1* transcripts initially decreased in both sub-strains following CCl<sub>4</sub> exposure (Figure 6-5D). By 48 hours post CCl<sub>4</sub> exposure, *Emr1* transcripts increased above baseline in 6N mice (Figure 6-5D). However, it was not until 72 hours after CCl<sub>4</sub> that *Emr1* transcripts increased above baseline in 6J mice; *Emr1* transcripts were still greater in 6N mice at this time point (Figure 6-5D). Consistent with earlier and increased *Emr1* transcript levels, 6N mice exhibited increased F4/80-positive staining compared to 6J mice 96 hours after CCl<sub>4</sub> exposure (Figure 6-5E and F).

Tumor necrosis factor  $\alpha$  (*Tnfa*) is a cytokine produced mainly by macrophages (Dixon *et al.*, 2013). TNF $\alpha$  can induce hepatocyte death or drive liver regeneration depending on cellular context (Webber *et al.*, 1998; Malhi *et al.*, 2010; Seki *et al.*, 2012; Deshpande *et al.*, 2016). Therefore, we evaluated *Tnfa* transcripts in liver after CCl<sub>4</sub> exposure. *Tnfa* increased above baseline in 6N mice earlier (12 hours) and was greater than in 6J mice (24 and 48 hours) (Figure 6-5G). While *Tnfa* transcripts returned to baseline by 96 hours in 6N mice, these transcripts remained elevated in 6J mice (Figure 6-5G).

Together, all of these data suggest that 6N mice exhibited a greater capacity to recruit cells, including macrophages, into the liver where they participated in more rapid removal of necrotic tissue, hastening liver repair after CCl<sub>4</sub> exposure. However,

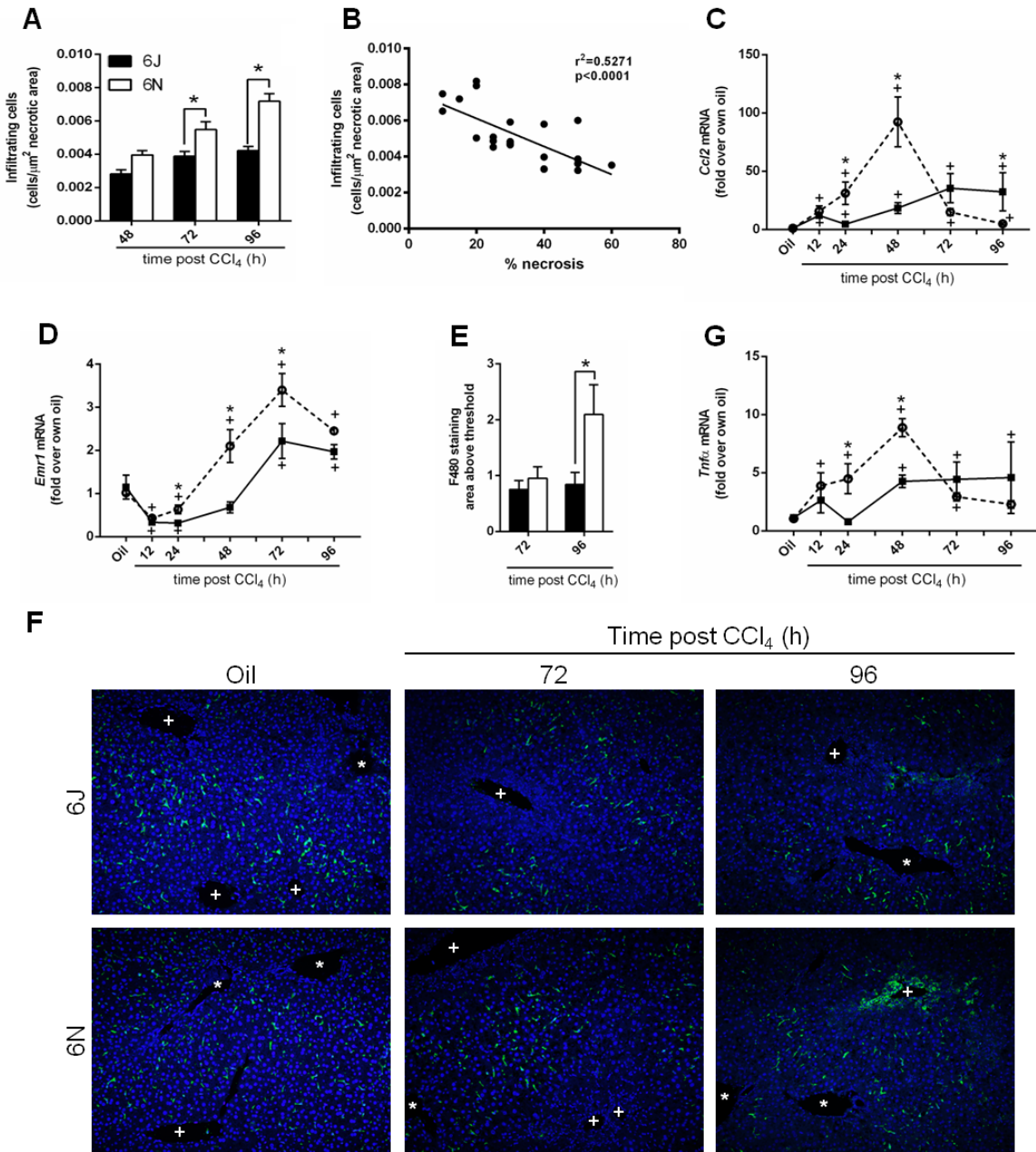


Figure 6-5: Infiltrating cells and macrophages in liver after acute  $\text{CCl}_4$  exposure.

A. The number of non-parenchymal cells infiltrating the necrotic area was counted in livers from mice euthanized 48, 72, and 96 hours post CCl<sub>4</sub> exposure. B. The number of cells was correlated to the % necrosis determined from H&E stained sections. Indices of macrophage accumulation were evaluated by determining hepatic transcript accumulation of C. *Ccl2*, and D. *Emr1* by real time PCR. E. Quantification of F4/80+ macrophages determined by immunofluorescence 72 and 96h after CCl<sub>4</sub> exposure. F. Representative F4/80 immunofluorescence images. In each image, central veins are marked with a + and portal veins are marked with a \*. G. Quantification of *Tnfa* transcripts by real time PCR. n=5-6 per group, \*, p ≤ 0.05 when comparing sub-strains at a single time point; +, p ≤ 0.05 when comparing the indicated CCl<sub>4</sub> time point to the oil (control) of the same sub-strain.

the increased cell recruitment observed in 6N mice may have also promoted increased liver injury, perhaps through increased TNF $\alpha$ -induced hepatotoxicity.

### **Liver regeneration following CCl<sub>4</sub> exposure**

Following the massive necrosis caused by CCl<sub>4</sub> and subsequent inflammation, the liver regenerates to restore normal mass and function (Hogaboam *et al.*, 1999; Cienfuegos *et al.*, 2014). This occurs at the later time points, 48, 72, and 96 hours, post CCl<sub>4</sub> exposure. We evaluated regeneration by analyzing hepatic gene expression and protein levels of proliferating cell nuclear antigen (*Pcna*), a DNA protein clamp essential for replication, and Cyclin D1 (*Ccnd1*), a protein required for cell cycle progression. Hepatic *Pcna* transcript levels increased in both genotypes following CCl<sub>4</sub> exposure. The increase in the 6N mice occurred earlier, at 48 hours post CCl<sub>4</sub> exposure, compared to 6J mice, which increased 72 hours post CCl<sub>4</sub> exposure (Figure 6-6A). PCNA protein increased in both sub-strains 48 hours post CCl<sub>4</sub> exposure, however, in parallel to mRNA data, 6N had higher PCNA levels compared to 6J mice (Figure 6-6B, C). The PCNA protein levels remained elevated in both sub-strains 96 hours post CCl<sub>4</sub> exposure. *Ccnd1* expression increased following CCl<sub>4</sub> exposure in both sub-strains 48 hours post CCl<sub>4</sub> exposure; there was no difference in *Ccnd1* transcript levels between 6N and 6J mice (Figure 6-6D). CCND1 protein levels also increased in both sub-strains following CCl<sub>4</sub> exposure, however there was no difference between sub-strains at any time point (Figure 6-6E, F). Ki67, which is present throughout the active phases of the cell cycle, increased in both sub-strains following CCl<sub>4</sub> exposure, however with different kinetics (Figure 6-6G, H). Specifically, Ki67-positive cells were present 48 hours after

CCl<sub>4</sub> exposure in 6N mice but were not present until 72 hours post CCl<sub>4</sub> exposure in 6J mice (Figure 6-6G, H). Together, these data suggest that 6N mice initiated regeneration earlier than 6J mice.

### **Matrix remodeling following CCl<sub>4</sub> exposure**

The final stage of wound healing is matrix remodeling (matrix synthesis and degradation) and similar to regeneration, it occurs at 48, 72, and 96 hours post CCl<sub>4</sub> exposure (Balaji *et al.*, 2015; Deshpande *et al.*, 2016). Activated hepatic stellate cells (HSC) contribute to matrix synthesis (Friedman, 2008a). HSC transdifferentiate into myofibroblasts and begin expressing  $\alpha$  smooth muscle actin (*Acta2*) and synthesize type 1 collagen (*Col1a1*) (Friedman, 2008a). Hepatic *Acta2* transcript levels increased following CCl<sub>4</sub> exposure in both 6J and 6N mice; *Acta2* transcript levels were higher in 6N mice 48 hours after CCl<sub>4</sub> exposure when compared to 6J mice (Figure 6-7A). Expression of *Col1a1* also increased in both sub-strains following CCl<sub>4</sub> exposure and was higher in 6N mice at 48 and 72 hours post CCl<sub>4</sub> exposure compared to 6J mice (Figure 6-7B). Immunohistochemistry revealed that  $\alpha$ SMA increased in both sub-strains following CCl<sub>4</sub> exposure (Figure 6-7C and D). However,  $\alpha$ SMA increased over baseline in 6N mice at 72 hours post CCl<sub>4</sub> exposure while  $\alpha$ SMA protein did not increase above baseline in 6J mice until 96 hours post CCl<sub>4</sub> exposure (Figure 6-7C and D). At this point,  $\alpha$ SMA levels were not different from baseline in 6N mice (48 hours is not included due to high non-specific staining in the necrotic tissue) (Figure 67C and D).

Matrix synthesis is opposed by matrix metabolism, which can be evaluated using *in situ* zymography (Lindsey *et al.*, 2001; Yan and Blomme, 2003). Very little matrix

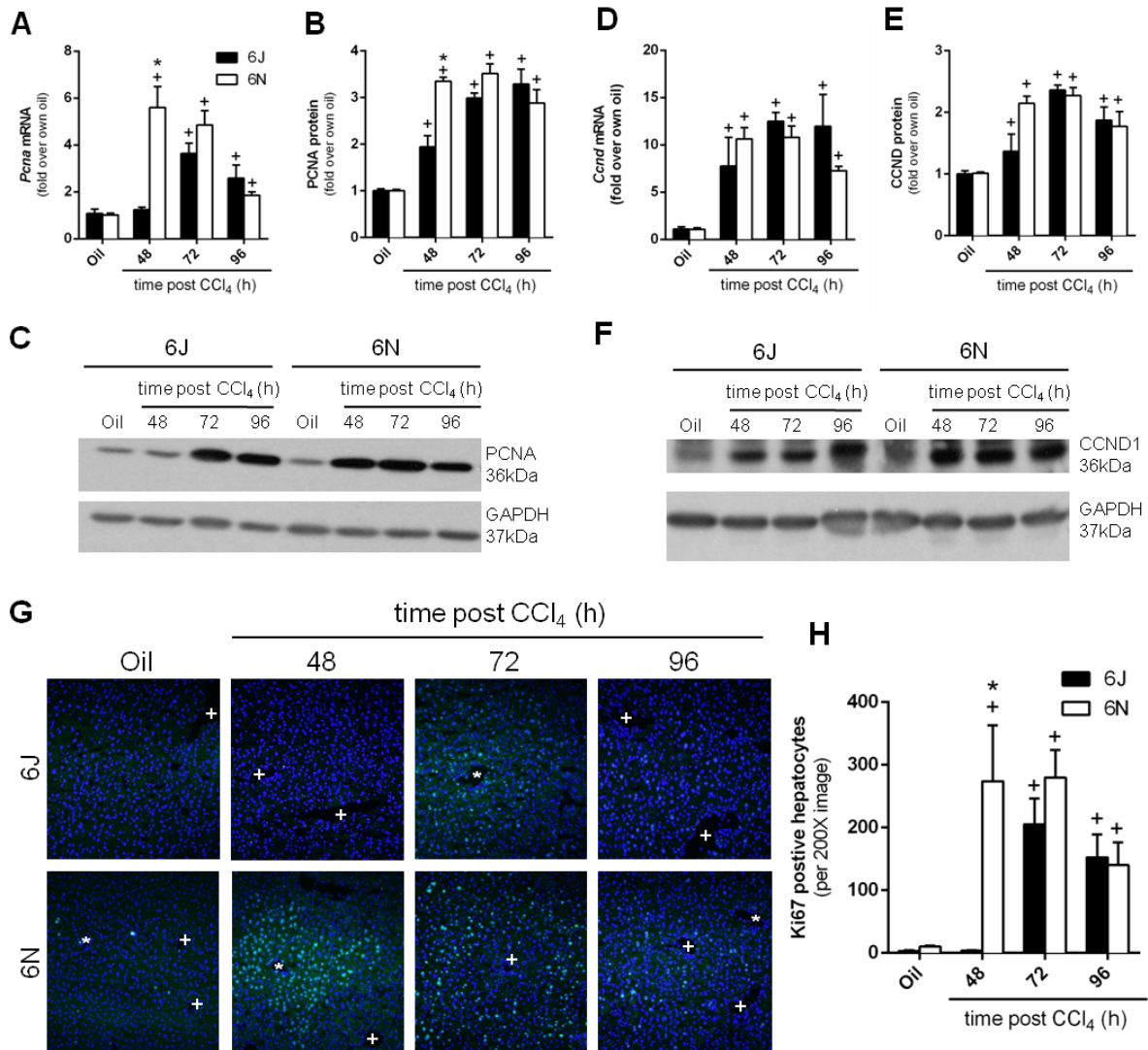


**Figure 6-6: Hepatic regeneration following acute CCl<sub>4</sub> exposure.**

Mice were exposed to CCl<sub>4</sub> and euthanized 48, 72, or 96 hours later. *Pcna* was evaluated at both the A. mRNA and B, C. protein level, by real time PCR or Western blotting, respectively. *Ccnd1* was evaluated at both the D. mRNA and E, F. protein level. G. Ki67 immunofluorescence was performed to identify proliferating hepatocytes. DAPI was used to visualize nuclei. In each image, central veins are marked with a + and portal veins are marked with a \*. H. Quantification of Ki67-positive cells. n=5-6 per group, \* represents  $p \leq 0.05$  when comparing sub-strains at a single time point; +,  $p \leq 0.05$  when comparing the indicated CCl<sub>4</sub> time point to the oil (control) of the same sub-strain.

metabolism occurred at baseline (Figure 6-7E, top panels, not quantified) or early time points (not shown), but matrix metabolism did occur 72 and 96 hours post CCl<sub>4</sub> exposure in both sub-strains. However, matrix metabolism was not different (area or intensity) between 6J and 6N mice at either time point (Figure 6-7F and G). These data together suggest that matrix remodeling was only partially different (synthesis but not metabolism) between sub-strains.

### **Fibrosis in 6N and 6J mice following chronic CCl<sub>4</sub> exposure**

Following acute liver injury induced by CCl<sub>4</sub> exposure, 6N mice have increased injury and inflammation. We, therefore, hypothesized that 6N mice would have increased fibrosis following chronic CCl<sub>4</sub>. 6N and 6J mice were exposed to CCl<sub>4</sub> twice a week for five weeks to establish liver fibrosis. Hepatic transcript accumulation of *Acta2*, the gene encoding  $\alpha$ SMA, a marker for HSC activation is increased in both 6N and 6J mice following chronic CCl<sub>4</sub> exposure and was not different between sub-strains (Figure 6-8A). Hepatic content of mRNAs that make up type 1 collagen, *Col1a1* and *Col1a2*, were increased in both sub-strains after chronic CCl<sub>4</sub> and were greater in 6N compared to 6J (Figure 6-8B and C). Picrosirius red was used to monitor ECM accumulation in both sub-strains after chronic CCl<sub>4</sub> and shows a similar trend as collagen transcripts, increasing in both sub-strains and having more in 6N than 6J (Figure 6-8D and E). These data support the hypothesis that 6N mice have increased fibrosis following chronic CCl<sub>4</sub> exposure compared to 6J mice, and shows the importance of choosing the correct sub-strain for controls in order to avoid data interpretation errors when using transgenic mice.

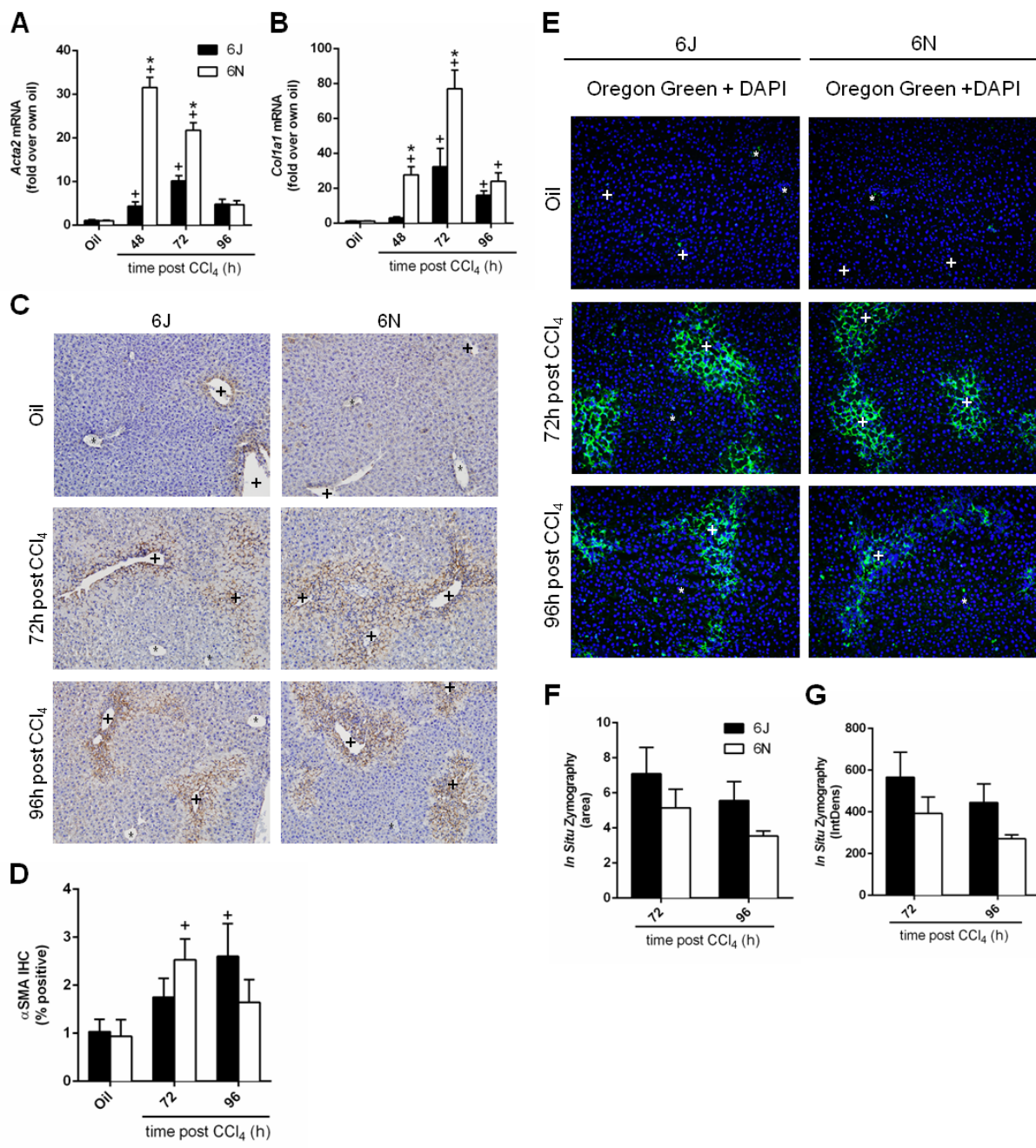
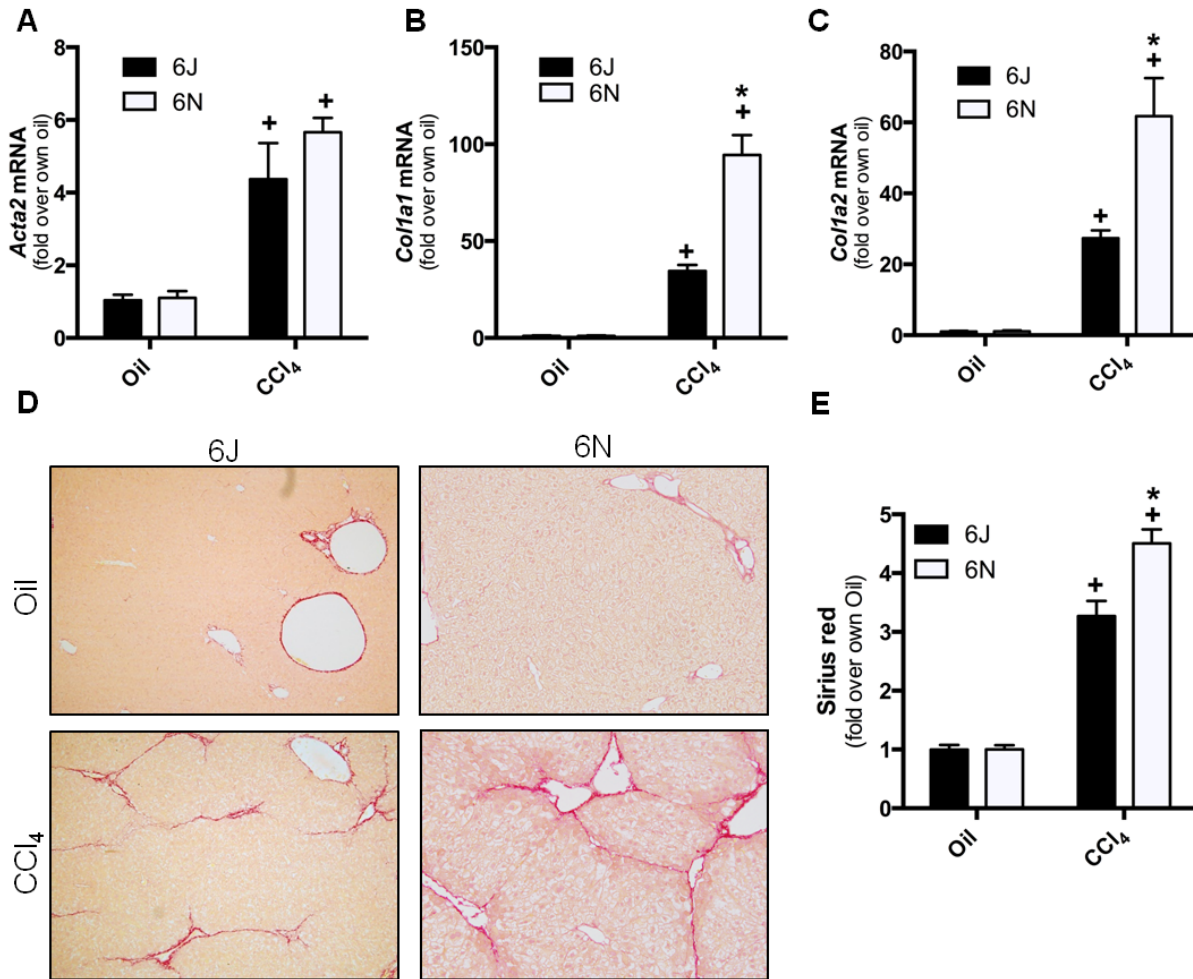


Figure 6-7: Matrix remodeling following acute CCl<sub>4</sub> exposure.

Mice were exposed to CCl<sub>4</sub> and euthanized 48, 72, or 96 hours later. Hepatic transcript accumulation of A. *Acta2* and B. *Col1a1* were evaluated by real time PCR. C. Immunohistochemistry for  $\alpha$ SMA, the *Acta2* gene product, was performed and D. quantified as the percent area of positive staining in each image. E. *In situ* zymography was used to detect matrix metabolism in frozen liver sections at baseline, 72 and 96 hours post CCl<sub>4</sub> exposure. The green fluorescence indicates areas of matrix metabolism. DAPI was used to visualize nuclei. F. The area and G. intensity above a set threshold was quantified after *in situ* zymography. Baseline matrix metabolism was too low to quantify. Central veins are marked with a + and portal veins are marked with a \*. n=5-6 per group, \*, p  $\leq$  0.05 when comparing sub-strains at a single time point; +, p  $\leq$  0.05 when comparing the indicated CCl<sub>4</sub> time point to the oil (control) of the same sub-strain.



**Figure 6-8: Hepatic fibrosis in C57BL/6J and C57BL/6N mice, after chronic CCl<sub>4</sub> exposure.**

Mice were exposed to CCl<sub>4</sub> twice a week for five weeks and euthanized 72 hours after the last injection. Control mice received olive oil (oil) injections twice a week for five weeks. Real time PCR was used to evaluate hepatic transcript levels of A. *Acta2*, B. *Col1a1*, and C. *Col1a2* in 6J and 6N mice. Data are normalized to 18s and expressed as fold change over each genotypes own oil. D. Representative histology images of picrosirius red and E. quantification to evaluate ECM accumulation. Central veins are marked with a + and portal veins are marked with a \*. Data are expressed as fold change over own oil. n=6-7 per group. \*, p ≤ 0.05 when comparing sub-strains at a single time point; +, p ≤ 0.05 when comparing CCl<sub>4</sub> to the oil (control) of the same sub-strain.

## **Genotypes of genetically modified mice used in this dissertation**

As stated above, the use of improper controls has caused data interpretation errors (Bourdi *et al.*, 2011). Bourdi, *et al.* discovered the reason for the discrepancy of *Jnk2*<sup>-/-</sup> mice being protected versus having exacerbated liver injury following acute APAP overdose was due to which sub-strain the *Jnk2*<sup>-/-</sup> were compared (Bourdi *et al.*, 2011). The differences in the wound healing response following acute CCl<sub>4</sub> exposure we observe in our study is important for our studies because the genetically modified mice used throughout this dissertation are on two different backgrounds. Specifically *Has3*<sup>-/-</sup> mice are on a 6J background with a mutant *Nnt* enzyme and *Hmnr*<sup>-/-</sup> mice are on a 6N background with a wild-type *Nnt* enzyme. This was confirmed by genotyping (Figure 6-9).

## **Discussion**

One goal of this study was to determine whether C57BL/6 sub-strains differed in their response to a single exposure to CCl<sub>4</sub>. We evaluated indices central to liver injury and wound healing, including inflammation, regeneration, and matrix remodeling. Similar to APAP-induced liver injury (Bourdi *et al.*, 2011; Duan *et al.*, 2016), we report here that 6N mice have increased injury compared to 6J mice; this increased injury was not due to differences in CYP2E1 bioactivation, or hepatocyte sensitivity to CCl<sub>4</sub> between sub-strains, but might be due to increased numbers of neutrophils and/or earlier and greater TNF $\alpha$  production observed in 6N mice.

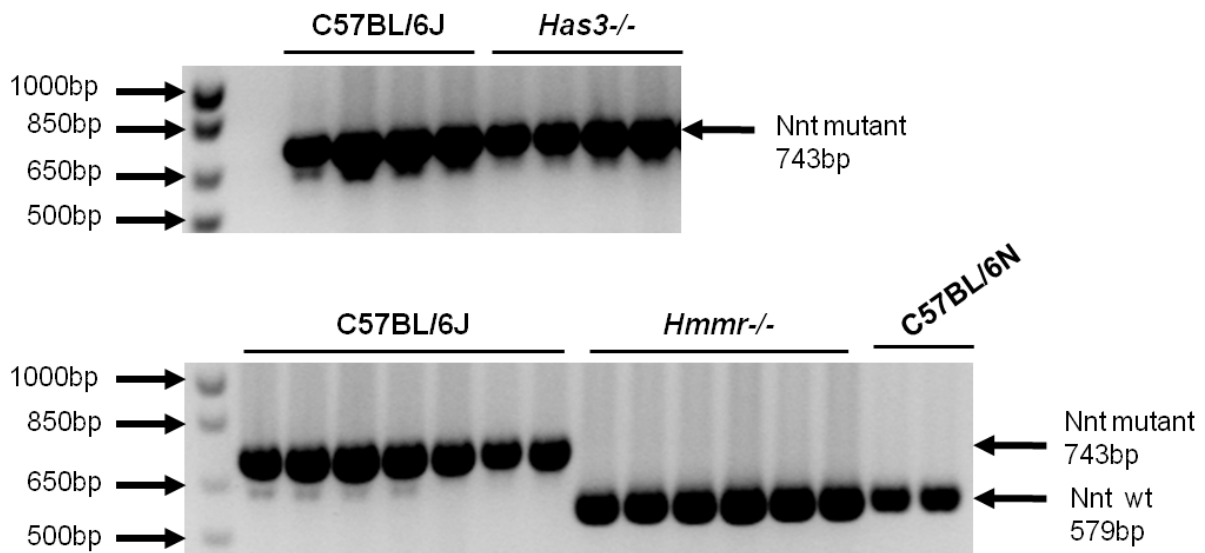


**Figure 6-9: *Nnt* genotypes of genetically modified mice used in this dissertation.**

Genomic DNA was isolated from livers of purchased 6J and 6N mice as well as in-house bred *Has3*<sup>-/-</sup> and *Hmnr*<sup>-/-</sup> mice and genotyped for *Nnt* status. Using appropriate primers described in Chapter 2, wild-type *Nnt* is 579 bp and mutant *Nnt* is 743 bp.

Paradoxically, the increase in TNF $\alpha$  in 6N mice may have also contributed to the more rapid onset of liver regeneration in 6N mice, relative to 6J mice, after CCl<sub>4</sub> exposure (Webber *et al.*, 1998; Bohm *et al.*, 2010). This apparent dichotomy may be due, in part, to the location where hepatocytes are exposed to TNF $\alpha$ . For example, the stressed hepatocytes found immediately around the necrotic pericentral area may be more sensitive to TNF $\alpha$ -mediated cell death, while the hepatocytes found in the periportal area may be more sensitive to TNF $\alpha$ -mediated promotion of liver regeneration. Our own data support this notion, as the area of necrosis was greater in 6N mice compared to 6J mice 48h after CCl<sub>4</sub>, while at the same time point, hepatocytes in the periportal areas of 6N expressed Ki67 while 6J mice did not; these phenomena occurred when *Tnfa* expression was greatest in 6N liver. Subsequently, increased infiltration of NPC, including macrophages, 72 and 96 hours after CCl<sub>4</sub>, into the necrotic areas was correlated to more rapid clearing of the necrotic tissue in the 6N mice compared to the 6J mice. While matrix synthesis began earlier in 6N mice, matrix metabolism was similar between 6J and 6N mice. Therefore, despite increased liver injury in 6N mice, liver repair was more rapid when compared to repair in the less-injured 6J mice. This is likely due to the more rapid inflammatory, regenerative and HSC responses observed in 6N mice.

Because CCl<sub>4</sub> causes mitochondrial damage, mutations in the *Nnt* gene would be expected to exacerbate injury due to the decreased antioxidant capacity in 6J mice. Despite this, and similar to APAP-induced liver injury, we report here that liver injury is increased in 6N mice compared to 6J mice. Cellular lipid membranes are disrupted after CCl<sub>4</sub> bioactivation. This bioactivation also causes mitochondrial damage and oxidative

stress reflected in a decrease in mitochondrial GSH/GSSG ratio (Ip and Ko, 1996; Wong *et al.*, 2014). In addition, CCl<sub>4</sub>-induced liver damage can be attenuated using antioxidants to raise the mitochondrial GSH/GSSG ratio. This, in turn, decreases cell damage and lowers plasma ALT levels (Ip and Ko, 1996; Wong *et al.*, 2014). *Nnt* mutant mice have a decreased basal GSH/GSSG ratio. Thus, it should follow that the *Nnt* mutant mice would have increased injury (Ronchi *et al.*, 2013). However, this does not occur after APAP (Bourdi *et al.*, 2011; Duan *et al.*, 2016) or CCl<sub>4</sub>-induced liver injury (described in this study), which suggests that factors other than the mutated *Nnt* may play a more prominent role in sub-strain-specific responses to hepatic injury triggered by APAP and CCl<sub>4</sub>. We also report that there is no difference in hepatocyte sensitivity to cell death caused by CCl<sub>4</sub>, *in vitro*, which further supports the idea that other factors, besides the mutated *Nnt* gene, are responsible for increased sensitivity of 6N mice to CCl<sub>4</sub>-induced liver injury.

Studies demonstrating that 6J mice are more sensitive to oxidative stress contradict our findings that 6N mice exhibited increased injury following acute CCl<sub>4</sub> exposure. In a number of model systems, mutated *Nnt* results in several redox alterations, including higher rates of H<sub>2</sub>O<sub>2</sub> release and the spontaneous oxidation of NADPH, along with a reduced GSH/GSSG ratio (Arkblad *et al.*, 2005; Sheeran *et al.*, 2010; Ronchi *et al.*, 2013). Mutant *Nnt* is a genetic modifier in two separate, transgenic mice. *Bcl2l2* encodes for BCL-W, which protects cells from apoptosis during cellular and oxidative stress (Ross *et al.*, 1998). When *Bcl2l2*<sup>-/-</sup> mice are on an *Nnt* mutant (6J) background, they display increased embryonic lethality compared to *Bcl2l2*<sup>-/-</sup> on an *Nnt* wild-type (6N) background (Ross *et al.*, 1998; Navarro *et al.*, 2012). Similarly, mice

deficient in mitochondrial superoxide dismutase (*Sod2*<sup>-/-</sup>) exhibit enhanced tissue damage and increased lethality shortly after birth when they are on an *Nnt* mutant background compared to *Sod2*<sup>-/-</sup> mice on an *Nnt* wild-type background (Huang *et al.*, 2006). In contrast to what is observed after APAP overdose (Bourdi *et al.*, 2011; Duan *et al.*, 2016) or after acute CCl<sub>4</sub> in the present study, these studies show that a mutant *Nnt* leads to increased sensitivity to oxidative stress.

Additional studies comparing 6J and 6N mice in models of diet-induced obesity show that the *Nnt* mutation is linked to glucose intolerance and reduced insulin secretion (Freeman *et al.*, 2006a; Freeman *et al.*, 2006b). Although both sub-strains are sensitive to diet-induced obesity, after high fat diet (60% of calories from fat) feeding, 6J mice gain more weight and display increased glucose intolerance compared to 6N mice (Nicholson *et al.*, 2010). Rescuing the mutated *Nnt* back to wild-type using bacterial artificial chromosomes improves glucose tolerance (Freeman *et al.*, 2006b). These data suggest that the mutated *Nnt* gene itself is at least partially responsible for the difference in glucose intolerance between the 6J and 6N mice (Freeman *et al.*, 2006b). However, after feeding these sub-strains a diet that contains 45% calories from fat, 6N mice display greater hepatic inflammation despite having a functional NNT enzyme (Freeman *et al.*, 2006b), which is similar to what we observe after acute CCl<sub>4</sub> exposure. Collectively, and similar to APAP overdose (Bourdi *et al.*, 2011; Duan *et al.*, 2016) and to acute CCl<sub>4</sub> exposure, a mutant *Nnt* can help protect mice from liver inflammation despite leading to impaired glucose tolerance. When thinking about these published studies and the data presented here, one must begin to consider what other factors, besides a mutated *Nnt*, are contributing to sub-strain specific differences in various

animal models of human disease, particularly when inflammation, liver damage, and hepatic repair are concerned.

Additional investigations document single nucleotide polymorphisms (SNPs) between the two sub-strains, which may account for differences between 6J and 6N mice, dependent or independent of *Nnt* status. Indeed, eleven different SNPs exist between 6J and 6N mice (Mekada *et al.*, 2009; Zurita *et al.*, 2011). Most of the SNPs map to non-coding regions of the genome, but 5 SNPs are linked to specific genes including *Naaladl2* (N-acetylated alpha-linked acidic dipeptidase-like 2), *Aplp2* (amyloid precursor-like protein 2), *Lims2* (LIM and senescent cell antigen-like-containing domain protein 1), *Fgf14* (Fibroblast growth factor 14), and *Snap29* (Synaptosomal-associated protein 29) (Mekada *et al.*, 2009; Zurita *et al.*, 2011). Although it is beyond the scope of this study, it is possible that one or more of these SNPs alone or together with the well-established *Nnt* mutation may contribute to the differences seen between the 6J and 6N mice following acute CCl<sub>4</sub> exposure.

Another explanation for the, at first, unexpected results found here may be explained by “hormesis”. Hormesis can be defined as low doses of a stressor being beneficial to survival while high doses of the same stressor are detrimental. It often refers to a chemical insult, but can also refer to adaptations to stress (Milisav *et al.*, 2012). If hormesis is considered in this scenario, 6J mice, which have had a non-functional NNT enzyme for decades, have likely adapted to the lower antioxidant capacity in other ways. Therefore, they can withstand higher oxidative stress, relative to non-adapted mice, resulting in reduced cell death and subsequently a limited inflammatory response. It is not until an injurious insult has overcome this new

homeostasis that robust injury and inflammation occurs. This concept has been applied to several phenomena in toxicology (Counts and Goodman, 1995; Williams and Iatropoulos, 2002). To determine if 6J mice compensated for reduced NNT activity by increasing other antioxidant defenses according to the principals of hormesis, we evaluated *Gclc* and *Nqo1* mRNA and NQO1 protein; we found little difference in these antioxidant molecules between the sub-strains. While beyond the scope of this study, further studies should evaluate additional antioxidant defense pathways in 6J and 6N mice to determine if differences in the observed antioxidant response contribute to differences in liver injury and subsequent inflammation noted in these sub-strains after acute CCl<sub>4</sub> exposure.

Our thorough characterization of differences between sub-strains after acute CCl<sub>4</sub> exposure is a critical first step in understanding differences between 6J and 6N mice. Our study shows, for the first time, that despite the fact that CCl<sub>4</sub>-induced liver injury is worse in 6N mice, liver repair was more rapid when compared to repair in the less-injured 6J mice. This is likely due to the more robust inflammatory, regenerative, and HSC responses observed in 6N mice, but other mechanisms may also be involved. In addition to exploration of whether or not hormesis is involved in protecting 6J mice from CCl<sub>4</sub>-induced liver injury relative to 6N mice as suggested above, it might be beneficial to determine if a zone-specific role for TNF $\alpha$  exists in driving hepatocyte death versus hepatocyte proliferation 48 hours after CCl<sub>4</sub> exposure. Additionally, further evaluation of the role neutrophils play in exacerbation of liver injury in 6N mice is also warranted. These would be excellent next steps to understanding sub-strain differences in this commonly used model of acute hepatotoxin exposure.

We also investigated potential differences in frank fibrosis between these two sub-strains following chronic CCl<sub>4</sub> exposure. In accordance with the acute data, we hypothesized that 6N mice would have increased hepatic fibrosis. They did in fact have increased pro-fibrotic transcripts and increased ECM accumulation evaluated by picrosirius red staining. Similar to acute data, this is surprising due to the mitochondrial defect in 6J mice. In fact, in a genetically modified mouse strain that has increased mitochondrial antioxidant capacity, CCl<sub>4</sub> induced fibrosis was decreased, suggesting that 6N mice would have decreased hepatic fibrosis (Mitchell *et al.*, 2009b). Even so, in a model of angiotensin II-induced left ventricular cardiac remodeling, 6N mice have increased collagen content compared to 6J mice (Cardin *et al.*, 2014). The fibroblasts isolated from these mice also have increased *Col1a1* transcript accumulation, and this supports the findings of our chronic CCl<sub>4</sub> study (Cardin *et al.*, 2014). As stated above, there have been several reported SNPs and it is possible that one of the SNPs alone or in combination with *Nnt* may be contributing to the differences observed in 6N vs 6J mice after chronic CCl<sub>4</sub> exposure (Zurita *et al.*, 2011). 6N mice heal faster than 6J mice after acute CCl<sub>4</sub> exposure and while the 6N mice display increased fibrosis at this time point after chronic CCl<sub>4</sub>, it would be interesting to evaluate fibrosis resolution in these two sub-strains to see if 6N mice can also resolve fibrosis faster than 6J mice.

Our study highlights the importance of identifying and choosing the correct control sub-strain when using genetically-modified mice in studies which utilize acute and chronic CCl<sub>4</sub>. Similar to the contradictory reports on *Jnk2*<sup>-/-</sup> mice in APAP-induced liver injury, comparing a genetically modified mouse to the wrong C57BL/6 sub-strain after CCl<sub>4</sub> exposure may lead to data misinterpretations. This experimental caveat is

vitaly important in this new age of experimental rigor, transparency and reproducibility required by the National Institute of Health (Collins and Tabak, 2014; Omary *et al.*, 2016). Also, as stated above, it is especially important when interpreting the data presented in this dissertation, as the genetically modified mice that were utilized are on two different sub-strain backgrounds.

## Chapter 7: Discussion, Conclusions, and Future Directions

*Portions of this chapter are adapted from 1) McCracken, JM et al. "Differential effects of hyaluronan synthase 3 deficiency after acute vs chronic liver injury in mice" Fibrogenesis and Tissue Repair 2016; Licensed under Creative Commons Attribution 4.0 International License and 2) McCracken, JM et al. "C57BL/6 substrains exhibit different responses to acute carbon tetrachloride exposure: Implications for work involving transgenic mice" Gene Expression: The Journal of Basic Liver Research. 17#3, doi: 10.3727/105221617X695050 with permission Cognizant, LLC; [www.cognizantcommunications.com](http://www.cognizantcommunications.com) copyright 2017 in press.*

Chronic liver disease and the complications that arise from it have become a major problem in the world (Abu-Wasel *et al.*, 2013; Roberts *et al.*, 2014; Kochanek *et al.*, 2016). In 2014, liver disease was rated the 12<sup>th</sup> leading cause of death in the United States (Kochanek *et al.*, 2016). In developed countries, like the United States, chronic liver disease is often caused by alcohol and drug abuse and/or over nutrition and obesity (Penny, 2013; Corey and Kaplan, 2014; Woolbright and Jaeschke, 2015). Patients are initially diagnosed with steatosis, but if injury becomes chronic the patient can progress to fibrosis, cirrhosis, and hepatocellular carcinoma (HCC) (Llovet *et al.*, 2003; Postic and Girard, 2008; Pellicoro *et al.*, 2014). Some patients are able to reverse steatosis and fibrosis if the etiologic agent is removed and their liver can return to normal function (Bataller and Brenner, 2005; Pellicoro *et al.*, 2014). Unfortunately, for the patients that progress past fibrosis to cirrhosis and HCC a liver transplant becomes the only treatment option for survival (Llovet *et al.*, 2003; Rai, 2013). Liver transplants are invasive, costly, and require lifelong immunosuppressive drugs (Rai, 2013). An additional complication is the shortage of healthy livers available for transplant (Parikh *et al.*, 2015). Basic science has provided a number of potential therapeutic targets, but none have translated to the clinic as viable treatment options for advanced liver disease (Cohen-Naftaly and Friedman, 2011; Mehal and To, 2016). Thus, increased research into the mechanisms of hepatic wound healing, and disease progression/regression are needed, which was an overarching goal of this dissertation. We hypothesized that the extracellular matrix (ECM) molecule hyaluronan (HA), HA binding proteins, and receptors (collectively referred to as the HA network) aid in hepatic wound healing after

both acute and chronic hepatotoxin induced liver injury, with a specific focus on HA itself and the HA receptor HA mediated motility receptor (HMMR).

### **Role for Hyaluronan (HA) and HA mediated motility receptor (HMMR) in acute and chronic liver injury induced by CCl<sub>4</sub>**

#### **Discussion**

Hyaluronan (HA) is a non-sulfated glycosaminoglycan that is ubiquitously present in the ECM (Fraser *et al.*, 1997; Jiang *et al.*, 2011). High levels of HA are found in the vitreous humor of the eyes, the skin, and synovial fluid (Cowman *et al.*, 2015). There, it acts as a space filler, ECM stabilizer, and shock absorber, respectively (Meyer and Palmer, 1934; Anderegg *et al.*, 2014; Guidolin and Franceschi, 2014). HA is also present in high amounts in fetal tissue and contributes to fetal tissues' ability to heal without a scar, also called regenerative healing (Longaker *et al.*, 1991; Leung *et al.*, 2012). Following injury, HA is transiently increased in many adult tissues including the skin, lung, and intestine and plays a role in the wound healing process and disease progression in each of these tissues (Bai *et al.*, 2005; Kessler *et al.*, 2008; Mack *et al.*, 2012). This transient increase in HA contrasts with the high basal HA found in fetal tissue and is thought to contribute to the fibrotic healing observed in adult tissue (West *et al.*, 1997).

Over 30 years ago, HA was identified as a potential biomarker for liver disease (Engstrom-Laurent *et al.*, 1985). It is increased in the plasma of patients with liver disease and since its discovery has been closely correlated with disease severity (Lee

*et al.*, 2010; Lee *et al.*, 2013). Despite the established role for HA in disease progression in other tissues and its use as a biomarker for liver injury, there has been little research into a possible pathogenic role of HA in the progression of liver disease. We are the first to show, using genetically modified mice, that there is a potential link between HA, a HA receptor (HA mediated motility receptor, HMMR), and several aspects of the acute hepatic wound healing process, including inflammation and matrix remodeling. We propose HA aids in the regenerative wound healing that occurs after acute hepatic injury, resulting in no excess ECM, similar to healing observed in fetal tissue. We have also proposed a link between HA, HMMR, and chronic wound healing, specifically that these two molecules are required for matrix remodeling and ECM clearance.

Using mice deficient in one of the hyaluronan synthase genes (*Has3*<sup>-/-</sup>) and carbon tetrachloride (CCl<sub>4</sub>) to induce acute liver injury, we show an increase in not only injury and inflammation, but a subsequent increase in wound healing including regeneration and matrix remodeling (Chapter 3). Surprisingly, we also observed increased hepatic HA content in *Has3*<sup>-/-</sup> mice compared to wild-type mice, and this HA was found in the centrilobular regions of the liver where CCl<sub>4</sub> caused necrosis. These differences, particularly the increased wound healing, are associated with an increase in both the gene expression and protein levels of HMMR. We therefore examined wound healing following acute CCl<sub>4</sub> in *Hmmr*<sup>-/-</sup> mice and found a delay in inflammation and wound healing compared to wild-type mice (Chapter 4). *Hmmr*<sup>-/-</sup> mice also had delayed hepatic HA accumulation. Following chronic CCl<sub>4</sub> we observed a similar reciprocal relationship. *Has3*<sup>-/-</sup> mice displayed increased pro-fibrotic markers but increased matrix

remodeling compared to wild-type mice. In contrast *Hmnr*<sup>-/-</sup> mice displayed decreased pro-fibrotic markers and decreased matrix remodeling compared to wild-type mice (Chapter 5). A summary of these findings can be found in Figure 7-1.

The observed increases in injury and inflammation in *Has3*<sup>-/-</sup> mice was unexpected and opposite of what is found in published literature. In a dextran sodium sulfate (DSS)-induced model of colitis, *Has3*<sup>-/-</sup> mice are protected from colon damage and had decreased inflammation (Kessler *et al.*, 2015). Unlike the increase in hepatic HA content we observed, *Has3*<sup>-/-</sup> mice have decreased intestinal HA content following DSS-induced colitis (Kessler *et al.*, 2015). Additionally, in the lung, *Has3*<sup>-/-</sup> mice have decreased injury, neutrophil recruitment, and macrophage inhibitory protein (MIP2) compared to wild-type mice after ventilator induced lung injury (Bai *et al.*, 2005). This was associated with decreased low molecular weight (LMW) HA fragments in *Has3*<sup>-/-</sup> mice compared to wild-type mice (Bai *et al.*, 2005). This, again, is in contrast our study, where we see increased inflammation and increased hepatic HA content in *Has3*<sup>-/-</sup> mice compared to wild-type mice after acute CCl<sub>4</sub> exposure. This suggests a potential difference in cell type expression of HAS enzymes exists and that these differences contribute to differential responses to injury depending on the tissue type.

There are three possible ways that HA and inflammation are related during tissue injury and repair (discussed in detail below and outlined in Figure 7-2). The first way HA can contribute to inflammation is by directly stimulating pro-inflammatory mediators. During tissue injury, endogenous HA (considered high molecular weight, HMW-HA) is cleaved to LMW-HA fragments that induce inflammatory changes within the tissue. In alveolar macrophages, LMW-HA fragments induce pro-inflammatory chemokines

**A**

<b>Acute CCl<sub>4</sub></b>	<i>Has3</i> <sup>-/-</sup>	<i>Hmmr</i> <sup>-/-</sup>
Injury	↑	=
Pro-inflammatory microenvironment	↑	↓
Macrophage migration	↑	↓
HSC activation markers	↑	↓
Matrix metabolism	↑	↓

**B**

<b>Chronic CCl<sub>4</sub></b>	<i>Has3</i> <sup>-/-</sup>	<i>Hmmr</i> <sup>-/-</sup>
Pro-fibrotic transcripts	↑	↓
Fibrosis	=	=
Matrix metabolism	↑	↓

**Figure 7-1: Summary of findings for acute and chronic CCl<sub>4</sub> exposure in *Has3*<sup>-/-</sup> and *Hmmr*<sup>-/-</sup> mice.**

A. Mice were exposed to a single injection of CCl<sub>4</sub> and parameters of hepatic injury and wound healing were evaluated. B. Mice were exposed to 2 injections of CCl<sub>4</sub> per week for 5 weeks to induce fibrosis and parameters of fibrosis and matrix remodeling. *Has3*<sup>-/-</sup> mice were compared to C57BL/6J control mice and *Hmmr*<sup>-/-</sup> mice were compared to C57BL/6N control mice. ↑ represents genetically modified mouse response is increased compared to wild-type; ↓ represents genetically modified mouse is decreased compared to wild-type; = represents genetically modified mouse has similar response compared to wild-type

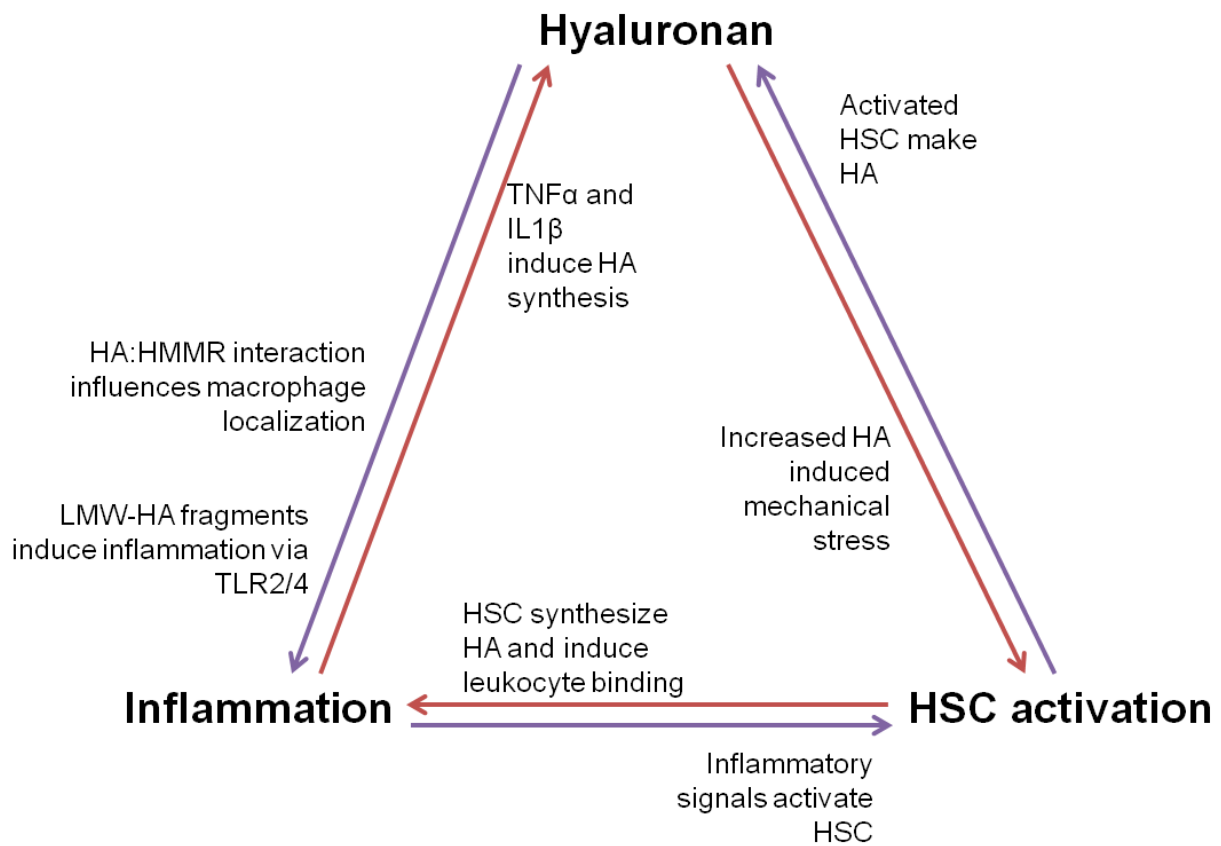


**Figure 7-2: Hyaluronan, inflammation, and hepatic stellate cells influence one another.**

Pro-inflammatory signals like TNF $\alpha$  and IL1 $\beta$  can induce HA synthesis. Reciprocally LMW-HA fragments induce inflammation via TLR2 and TLR4. Additionally the HA:HMMR interaction aids in macrophage localization. HA is synthesized by activated HSC and subsequently increases mechanical stress further activating HSC in a feed forward loop. Lastly, HSC synthesized HA increased leukocyte binding and localization and conversely, pro-inflammatory signals activate HSC.

including CCL2 and CXCL10, which promote a pro-inflammatory microenvironment (Horton *et al.*, 1998). In *Has3*<sup>-/-</sup> mice we observe an increase in hepatic HA content, which may be being cleaved to LMW-HA fragments and directly induces inflammation. We also observe an increased percentage of <100 kDa HA fragments in *Has3*<sup>-/-</sup> mice, which again could be contributing to the increased *Ccl2* and *Cxcl10* transcripts in *Has3*<sup>-/-</sup> mice. Conversely, *Hmmr*<sup>-/-</sup> mice have decreased hepatic HA, which would limit LMW-HA fragment formation and subsequent inflammation in *Hmmr*<sup>-/-</sup> mice compared to wild-type mice.

As stated above, HA itself could be inducing inflammation, but a second way HA and inflammation could be related is that inflammation could be inducing HA deposition as has been demonstrated previously. Interleukin (IL) 1 $\beta$  and TNF $\alpha$  induce HA synthesis in endothelial cells that then subsequently binds monocytes *in vitro* (Vigetti *et al.*, 2010). IL1 $\beta$  also stimulates HA synthesis by fibroblasts, which then forms protrusions with CD44 and ICAM1 and becomes adhesive for monocytes *in vitro* (Meran *et al.*, 2013). In both of these studies, increased *Has2* expression was considered the cause of the increased HA synthesis. We also observe increased *Has2* expression following acute CCl<sub>4</sub> exposure, although *Has1* is expressed to a higher degree in both wild-type and *Has3*<sup>-/-</sup> mice. However, it is possible that the differential inflammatory response we observe in *Has3*<sup>-/-</sup> and *Hmmr*<sup>-/-</sup> mice is contributing to the differential hepatic HA content. Thus more inflammation equals more HA deposition in *Has3*<sup>-/-</sup> mice compared to wild-type mice, and less inflammation equals less HA deposition in *Hmmr*<sup>-/-</sup> mice compared to wild-type mice.

Finally, HA interacting with HMMR may be contributing to localization of recruited macrophages and, subsequently, inflammation. In addition to the increased inflammatory microenvironment we saw in *Has3*<sup>-/-</sup> mice, we saw an increase in hepatic HA and HMMR. We propose that recruited macrophages express HMMR on their surface and use HA to localize to the necrotic area and contribute to inflammation. Preliminary work in our lab shows a 20-fold increase in expression of *Hmmr* in non-parenchymal cells (NPC) compared to hepatocytes isolated from the liver both 48 and 72 hours after acute liver injury induced by CCl<sub>4</sub>, supporting the hypothesis that HMMR is expressed by macrophages following acute liver injury. HMMR is already linked to macrophage migration in other models of tissue injury, including excisional skin wounding and bleomycin induced lung injury. Specifically, using a HMMR mimetic that prevents the interaction between HA and HMMR inhibits macrophage migration into excisional skin wounds (Tolg *et al.*, 2012). Similarly, a HMMR blocking antibody prevents macrophage migration into the lung during bleomycin induced lung injury (Zaman *et al.*, 2005). When we evaluated inflammation in *Hmmr*<sup>-/-</sup> mice exposed to CCl<sub>4</sub>, we observed decreased inflammation compared to wild-type mice. This further supports the hypothesis that a HA:HMMR interaction is important for macrophage migration into the liver following acute liver injury. Still further work should be done (as described below) in order to determine more specifically macrophage localization and what contribution HA is playing in that localization. The localization of hepatic macrophages becomes important in not only the inflammatory phase of wound healing but also matrix remodeling and will be described in more detail below.

Another aspect of liver wound healing we found affected by HA and HMMR was liver regeneration. There are two potential ways that regeneration could be affected. The first could be related to inflammation. Inflammation plays a vital role in liver regeneration. In fact, TNF $\alpha$  primes rat hepatocytes to enter the cell cycle and proliferate (Webber *et al.*, 1998). Additionally, when inflammation is prevented by depleting Kupffer cells, effectively lowering *Tnfa* transcripts, ethanol induced DNA synthesis is inhibited (Owumi *et al.*, 2014). Therefore, it is possible that the increased inflammation in *Has3*<sup>-/-</sup> is priming hepatocytes to enter the cell cycle earlier than their wild-type counterparts. This may be why we observe increased regeneration in *Has3*<sup>-/-</sup> mice compared to wild-type mice. Conversely, the decreased inflammation observed in *Hmmr*<sup>-/-</sup> mice may be the reason that there is a delay in regeneration in *Hmmr*<sup>-/-</sup> mice compared to wild-type mice after acute CCl<sub>4</sub> exposure.

While HA and HMMR may be playing a role in the increased inflammation and subsequent regeneration, it is possible that HMMR, potentially independent of HA, may be playing a direct role in regeneration. In addition to HMMR's extracellular role in cell migration, intracellular HMMR plays a vital role in cell cycle regulation. After HMMR knockdown in HeLa cells, there is an increase in mitotic spindle abnormalities; these cells are still able to enter the cell cycle but are arrested at the G2/M phase transition (Chen *et al.*, 2014). A portion of the HeLa cells will eventually complete mitosis, but it takes significantly more time to complete than the HeLa cells expressing HMMR (Chen *et al.*, 2014). This parallels the delay in regeneration we see in *Hmmr*<sup>-/-</sup> mice 48 hours after CCl<sub>4</sub> and the subsequent recovery to wild-type regeneration levels by 72 hours after CCl<sub>4</sub>. Because the liver is required for survival, it is likely that there are multiple

mechanisms that can compensate for and overcome HMMR deficiency. While we do observe increased *Hmmr* expression in NPC fractions compared to hepatocyte fractions after CCl<sub>4</sub> induced liver injury, there is also increased expression of *Hmmr* in hepatocytes from 48 to 72 hours (Hmmr expression at basal levels in hepatocytes and nonparenchymal cells has not been evaluated). Similarly, the increased proliferation in *Has3*<sup>-/-</sup> mice compared to wild-type mice occurs at 48 and 72 hours, and at both time points HMMR is higher in *Has3*<sup>-/-</sup> mice compared to wild-type mice. This further supports a role for HMMR in hepatocyte proliferation. *In vitro* experiments could help elucidate a role for intracellular HMMR in hepatocyte proliferation (described below).

Matrix remodeling, including both synthesis and degradation can also contribute to/be affected by HA and the HA network (outlined in Figure 7.2). Matrix synthesis occurs in the liver after both acute and chronic liver injury and requires activation of hepatic stellate cells (HSC), which differentiate into myofibroblasts and synthesize ECM. As stated above, HA is increased after dermal tissue injuries in the skin, and as we have shown, HA deposition also occurs in the liver after injury. Previous studies show that HSC isolated from livers following partial hepatectomy synthesize HA (Vrochides *et al.*, 1996). We have demonstrated here that HA is deposited around the central vein regions of the liver. This is the region damaged by CCl<sub>4</sub> and is also where the activated HSC localize, supporting the role of HSC in the synthesis of HA after toxin induced liver injury. Similar to the transient increase of HA in the skin, HA is removed from the liver after wound healing, likely being degraded by hyaluronidases and subsequently taken up by liver sinusoidal endothelial cells (Csoka *et al.*, 2001; Harris *et al.*, 2007). Future work will help to elucidate how HA is removed following liver injury.

In addition to fibroblasts being a main producer of HA, HA can also affect fibroblast phenotype. Animals deficient in both *Has1* and *Has3* (*Has1/3-/-*) have decreased HA deposition following excisional skin wounding as expected due to the lack of two HA synthase enzymes (Mack *et al.*, 2012). *Has1/3-/-* mice also have faster myofibroblast differentiation and dermal wound closure compared to wild-type mice (Mack *et al.*, 2012). This study has similarities and differences to the outcomes we observed in our study. While we do not see decreased hepatic HA content as was observed in the dermal injury study, we do see increased markers of HSC activation in *Has3-/-* mice after both acute and chronic CCl<sub>4</sub> exposure. This study, as well as ours, points out that HA synthesis is likely a cell type- and tissue-specific response to injury.

Additional studies in the skin further support a role for HA in wound healing and fibroblast activation. When a HA-based filler is injected intradermally into photodamaged human skin, collagen production increases (Turlier *et al.*, 2013). This is likely due to increased mechanical stress on the fibroblasts caused by the HA injection coupled to the large amounts of water organized around each HA molecule (Turlier *et al.*, 2013). A similar mechanism influences HSC activation; increased stiffness increases HSC activation, both *in vitro* and *in vivo* after acute liver failure (Dechene *et al.*, 2010; Olsen *et al.*, 2011). It is therefore possible that the increased HA in *Has3-/-* mice is attracting fluid to the liver, causing increased mechanical stress sensed by HSC, and thereby increasing HSC activation markers. The reverse could be happening in *Hmmr-/-* mice, where decreased HSC activation markers are observed in the context of an acutely injured liver with profoundly reduced HA content.

HMMR itself is linked to both fibroblast activation and migration (Tolg *et al.*, 2006). Similar to many parameters listed above, *Hmmr*<sup>-/-</sup> mice show a fibrotic response reciprocal to that observed in *Has3*<sup>-/-</sup> mice; i.e. *Hmmr*<sup>-/-</sup> mice have lower induction of pro-fibrotic genes after both acute and chronic CCl<sub>4</sub> exposure compared to wild-type or *Has3*<sup>-/-</sup> mice. *Hmmr*<sup>-/-</sup> mice also have decreased hepatic HA deposition after acute CCl<sub>4</sub> exposure. Tolg, *et al.* demonstrated *Hmmr*<sup>-/-</sup> fibroblasts are unable to migrate to the extent of wild-type mice *in vitro* and this leads to defective wound healing, *in vivo* (Tolg *et al.*, 2006). Additionally, using a HMMR mimetic that prevents the HA:HMMR interaction, wound healing is delayed and associated with decreased collagen content in the wound bed (Tolg *et al.*, 2012). This published literature, along with the data presented in this dissertation, support a role for HMMR and HA in HSC localization.

The final step in wound healing after acute liver injury is matrix degradation. This is also important to fibrosis regression after chronic liver injury. Matrix degradation occurs through a coordinated action of matrix metalloproteinases (MMPs) and their inhibitors (TIMPs) (Hemmann *et al.*, 2007; Duarte *et al.*, 2015). Similar to many parameters outlined above, we observed a reciprocal pattern of matrix degradation between *Has3*<sup>-/-</sup> mice and *Hmmr*<sup>-/-</sup> mice after acute CCl<sub>4</sub>. Specifically, *Has3*<sup>-/-</sup> mice have increased matrix metabolism compared to wild-type mice and *Hmmr*<sup>-/-</sup> mice have decreased matrix metabolism compared to wild-type mice, which mirrors the HA deposition between the transgenic strains. After chronic CCl<sub>4</sub>, matrix remodeling was increased in *Has3*<sup>-/-</sup> mice and decreased in *Hmmr*<sup>-/-</sup> mice, paralleling the results of our acute CCl<sub>4</sub> studies

In the liver, MMPs are primarily produced by macrophages (Fallowfield *et al.*, 2007b; Duarte *et al.*, 2015). CCR2, the receptor for CCL2, is expressed by macrophages, and is required for the recruitment of macrophages to the liver after injury (Mitchell *et al.*, 2009a). *Ccr2*<sup>-/-</sup> mice have delayed fibrosis resolution following chronic CCl<sub>4</sub> exposure and this is associated with delayed *Mmp2* and *Mmp13* transcript expression (Mitchell *et al.*, 2009a). Similar results are found when macrophages are depleted using a Cd11b-DTR transgenic mouse model (Duffield *et al.*, 2005). Since macrophages are vital for matrix metabolism in the liver following liver injury, the results we obtained (i.e. increased matrix metabolism and HA deposition in *Has3*<sup>-/-</sup> mice and decreased matrix metabolism and HA deposition in *Hmmr*<sup>-/-</sup> mice) further support a role for HA and HMMR in macrophage localization to areas which require matrix degradation. Additionally, HA itself induces both *Mmp9* and *Mmp13* transcripts in Lewis Lung Carcinoma cells and primary embryonic fibroblasts (Fieber *et al.*, 2004). It is therefore possible that the increased HA in *Has3*<sup>-/-</sup> mice may be contributing directly to the increased matrix metabolism. Conversely, the reduced HA deposition in *Hmmr*<sup>-/-</sup> mice may be contributing to decreased matrix metabolism after acute CCl<sub>4</sub>.

Hepatic wound healing after acute liver injury is regenerative, similar to that observed in injured fetal tissue, and does not result in ECM accumulation (Constandinou *et al.*, 2005; Leung *et al.*, 2012). We have observed an increase in hepatic HA, which is associated with wound healing. However after chronic CCl<sub>4</sub> we do not see the same extent of HA present in wild-type or *Has3*<sup>-/-</sup> mice as we do after acute liver injury. Chronic liver injury is analogous to adult tissue healing in the skin, which heals with a collagen-containing scar (Bayat *et al.*, 2003; Pellicoro *et al.*, 2014). It is

therefore tempting to speculate that the increased HA found following acute liver injury is contributing to the regenerative response, and because this HA accumulation is limited after chronic injury, perhaps this prevents regenerative repair. However, because we have only evaluated a single time point after chronic CCl<sub>4</sub> we cannot conclusively say that there is not as much hepatic HA after chronic liver injury as we see after acute liver injury. Despite the limited HA found after chronic liver injury, we do see increased matrix metabolism in *Has3*<sup>-/-</sup> mice and decreased matrix metabolism in *Hmmer*<sup>-/-</sup> mice. This further supports our hypothesis that HA and HMMR are involved in not only acute hepatic wound healing, but fibrosis resolution.

## **Conclusions**

We provide the first evidence of a role for HA and HMMR in both hepatic wound healing after acute liver injury as well as in fibrosis resolution. Specifically, we propose that following acute liver injury, hepatocytes and Kupffer cells release pro-inflammatory cytokines that activate HSC to produce HA. We suspect that there is a feed-forward loop between HA, inflammation, and HSC activation driving wound healing after acute and chronic liver injury (outlined in Figure 7-2). This likely involves a critical HA:HMMR interaction aiding in macrophage migration. This increased pro-inflammatory environment then likely contributes to hepatocyte proliferation required to repair the liver after acute injury. However, it is currently unknown what, if any, role intracellular HMMR plays in hepatocyte proliferation. As HA accumulates, there is increased mechanical stress, in turn increasing HSC activation. This could again be another feed forward loop as activated HSC synthesize HA (outlined in Figure 7-2). Finally, in both acute and

chronic liver disease, HA and HMMR continue to contribute to macrophage localization which aids in matrix degradation. A working model as described above can be found in Figure 7-3.

### **Future directions**

We are the first to propose a role for the HA network in liver injury and repair after acute and chronic liver injury. However, future work, both *in vitro* and *in vivo*, is required to determine precise mechanisms by which this occurs. *Has3*<sup>-/-</sup> mice have increased HA synthesis, most likely from activated HSC. In order to determine if the *Has3*<sup>-/-</sup> HSC actually have increased HA synthetic capacity or if they are influenced by the increased inflammation observed in *Has3*<sup>-/-</sup> mice, HSC can be isolated from both *Has3*<sup>-/-</sup> and wild-type mice. The HSC can be plated on plastic, which will stimulate activation and HA content can be measured in the cell culture supernatant using the same HA ELISA-like assay used to measure HA content in the plasma. A similar experiment can be done with isolated *Hmmr*<sup>-/-</sup> HSC. This will allow us to separate pure HSC HA synthetic capacity from inflammation induced HA synthesis.

In order to determine what role HMMR is playing in migration and activation of macrophages and/or HSC, it would first be important to determine where HMMR is expressed. Although we have preliminary evidence that HMMR has higher expression in non-parenchymal cells than in hepatocytes, it would be important to co-localize HMMR with known markers for hepatic macrophages (F4/80, CD11b, or CCR2), hepatocytes (Albumin), liver sinusoidal endothelial cells (CD31), and activated HSC ( $\alpha$ SMA) or to separate each cell fraction and monitor HMMR expression either by qPCR, Western

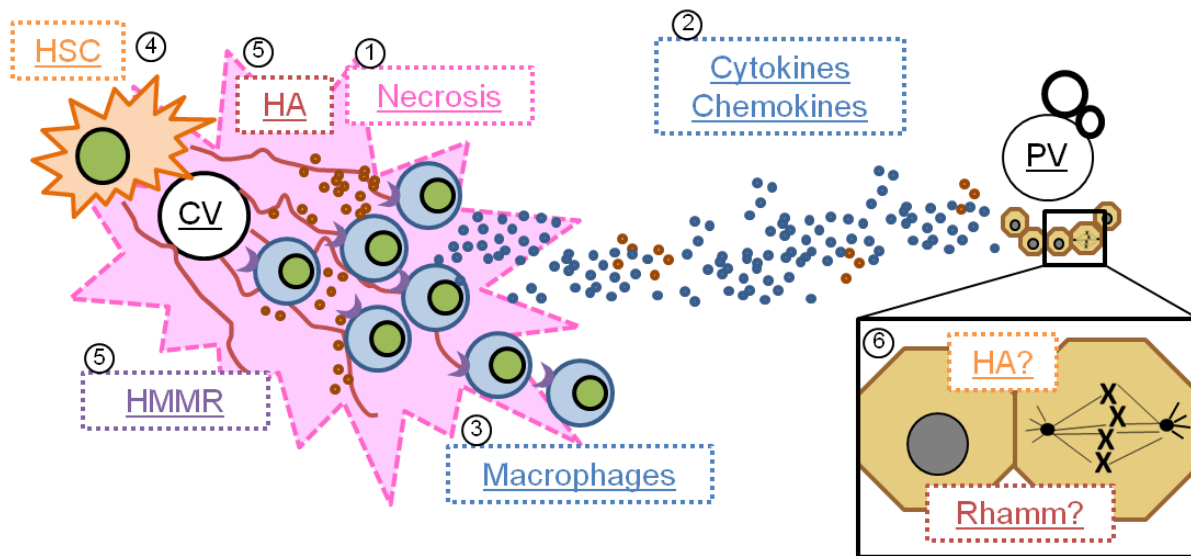


**Figure 7-3: Current working model describing a role for HA and HMMR in hepatic wound healing.**

1. Acute  $\text{CCl}_4$  exposure causes centrilobular necrosis leading to 2. the production of cytokines and chemokines. 3. These chemokines recruit macrophages to the liver; subsequently increasing the pro-inflammatory microenvironment. 4. At the same time, HSC become activated and begin synthesizing HA. 5. The chemokines recruit monocytes to the liver that then differentiate into macrophages. We propose these macrophages express HMMR and use both the chemokine gradient and the HA being synthesized by HSC to localize to the necrotic area and remove cellular debris. 6. What remains a question is what role if any intracellular HA and intracellular HMMR is playing in hepatocyte regeneration.

blotting, or flow cytometric analysis. While this will tell us what cells are expressing HMMR, using HMMR floxed mice to make cell type specific HMMR-deficient mice will allow us to determine how important HMMR is in each of these cell types and how it contributes to the wound healing process.

Because HMMR has critical functions in cell migration and proliferation, both of which contribute to hepatic wound healing, it will be important to separate the two aspects. To understand more mechanistically what role HMMR plays in migration, *in vitro* scratch wound assays or Boyden chambers could be used. For example, plating HSC or macrophages that are HMMR-deficient and monitoring their migration will tell us if HMMR is in fact playing a role in the migration of either of these hepatic cell types. Stimulating migration with HA, both HMW and LMW, in the presence or absence of peptides which prevent HA from binding HMMR, will help show if it is truly a HA:HMMR interaction aiding in the migration of these cell types. Additionally, in order to determine if HMMR plays a direct role in hepatocyte proliferation, cell cycle flow cytometry could be utilized to evaluate the cell cycle phases of both wild-type and *Hmmr*<sup>-/-</sup> hepatocytes after acute CCl<sub>4</sub> exposure. This would aid in determining if *Hmmr*<sup>-/-</sup> hepatocytes become stalled at the G2/M phase transition. Additionally, *in vitro* *Hmmr* could be knocked down in primary hepatocytes or HepG2 cells and proliferation monitored, and should include an assessment of spindle defects that may occur. If HMMR is playing a role in hepatocyte proliferation, I would expect HMMR to localize to hepatocytes, *Hmmr*<sup>-/-</sup> hepatocytes to be stuck in G2/M phase, and that the knockdown of *Hmmr* would inhibit hepatocyte proliferation. If none of these occur, it is likely that the

differential regenerative response in *Has3*<sup>-/-</sup> and *Hmnr*<sup>-/-</sup> mice is due to the differences in inflammation.

Since we propose possible feed forward mechanisms are contributing to HA synthesis, inflammation, and HSC activation, a good next step would be to inhibit HA synthesis and monitor the effect that has on inflammation and HSC activation. 4-methylumbelliferone (4-MU) is a pharmacologic HA synthesis inhibitor that works in two ways. First, it is conjugated to glucuronic acid, one of the two monosaccharide components of HA, by UDP-glucuronosyltransferase which then makes glucuronic acid unavailable for HAS enzymes to use for HA synthesis. This effectively depletes the substrate pool and prevents HA synthesis (Kakizaki *et al.*, 2004; Nagy *et al.*, 2015b). Second, 4-MU reduces *Has* enzyme expression (Kultti *et al.*, 2009). Paul Bollyky has described the use of 4-MU incorporated into a chow diet at 5% (wt/wt) and shows it effectively inhibits HA synthesis in mouse models of diabetes (Nagy *et al.*, 2015a; Kuipers *et al.*, 2016). We have preliminary data showing we are also able to inhibit HA synthesis following acute CCl<sub>4</sub> exposure by feeding mice the same 5% 4-MU diet for 2 weeks prior to CCl<sub>4</sub> exposure. Importantly, 4-MU feeding does not alter peak liver injury, measured by ALT activity, allowing us to understand how HA affects wound healing parameters after liver injury. We hypothesize that while decreased HA may inhibit early inflammation, it may have a detrimental effect when it comes to wound healing, namely on cell proliferation and matrix remodeling. In other words, if HA is important for wound healing, then preventing HA should limit wound healing.

A way to determine if the HA:HMMR interaction is required for hepatic wound healing would be to use mice that over-express HMMR in macrophages that cannot

bind HA and mice that over express a wild-type (HA-binding competent) HMMR. These mice were recently developed by our collaborator, Dr. Rashmin Savani and will be used in future collaborative studies. The three studies outlined above will allow us to determine the specific roles that HA, HMMR, or the HA:HMMR interaction play in inflammation and wound healing in the injured liver. If HA:HMMR is critical to the wound healing process, we would hypothesize that the mice expressing HMMR that can not bind HA will have delayed wound healing.

HA signaling largely depends on size. ELISA-like assays provide a quantitative value for total amount of HA in a sample, however they do not distinguish between different HA sizes. Isolation of HA from tissue can be accomplished through a series of ethanol precipitations and by digesting everything but glycosaminoglycans from the sample (Cowman *et al.*, 2015). Once the HA has been isolated, simple agarose gel electrophoresis and staining with a cationic molecule called Stains All can be used to visualize HA (Cowman *et al.*, 2011). Because HA is polydisperse, HA will appear as a smear in the gel and an average molecular mass can be determined when compared against HA standards of known molecular weights (Cowman *et al.*, 2011). We have isolated HA from mouse intestine (as a positive control) with success, however isolating HA from liver tissue has been more difficult and is something we are working to optimize. As a second approach to learn something about HA molecular weight, we utilized molecular weight cut off columns in combination with the ELISA-like assay to determine amounts of HA over a broad range of sizes. Alternatively, using size exclusion chromatography or anion exchange columns in combination with an ELISA-like assay would be a better way to monitor narrower size fractions (Cowman *et al.*,

2015; Yuan *et al.*, 2015). Any of these methods would help to better understand the size of both plasma HA and intrahepatic HA and help to better predict what roles HA is playing in wound healing based on the size.

Once HA is synthesized and extruded into the extracellular space it can interact with a number of HA binding proteins and receptors, and together this constitutes the HA network. For our initial studies, we focused on HA and a single HA receptor, HMMR, and largely ignored the rest of the HA network. Evaluating other HA receptors, like CD44 and TLR2/4, which play roles in cell migration and inflammation, respectively, will give us a better understanding of the HA signaling occurring in acute and chronic liver injury (Jiang *et al.*, 2005; Decleves *et al.*, 2006). Similarly, HA binding proteins such as tumor necrosis factor-stimulating gene 6 (TSG-6), which plays a role in HA matrix stabilization and aids in the transfer of heavy chain (HC) from inter- $\alpha$ -inhibitor (I $\alpha$ I) to HA, can be monitored (Baranova *et al.*, 2011; Martin *et al.*, 2016). The addition of HC to HA increases leukocyte recruitment and could play a role in hepatic wound healing (Lauer *et al.*, 2013). By examining the expression and localization of other portions of the HA network we could gain a more comprehensive understanding of HA's role in liver disease pathology.

Based on the increased injury and pro-fibrotic response we observed in *Has3*<sup>-/-</sup> mice after acute CCl<sub>4</sub> exposure, we were surprised we did not see increased fibrosis after chronic CCl<sub>4</sub>. Similarly, we were also surprised that delayed inflammation and reduced pro-fibrotic signature in the liver after acute CCl<sub>4</sub> in *Hmmr*<sup>-/-</sup> mice did not decrease fibrosis after chronic CCl<sub>4</sub>. The apparent disconnect in both transgenic mice can be attributed to differences in matrix degradation following chronic CCl<sub>4</sub>.

Specifically, matrix degradation is enhanced in *Has3*<sup>-/-</sup> mice, while matrix degradation is reduced in *Hmmr*<sup>-/-</sup> mice after chronic CCl<sub>4</sub> exposure, relative to each knockout's wild-type control. A caveat to this interpretation of our data is that we only looked 72 hours after the last CCl<sub>4</sub> injection. Based on the single time point, we would hypothesize that *Has3*<sup>-/-</sup> mice will have faster fibrosis resolution compared to wild-type mice and conversely, *Hmmr*<sup>-/-</sup> mice will have slower fibrosis resolution compared to wild-type mice after chronic CCl<sub>4</sub> exposure. In order to test this hypothesis, several time points after the cessation of CCl<sub>4</sub> should be monitored. By euthanizing mice 1, 3, 5, 7, and 14 days after the last exposure, it will be possible to monitor the regression of the fibrotic scar. By looking at 1 day after the last CCl<sub>4</sub> exposure it will also be possible to determine if *Has3*<sup>-/-</sup> mice do in fact have increased fibrosis and if *Hmmr*<sup>-/-</sup> mice do have decreased fibrosis as would be predicted based on the transcript accumulation of pro-fibrogenic markers we observed.

Lastly, an important next step in both the acute and chronic CCl<sub>4</sub> exposure would be better localization of both macrophages and fibroblasts in injured liver over the time course of repair/fibrosis since we are implicating the HA:HMMR interaction in both. We have experienced some problems using F4/80 immunofluorescence to monitor macrophage migration into the liver. Specifically, we see a high amount of variability, in both the intensity and staining patterns observed in a single tissue section. Use of CCR2 reporter mice (CCR2-RFP mice) would bypass this problem and provide an easier way to determine recruited macrophage localization (Saederup *et al.*, 2010). Also because these macrophages express RFP, we can combine that with the HABP (GFP) staining already optimized in the lab to co-localize HA and the CCR2<sup>+</sup> macrophages.

Using  $\alpha$ SMA as a marker for HSC is an effective way to monitor HSC localization and could be done to localize HSC with and without HABP-costaining in *Has3*<sup>-/-</sup> and *Hmmer*<sup>-/-</sup> mice after acute and chronic CCl<sub>4</sub> exposure. We would expect that using these different techniques we could confirm the hypothesis that HA and HMMR are important for macrophage localization to the necrotic area and fibrotic septae after acute and chronic CCl<sub>4</sub> exposure respectively.

Overall, by delving into *in vitro* methods to try to tease apart the different feed forward loops that may be present in inflammation, HA, HSC activation, and regeneration, we can provide a better mechanistic understanding of the role of HA and HMMR in liver injury and wound healing after both acute and chronic hepatotoxin-induced injury. Considering other aspects of the HA network, including additional receptors and binding proteins, will give a more comprehensive look at what role HA is playing in liver disease pathology. Additionally, by inhibiting HA synthesis *in vivo* we will be able to monitor how HA itself effects the wound healing process. In terms of chronic CCl<sub>4</sub> and fibrosis regression, monitoring several time points in the healing process will give us a better understanding of how HA and HMMR contribute to fibrosis regression. Finally, utilizing better techniques to localize macrophages during the wound healing process, as well as using  $\alpha$ SMA to localize HSC will help to determine if the HA:HMMR interaction does, as we propose, contribute to the localization of these cells during both acute and chronic wound healing.

**Differences in C57BL/6 sub-strain response to acute and chronic CCl<sub>4</sub>: implications for genetically modified mice**

## Discussion

During the course of this dissertation, we discovered that the two genetically modified mice being utilized were on different C57BL/6 sub-strain backgrounds; *Has3*<sup>-/-</sup> mice are on a C57BL/6J (6J) background while *Hmmr*<sup>-/-</sup> mice are on a C57BL/6N (6N) background. We therefore sought to explore differences in hepatotoxicity and the wound healing response to acute and chronic CCl<sub>4</sub> exposure between these two commonly used mouse sub-strains thinking this could provide better insight into understanding how HA and HMMR affect wound healing and fibrosis after acute and chronic liver injury. Differential hepatotoxicity to APAP overdose has been described in these two sub-strains (Bourdi *et al.*, 2011; Duan *et al.*, 2016). We hypothesized that, similar to APAP induced liver injury, 6N mice would have increased liver injury after acute CCl<sub>4</sub> exposure. We also hypothesized that due to 6N mice having increased injury, they would have a more robust wound healing response leading to fibrosis after chronic CCl<sub>4</sub> exposure.

We found that the 6N mice do in fact have increased injury, but this is not due to a difference in CCl<sub>4</sub> bioactivation by CYP2E1 *in vivo* or in hepatocyte sensitivity to CCl<sub>4</sub> *in vitro*. Increased injury results in increased wound healing response as has been shown previously and is likely contributing to the many differences we observed between 6N and 6J mice in acute liver injury (Mehendale, 2005). Following acute liver injury induced by CCl<sub>4</sub>, we observed increased inflammation, regeneration, and matrix synthesis in 6N mice compared to 6J mice. The increased inflammatory microenvironment observed in 6N mice is likely influencing the increased regeneration,

as has been shown previously (Strey *et al.*, 2003; Owumi *et al.*, 2014). Pro-inflammatory cytokines can activate HSC, so it is also likely that the increased inflammation in 6N mice is also contributing to the earlier HSC activation we observed (Imamura *et al.*, 2005).

In accordance with the increased liver injury and wound healing we observed in 6N mice compared to 6J mice after acute CCl<sub>4</sub> exposure, we hypothesized that 6N mice would have increased fibrosis following chronic CCl<sub>4</sub>. We did, in fact, see increased pro-fibrotic markers and ECM accumulation visualized by picrosirius red staining in 6N mice. We did not evaluate matrix remodeling in 6N and 6J mice after chronic CCl<sub>4</sub> exposure because there was no difference in matrix remodeling between sub-strains after acute CCl<sub>4</sub> exposure and because we observed increased fibrosis in 6N mice compared to 6J mice. However, future studies could explore matrix metabolism and fibrosis resolution between these sub-strains to gain additional mechanistic clarity into the ability of the liver to heal after chronic liver injury. Because matrix remodeling was not different between sub-strains after acute liver injury, we hypothesize that fibrosis in 6N mice would resolve at the same rate as that found in 6J mice, but that complete fibrosis resolution would take longer in 6N mice as they have more fibrosis to begin with.

Similar to observations in the acetaminophen overdose literature, the implications of our work are important for labs that utilize CCl<sub>4</sub> to induce acute and chronic liver injury in genetically modified mice and purchase wild-type control mice instead of using littermate controls. Because differences in injury and wound healing were discovered between 6J and 6N mice following both acute and chronic CCl<sub>4</sub> exposure, comparing the genetically modified mice used in this dissertation to the wrong sub-strain would

have led to data interpretation errors. For example, by graphing ALT activity of all four genotypes used in this dissertation, it is evident that we could have incorrectly interpreted the *Has3*<sup>-/-</sup> data; i.e. there is no difference in ALT activities between *Has3*<sup>-/-</sup> and 6N mice (incorrect sub-strain) but there is increased ALT activity when comparing *Has3*<sup>-/-</sup> and 6J mice (correct sub-strain) (Figure 7-4).

## **Conclusions**

By evaluating both hepatotoxicity and wound healing following acute CCl<sub>4</sub> exposure, as well as fibrosis following chronic CCl<sub>4</sub> exposure, we were able to discern differential responses in 6N and 6J mice. Following acute CCl<sub>4</sub> exposure, 6N mice have increased injury and subsequent wound healing compared to 6J mice and following chronic CCl<sub>4</sub> exposure, 6N mice have increased fibrosis compared to 6J mice. These sub-strain differences highlight the importance of using the correct sub-strain control when trying to correctly identify the impact HAS3 and HMMR deficiency has on hepatic wound healing and fibrosis after acute and chronic liver injury, respectively. Additionally, the NIH is currently stressing the importance of reproducibility and transparency in study design and reporting (Collins and Tabak, 2014). We believe that these studies show that it is important to report not only what strain of mouse the studies were completed in, but also what sub-strain, particularly if CCl<sub>4</sub> is being used to induce liver injury.

## **Future Directions**

In Chapter 6, we proposed a number of possible explanations for the increased injury we observed in 6N versus 6J mice. One possible mechanism we propose is the

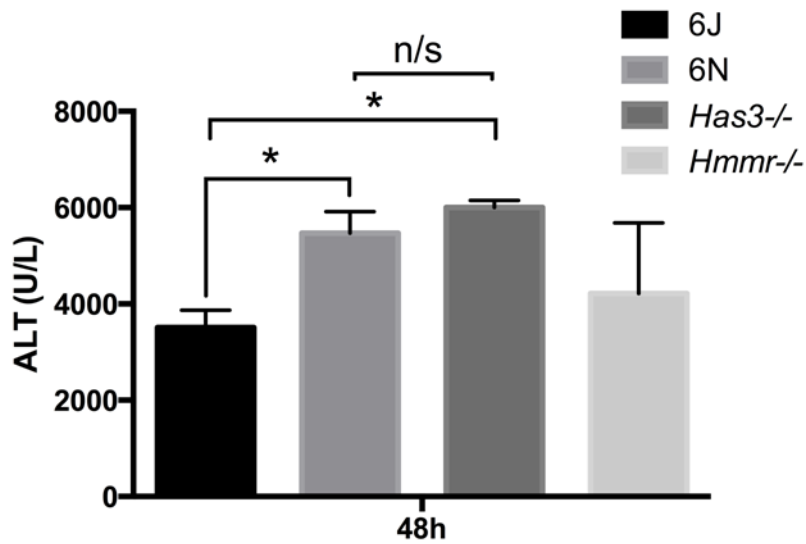


**Figure 7-4: ALT activity 48 hours after CCl<sub>4</sub> exposure in all four strains of mice used in this dissertation.**

Due to the observed differences in peak ALT levels between 6J and 6N mice, comparing the genetically modified mice to the wrong sub-strain would have led to interpretation error. This is evident in the significant difference between 6J mice and *Has3*<sup>-/-</sup> mice (correct control) and no significant (n/s) difference between 6N mice and *Has3*<sup>-/-</sup> mice (incorrect control).

idea of hormesis (Milisav *et al.*, 2012). 6J mice have a mutation in nucleotide nicotinamide (*Nnt*), which reduces antioxidant capacity within the mitochondria (Ronchi *et al.*, 2013). It is possible that over time, 6J mice have adapted to the constant reduction in antioxidant capacity and thus require higher stress to induce inflammation. We have shown that the two sub-strains have equivalent cell death *in vitro*, but it may be possible that the cell death is not sending the same signals; i.e. that 6N mice have increased pro-inflammatory signals, thus increasing the innate immune response and resulting in increased injury. It would be interesting to evaluate macrophage chemoattractant proteins (like CCL2) production in mice exposed to CCl<sub>4</sub>. If 6J mice have adapted to the lower antioxidant capacity, it is possible that the same amount of cell death will not trigger the same inflammatory response.

It is possible that the increase in wound healing response in 6N mice compared to 6J mice after acute CCl<sub>4</sub> exposure is entirely based upon the increased injury. It is known that following any form of liver injury, tissue repair follows a dose response; i.e. the more injury, the more robust the repair up to a threshold when the repair can no longer compensate for the increased injury (Mehendale, 2005). If we could determine an equitoxic dose of CCl<sub>4</sub> to administer in order to have the same amount of hepatic injury in both 6J and 6N mice, we could observe what effect this has on the wound healing response. If the sub-strains no longer have a differential response (for example regeneration does not start earlier in 6N mice than 6J mice), then the wound healing response is entirely dependent on the extent of liver injury.

We observed an increase in fibrosis in 6N mice compared to 6J mice after chronic CCl<sub>4</sub> exposure. We did not, however, evaluate matrix remodeling in these mice.

Because there was no difference in matrix remodeling in 6N mice after acute CCl<sub>4</sub> exposure, we hypothesize that there would be no difference in matrix remodeling in 6N mice compared to 6J mice after chronic CCl<sub>4</sub> exposure. This can be measured by *in situ* zymography to directly measure MMP activity, as was done in Chapters 3 - 6. Similar to what was described above, looking at a single time point after chronic CCl<sub>4</sub> has limitations, therefore to evaluate fibrosis resolution several time points after cessation of CCl<sub>4</sub> should be evaluated.

Lastly, we propose that HA and HMMR play a role in hepatic wound healing after both acute and chronic CCl<sub>4</sub> exposure. Because these two sub-strains have differential responses in both settings, it would be interesting to evaluate hepatic HA and HMMR levels. We hypothesize that 6N mice would have increased HA early, contributing to the increased inflammation we observe. However, because there is no difference in matrix remodeling, perhaps 6J mice reach 6N hepatic HA levels quickly, or hepatic HA is degraded more rapidly in 6N mice, and thus drive increased inflammation. Lastly, 6N mice have earlier regeneration, which again may be due to increased inflammation, but it may also be because 6N have increased intracellular HMMR expression. Evaluating HA and HMMR in these two sub-strains could provide more evidence of a role for the HA network in hepatic wound healing.

## **Chapter 8: References**

- Abdelmegeed, M.A., Moon, K.H., Chen, C., Gonzalez, F.J., Song, B.J., 2010. Role of cytochrome P450 2E1 in protein nitration and ubiquitin-mediated degradation during acetaminophen toxicity. *Biochem. Pharmacol.* **79**, 57-66.
- Abu-Wasel, B., Walsh, C., Keough, V., Molinari, M., 2013. Pathophysiology, epidemiology, classification and treatment options for polycystic liver diseases. *World J. Gastroenterol.* **19**, 5775-5786.
- Adhyatmika, A., Putri, K.S., Beljaars, L., Melgert, B.N., 2015. The Elusive Antifibrotic Macrophage. *Front Med (Lausanne)* **2**, 81.
- Albeiroti, S., Ayasoufi, K., Hill, D.R., Shen, B., de la Motte, C.A., 2015. Platelet hyaluronidase-2: an enzyme that translocates to the surface upon activation to function in extracellular matrix degradation. *Blood* **125**, 1460-1469.
- Alwayn, I.P., Verbese, J.E., Kim, S., Roy, R., Arsenault, D.A., Greene, A.K., Novak, K., Laforme, A., Lee, S., Moses, M.A., Puder, M., 2008. A critical role for matrix metalloproteinases in liver regeneration. *J. Surg. Res.* **145**, 192-198.
- Anderegg, U., Simon, J.C., Averbek, M., 2014. More than just a filler - the role of hyaluronan for skin homeostasis. *Exp. Dermatol.* **23**, 295-303.
- Apte, U., Gkretsi, V., Bowen, W.C., Mars, W.M., Luo, J.H., Donthamsetty, S., Orr, A., Monga, S.P., Wu, C., Michalopoulos, G.K., 2009. Enhanced liver regeneration following changes induced by hepatocyte-specific genetic ablation of integrin-linked kinase. *Hepatology* **50**, 844-851.
- Arkblad, E.L., Tuck, S., Pestov, N.B., Dmitriev, R.I., Kostina, M.B., Stenvall, J., Tranberg, M., Rydstrom, J., 2005. A *Caenorhabditis elegans* mutant lacking

- functional nicotinamide nucleotide transhydrogenase displays increased sensitivity to oxidative stress. *Free Radic. Biol. Med.* **38**, 1518-1525.
- Aruffo, A., Stamenkovic, I., Melnick, M., Underhill, C., Seed, B., 1990. CD44 is the principal cell surface receptor for hyaluronate. *Cell* **61**, 1303-1313.
- Assmann, V., Jenkinson, D., Marshall, J.F., Hart, I.R., 1999. The intracellular hyaluronan receptor RHAMM/IHABP interacts with microtubules and actin filaments. *J. Cell Sci.* **112 ( Pt 22)**, 3943-3954.
- Auvinen, P., Tammi, R., Kosma, V.M., Sironen, R., Soini, Y., Mannermaa, A., Tumelius, R., Uljas, E., Tammi, M., 2013. Increased hyaluronan content and stromal cell CD44 associate with HER2 positivity and poor prognosis in human breast cancer. *Int. J. Cancer* **132**, 531-539.
- Aziz-Seible, R.S., Lee, S.M., Kharbanda, K.K., McVicker, B.L., Casey, C.A., 2011. Ethanol feeding potentiates the pro-inflammatory response of Kupffer cells to cellular fibronectin. *Alcohol. Clin. Exp. Res.* **35**, 717-725.
- Baeck, C., Wehr, A., Karlmark, K.R., Heymann, F., Vucur, M., Gassler, N., Huss, S., Klussmann, S., Eulberg, D., Luedde, T., Trautwein, C., Tacke, F., 2012. Pharmacological inhibition of the chemokine CCL2 (MCP-1) diminishes liver macrophage infiltration and steatohepatitis in chronic hepatic injury. *Gut* **61**, 416-426.
- Bagli, D.J., Joyner, B.D., Mahoney, S.R., McCulloch, L., 1999. The hyaluronic acid receptor RHAMM is induced by stretch injury of rat bladder in vivo and influences smooth muscle cell contraction in vitro [corrected]. *J. Urol.* **162**, 832-840.

- Bai, K.J., Spicer, A.P., Mascarenhas, M.M., Yu, L., Ochoa, C.D., Garg, H.G., Quinn, D.A., 2005. The role of hyaluronan synthase 3 in ventilator-induced lung injury. *Am. J. Respir. Crit. Care Med.* **172**, 92-98.
- Bajt, M.L., Knight, T.R., Lemasters, J.J., Jaeschke, H., 2004. Acetaminophen-induced oxidant stress and cell injury in cultured mouse hepatocytes: protection by N-acetyl cysteine. *Toxicol. Sci.* **80**, 343-349.
- Balaji, S., Watson, C.L., Ranjan, R., King, A., Bollyky, P.L., Keswani, S.G., 2015. Chemokine Involvement in Fetal and Adult Wound Healing. *Adv Wound Care (New Rochelle)* **4**, 660-672.
- Balazs, E.A., Laurent, T.C., Jeanloz, R.W., 1986. Nomenclature of hyaluronic acid. *Biochem. J.* **235**, 903.
- Band, P.A., Heeter, J., Wisniewski, H.G., Liublinska, V., Pattanayak, C.W., Karia, R.J., Stabler, T., Balazs, E.A., Kraus, V.B., 2015. Hyaluronan molecular weight distribution is associated with the risk of knee osteoarthritis progression. *Osteoarthritis Cartilage* **23**, 70-76.
- Baranova, N.S., Nileback, E., Haller, F.M., Briggs, D.C., Svedhem, S., Day, A.J., Richter, R.P., 2011. The inflammation-associated protein TSG-6 cross-links hyaluronan via hyaluronan-induced TSG-6 oligomers. *J. Biol. Chem.* **286**, 25675-25686.
- Bart, G., Vico, N.O., Hassinen, A., Pujol, F.M., Deen, A.J., Ruusala, A., Tammi, R.H., Squire, A., Heldin, P., Kellokumpu, S., Tammi, M.I., 2015. Fluorescence resonance energy transfer (FRET) and proximity ligation assays reveal

- functionally relevant homo- and heteromeric complexes among hyaluronan synthases HAS1, HAS2, and HAS3. *J. Biol. Chem.* **290**, 11479-11490.
- Bastard, J.P., Maachi, M., Lagathu, C., Kim, M.J., Caron, M., Vidal, H., Capeau, J., Feve, B., 2006. Recent advances in the relationship between obesity, inflammation, and insulin resistance. *Eur. Cytokine Netw.* **17**, 4-12.
- Bataller, R., Brenner, D.A., 2005. Liver fibrosis. *J. Clin. Invest.* **115**, 209-218.
- Bayat, A., McGrouther, D.A., Ferguson, M.W., 2003. Skin scarring. *BMJ* **326**, 88-92.
- Bertola, A., Mathews, S., Ki, S.H., Wang, H., Gao, B., 2013. Mouse model of chronic and binge ethanol feeding (the NIAAA model). *Nat. Protoc.* **8**, 627-637.
- Bilbao, I., Armadans, L., Lazaro, J.L., Hidalgo, E., Castells, L., Margarit, C., 2003. Predictive factors for early mortality following liver transplantation. *Clin. Transplant.* **17**, 401-411.
- Bjermer, L., Lundgren, R., Hallgren, R., 1989. Hyaluronan and type III procollagen peptide concentrations in bronchoalveolar lavage fluid in idiopathic pulmonary fibrosis. *Thorax* **44**, 126-131.
- Bohm, F., Kohler, U.A., Speicher, T., Werner, S., 2010. Regulation of liver regeneration by growth factors and cytokines. *EMBO Mol. Med.* **2**, 294-305.
- Bollyky, P.L., Falk, B.A., Wu, R.P., Buckner, J.H., Wight, T.N., Nepom, G.T., 2009. Intact extracellular matrix and the maintenance of immune tolerance: high molecular weight hyaluronan promotes persistence of induced CD4+CD25+ regulatory T cells. *J. Leukoc. Biol.* **86**, 567-572.
- Bourdi, M., Davies, J.S., Pohl, L.R., 2011. Mispairing C57BL/6 substrains of genetically engineered mice and wild-type controls can lead to confounding results as it did

- in studies of JNK2 in acetaminophen and concanavalin A liver injury. *Chem. Res. Toxicol.* **24**, 794-796.
- Bourdi, M., Korrapati, M.C., Chakraborty, M., Yee, S.B., Pohl, L.R., 2008. Protective role of c-Jun N-terminal kinase 2 in acetaminophen-induced liver injury. *Biochem. Biophys. Res. Commun.* **374**, 6-10.
- Bousquet, J., Chanez, P., Lacoste, J.Y., Enander, I., Venge, P., Peterson, C., Ahlstedt, S., Michel, F.B., Godard, P., 1991. Indirect evidence of bronchial inflammation assessed by titration of inflammatory mediators in BAL fluid of patients with asthma. *J. Allergy Clin. Immunol.* **88**, 649-660.
- Camenisch, T.D., Spicer, A.P., Brehm-Gibson, T., Biesterfeldt, J., Augustine, M.L., Calabro, A., Jr., Kubalak, S., Klewer, S.E., McDonald, J.A., 2000. Disruption of hyaluronan synthase-2 abrogates normal cardiac morphogenesis and hyaluronan-mediated transformation of epithelium to mesenchyme. *J. Clin. Invest.* **106**, 349-360.
- Campo, G.M., Avenoso, A., Campo, S., Ferlazzo, A.M., Micali, C., Zanghì, L., Calatroni, A., 2004. Hyaluronic acid and chondroitin-4-sulphate treatment reduces damage in carbon tetrachloride-induced acute rat liver injury. *Life Sci.* **74**, 1289-1305.
- Campo, G.M., Avenoso, A., Nastasi, G., Micali, A., Prestipino, V., Vaccaro, M., D'Ascola, A., Calatroni, A., Campo, S., 2011. Hyaluronan reduces inflammation in experimental arthritis by modulating TLR-2 and TLR-4 cartilage expression. *Biochim. Biophys. Acta* **1812**, 1170-1181.
- Cardin, S., Scott-Boyer, M.P., Praktiknjo, S., Jeidane, S., Picard, S., Reudelhuber, T.L., Deschepper, C.F., 2014. Differences in cell-type-specific responses to

- angiotensin II explain cardiac remodeling differences in C57BL/6 mouse substrains. *Hypertension* **64**, 1040-1046.
- Chang, B., Xu, M.J., Zhou, Z., Cai, Y., Li, M., Wang, W., Feng, D., Bertola, A., Wang, H., Kunos, G., Gao, B., 2015a. Short- or long-term high-fat diet feeding plus acute ethanol binge synergistically induce acute liver injury in mice: an important role for CXCL1. *Hepatology* **62**, 1070-1085.
- Chang, W.J., Song, L.J., Yi, T., Shen, K.T., Wang, H.S., Gao, X.D., Li, M., Xu, J.M., Niu, W.X., Qin, X.Y., 2015b. Early activated hepatic stellate cell-derived molecules reverse acute hepatic injury. *World J. Gastroenterol.* **21**, 4184-4194.
- Charlton, M., 2004. Nonalcoholic fatty liver disease: a review of current understanding and future impact. *Clin. Gastroenterol. Hepatol.* **2**, 1048-1058.
- Chen, H., Mohan, P., Jiang, J., Nemirovsky, O., He, D., Fleisch, M.C., Niederacher, D., Pilarski, L.M., Lim, C.J., Maxwell, C.A., 2014. Spatial regulation of Aurora A activity during mitotic spindle assembly requires RHAMM to correctly localize TPX2. *Cell cycle* **13**, 2248-2261.
- Cheng, G., Swaidani, S., Sharma, M., Lauer, M.E., Hascall, V.C., Aronica, M.A., 2011. Hyaluronan deposition and correlation with inflammation in a murine ovalbumin model of asthma. *Matrix Biol.* **30**, 126-134.
- Chow, G., Knudson, C.B., Knudson, W., 2006. Expression and cellular localization of human hyaluronidase-2 in articular chondrocytes and cultured cell lines. *Osteoarthritis Cartilage* **14**, 849-858.

- Chung, L., Dinakarbandian, D., Yoshida, N., Lauer-Fields, J.L., Fields, G.B., Visse, R., Nagase, H., 2004. Collagenase unwinds triple-helical collagen prior to peptide bond hydrolysis. *EMBO J.* **23**, 3020-3030.
- Cienfuegos, J.A., Rotellar, F., Baixauli, J., Martinez-Regueira, F., Pardo, F., Hernandez-Lizoain, J.L., 2014. Liver regeneration--the best kept secret. A model of tissue injury response. *Rev. Esp. Enferm. Dig.* **106**, 171-194.
- Cohen-Naftaly, M., Friedman, S.L., 2011. Current status of novel antifibrotic therapies in patients with chronic liver disease. *Therap. Adv. Gastroenterol.* **4**, 391-417.
- Collins, F., Tabak, L., 2014. Policy: NIH plans to enhance reproducibility. *Nature* **505**, 612-613.
- Constandinou, C., Henderson, N., Iredale, J.P., 2005. Modeling liver fibrosis in rodents. *Methods Mol. Med.* **117**, 237-250.
- Cook, A.C., Chambers, A.F., Turley, E.A., Tuck, A.B., 2006. Osteopontin induction of hyaluronan synthase 2 expression promotes breast cancer malignancy. *J. Biol. Chem.* **281**, 24381-24389.
- Corey, K.E., Kaplan, L.M., 2014. Obesity and liver disease: the epidemic of the twenty-first century. *Clin. Liver Dis.* **18**, 1-18.
- Counts, J.L., Goodman, J.I., 1995. Principles underlying dose selection for, and extrapolation from, the carcinogen bioassay: dose influences mechanism. *Regul. Toxicol. Pharmacol.* **21**, 418-421.
- Cowman, M.K., Chen, C.C., Pandya, M., Yuan, H., Ramkishun, D., LoBello, J., Bhilocha, S., Russell-Puleri, S., Skendaj, E., Mijovic, J., Jing, W., 2011. Improved

- agarose gel electrophoresis method and molecular mass calculation for high molecular mass hyaluronan. *Anal. Biochem.* **417**, 50-56.
- Cowman, M.K., Lee, H.G., Schwertfeger, K.L., McCarthy, J.B., Turley, E.A., 2015. The Content and Size of Hyaluronan in Biological Fluids and Tissues. *Front. Immunol.* **6**, 261.
- Crespo Yanguas, S., Cogliati, B., Willebrords, J., Maes, M., Colle, I., van den Bossche, B., de Oliveira, C.P., Andraus, W., Alves, V.A., Leclercq, I., Vinken, M., 2016. Experimental models of liver fibrosis. *Arch. Toxicol.* **90**, 1025-1048.
- Csoka, A.B., Frost, G.I., Stern, R., 2001. The six hyaluronidase-like genes in the human and mouse genomes. *Matrix Biol.* **20**, 499-508.
- Csoka, A.B., Scherer, S.W., Stern, R., 1999. Expression analysis of six paralogous human hyaluronidase genes clustered on chromosomes 3p21 and 7q31. *Genomics* **60**, 356-361.
- Czaja, A.J., 2014. Hepatic inflammation and progressive liver fibrosis in chronic liver disease. *World J. Gastroenterol.* **20**, 2515-2532.
- Dalton, T.P., Chen, Y., Schneider, S.N., Nebert, D.W., Shertzer, H.G., 2004. Genetically altered mice to evaluate glutathione homeostasis in health and disease. *Free Radic. Biol. Med.* **37**, 1511-1526.
- Dambach, D.M., Watson, L.M., Gray, K.R., Durham, S.K., Laskin, D.L., 2002. Role of CCR2 in macrophage migration into the liver during acetaminophen-induced hepatotoxicity in the mouse. *Hepatology* **35**, 1093-1103.

- de la Motte, C.A., 2011. Hyaluronan in intestinal homeostasis and inflammation: implications for fibrosis. *Am. J. Physiol. Gastrointest. Liver Physiol.* **301**, G945-949.
- de la Motte, C.A., Hascall, V.C., Drazba, J., Bandyopadhyay, S.K., Strong, S.A., 2003. Mononuclear leukocytes bind to specific hyaluronan structures on colon mucosal smooth muscle cells treated with polyinosinic acid:polycytidylic acid: inter-alpha-trypsin inhibitor is crucial to structure and function. *Am. J. Pathol.* **163**, 121-133.
- Dechene, A., Sowa, J.P., Gieseler, R.K., Jochum, C., Bechmann, L.P., El Fouly, A., Schlattjan, M., Saner, F., Baba, H.A., Paul, A., Dries, V., Odenthal, M., Gerken, G., Friedman, S.L., Canbay, A., 2010. Acute liver failure is associated with elevated liver stiffness and hepatic stellate cell activation. *Hepatology* **52**, 1008-1016.
- Decleves, A.E., Caron, N., Nonclercq, D., Legrand, A., Toubeau, G., Kramp, R., Flamion, B., 2006. Dynamics of hyaluronan, CD44, and inflammatory cells in the rat kidney after ischemia/reperfusion injury. *Int. J. Mol. Med.* **18**, 83-94.
- Decleves, A.E., Caron, N., Voisin, V., Legrand, A., Bouby, N., Kultti, A., Tammi, M.I., Flamion, B., 2012. Synthesis and fragmentation of hyaluronan in renal ischaemia. *Nephrol. Dial. Transplant.* **27**, 3771-3781.
- DeLeve, L.D., 2013. Liver sinusoidal endothelial cells and liver regeneration. *J. Clin. Invest.* **123**, 1861-1866.
- DeLeve, L.D., 2015. Liver sinusoidal endothelial cells in hepatic fibrosis. *Hepatology* **61**, 1740-1746.

- Deshpande, K.T., Liu, S., McCracken, J.M., Jiang, L., Gaw, T.E., Kaydo, L.N., Richard, Z.C., O'Neil, M.F., Pritchard, M.T., 2016. Moderate (2%, v/v) Ethanol Feeding Alters Hepatic Wound Healing after Acute Carbon Tetrachloride Exposure in Mice. *Biomolecules* **6**.
- Dixon, L.J., Barnes, M., Tang, H., Pritchard, M.T., Nagy, L.E., 2013. Kupffer cells in the liver. *Comprehensive Physiology* **3**, 785-797.
- Dominguez, M., Miquel, R., Colmenero, J., Moreno, M., Garcia-Pagan, J.C., Bosch, J., Arroyo, V., Gines, P., Caballeria, J., Bataller, R., 2009. Hepatic expression of CXC chemokines predicts portal hypertension and survival in patients with alcoholic hepatitis. *Gastroenterology* **136**, 1639-1650.
- Duan, L., Davis, J.S., Woolbright, B.L., Du, K., Cahkraborty, M., Weemhoff, J., Jaeschke, H., Bourdi, M., 2016. Differential susceptibility to acetaminophen-induced liver injury in sub-strains of C57BL/6 mice: 6N versus 6J. *Food Chem. Toxicol.* **98**, 107-118.
- Duarte, S., Baber, J., Fujii, T., Coito, A.J., 2015. Matrix metalloproteinases in liver injury, repair and fibrosis. *Matrix Biol.* **44-46**, 147-156.
- Duffield, J.S., Forbes, S.J., Constandinou, C.M., Clay, S., Partolina, M., Vuthoori, S., Wu, S., Lang, R., Iredale, J.P., 2005. Selective depletion of macrophages reveals distinct, opposing roles during liver injury and repair. *J. Clin. Invest.* **115**, 56-65.
- Edwards, M.J., Keller, B.J., Kauffman, F.C., Thurman, R.G., 1993. The involvement of Kupffer cells in carbon tetrachloride toxicity. *Toxicol. Appl. Pharmacol.* **119**, 275-279.

- El Taghdouini, A., Najimi, M., Sancho-Bru, P., Sokal, E., van Grunsven, L.A., 2015. In vitro reversion of activated primary human hepatic stellate cells. *Fibrogenesis Tissue Repair* **8**, 14.
- Engstrom-Laurent, A., Loof, L., Nyberg, A., Schroder, T., 1985. Increased serum levels of hyaluronate in liver disease. *Hepatology* **5**, 638-642.
- Esguerra, K.V., Tolg, C., Akentieva, N., Price, M., Cho, C.F., Lewis, J.D., McCarthy, J.B., Turley, E.A., Luyt, L.G., 2015. Identification, design and synthesis of tubulin-derived peptides as novel hyaluronan mimetic ligands for the receptor for hyaluronan-mediated motility (RHAMM/HMMR). *Integr. Biol. (Camb.)* **7**, 1547-1560.
- Fallowfield, J.A., Mizuno, M., Kendall, T.J., Constandinou, C.M., Benyon, R.C., Duffield, J.S., Iredale, J.P., 2007a. Scar-associated macrophages are a major source of hepatic matrix metalloproteinase-13 and facilitate the resolution of murine hepatic fibrosis. *J. Immunol.* **178**, 5288-5295.
- Fallowfield, J.A., Mizuno, M., Kendall, T.J., Constandinou, C.M., Benyon, R.C., Duffield, J.S., Iredale, J.P., 2007b. Scar-Associated Macrophages Are a Major Source of Hepatic Matrix Metalloproteinase-13 and Facilitate the Resolution of Murine Hepatic Fibrosis. *The Journal of Immunology* **178**, 5288-5295.
- Faroon, O., Taylor, J., Roney, N., Fransen, M.E., Bogaczyk, S., Diamon, G., 2003. Toxicological Profile for Caron Tetrachloride. Center for Disease Control, pp.
- Fieber, C., Baumann, P., Vallon, R., Termeer, C., Simon, J.C., Hofmann, M., Angel, P., Herrlich, P., Sleeman, J.P., 2004. Hyaluronan-oligosaccharide-induced transcription of metalloproteases. *J. Cell Sci.* **117**, 359-367.

- Foley, J.P., Lam, D., Jiang, H., Liao, J., Cheong, N., McDevitt, T.M., Zaman, A., Wright, J.R., Savani, R.C., 2012. Toll-like receptor 2 (TLR2), transforming growth factor-beta, hyaluronan (HA), and receptor for HA-mediated motility (RHAMM) are required for surfactant protein A-stimulated macrophage chemotaxis. *J. Biol. Chem.* **287**, 37406-37419.
- Foxman, E.F., Campbell, J.J., Butcher, E.C., 1997. Multistep navigation and the combinatorial control of leukocyte chemotaxis. *J. Cell Biol.* **139**, 1349-1360.
- Fraser, J.R., Laurent, T.C., Laurent, U.B., 1997. Hyaluronan: its nature, distribution, functions and turnover. *J. Intern. Med.* **242**, 27-33.
- Freeman, H., Shimomura, K., Cox, R.D., Ashcroft, F.M., 2006a. Nicotinamide nucleotide transhydrogenase: a link between insulin secretion, glucose metabolism and oxidative stress. *Biochem. Soc. Trans.* **34**, 806-810.
- Freeman, H.C., Hugill, A., Dear, N.T., Ashcroft, F.M., Cox, R.D., 2006b. Deletion of nicotinamide nucleotide transhydrogenase: a new quantitative trait locus accounting for glucose intolerance in C57BL/6J mice. *Diabetes* **55**, 2153-2156.
- Friedman, S.L., 2000. Molecular regulation of hepatic fibrosis, an integrated cellular response to tissue injury. *J. Biol. Chem.* **275**, 2247-2250.
- Friedman, S.L., 2008a. Hepatic stellate cells: protean, multifunctional, and enigmatic cells of the liver. *Physiol. Rev.* **88**, 125-172.
- Friedman, S.L., 2008b. Mechanisms of hepatic fibrogenesis. *Gastroenterology* **134**, 1655-1669.

- Gao, Y., Foster, R., Yang, X., Feng, Y., Shen, J.K., Mankin, H.J., Hornicek, F.J., Amiji, M.M., Duan, Z., 2015. Up-regulation of CD44 in the development of metastasis, recurrence and drug resistance of ovarian cancer. *Oncotarget* **6**, 9313-9326.
- Garbuzenko, D.V., 2015. Contemporary concepts of the medical therapy of portal hypertension under liver cirrhosis. *World J. Gastroenterol.* **21**, 6117-6126.
- Gogel, B.M., Goldstein, R.M., Kuhn, J.A., McCarty, T.M., Donahoe, A., Glastad, K., 2000. Diagnostic evaluation of hepatocellular carcinoma in a cirrhotic liver. *Oncology (Williston Park)* **14**, 15-20.
- Gressner, A.M., Bachem, M.G., 1990. Cellular sources of noncollagenous matrix proteins: role of fat-storing cells in fibrogenesis. *Semin. Liver Dis.* **10**, 30-46.
- Grisham, J.W., 1962. A morphologic study of deoxyribonucleic acid synthesis and cell proliferation in regenerating rat liver; autoradiography with thymidine-H3. *Cancer Res.* **22**, 842-849.
- Gudowska, M., Gruszewska, E., Panasiuk, A., Cylwik, B., Flisiak, R., Swiderska, M., Szmitekowski, M., Chrostek, L., 2016. Hyaluronic acid concentration in liver diseases. *Clin. Exp. Med.* **16**, 523-528.
- Guidolin, D., Franceschi, F., 2014. Viscosupplementation with high molecular weight native hyaluronan. Focus on a 1500-2000 KDa fraction (Hyalubrix(R)). *Eur. Rev. Med. Pharmacol. Sci.* **18**, 3326-3338.
- Gujral, J.S., Knight, T.R., Farhood, A., Bajt, M.L., Jaeschke, H., 2002. Mode of cell death after acetaminophen overdose in mice: apoptosis or oncotic necrosis? *Toxicol. Sci.* **67**, 322-328.

- Gunawan, B.K., Liu, Z.X., Han, D., Hanawa, N., Gaarde, W.A., Kaplowitz, N., 2006. c-Jun N-terminal kinase plays a major role in murine acetaminophen hepatotoxicity. *Gastroenterology* **131**, 165-178.
- Guo, J., Friedman, S.L., 2007. Hepatic fibrogenesis. *Semin. Liver Dis.* **27**, 413-426.
- Gurtner, G.C., Werner, S., Barrandon, Y., Longaker, M.T., 2008. Wound repair and regeneration. *Nature* **453**, 314-321.
- Gushulak, L., Hemming, R., Martin, D., Seyrantepe, V., Pshezhetsky, A., Triggs-Raine, B., 2012. Hyaluronidase 1 and beta-hexosaminidase have redundant functions in hyaluronan and chondroitin sulfate degradation. *J. Biol. Chem.* **287**, 16689-16697.
- Ha, U.S., Koh, J.S., Cho, K.J., Yoon, B.I., Lee, K.W., Hong, S.H., Lee, J.Y., 2016. Hyaluronic acid-carboxymethylcellulose reduced postoperative bowel adhesions following laparoscopic urologic pelvic surgery: a prospective, randomized, controlled, single-blind study. *BMC Urol.* **16**, 28.
- Han, N.K., Shin, D.H., Kim, J.S., Weon, K.Y., Jang, C.Y., Kim, J.S., 2016. Hyaluronan-conjugated liposomes encapsulating gemcitabine for breast cancer stem cells. *Int J Nanomedicine* **11**, 1413-1425.
- Hardingham, T.E., Fosang, A.J., 1992. Proteoglycans: many forms and many functions. *FASEB J.* **6**, 861-870.
- Hardwick, C., Hoare, K., Owens, R., Hohn, H.P., Hook, M., Moore, D., Cripps, V., Austen, L., Nance, D.M., Turley, E., 1992. Molecular Cloning of a Novel Hyaluronan Receptor that Mediates Tumor Cell Motility. *J. Cell Biol.* **117**, 1343-1350.

- Harris, E.N., Kyosseva, S.V., Weigel, J.A., Weigel, P.H., 2007. Expression, processing, and glycosaminoglycan binding activity of the recombinant human 315-kDa hyaluronic acid receptor for endocytosis (HARE). *J. Biol. Chem.* **282**, 2785-2797.
- Hasegawa, K., Yoneda, M., Kuwabara, H., Miyaishi, O., Itano, N., Ohno, A., Zako, M., Isogai, Z., 2007. Versican, a major hyaluronan-binding component in the dermis, loses its hyaluronan-binding ability in solar elastosis. *J. Invest. Dermatol.* **127**, 1657-1663.
- Hatano, H., Shigeishi, H., Kudo, Y., Higashikawa, K., Tobiume, K., Takata, T., Kamata, N., 2012. Overexpression of receptor for hyaluronan-mediated motility (RHAMM) in MC3T3-E1 cells induces proliferation and differentiation through phosphorylation of ERK1/2. *J. Bone Miner. Metab.* **30**, 293-303.
- He, Y., Jin, L., Wang, J., Yan, Z., Chen, T., Zhao, Y., 2015. Mechanisms of fibrosis in acute liver failure. *Liver international : official journal of the International Association for the Study of the Liver* **35**, 1877-1885.
- Heit, B., Tavener, S., Raharjo, E., Kubes, P., 2002. An intracellular signaling hierarchy determines direction of migration in opposing chemotactic gradients. *J. Cell Biol.* **159**, 91-102.
- Hemann, S., Graf, J., Roderfeld, M., Roeb, E., 2007. Expression of MMPs and TIMPs in liver fibrosis - a systematic review with special emphasis on anti-fibrotic strategies. *J. Hepatol.* **46**, 955-975.
- Herrnberger, L., Hennig, R., Kremer, W., Hellerbrand, C., Goepferich, A., Kalbitzer, H.R., Tamm, E.R., 2014. Formation of fenestrae in murine liver sinusoids

- depends on plasmalemma vesicle-associated protein and is required for lipoprotein passage. PLoS One **9**, e115005.
- Hoek, J.B., Rydstrom, J., 1988. Physiological roles of nicotinamide nucleotide transhydrogenase. Biochem. J. **254**, 1-10.
- Hofmann, A.F., 1999. The continuing importance of bile acids in liver and intestinal disease. Arch. Intern. Med. **159**, 2647-2658.
- Hogaboam, C.M., Bone-Larson, C.L., Steinhauer, M.L., Lukacs, N.W., Colletti, L.M., Simpson, K.J., Strieter, R.M., Kunkel, S.L., 1999. Novel CXCR2-dependent liver regenerative qualities of ELR-containing CXC chemokines. FASEB J. **13**, 1565-1574.
- Horton, M.R., McKee, C.M., Bao, C., Liao, F., Farber, J.M., Hodge-DuFour, J., Pure, E., Oliver, B.L., Wright, T.M., Noble, P.W., 1998. Hyaluronan fragments synergize with interferon-gamma to induce the C-X-C chemokines mig and interferon-inducible protein-10 in mouse macrophages. J. Biol. Chem. **273**, 35088-35094.
- Hu, J., Srivastava, K., Wieland, M., Runge, A., Mogler, C., Besemfelder, E., Terhardt, D., Vogel, M.J., Cao, L., Korn, C., Bartels, S., Thomas, M., Augustin, H.G., 2014. Endothelial cell-derived angiopoietin-2 controls liver regeneration as a spatiotemporal rheostat. Science **343**, 416-419.
- Huang, H., Tohme, S., Al-Khafaji, A.B., Tai, S., Loughran, P., Chen, L., Wang, S., Kim, J., Billiar, T., Wang, Y., Tsung, A., 2015. Damage-associated molecular pattern-activated neutrophil extracellular trap exacerbates sterile inflammatory liver injury. Hepatology **62**, 600-614.

- Huang, T.T., Naeemuddin, M., Elchuri, S., Yamaguchi, M., Kozy, H.M., Carlson, E.J., Epstein, C.J., 2006. Genetic modifiers of the phenotype of mice deficient in mitochondrial superoxide dismutase. *Hum. Mol. Genet.* **15**, 1187-1194.
- Huh, C.G., Factor, V.M., Sanchez, A., Uchida, K., Conner, E.A., Thorgeirsson, S.S., 2004. Hepatocyte growth factor/c-met signaling pathway is required for efficient liver regeneration and repair. *Proc. Natl. Acad. Sci. U. S. A.* **101**, 4477-4482.
- Hwang, J.H., Kim, Y.H., Noh, J.R., Gang, G.T., Kim, K.S., Chung, H.K., Tadi, S., Yim, Y.H., Shong, M., Lee, C.H., 2015. The protective role of NAD(P)H:quinone oxidoreductase 1 on acetaminophen-induced liver injury is associated with prevention of adenosine triphosphate depletion and improvement of mitochondrial dysfunction. *Arch. Toxicol.* **89**, 2159-2166.
- Ikarashi, M., Nakashima, H., Kinoshita, M., Sato, A., Nakashima, M., Miyazaki, H., Nishiyama, K., Yamamoto, J., Seki, S., 2013. Distinct development and functions of resident and recruited liver Kupffer cells/macrophages. *J. Leukoc. Biol.* **94**, 1325-1336.
- Ikenaga, N., Peng, Z.W., Vaid, K.A., Liu, S.B., Yoshida, S., Sverdlov, D.Y., Mikels-Vigdal, A., Smith, V., Schuppan, D., Popov, Y.V., 2017. Selective targeting of lysyl oxidase-like 2 (LOXL2) suppresses hepatic fibrosis progression and accelerates its reversal. *Gut*.
- Imamura, M., Ogawa, T., Sasaguri, Y., Chayama, K., Ueno, H., 2005. Suppression of macrophage infiltration inhibits activation of hepatic stellate cells and liver fibrogenesis in rats. *Gastroenterology* **128**, 138-146.

- Ip, S.P., Ko, K.M., 1996. The crucial antioxidant action of schisandrin B in protecting against carbon tetrachloride hepatotoxicity in mice: a comparative study with butylated hydroxytoluene. *Biochem. Pharmacol.* **52**, 1687-1693.
- Issa, R., Williams, E., Trim, N., Kendall, T., Arthur, M.J., Reichen, J., Benyon, R.C., Iredale, J.P., 2001. Apoptosis of hepatic stellate cells: involvement in resolution of biliary fibrosis and regulation by soluble growth factors. *Gut* **48**, 548-557.
- Itano, N., Sawai, T., Yoshida, M., Lenas, P., Yamada, Y., Imagawa, M., Shinomura, T., Hamaguchi, M., Yoshida, Y., Ohnuki, Y., Miyauchi, S., Spicer, A.P., McDonald, J.A., Kimata, K., 1999. Three Isoforms of Mammalian Hyaluronan Synthases Have Distinct Enzymatic Properties. *J. Biol. Chem.* **274**, 25085-25092.
- Jacobson, A., Brinck, J., Briskin, M.J., Spicer, A.P., Heldin, P., 2000. Expression of human hyaluronan synthases in response to external stimuli. *Biochem. J.* **348 Pt 1**, 29-35.
- Jaeschke, H., 2003. Molecular mechanisms of hepatic ischemia-reperfusion injury and preconditioning. *Am. J. Physiol. Gastrointest. Liver Physiol.* **284**, G15-26.
- Jaeschke, H., 2015. Acetaminophen: Dose-Dependent Drug Hepatotoxicity and Acute Liver Failure in Patients. *Dig. Dis.* **33**, 464-471.
- Jiang, D., Liang, J., Fan, J., Yu, S., Chen, S., Luo, Y., Prestwich, G.D., Mascarenhas, M.M., Garg, H.G., Quinn, D.A., Homer, R.J., Goldstein, D.R., Bucala, R., Lee, P.J., Medzhitov, R., Noble, P.W., 2005. Regulation of lung injury and repair by Toll-like receptors and hyaluronan. *Nat. Med.* **11**, 1173-1179.
- Jiang, D., Liang, J., Noble, P.W., 2007. Hyaluronan in tissue injury and repair. *Annu. Rev. Cell Dev. Biol.* **23**, 435-461.

- Jiang, D., Liang, J., Noble, P.W., 2011. Hyaluronan as an immune regulator in human diseases. *Physiol. Rev.* **91**, 221-264.
- Jiang, J., Casalegno-Garduno, R., Chen, H., Schmitt, A., Schmitt, M., Maxwell, C.A., 2010. Multifunctional proteins bridge mitosis with motility and cancer with inflammation and arthritis. *TheScientificWorldJournal* **10**, 1244-1257.
- Jiao, J., Sastre, D., Fiel, M.I., Lee, U.E., Ghiassi-Nejad, Z., Ginhoux, F., Vivier, E., Friedman, S.L., Merad, M., Aloman, C., 2012. Dendritic cell regulation of carbon tetrachloride-induced murine liver fibrosis regression. *Hepatology* **55**, 244-255.
- Jin, H., Lian, N., Zhang, F., Chen, L., Chen, Q., Lu, C., Bian, M., Shao, J., Wu, L., Zheng, S., 2016. Activation of PPARgamma/P53 signaling is required for curcumin to induce hepatic stellate cell senescence. *Cell Death Dis.* **7**, e2189.
- Jin, J., Hong, I.H., Lewis, K., Iakova, P., Breaux, M., Jiang, Y., Sullivan, E., Jawanmardi, N., Timchenko, L., Timchenko, N.A., 2015. Cooperation of C/EBP family proteins and chromatin remodeling proteins is essential for termination of liver regeneration. *Hepatology* **61**, 315-325.
- Jonker, A.M., Dijkhuis, F.W., Boes, A., Hardonk, M.J., Grond, J., 1992. Immunohistochemical study of extracellular matrix in acute galactosamine hepatitis in rats. *Hepatology* **15**, 423-431.
- Joron, G.E., Hollenburg, C.H., Bensley, E.H., 1957. Carbon Tetrachloride-An Underrated Hazard. *The Canadian Medical Association Journal* **76**.
- Kakizaki, I., Kojima, K., Takagaki, K., Endo, M., Kannagi, R., Ito, M., Maruo, Y., Sato, H., Yasuda, T., Mita, S., Kimata, K., Itano, N., 2004. A novel mechanism for the

- inhibition of hyaluronan biosynthesis by 4-methylumbelliferone. *J. Biol. Chem.* **279**, 33281-33289.
- Kessler, S., Rho, H., West, G., Fiocchi, C., Drazba, J., de la Motte, C., 2008. Hyaluronan (HA) deposition precedes and promotes leukocyte recruitment in intestinal inflammation. *Clin. Transl. Sci.* **1**, 57-61.
- Kessler, S.P., Obery, D.R., de la Motte, C., 2015. Hyaluronan Synthase 3 Null Mice Exhibit Decreased Intestinal Inflammation and Tissue Damage in the DSS-Induced Colitis Model. *Int. J. Cell Biol.* **2015**, 745237.
- Kim, Y., Kumar, S., 2014. CD44-mediated adhesion to hyaluronic acid contributes to mechanosensing and invasive motility. *Mol. Cancer Res.* **12**, 1416-1429.
- Kinoshita, M., Uchida, T., Sato, A., Nakashima, M., Nakashima, H., Shono, S., Habu, Y., Miyazaki, H., Hiroi, S., Seki, S., 2010. Characterization of two F4/80-positive Kupffer cell subsets by their function and phenotype in mice. *J. Hepatol.* **53**, 903-910.
- Kiso, K., Ueno, S., Fukuda, M., Ichi, I., Kobayashi, K., Sakai, T., Fukui, K., Kojo, S., 2012. The role of Kupffer cells in carbon tetrachloride intoxication in mice. *Biol. Pharm. Bull.* **35**, 980-983.
- Knockaert, L., Berson, A., Ribault, C., Prost, P.E., Fautrel, A., Pajaud, J., Lepage, S., Lucas-Clerc, C., Begue, J.M., Fromenty, B., Robin, M.A., 2012. Carbon tetrachloride-mediated lipid peroxidation induces early mitochondrial alterations in mouse liver. *Lab. Invest.* **92**, 396-410.

- Knudson, W., Aguiar, D.J., Hua, Q., Knudson, C.B., 1996. CD44-anchored hyaluronan-rich pericellular matrices: an ultrastructural and biochemical analysis. *Exp. Cell Res.* **228**, 216-228.
- Knudson, W., Chow, G., Knudson, C.B., 2002. CD44-mediated uptake and degradation of hyaluronan. *Matrix Biol.* **21**, 15-23.
- Kobayashi, N., Miyoshi, S., Mikami, T., Koyama, H., Kitazawa, M., Takeoka, M., Sano, K., Amano, J., Isogai, Z., Niida, S., Oguri, K., Okayama, M., McDonald, J.A., Kimata, K., Taniguchi, S., Itano, N., 2010. Hyaluronan deficiency in tumor stroma impairs macrophage trafficking and tumor neovascularization. *Cancer Res.* **70**, 7073-7083.
- Kochanek, K.D., Murphy, S.L., Xu, J., Tejada-Vera, B., 2016. Deaths: Final Data for 2014. *Natl. Vital Stat. Rep.* **65**, 122.
- Kosinska, M.K., Ludwig, T.E., Liebisch, G., Zhang, R., Siebert, H.C., Wilhelm, J., Kaesser, U., Dettmeyer, R.B., Klein, H., Ishaque, B., Rickert, M., Schmitz, G., Schmidt, T.A., Steinmeyer, J., 2015. Articular Joint Lubricants during Osteoarthritis and Rheumatoid Arthritis Display Altered Levels and Molecular Species. *PLoS One* **10**, e0125192.
- Kuipers, H.F., Nagy, N., Ruppert, S.M., Sunkari, V.G., Marshall, P.L., Gebe, J.A., Ishak, H.D., Keswani, S.G., Bollyky, J., Frymoyer, A.R., Wight, T.N., Steinman, L., Bollyky, P.L., 2016. The pharmacokinetics and dosing of oral 4-methylumbelliferone for inhibition of hyaluronan synthesis in mice. *Clin. Exp. Immunol.* **185**, 372-381.

- Kultti, A., Pasonen-Seppanen, S., Jauhiainen, M., Rilla, K.J., Karna, R., Pyoria, E., Tammi, R.H., Tammi, M.I., 2009. 4-Methylumbelliferone inhibits hyaluronan synthesis by depletion of cellular UDP-glucuronic acid and downregulation of hyaluronan synthase 2 and 3. *Exp. Cell Res.* **315**, 1914-1923.
- Kupiec-Weglinski, J.W., Busuttil, R.W., 2005. Ischemia and reperfusion injury in liver transplantation. *Transplant. Proc.* **37**, 1653-1656.
- Kusayama, Y., Akamatsu, Y., Kumagai, K., Kobayashi, H., Aratake, M., Saito, T., 2014. Changes in synovial fluid biomarkers and clinical efficacy of intra-articular injections of hyaluronic acid for patients with knee osteoarthritis. *Journal of experimental orthopaedics* **1**, 16.
- Kuwabara, H., Yoneda, M., Nagai, M., Nishio, H., Tasaka, T., Suzuki, K., Mori, H., 2003. High levels of hyaluronan production by a malignant lymphoma cell line with primary effusion lymphoma immunophenotype OHK. *Br. J. Haematol.* **120**, 1055-1057.
- Lauer, M.E., Cheng, G., Swaidani, S., Aronica, M.A., Weigel, P.H., Hascall, V.C., 2013. Tumor necrosis factor-stimulated gene-6 (TSG-6) amplifies hyaluronan synthesis by airway smooth muscle cells. *J. Biol. Chem.* **288**, 423-431.
- Laurent, T.C., Fraser, J.R., 1992. Hyaluronan. *FASEB J.* **6**, 2397-2404.
- LeBaron, R.G., Zimmermann, D.R., Ruoslahti, E., 1992. Hyaluronate binding properties of versican. *J. Biol. Chem.* **267**, 10003-10010.
- Lee, C.K., Perez-Atayde, A.R., Mitchell, P.D., Raza, R., Afdhal, N.H., Jonas, M.M., 2013. Serum biomarkers and transient elastography as predictors of advanced

- liver fibrosis in a United States cohort: the Boston children's hospital experience. *J. Pediatr.* **163**, 1058-1064 e1052.
- Lee, H.H., Seo, Y.S., Um, S.H., Won, N.H., Yoo, H., Jung, E.S., Kwon, Y.D., Park, S., Keum, B., Kim, Y.S., Yim, H.J., Jeon, Y.T., Chun, H.J., Kim, C.D., Ryu, H.S., 2010. Usefulness of non-invasive markers for predicting significant fibrosis in patients with chronic liver disease. *J. Korean Med. Sci.* **25**, 67-74.
- Lee, S.S., Buters, J.T., Pineau, T., Fernandez-Salguero, P., Gonzalez, F.J., 1996. Role of CYP2E1 in the hepatotoxicity of acetaminophen. *J. Biol. Chem.* **271**, 12063-12067.
- Leeman, M.F., McKay, J.A., Murray, G.I., 2002. Matrix metalloproteinase 13 activity is associated with poor prognosis in colorectal cancer. *J. Clin. Pathol.* **55**, 758-762.
- Leise, M.D., Poterucha, J.J., Talwalkar, J.A., 2014. Drug-induced liver injury. *Mayo Clin. Proc.* **89**, 95-106.
- Leung, A., Crombleholme, T.M., Keswani, S.G., 2012. Fetal wound healing: implications for minimal scar formation. *Curr. Opin. Pediatr.* **24**, 371-378.
- Li, J., Li, R.J., Lv, G.Y., Liu, H.Q., 2015. The mechanisms and strategies to protect from hepatic ischemia-reperfusion injury. *Eur. Rev. Med. Pharmacol. Sci.* **19**, 2036-2047.
- Liang, J., Jiang, D., Jung, Y., Xie, T., Ingram, J., Church, T., Degan, S., Leonard, M., Kraft, M., Noble, P.W., 2011. Role of hyaluronan and hyaluronan-binding proteins in human asthma. *J. Allergy Clin. Immunol.* **128**, 403-411 e403.

- Limaye, P.B., Bowen, W.C., Orr, A., Apte, U.M., Michalopoulos, G.K., 2010. Expression of hepatocytic- and biliary-specific transcription factors in regenerating bile ducts during hepatocyte-to-biliary epithelial cell transdifferentiation. *Comp Hepatol* **9**, 9.
- Lindsey, M., Wedin, K., Brown, M.D., Keller, C., Evans, A.J., Smolen, J., Burns, A.R., Rossen, R.D., Michael, L., Entman, M., 2001. Matrix-dependent mechanism of neutrophil-mediated release and activation of matrix metalloproteinase 9 in myocardial ischemia/reperfusion. *Circulation* **103**, 2181-2187.
- Liu, K., Wang, Z.Q., Wang, S.J., Liu, P., Qin, Y.H., Ma, Y., Li, X.C., Huo, Z.J., 2015. Hyaluronic acid-tagged silica nanoparticles in colon cancer therapy: therapeutic efficacy evaluation. *Int J Nanomedicine* **10**, 6445-6454.
- Liu, Y., Wen, X.M., Lui, E.L., Friedman, S.L., Cui, W., Ho, N.P., Li, L., Ye, T., Fan, S.T., Zhang, H., 2009. Therapeutic targeting of the PDGF and TGF-beta-signaling pathways in hepatic stellate cells by PTK787/ZK22258. *Lab. Invest.* **89**, 1152-1160.
- Llovet, J.M., Burroughs, A., Bruix, J., 2003. Hepatocellular carcinoma. *Lancet* **362**, 1907-1917.
- Lokeshwar, V.B., Obek, C., Pham, H.T., Wei, D., Young, M.J., Duncan, R.C., Soloway, M.S., Block, N.L., 2000. Urinary hyaluronic acid and hyaluronidase: markers for bladder cancer detection and evaluation of grade. *J. Urol.* **163**, 348-356.
- Longaker, M.T., Chiu, E.S., Adzick, N.S., Stern, M., Harrison, M.R., Stern, R., 1991. Studies in fetal wound healing. V. A prolonged presence of hyaluronic acid characterizes fetal wound fluid. *Ann. Surg.* **213**, 292-296.

- Lovvorn, H.N., 3rd, Cass, D.L., Sylvester, K.G., Yang, E.Y., Crombleholme, T.M., Adzick, N.S., Savani, R.C., 1998. Hyaluronan receptor expression increases in fetal excisional skin wounds and correlates with fibroplasia. *J. Pediatr. Surg.* **33**, 1062-1069; discussion 1069-1070.
- Lu, B., Rutledge, B.J., Gu, L., Fiorillo, J., Lukacs, N.W., Kunkel, S.L., North, R., Gerard, C., Rollins, B.J., 1998. Abnormalities in monocyte recruitment and cytokine expression in monocyte chemoattractant protein 1-deficient mice. *J. Exp. Med.* **187**, 601-608.
- Lu, Y., Zhuge, J., Wang, X., Bai, J., Cederbaum, A.I., 2008. Cytochrome P450 2E1 contributes to ethanol-induced fatty liver in mice. *Hepatology* **47**, 1483-1494.
- Mack, J.A., Feldman, R.J., Itano, N., Kimata, K., Lauer, M., Hascall, V.C., Maytin, E.V., 2012. Enhanced inflammation and accelerated wound closure following tetraphorbol ester application or full-thickness wounding in mice lacking hyaluronan synthases Has1 and Has3. *J. Invest. Dermatol.* **132**, 198-207.
- Malhi, H., Guicciardi, M.E., Gores, G.J., 2010. Hepatocyte death: a clear and present danger. *Physiol. Rev.* **90**, 1165-1194.
- Manasa, M., Sridevi, V., Chandana Lakshmi, M.V.V., Dedeepy, J., 2012. A Review on Hyaluronic Acid. *International Journal of Research in Chemistry and Environment* **2**, 5.
- Mao, S.A., Glorioso, J.M., Nyberg, S.L., 2014. Liver regeneration. *Transl. Res.* **163**, 352-362.
- Marangoni, A., Accardo, S., Aldini, R., Guardigli, M., Cavrini, F., Sambri, V., Montagnani, M., Roda, A., Cevenini, R., 2006. Production of reactive oxygen

- species and expression of inducible nitric oxide synthase in rat isolated Kupffer cells stimulated by *Leptospira interrogans* and *Borrelia burgdorferi*. *World J. Gastroenterol.* **12**, 3077-3081.
- Marhaba, R., Zoller, M., 2004. CD44 in cancer progression: adhesion, migration and growth regulation. *J Mol Histol* **35**, 211-231.
- Martin, J., Midgley, A., Meran, S., Woods, E., Bowen, T., Phillips, A.O., Steadman, R., 2016. Tumor Necrosis Factor-stimulated Gene 6 (TSG-6)-mediated Interactions with the Inter-alpha-inhibitor Heavy Chain 5 Facilitate Tumor Growth Factor beta1 (TGFbeta1)-dependent Fibroblast to Myofibroblast Differentiation. *J. Biol. Chem.* **291**, 13789-13801.
- Martin-Murphy, B.V., Holt, M.P., Ju, C., 2010. The role of damage associated molecular pattern molecules in acetaminophen-induced liver injury in mice. *Toxicol. Lett.* **192**, 387-394.
- Matsumoto, K., Li, Y., Jakuba, C., Sugiyama, Y., Sayo, T., Okuno, M., Dealy, C.N., Toole, B.P., Takeda, J., Yamaguchi, Y., Kosher, R.A., 2009. Conditional inactivation of Has2 reveals a crucial role for hyaluronan in skeletal growth, patterning, chondrocyte maturation and joint formation in the developing limb. *Development* **136**, 2825-2835.
- Maxwell, C.A., Keats, J.J., Crainie, M., Sun, X., Yen, T., Shibuya, E., Hendzel, M., Chan, G., Pilarski, L.M., 2003. RHAMM is a centrosomal protein that interacts with dynein and maintains spindle pole stability. *Mol. Biol. Cell* **14**, 2262-2276.
- McAtee, C.O., Berkebile, A.R., Elowsky, C.G., Fangman, T., Barycki, J.J., Wahl, J.K., 3rd, Khalimonchuk, O., Naslavsky, N., Caplan, S., Simpson, M.A., 2015.

- Hyaluronidase Hyal1 Increases Tumor Cell Proliferation and Motility through Accelerated Vesicle Trafficking. *J. Biol. Chem.* **290**, 13144-13156.
- McCay, P.B., Lai, E.K., Poyer, J.L., DuBose, C.M., Janzen, E.G., 1984. Oxygen- and carbon-centered free radical formation during carbon tetrachloride metabolism. Observation of lipid radicals in vivo and in vitro. *J. Biol. Chem.* **259**, 2135-2143.
- McCracken, J.M., Chalise, P., Briley, S.M., Dennis, K.L., Jiang, L., Duncan, F.E., Pritchard, M.T., 2017 in press. C57BL/6 substrains exhibit different responses to acute carbon tetrachloride exposure: Implications for work involving transgenic mice. *Gene Expression: The Journal of Basic Liver Research* **17**.
- McCracken, J.M., Jiang, L., Deshpande, K.T., O'Neil, M.F., Pritchard, M.T., 2016. Differential effects of hyaluronan synthase 3 deficiency after acute vs chronic liver injury in mice. *Fibrogenesis Tissue Repair* **9**, 4.
- McDonald, B., Kubes, P., 2015. Interactions between CD44 and Hyaluronan in Leukocyte Trafficking. *Front. Immunol.* **6**, 68.
- McDonald, B., Kubes, P., 2016. Innate Immune Cell Trafficking and Function During Sterile Inflammation of the Liver. *Gastroenterology* **151**, 1087-1095.
- McDonald, B., Pittman, K., Menezes, G.B., Hirota, S.A., Slaba, I., Waterhouse, C.C., Beck, P.L., Muruve, D.A., Kubes, P., 2010. Intravascular danger signals guide neutrophils to sites of sterile inflammation. *Science* **330**, 362-366.
- McGill, M.R., Williams, C.D., Xie, Y., Ramachandran, A., Jaeschke, H., 2012. Acetaminophen-induced liver injury in rats and mice: comparison of protein adducts, mitochondrial dysfunction, and oxidative stress in the mechanism of toxicity. *Toxicol. Appl. Pharmacol.* **264**, 387-394.

- McKee, C.M., Penno, M.B., Cowman, M., Burdick, M.D., Strieter, R.M., Bao, C., Noble, P.W., 1996. Hyaluronan (HA) fragments induce chemokine gene expression in alveolar macrophages. The role of HA size and CD44. *J. Clin. Invest.* **98**, 2403-2413.
- Mederacke, I., Hsu, C.C., Troeger, J.S., Huebener, P., Mu, X., Dapito, D.H., Pradere, J.P., Schwabe, R.F., 2013. Fate tracing reveals hepatic stellate cells as dominant contributors to liver fibrosis independent of its aetiology. *Nat Commun* **4**, 2823.
- Mehal, W., To, U., 2016. New approaches for fibrosis regression in alcoholic cirrhosis. *Hepatol Int* **10**, 773-778.
- Mehendale, H.M., 2005. Tissue repair: an important determinant of final outcome of toxicant-induced injury. *Toxicol. Pathol.* **33**, 41-51.
- Mekada, K., Abe, K., Murakami, A., Nakamura, S., Nakata, H., Moriwaki, K., Obata, Y., Yoshiki, A., 2009. Genetic differences among C57BL/6 substrains. *Exp. Anim.* **58**, 141-149.
- Mencin, A., Kluwe, J., Schwabe, R.F., 2009. Toll-like receptors as targets in chronic liver diseases. *Gut* **58**, 704-720.
- Meran, S., Martin, J., Luo, D.D., Steadman, R., Phillips, A., 2013. Interleukin-1beta induces hyaluronan and CD44-dependent cell protrusions that facilitate fibroblast-monocyte binding. *Am. J. Pathol.* **182**, 2223-2240.
- Meyer, K., 1958. Chemical structure of hyaluronic acid. *Fed. Proc.* **17**, 1075-1077.
- Meyer, K., Palmer, J.W., 1934. The polysaccharide of the vitreous humor. *J. Biol. Chem.*, 629-634.

- Meyer-Kirchrath, J., Debey, S., Glandorff, C., Kirchrath, L., Schror, K., 2004. Gene expression profile of the Gs-coupled prostacyclin receptor in human vascular smooth muscle cells. *Biochem. Pharmacol.* **67**, 757-765.
- Michalopoulos, G.K., DeFrances, M.C., 1997. Liver regeneration. *Science* **276**, 60-66.
- Milisav, I., Poljsak, B., Suput, D., 2012. Adaptive response, evidence of cross-resistance and its potential clinical use. *Int J Mol Sci* **13**, 10771-10806.
- Mine, S., Okada, Y., Kawahara, C., Tabata, T., Tanaka, Y., 2006. Serum hyaluronan concentration as a marker of angiopathy in patients with diabetes mellitus. *Endocr. J.* **53**, 761-766.
- Mitchell, C., Couton, D., Couty, J.P., Anson, M., Crain, A.M., Bizet, V., Renia, L., Pol, S., Mallet, V., Gilgenkrantz, H., 2009a. Dual role of CCR2 in the constitution and the resolution of liver fibrosis in mice. *Am. J. Pathol.* **174**, 1766-1775.
- Mitchell, C., Robin, M.A., Mayeuf, A., Mahrouf-Yorgov, M., Mansouri, A., Hamard, M., Couton, D., Fromenty, B., Gilgenkrantz, H., 2009b. Protection against hepatocyte mitochondrial dysfunction delays fibrosis progression in mice. *Am. J. Pathol.* **175**, 1929-1937.
- Mochizuki, A., Pace, A., Rockwell, C.E., Roth, K.J., Chow, A., O'Brien, K.M., Albee, R., Kelly, K., Towery, K., Luyendyk, J.P., Copple, B.L., 2014. Hepatic stellate cells orchestrate clearance of necrotic cells in a hypoxia-inducible factor-1alpha-dependent manner by modulating macrophage phenotype in mice. *J. Immunol.* **192**, 3847-3857.
- Mohanraj, R., Sato, A., Nakashima, H., Nakashima, M., Ikarashi, M., Nishiyama, K., Kinoshita, M., Seki, S., 2014. Involvement of the TNF and FasL Produced by

- CD11b Kupffer Cells/Macrophages in CCl<sub>4</sub>-Induced Acute Hepatic Injury. *PLoS One* **9**, e92515.
- Moles, A., Murphy, L., Wilson, C.L., Chakraborty, J.B., Fox, C., Park, E.J., Mann, J., Oakley, F., Howarth, R., Brain, J., Masson, S., Karin, M., Seki, E., Mann, D.A., 2014. A TLR2/S100A9/CXCL-2 signaling network is necessary for neutrophil recruitment in acute and chronic liver injury in the mouse. *J. Hepatol.* **60**, 782-791.
- Moseley, R., Waddington, R.J., Embery, G., 1997. Degradation of glycosaminoglycans by reactive oxygen species derived from stimulated polymorphonuclear leukocytes. *Biochim. Biophys. Acta* **1362**, 221-231.
- Nagy, N., Kaber, G., Johnson, P.Y., Gebe, J.A., Preisinger, A., Falk, B.A., Sunkari, V.G., Gooden, M.D., Vernon, R.B., Bogdani, M., Kuipers, H.F., Day, A.J., Campbell, D.J., Wight, T.N., Bollyky, P.L., 2015a. Inhibition of hyaluronan synthesis restores immune tolerance during autoimmune insulinitis. *J. Clin. Invest.* **125**, 3928-3940.
- Nagy, N., Kuipers, H.F., Frymoyer, A.R., Ishak, H.D., Bollyky, J.B., Wight, T.N., Bollyky, P.L., 2015b. 4-methylumbelliferone treatment and hyaluronan inhibition as a therapeutic strategy in inflammation, autoimmunity, and cancer. *Front. Immunol.* **6**, 123.
- Nakagawa, H., Maeda, S., Hikiba, Y., Ohmae, T., Shibata, W., Yanai, A., Sakamoto, K., Ogura, K., Noguchi, T., Karin, M., Ichijo, H., Omata, M., 2008. Deletion of apoptosis signal-regulating kinase 1 attenuates acetaminophen-induced liver

- injury by inhibiting c-Jun N-terminal kinase activation. *Gastroenterology* **135**, 1311-1321.
- Nakamura, K., Yokohama, S., Yoneda, M., Okamoto, S., Tamaki, Y., Ito, T., Okada, M., Aso, K., Makino, I., 2004. High, but not low, molecular weight hyaluronan prevents T-cell-mediated liver injury by reducing proinflammatory cytokines in mice. *J. Gastroenterol.* **39**, 346-354.
- Natarajan, A., Wagner, B., Sibilica, M., 2007. The EGF receptor is required for efficient liver regeneration. *Proc. Natl. Acad. Sci. U. S. A.* **104**, 17081-17086.
- Navarro, S.J., Trinh, T., Lucas, C.A., Ross, A.J., Waymire, K.G., Macgregor, G.R., 2012. The C57BL/6J Mouse Strain Background Modifies the Effect of a Mutation in Bcl2l2. *G3* **2**, 99-102.
- Necas, J., Bartosikova, L., Brauner, P., Kolar, J., 2008. Hyaluronic acid (hyaluronan): a review. *Veterinari Medicina* **53**, 397-411.
- Neuman, M.G., Cohen, L.B., Nanau, R.M., 2016. Hyaluronic acid as a non-invasive biomarker of liver fibrosis. *Clin. Biochem.* **49**, 302-315.
- Nicholson, A., Reifsnyder, P.C., Malcolm, R.D., Lucas, C.A., MacGregor, G.R., Zhang, W., Leiter, E.H., 2010. Diet-induced obesity in two C57BL/6 substrains with intact or mutant nicotinamide nucleotide transhydrogenase (Nnt) gene. *Obesity* **18**, 1902-1905.
- Nieto, N., Friedman, S.L., Cederbaum, A.I., 2002. Cytochrome P450 2E1-derived reactive oxygen species mediate paracrine stimulation of collagen I protein synthesis by hepatic stellate cells. *J. Biol. Chem.* **277**, 9853-9864.

- Nikitovic, D., Kouvidi, K., Karamanos, N.K., Tzanakakis, G.N., 2013. The roles of hyaluronan/RHAMM/CD44 and their respective interactions along the insidious pathways of fibrosarcoma progression. *BioMed research international* **2013**, 929531.
- Nishiyama, K., Nakashima, H., Ikarashi, M., Kinoshita, M., Nakashima, M., Aosasa, S., Seki, S., Yamamoto, J., 2015. Mouse CD11b+Kupffer Cells Recruited from Bone Marrow Accelerate Liver Regeneration after Partial Hepatectomy. *PLoS One* **10**, e0136774.
- Noble, P.W., 2002. Hyaluronan and its catabolic products in tissue injury and repair. *Matrix Biol.* **21**, 25-29.
- Oakley, F., Meso, M., Iredale, J.P., Green, K., Marek, C.J., Zhou, X., May, M.J., Millward-Sadler, H., Wright, M.C., Mann, D.A., 2005. Inhibition of inhibitor of kappaB kinases stimulates hepatic stellate cell apoptosis and accelerated recovery from rat liver fibrosis. *Gastroenterology* **128**, 108-120.
- Olsen, A.L., Bloomer, S.A., Chan, E.P., Gaca, M.D., Georges, P.C., Sackey, B., Uemura, M., Janmey, P.A., Wells, R.G., 2011. Hepatic stellate cells require a stiff environment for myofibroblastic differentiation. *Am. J. Physiol. Gastrointest. Liver Physiol.* **301**, G110-118.
- Omary, M.B., Cohen, D.E., El-Omar, E.M., Jalan, R., Low, M.J., Nathanson, M.H., Peek, R.M., Jr., Turner, J.R., 2016. Not All Mice Are the Same: Standardization of Animal Research Data Presentation. *Gastroenterology* **150**, 1503-1504.
- Osawa, Y., Hoshi, M., Yasuda, I., Saibara, T., Moriwaki, H., Kozawa, O., 2013. Tumor necrosis factor-alpha promotes cholestasis-induced liver fibrosis in the mouse

- through tissue inhibitor of metalloproteinase-1 production in hepatic stellate cells. *PLoS One* **8**, e65251.
- Owumi, S.E., Corthals, S.M., Uwaifo, A.O., Kamendulis, L.M., Klaunig, J.E., 2014. Depletion of Kupffer cells modulates ethanol-induced hepatocyte DNA synthesis in C57Bl/6 mice. *Environ. Toxicol.* **29**, 867-875.
- Paliwal, S., Fagien, S., Sun, X., Holt, T., Kim, T., Hee, C.K., Van Epps, D., Messina, D.J., 2014. Skin extracellular matrix stimulation following injection of a hyaluronic acid-based dermal filler in a rat model. *Plast. Reconstr. Surg.* **134**, 1224-1233.
- Parikh, N.D., Hutton, D., Marrero, W., Sanghani, K., Xu, Y., Laveri, M., 2015. Projections in donor organs available for liver transplantation in the United States: 2014-2025. *Liver Transpl.* **21**, 855-863.
- Park, J.Y., Duong, C.T., Sharma, A.R., Son, K.M., Thompson, M.S., Park, S., Chang, J.D., Nam, J.S., Park, S., Lee, S.S., 2014. Effects of hyaluronic acid and gamma-globulin concentrations on the frictional response of human osteoarthritic articular cartilage. *PLoS One* **9**, e112684.
- Pascual, M., Fernandez-Lizarbe, S., Guerri, C., 2011. Role of TLR4 in ethanol effects on innate and adaptive immune responses in peritoneal macrophages. *Immunol. Cell Biol.* **89**, 716-727.
- Pasonen-Seppanen, S., Hyttinen, J.M., Rilla, K., Jokela, T., Noble, P.W., Tammi, M., Tammi, R., 2012. Role of CD44 in the organization of keratinocyte pericellular hyaluronan. *Histochem. Cell Biol.* **137**, 107-120.
- Pasonen-Seppanen, S., Karvinen, S., Torronen, K., Hyttinen, J.M., Jokela, T., Lammi, M.J., Tammi, M.I., Tammi, R., 2003. EGF upregulates, whereas TGF-beta

- downregulates, the hyaluronan synthases Has2 and Has3 in organotypic keratinocyte cultures: correlations with epidermal proliferation and differentiation. *J. Invest. Dermatol.* **120**, 1038-1044.
- Pellicoro, A., Ramachandran, P., Iredale, J.P., Fallowfield, J.A., 2014. Liver fibrosis and repair: immune regulation of wound healing in a solid organ. *Nat. Rev. Immunol.* **14**, 181-194.
- Peng, C., Wallwiener, M., Rudolph, A., Cuk, K., Eilber, U., Celik, M., Modugno, C., Trumpp, A., Heil, J., Marme, F., Madhavan, D., Nees, J., Riethdorf, S., Schott, S., Sohn, C., Pantel, K., Schneeweiss, A., Chang-Claude, J., Yang, R., Burwinkel, B., 2016. Plasma hyaluronic acid level as a prognostic and monitoring marker of metastatic breast cancer. *Int. J. Cancer* **138**, 2499-2509.
- Penny, S.M., 2013. Alcoholic liver disease. *Radiol. Technol.* **84**, 577-592; quiz 593-575.
- Perepelyuk, M., Terajima, M., Wang, A.Y., Georges, P.C., Janmey, P.A., Yamauchi, M., Wells, R.G., 2013. Hepatic stellate cells and portal fibroblasts are the major cellular sources of collagens and lysyl oxidases in normal liver and early after injury. *Am. J. Physiol. Gastrointest. Liver Physiol.* **304**, G605-614.
- Picaud, L., Thibault, B., Mery, E., Ouali, M., Martinez, A., Delord, J.P., Couderc, B., Ferron, G., 2014. Evaluation of the effects of hyaluronic acid-carboxymethyl cellulose barrier on ovarian tumor progression. *J Ovarian Res* **7**, 40.
- Pluta, A., Gutkowski, K., Hartleb, M., 2010. Coagulopathy in liver diseases. *Adv. Med. Sci.* **55**, 16-21.

- Poisson, J., Lemoine, S., Boulanger, C., Durand, F., Moreau, R., Valla, D., Rautou, P.E., 2017. Liver sinusoidal endothelial cells: Physiology and role in liver diseases. *J. Hepatol.* **66**, 212-227.
- Poole, L.G., Arteel, G.E., 2016. Transitional Remodeling of the Hepatic Extracellular Matrix in Alcohol-Induced Liver Injury. *BioMed research international* **2016**, 3162670.
- Possamai, L.A., 2010. Role of monocytes and macrophages in experimental and human acute liver failure. *World J. Gastroenterol.* **16**, 1811.
- Postic, C., Girard, J., 2008. Contribution of de novo fatty acid synthesis to hepatic steatosis and insulin resistance: lessons from genetically engineered mice. *J. Clin. Invest.* **118**, 829-838.
- Pritchard, M.T., Malinak, R.N., Nagy, L.E., 2011. Early growth response (EGR)-1 is required for timely cell-cycle entry and progression in hepatocytes after acute carbon tetrachloride exposure in mice. *Am. J. Physiol. Gastrointest. Liver Physiol.* **300**, G1124-1131.
- Pritchard, M.T., McCracken, J.M., 2015. Identifying Novel Targets for Treatment of Liver Fibrosis: What Can We Learn from Injured Tissues which Heal Without a Scar? *Curr. Drug Targets* **16**, 1332-1346.
- Pritchard, M.T., McMullen, M.R., Stavitsky, A.B., Cohen, J.I., Lin, F., Medof, M.E., Nagy, L.E., 2007. Differential contributions of C3, C5, and decay-accelerating factor to ethanol-induced fatty liver in mice. *Gastroenterology* **132**, 1117-1126.
- Rai, R., 2013. Liver transplantatation- an overview. *Indian J. Surg.* **75**, 185-191.

- Rai, S.K., Duh, F.M., Vigdorovich, V., Danilkovitch-Miagkova, A., Lerman, M.I., Miller, A.D., 2001. Candidate tumor suppressor HYAL2 is a glycosylphosphatidylinositol (GPI)-anchored cell-surface receptor for jaagsiekte sheep retrovirus, the envelope protein of which mediates oncogenic transformation. *Proc. Natl. Acad. Sci. U. S. A.* **98**, 4443-4448.
- Ramachandra, V., Phuc, S., Franco, A.C., Gonzales, R.A., 2007. Ethanol preference is inversely correlated with ethanol-induced dopamine release in 2 substrains of C57BL/6 mice. *Alcohol. Clin. Exp. Res.* **31**, 1669-1676.
- Ramachandran, P., Pellicoro, A., Vernon, M.A., Boulter, L., Aucott, R.L., Ali, A., Hartland, S.N., Snowdon, V.K., Cappon, A., Gordon-Walker, T.T., Williams, M.J., Dunbar, D.R., Manning, J.R., van Rooijen, N., Fallowfield, J.A., Forbes, S.J., Iredale, J.P., 2012. Differential Ly-6C expression identifies the recruited macrophage phenotype, which orchestrates the regression of murine liver fibrosis. *Proc. Natl. Acad. Sci. U. S. A.* **109**, E3186-3195.
- Ramaiah, S.K., Jaeschke, H., 2007. Role of neutrophils in the pathogenesis of acute inflammatory liver injury. *Toxicol. Pathol.* **35**, 757-766.
- Rangel, M.P., de Sa, V.K., Martins, V., Martins, J.R., Parra, E.R., Mendes, A., Andrade, P.C., Reis, R.M., Longatto-Filho, A., Oliveira, C.Z., Takagaki, T., Carraro, D.M., Nader, H.B., Capelozzi, V.L., 2015. Tissue hyaluronan expression, as reflected in the sputum of lung cancer patients, is an indicator of malignancy. *Braz. J. Med. Biol. Res.* **48**, 557-567.
- Reddy, G.K., Enwemeka, C.S., 1996. A simplified method for the analysis of hydroxyproline in biological tissues. *Clin. Biochem.* **29**, 225-229.

- Reed, R.K., Lilja, K., Laurent, T.C., 1988. Hyaluronan in the rat with special reference to the skin. *Acta Physiol. Scand.* **134**, 405-411.
- Reynolds, J., 2011. Strain differences and the genetic basis of experimental autoimmune anti-glomerular basement membrane glomerulonephritis. *Int. J. Exp. Pathol.* **92**, 211-217.
- Rilla, K., Oikari, S., Jokela, T.A., Hyttinen, J.M., Karna, R., Tammi, R.H., Tammi, M.I., 2013. Hyaluronan synthase 1 (HAS1) requires higher cellular UDP-GlcNAc concentration than HAS2 and HAS3. *J. Biol. Chem.* **288**, 5973-5983.
- Roberts, H.W., Utuama, O.A., Klevens, M., Teshale, E., Hughes, E., Jiles, R., 2014. The contribution of viral hepatitis to the burden of chronic liver disease in the United States. *Am. J. Gastroenterol.* **109**, 387-393; quiz 386, 394.
- Rock, K.L., Kono, H., 2008. The Inflammatory Response to Cell Death. *Annual Review of Pathology: Mechanisms of Disease* **3**, 99-126.
- Ronchi, J.A., Figueira, T.R., Ravagnani, F.G., Oliveira, H.C., Vercesi, A.E., Castilho, R.F., 2013. A spontaneous mutation in the nicotinamide nucleotide transhydrogenase gene of C57BL/6J mice results in mitochondrial redox abnormalities. *Free Radic. Biol. Med.* **63**, 446-456.
- Ross, A.J., Waymire, K.G., Moss, J.E., Parlow, A.F., Skinner, M.K., Russell, L.D., MacGregor, G.R., 1998. Testicular degeneration in Bclw-deficient mice. *Nat. Genet.* **18**, 251-256.
- Rosso, N., Chavez-Tapia, N.C., Tiribelli, C., Bellentani, S., 2014. Translational approaches: from fatty liver to non-alcoholic steatohepatitis. *World J. Gastroenterol.* **20**, 9038-9049.

- Rostami, S., Parsian, H., 2013. Hyaluronic Acid: From Biochemical Characteristics to its Clinical Translation in Assessment of Liver Fibrosis. *Hepat Mon* **13**, e13787.
- Ruffell, B., Poon, G.F., Lee, S.S., Brown, K.L., Tjew, S.L., Cooper, J., Johnson, P., 2011. Differential use of chondroitin sulfate to regulate hyaluronan binding by receptor CD44 in Inflammatory and Interleukin 4-activated Macrophages. *J. Biol. Chem.* **286**, 19179-19190.
- Rugheimer, L., Carlsson, C., Johnsson, C., Hansell, P., 2008. Renal hyaluronan content during experimental uncontrolled diabetes in rats. *J. Physiol. Pharmacol.* **59**, 115-128.
- Ruppert, S.M., Hawn, T.R., Arrigoni, A., Wight, T.N., Bollyky, P.L., 2014. Tissue integrity signals communicated by high-molecular weight hyaluronan and the resolution of inflammation. *Immunol. Res.* **58**, 186-192.
- Rychtrmc, D., Hubalkova, L., Viskova, A., Libra, A., Buncek, M., Cervinkova, Z., 2012. Transcriptome temporal and functional analysis of liver regeneration termination. *Physiol. Res.* **61 Suppl 2**, S77-92.
- Saederup, N., Cardona, A.E., Croft, K., Mizutani, M., Cotleur, A.C., Tsou, C.L., Ransohoff, R.M., Charo, I.F., 2010. Selective chemokine receptor usage by central nervous system myeloid cells in CCR2-red fluorescent protein knock-in mice. *PLoS One* **5**, e13693.
- Saidi, R.F., Markmann, J.F., Jabbour, N., Li, Y., Shah, S.A., Cosimi, A.B., Bozorgzadeh, A., 2012. The faltering solid organ donor pool in the United States (2001-2010). *World J. Surg.* **36**, 2909-2913.

- Savani, R., Bagli, D.J., Harrison, R., Turley, E., 2000. The Role of Hyaluronan-Receptor Interactions in Wound Repair. In Garg, H.G., Longaker, M.T., (Eds.), Scarless Wound Healing. Marcel Dekker, Inc., New York, pp. 115-142.
- Savani, R.C., Cao, G., Pooler, P.M., Zaman, A., Zhou, Z., DeLisser, H.M., 2001. Differential Involvement of the Hyaluronan (HA) Receptors CD44 and Receptor for HA-mediated Motility in Endothelial Cell Function and Angiogenesis. *J. Biol. Chem.* **276**, 36770-36778.
- Schaffert, C.-S., 2009. Alcohol metabolites and lipopolysaccharide: Roles in the development and/or progression of alcoholic liver disease. *World J. Gastroenterol.* **15**, 1209.
- Schumacher, J.D., Guo, G.L., 2016. Regulation of Hepatic Stellate Cells and Fibrogenesis by Fibroblast Growth Factors. *BioMed research international* **2016**, 8323747.
- Scott, C.L., Zheng, F., De Baetselier, P., Martens, L., Saeys, Y., De Prijck, S., Lippens, S., Abels, C., Schoonooghe, S., Raes, G., Devoogdt, N., Lambrecht, B.N., Beschin, A., Guilliams, M., 2016. Bone marrow-derived monocytes give rise to self-renewing and fully differentiated Kupffer cells. *Nat Commun* **7**, 10321.
- Sebastiani, G., Gkouvatsos, K., Pantopoulos, K., 2014. Chronic hepatitis C and liver fibrosis. *World J. Gastroenterol.* **20**, 11033-11053.
- Seki, E., Brenner, D.A., Karin, M., 2012. A liver full of JNK: signaling in regulation of cell function and disease pathogenesis, and clinical approaches. *Gastroenterology* **143**, 307-320.

- Seki, E., Schwabe, R.F., 2015. Hepatic inflammation and fibrosis: functional links and key pathways. *Hepatology* **61**, 1066-1079.
- Seror, J., Merkher, Y., Kampf, N., Collinson, L., Day, A.J., Maroudas, A., Klein, J., 2012. Normal and shear interactions between hyaluronan-aggrecan complexes mimicking possible boundary lubricants in articular cartilage in synovial joints. *Biomacromolecules* **13**, 3823-3832.
- Shariat, S.F., Karam, J.A., Lotan, Y., Karakiewicz, P.I., 2008. Critical evaluation of urinary markers for bladder cancer detection and monitoring. *Reviews in urology* **10**, 120-135.
- Sheeran, F.L., Rydstrom, J., Shakhparonov, M.I., Pestov, N.B., Pepe, S., 2010. Diminished NADPH transhydrogenase activity and mitochondrial redox regulation in human failing myocardium. *Biochim. Biophys. Acta* **1797**, 1138-1148.
- Siiskonen, H., Oikari, S., Pasonen-Seppanen, S., Rilla, K., 2015. Hyaluronan synthase 1: a mysterious enzyme with unexpected functions. *Front. Immunol.* **6**, 43.
- Simonetti, R.G., Camma, C., Fiorello, F., Politi, F., D'Amico, G., Pagliaro, L., 1991. Hepatocellular carcinoma. A worldwide problem and the major risk factors. *Dig. Dis. Sci.* **36**, 962-972.
- Sokolowska, M., Chen, L.Y., Eberlein, M., Martinez-Anton, A., Liu, Y., Alsaaty, S., Qi, H.Y., Logun, C., Horton, M., Shelhamer, J.H., 2014. Low molecular weight hyaluronan activates cytosolic phospholipase A2alpha and eicosanoid production in monocytes and macrophages. *J. Biol. Chem.* **289**, 4470-4488.
- Spandidos, A., Wang, X., Wang, H., Dragnev, S., Thurber, T., Seed, B., 2008. A comprehensive collection of experimentally validated primers for Polymerase

- Chain Reaction quantitation of murine transcript abundance. *BMC Genomics* **9**, 633.
- Spandidos, A., Wang, X., Wang, H., Seed, B., 2010. PrimerBank: a resource of human and mouse PCR primer pairs for gene expression detection and quantification. *Nucleic Acids Res.* **38**, D792-799.
- Spicer, A.P., McDonald, J.A., 1998. Characterization and molecular evolution of a vertebrate hyaluronan synthase gene family. *J. Biol. Chem.* **273**, 1923-1932.
- Stal, P., 2015. Liver fibrosis in non-alcoholic fatty liver disease - diagnostic challenge with prognostic significance. *World J. Gastroenterol.* **21**, 11077-11087.
- Stawicki, S.P., Green, J.M., Martin, N.D., Green, R.H., Cipolla, J., Seamon, M.J., Eiferman, D.S., Evans, D.C., Hazelton, J.P., Cook, C.H., Steinberg, S.M., Opus 12 Foundation, I.M.-C.T.G., Investigators, O., 2014. Results of a prospective, randomized, controlled study of the use of carboxymethylcellulose sodium hyaluronate adhesion barrier in trauma open abdomens. *Surgery* **156**, 419-430.
- Stefanovic, L., Stefanovic, B., 2012. Role of cytokine receptor-like factor 1 in hepatic stellate cells and fibrosis. *World J Hepatol* **4**, 356-364.
- Stern, R., 2003. Devising a pathway for hyaluronan catabolism: are we there yet? *Glycobiology* **13**, 105R-115R.
- Stern, R., Asari, A.A., Sugahara, K.N., 2006. Hyaluronan fragments: an information-rich system. *Eur. J. Cell Biol.* **85**, 699-715.
- Strey, C.W., Markiewski, M., Mastellos, D., Tudoran, R., Spruce, L.A., Greenbaum, L.E., Lambris, J.D., 2003. The proinflammatory mediators C3a and C5a are essential for liver regeneration. *J. Exp. Med.* **198**, 913-923.

- Szabo, G., Mandrekar, P., 2010. Focus on: Alcohol and the liver. *Alcohol Res Health* **33**, 87-96.
- Takeuchi, O., Hoshino, K., Kawai, T., Sanjo, H., Takada, H., Ogawa, T., Takeda, K., Akira, S., 1999. Differential roles of TLR2 and TLR4 in recognition of gram-negative and gram-positive bacterial cell wall components. *Immunity* **11**, 443-451.
- Tammi, R., Agren, U.M., Tuhkanen, A.L., Tammi, M., 1994. Hyaluronan metabolism in skin. *Prog. Histochem. Cytochem.* **29**, 1-81.
- Tang, H., Amara, U., Tang, D., Barnes, M.A., McDonald, C., Nagy, L.E., 2013. Synergistic interaction between C5a and NOD2 signaling in the regulation of chemokine expression in RAW 264.7 macrophages. *Adv Biosci Biotechnol* **4**, 30-37.
- Taniguchi, M., Takeuchi, T., Nakatsuka, R., Watanabe, T., Sato, K., 2004. Molecular process in acute liver injury and regeneration induced by carbon tetrachloride. *Life Sci.* **75**, 1539-1549.
- Taub, R., 2004. Liver regeneration: from myth to mechanism. *Nat. Rev. Mol. Cell Biol.* **5**, 836-847.
- Teder, P., Vandivier, R.W., Jiang, D., Liang, J., Cohn, L., Pure, E., Henson, P.M., Noble, P.W., 2002. Resolution of lung inflammation by CD44. *Science* **296**, 155-158.
- Telmer, P.G., Tolg, C., McCarthy, J.B., Turley, E.A., 2011. How does a protein with dual mitotic spindle and extracellular matrix receptor functions affect tumor susceptibility and progression? *Commun. Integr. Biol.* **4**, 182-185.

- Temple-Wong, M.M., Ren, S., Quach, P., Hansen, B.C., Chen, A.C., Hasegawa, A., D'Lima, D.D., Koziol, J., Masuda, K., Lotz, M.K., Sah, R.L., 2016. Hyaluronan concentration and size distribution in human knee synovial fluid: variations with age and cartilage degeneration. *Arthritis Res. Ther.* **18**, 18.
- ten Broek, R.P., Stommel, M.W., Strik, C., van Laarhoven, C.J., Keus, F., van Goor, H., 2014. Benefits and harms of adhesion barriers for abdominal surgery: a systematic review and meta-analysis. *Lancet* **383**, 48-59.
- Thannickal, V.J., Zhou, Y., Gaggar, A., Duncan, S.R., 2014. Fibrosis: ultimate and proximate causes. *J. Clin. Invest.* **124**, 4673-4677.
- Tolg, C., Hamilton, S.R., Morningstar, L., Zhang, J., Zhang, S., Esguerra, K.V., Telmer, P.G., Luyt, L.G., Harrison, R., McCarthy, J.B., Turley, E.A., 2010. RHAMM promotes interphase microtubule instability and mitotic spindle integrity through MEK1/ERK1/2 activity. *J. Biol. Chem.* **285**, 26461-26474.
- Tolg, C., Hamilton, S.R., Nakrieko, K.A., Kooshesh, F., Walton, P., McCarthy, J.B., Bissell, M.J., Turley, E.A., 2006. Rhamm-/- fibroblasts are defective in CD44-mediated ERK1,2 mitogenic signaling, leading to defective skin wound repair. *J. Cell Biol.* **175**, 1017-1028.
- Tolg, C., Hamilton, S.R., Zalinska, E., McCulloch, L., Amin, R., Akentieva, N., Winnik, F., Savani, R., Bagli, D.J., Luyt, L.G., Cowman, M.K., McCarthy, J.B., Turley, E.A., 2012. A RHAMM mimetic peptide blocks hyaluronan signaling and reduces inflammation and fibrogenesis in excisional skin wounds. *Am. J. Pathol.* **181**, 1250-1270.

- Tolg, C., Poon, R., Fodde, R., Turley, E.A., Alman, B.A., 2003. Genetic deletion of receptor for hyaluronan-mediated motility (Rhamm) attenuates the formation of aggressive fibromatosis (desmoid tumor). *Oncogene* **22**, 6873-6882.
- Tolg, C., Telmer, P., Turley, E., 2014. Specific sizes of hyaluronan oligosaccharides stimulate fibroblast migration and excisional wound repair. *PLoS One* **9**, e88479.
- Tomita, K., Freeman, B.L., Bronk, S.F., LeBrasseur, N.K., White, T.A., Hirsova, P., Ibrahim, S.H., 2016. CXCL10-Mediates Macrophage, but not Other Innate Immune Cells-Associated Inflammation in Murine Nonalcoholic Steatohepatitis. *Sci. Rep.* **6**, 28786.
- Tsochatzis, E.A., Bosch, J., Burroughs, A.K., 2014. Liver cirrhosis. *The Lancet* **383**, 1749-1761.
- Turley, E.A., 1982. Purification of a hyaluronate-binding protein fraction that modifies cell social behavior. *Biochem. Biophys. Res. Commun.* **108**, 1016-1024.
- Turley, E.A., Noble, P.W., Bourguignon, L.Y., 2002. Signaling properties of hyaluronan receptors. *J. Biol. Chem.* **277**, 4589-4592.
- Turlier, V., Delalleau, A., Casas, C., Rouquier, A., Bianchi, P., Alvarez, S., Josse, G., Briant, A., Dahan, S., Saint-Martory, C., Theunis, J., Bensafi-Benaouda, A., Degouy, A., Schmitt, A.M., Redoules, D., 2013. Association between collagen production and mechanical stretching in dermal extracellular matrix: in vivo effect of cross-linked hyaluronic acid filler. A randomised, placebo-controlled study. *J. Dermatol. Sci.* **69**, 187-194.
- van den Broek, M.A., Vreuls, C.P., Winstanley, A., Jansen, R.L., van Bijnen, A.A., Dello, S.A., Bemelmans, M.H., Dejong, C.H., Driessen, A., Olde Damink, S.W., 2013.

- Hyaluronic acid as a marker of hepatic sinusoidal obstruction syndrome secondary to oxaliplatin-based chemotherapy in patients with colorectal liver metastases. *Ann. Surg. Oncol.* **20**, 1462-1469.
- Vigetti, D., Genasetti, A., Karousou, E., Viola, M., Moretto, P., Clerici, M., Deleonibus, S., De Luca, G., Hascall, V.C., Passi, A., 2010. Proinflammatory cytokines induce hyaluronan synthesis and monocyte adhesion in human endothelial cells through hyaluronan synthase 2 (HAS2) and the nuclear factor-kappaB (NF-kappaB) pathway. *J. Biol. Chem.* **285**, 24639-24645.
- Vogel, R., Wiesinger, H., Hamprecht, B., Dringen, R., 1999. The regeneration of reduced glutathione in rat forebrain mitochondria identifies metabolic pathways providing the NADPH required. *Neurosci. Lett.* **275**, 97-100.
- Vrochides, D., Papanikolaou, V., Pertoft, H., Antoniadou, A.A., Heldin, P., 1996. Biosynthesis and degradation of hyaluronan by nonparenchymal liver cells during liver regeneration. *Hepatology* **23**, 1650-1655.
- Wagner, M., Zollner, G., Trauner, M., 2009. New molecular insights into the mechanisms of cholestasis. *J. Hepatol.* **51**, 565-580.
- Walkin, L., Herrick, S.E., Summers, A., Brenchley, P.E., Hoff, C.M., Korstanje, R., Margetts, P.J., 2013. The role of mouse strain differences in the susceptibility to fibrosis: a systematic review. *Fibrogenesis Tissue Repair* **6**, 18.
- Wang, A., de la Motte, C., Lauer, M., Hascall, V., 2011. Hyaluronan matrices in pathobiological processes. *The FEBS journal* **278**, 1412-1418.

- Wang, D.H., Wang, Y.N., Ge, J.Y., Liu, H.Y., Zhang, H.J., Qi, Y., Liu, Z.H., Cui, X.L., 2013. Role of activin A in carbon tetrachloride-induced acute liver injury. *World J. Gastroenterol.* **19**, 3802-3809.
- Wang, F., Garza, L.A., Kang, S., Varani, J., Orringer, J.S., Fisher, G.J., Voorhees, J.J., 2007. In vivo stimulation of de novo collagen production caused by cross-linked hyaluronic acid dermal filler injections in photodamaged human skin. *Arch. Dermatol.* **143**, 155-163.
- Wang, S., Pacher, P., De Lisle, R.C., Huang, H., Ding, W.X., 2016a. A Mechanistic Review of Cell Death in Alcohol-Induced Liver Injury. *Alcohol. Clin. Exp. Res.* **40**, 1215-1223.
- Wang, X., Seed, B., 2003. A PCR primer bank for quantitative gene expression analysis. *Nucleic Acids Res.* **31**, e154.
- Wang, Z., Tian, Y., Zhang, H., Qin, Y., Li, D., Gan, L., Wu, F., 2016b. Using hyaluronic acid-functionalized pH stimuli-responsive mesoporous silica nanoparticles for targeted delivery to CD44-overexpressing cancer cells. *Int J Nanomedicine* **11**, 6485-6497.
- Ward, B.C., Panitch, A., 2011. Abdominal adhesions: current and novel therapies. *J. Surg. Res.* **165**, 91-111.
- Webber, E.M., Bruix, J., Pierce, R.H., Fausto, N., 1998. Tumor necrosis factor primes hepatocytes for DNA replication in the rat. *Hepatology* **28**, 1226-1234.
- Weber, L.W., Boll, M., Stampfl, A., 2003. Hepatotoxicity and mechanism of action of haloalkanes: carbon tetrachloride as a toxicological model. *Crit. Rev. Toxicol.* **33**, 105-136.

- Wells, R.G., Schwabe, R.F., 2015. Origin and function of myofibroblasts in the liver. *Semin. Liver Dis.* **35**, 97-106.
- West, D.C., Shaw, D.M., Lorenz, P., Adzick, N.S., Longaker, M.T., 1997. Fibrotic healing of adult and late gestation fetal wounds correlates with increased hyaluronidase activity and removal of hyaluronan. *Int. J. Biochem. Cell Biol.* **29**, 201-210.
- Williams, G.M., Iatropoulos, M.J., 2002. Alteration of liver cell function and proliferation: differentiation between adaptation and toxicity. *Toxicol. Pathol.* **30**, 41-53.
- Wong, F.W., Chan, W.Y., Lee, S.S., 1998. Resistance to carbon tetrachloride-induced hepatotoxicity in mice which lack CYP2E1 expression. *Toxicol. Appl. Pharmacol.* **153**, 109-118.
- Wong, H.S., Chen, J.H., Leong, P.K., Leung, H.Y., Chan, W.M., Ko, K.M., 2014. beta-sitosterol protects against carbon tetrachloride hepatotoxicity but not gentamicin nephrotoxicity in rats via the induction of mitochondrial glutathione redox cycling. *Molecules* **19**, 17649-17662.
- Woolbright, B.L., Dorko, K., Antoine, D.J., Clarke, J.I., Gholami, P., Li, F., Kumer, S.C., Schmitt, T.M., Forster, J., Fan, F., Jenkins, R.E., Park, B.K., Hagenbuch, B., Olyae, M., Jaeschke, H., 2015. Bile acid-induced necrosis in primary human hepatocytes and in patients with obstructive cholestasis. *Toxicol. Appl. Pharmacol.* **283**, 168-177.
- Woolbright, B.L., Jaeschke, H., 2015. Sterile inflammation in acute liver injury: myth or mystery? *Expert Rev Gastroenterol Hepatol* **9**, 1027-1029.

- Wu, D., Cederbaum, A.I., 2008. Alcohol, Methods and Protocols. Humana Press, Totowa, NJ.
- Xie, J., Liu, J., Chen, T.M., Lan, Q., Zhang, Q.Y., Liu, B., Dai, D., Zhang, W.D., Hu, L.P., Zhu, R.Z., 2015. Dihydromyricetin alleviates carbon tetrachloride-induced acute liver injury via JNK-dependent mechanism in mice. *World J. Gastroenterol.* **21**, 5473-5481.
- Xu, R., Lin, F., He, J., Jin, L., Zhang, J.Y., Fu, J., Liu, H., Wang, S., Zhang, Z., Wang, F.S., 2013. Complement 5a stimulates hepatic stellate cells in vitro, and is increased in the plasma of patients with chronic hepatitis B. *Immunology* **138**, 228-234.
- Yamamoto, H., Tobisawa, Y., Inubushi, T., Irie, F., Oyama, C., Yamaguchi, Y., 2017. A Mammalian Homolog of the Zebrafish Transmembrane Protein 2 (TMEM2) Is the Long-sought-after Cell Surface Hyaluronidase. *J. Biol. Chem.*
- Yamamoto, T., Naito, M., Moriyama, H., Umezu, H., Matsuo, H., Kiwada, H., Arakawa, M., 1996. Repopulation of murine Kupffer cells after intravenous administration of liposome-encapsulated dichloromethylene diphosphonate. *Am. J. Pathol.* **149**, 1271-1286.
- Yan, S.J., Blomme, E.A., 2003. In situ zymography: a molecular pathology technique to localize endogenous protease activity in tissue sections. *Vet. Pathol.* **40**, 227-236.
- Yang, C., Cao, M., Liu, H., He, Y., Xu, J., Du, Y., Liu, Y., Wang, W., Cui, L., Hu, J., Gao, F., 2012. The high and low molecular weight forms of hyaluronan have distinct effects on CD44 clustering. *J. Biol. Chem.* **287**, 43094-43107.

- Yang, Y.M., Seki, E., 2015. TNFalpha in liver fibrosis. *Curr Pathobiol Rep* **3**, 253-261.
- Yasuda, T., 2007. Hyaluronan inhibits cytokine production by lipopolysaccharide-stimulated U937 macrophages through down-regulation of NF-kappaB via ICAM-1. *Inflamm. Res.* **56**, 246-253.
- Yata, Y., Takahara, T., Furui, K., Zhang, L.P., Watanabe, A., 1999. Expression of matrix metalloproteinase-13 and tissue inhibitor of metalloproteinase-1 in acute liver injury. *J. Hepatol.* **30**, 419-424.
- Yilmaz, Y., 2012. Review article: is non-alcoholic fatty liver disease a spectrum, or are steatosis and non-alcoholic steatohepatitis distinct conditions? *Aliment. Pharmacol. Ther.* **36**, 815-823.
- Yoshida, H., Nagaoka, A., Kusaka-Kikushima, A., Tobiishi, M., Kawabata, K., Sayo, T., Sakai, S., Sugiyama, Y., Enomoto, H., Okada, Y., Inoue, S., 2013. KIAA1199, a deafness gene of unknown function, is a new hyaluronan binding protein involved in hyaluronan depolymerization. *Proc. Natl. Acad. Sci. U. S. A.* **110**, 5612-5617.
- You, Q., Holt, M., Yin, H., Li, G., Hu, C.J., Ju, C., 2013. Role of hepatic resident and infiltrating macrophages in liver repair after acute injury. *Biochem. Pharmacol.* **86**, 836-843.
- Yuan, B., Dong, R., Shi, D., Zhou, Y., Zhao, Y., Miao, M., Jiao, B., 2011. Down-regulation of miR-23b may contribute to activation of the TGF-beta1/Smad3 signalling pathway during the termination stage of liver regeneration. *FEBS Lett.* **585**, 927-934.

- Yuan, H., Amin, R., Ye, X., de la Motte, C.A., Cowman, M.K., 2015. Determination of hyaluronan molecular mass distribution in human breast milk. *Anal. Biochem.* **474**, 78-88.
- Zaman, A., Cui, Z., Foley, J.P., Zhao, H., Grimm, P.C., Delisser, H.M., Savani, R.C., 2005. Expression and role of the hyaluronan receptor RHAMM in inflammation after bleomycin injury. *Am. J. Respir. Cell Mol. Biol.* **33**, 447-454.
- Zamara, E., Galastri, S., Aleffi, S., Petrai, I., Aragno, M., Mastrocola, R., Novo, E., Bertolani, C., Milani, S., Vizzutti, F., Vercelli, A., Pinzani, M., Laffi, G., LaVilla, G., Parola, M., Marra, F., 2007. Prevention of severe toxic liver injury and oxidative stress in MCP-1-deficient mice. *J. Hepatol.* **46**, 230-238.
- Zhan, S.S., Jiang, J.X., Wu, J., Halsted, C., Friedman, S.L., Zern, M.A., Torok, N.J., 2006. Phagocytosis of apoptotic bodies by hepatic stellate cells induces NADPH oxidase and is associated with liver fibrosis in vivo. *Hepatology* **43**, 435-443.
- Zhang, D., Jiang, M., Miao, D., 2011. Transplanted human amniotic membrane-derived mesenchymal stem cells ameliorate carbon tetrachloride-induced liver cirrhosis in mouse. *PLoS One* **6**, e16789.
- Zhou, W.C., Zhang, Q.B., Qiao, L., 2014. Pathogenesis of liver cirrhosis. *World J. Gastroenterol.* **20**, 7312-7324.
- Zhuang, Y., Yin, Q., 2013. Peroxisome proliferator-activated receptor gamma agonists attenuate hyperglycaemia-induced hyaluronan secretion in vascular smooth muscle cells by inhibiting PKCbeta2. *Cell Biochem. Biophys.* **67**, 583-590.
- Zigmond, E., Samia-Grinberg, S., Pasmanik-Chor, M., Brazowski, E., Shibolet, O., Halpern, Z., Varol, C., 2014. Infiltrating monocyte-derived macrophages and

resident kupffer cells display different ontogeny and functions in acute liver injury.  
J. Immunol. **193**, 344-353.

Zurita, E., Chagoyen, M., Cantero, M., Alonso, R., Gonzalez-Neira, A., Lopez-Jimenez, A., Lopez-Moreno, J.A., Landel, C.P., Benitez, J., Pazos, F., Montoliu, L., 2011. Genetic polymorphisms among C57BL/6 mouse inbred strains. Transgenic Res. **20**, 481-489.